Universität Basel

Evolutionary prospection of *Globorotalia menardii*: an investigation of tempo and mode of evolution since the Late Miocene

Inauguraldissertation

zur
Erlangung der Würde eines Doktors der Philosophie
vorgelegt der
Philosophisch-Naturwissenschaftlichen Fakultät
der Universität Basel

von

Thore Friesenhagen

2024

Genehmigt von der Philosophisch-Naturwissenschaftlichen Fakultät
auf Antrag von

Erstbetreuer/in:	PD Dr. Michael Knappertsbusch
Zweitbetreuer/in:	Prof erem. Dr. Andreas Wetzel
Externe/r Experte/in:	Prof. Dr. Martin R. Langer

Basel, den 26.04.2022

Prof. Dr. Marcel Mayor

Dekan

Für meine Eltern

Content

List of tables

List of figures

List of figures in Appendix

Acknowledgements

I thank the Swiss National Science Foundation (SNF) for funding this thesis and Freiwillige Akademische Gesellschaft (FAG) Basel for the financial support.

Thanks go to the International Ocean Discovery Program (IODP) and the Ocean Drilling Program (ODP) for providing the sample material for this thesis.

My supervisors deserve especially cordial thanks. I owe by far the most to Dr. Michael Knappertsbusch, who designed the study and wrote the proposal. I will never forget our long. thought-provoking discussions and his unlimited support.

I am indebt to Prof. em. Dr. Andreas Wetzel for his support and advice. Special thanks go to Prof. Dr. Martin Langer for agreeing to stand as my external expert.

Thanks go to the developers of the AMOR system, Michael Knappertsbusch and Jean Eisenecker. This machine is an amazing piece of work!

I greatly profited from the generous support of the Natural History Museum Basel, which integrated me very soon after my start (thank you so much Tandra, Bastien, Daniela, André, Edi, Loïc, Basil, Nora, Anna, Marlen, Patrizia) and provided a working place and infrastructure.

The acknowledgements would be incomplete without mentioning my friends and office mates, for their scientific, but also and especially moral support even in the most difficult times of my dissertation:

Thomas, you always gave ear to both scientifical but also private problems.

Diana Rendon-Mera, Gracias for the great time.

Alexandra Viertler, may your dice always roll in your favour (except if you are the DM).

Johannes, you helped me a lot to feel home in Basel soon. Thank you so much for introducing me to the wonderful world of Pen&Paper games!

Bastien, thank you for your ideas and for all the escape rooms we played together.

Tandra, thank you so much for your moral support and for all the Escape Rooms and Board Game evenings!

Oceané, I will never forget our conversations during coffee breaks!

Althaea, Alrikas, Firunz and Milomir, will never forget you!

For scientific support, advice, discussion, I wish to thank:

Daniel Burkhardt, Mark Charran, Loïc Costeur, Christian de Capitani, Dominik Fleitmann, Seraina Klopfstein, Thomas Kuhn, Sergio Kühni, Moritz Lehmann, David Marques, Bastien Mennecart, Johannes Pietsch, André Puschnig, Diana Rendon Mera, Tamara Spasojevic, Edi Stöckli and Alexandra Viertler.

Last but not least, I want to express my deep gratitude to my sister and my parents, for their absolute and unending support, kindness and belief in me.

Abstract

Deciphering tempo and mode of evolution from the fossil record is a challenge for evolutionary studies. The observed pattern in the fossil record often results in ambiguous interpretations due to lack of temporal and spatial information of distribution as well as first appearance and disappearance or extinction of species.

Evolutionary prospection, which is the tracking of morphological changes of a species or group of organisms through time and different locations, may serve as a strategy to decipher tempo and mode of evolution from the fossil record.

In this thesis, this strategy is used with the aim to unravel the processes which influenced the evolution of the planktonic foraminifer *Globorotalia menardii* the Atlantic Ocean since the late Miocene.

The initial point is the observation of a rapid test-size increase in the Atlantic Ocean, which took place in the early Pleistocene between 2.3 Ma and 1.95 Ma. Within this time interval, the maximum test size of *G. menardii* more than doubled from ca. 550 µm to ca. 1150 µm in the axial length. This size had never been reached in the Atlantic Ocean before, so that Knappertsbsuch (2016) postulated the occurrence of a new, giant *G. menardii* morphotype. The evolutionary history of the proposed new type remained unsolved, as this event happened after the closure of the Central American Seaway. Therefore, the giant morphotype could not have derived from the eastern Pacific Ocean, where specimens with a size of more than 1000 µm had already been observed before.

Two hypotheses are tested, which could explain the appearance of this giant type: The Agulhas leakage hypothesis proposes the dispersal of the giant morphotype from the Indian Ocean via the Agulhas leakage around the southern tip of Africa. Alternatively, the giant type evolved in the Atlantic Ocean by a punctuated evolutionary event.

Following the idea of evolutionary prospection, quantitative measurements of morphological characteristics of the test of menardiform globorotaliids in keel view were made on samples from ODP Hole 667A in the eastern equatorial Atlantic Ocean for the last 7.96 Myr and IODP Hole U1476A in the Mozambique Channel from 6.49 Ma to the present. A comparison of these two locations allows to track the first occurrence of the giant morphotype and thus if it could spatially originate in the Indian Ocean. In the eastern tropical Atlantic Ocean ODP Hole 667A, 6719 menardiform globorotaliids specimens, including 4482 specimens of *G. menardii*, were picked from 33 stratigraphic levels. 7823 menardiform globorotaliids of which 4978 specimens belong to *G. menardii*, were collected from 31 stratigraphic level at Hole U1476A.

The use of the "Automated Measurement system for shell mORphology" (AMOR; Knappertsbusch et al., 2009; Knappertsbusch and Eisenecker, 2022) guarantee the objectivity and comparability of the performed morphological measurements. This system is capable of processing a huge quantity of objects, as it automatically orientates and images tests of menardiform globorotaliids in keel view.

The results are in accordance with the Agulhas leakage hypothesis. In the eastern tropical Atlantic Ocean, the doubling of the test size is observed between 2.58 Ma and 2.057 Ma. It coincides with a change in the predominant coiling direction of *G. menardii* populations from dextral to sinistral. If the giant morphotype is defined as exhibiting a sinistral coiling direction and having an axial length of more than 1000 µm, it already appeared at 2.95 Ma in the tropical Indian Ocean. Thus, a precondition for the Agulhas Leakage hypothesis is fulfilled with the earlier, diachronic occurrence in the Indian Ocean.

The evolution of form and shape of *G. menardii*, which are two further parameters derived from the performed morphological measurements, through time do not allow to distinguish the giant morphotype from the ancestral, small type.

Yet, the possibility that the giant morphotype evolved in a regional, punctuated evolutionary event in the Atlantic Ocean between 2.3 Ma and 2.057 Ma cannot be excluded based on the gathered data.

Patterns in the test-size evolution of *G. menardii* show a coinciding trend to proxies for the strength of the Atlantic Meridional Overturning Circulation (AMOC) in the Atlantic Ocean and the Indian Monsoon in the Indian Ocean. It suggests that changes in the strength of these major oceanographic drivers influence the long-term test-size evolution of *G. menardii* in the investigated time interval, probably due to their influence on the hydrography of the upper water column, which is the habitat of *G. menardii*.

A further objective of the thesis is the observation of interspecific trends within the *G. menardii-Globorotalia limbata-Globorotalia multicamerata* lineage. Continuing morphological splitting of the descendants *G. limbata* and *G. multicamerata* from its ancestor *G. menardii* could point to an ongoing diverging evolution of those morphospecies. Diverging trends in mean population test size are observed at the investigated sites: at Hole 667A in the eastern tropical Atlantic Ocean, *G. limbata* and *G. multicamerata* increase in size in comparison to *G. menardii* from 5.268 Ma until 4.14 Ma, while in the Indian Ocean a similar trend is observed from 5.78 Ma until 3.44 Ma. However, those time intervals of divergent test-size evolution are followed by intervals of converging trends. This probably indicates that those trends were rather caused by changes in the environmental conditions than being based on ongoing genetic differentiation.

Evolutionary prospection of demonstrates a high potential as a strategy to investigate the tempo and mode of evolution in menardiform globorotaliids.

References

Knappertsbusch, M. W.: Evolutionary prospection in the Neogene planktic foraminifer Globorotalia menardii and related forms from ODP Hole 925B (Ceara Rise, western tropical Atlantic): evidence for gradual evolution superimposed by long distance dispersal?, Swiss Journal of Palaeontology, 135, 205–248, https://doi.org/10.1007/s13358-016-0113-6, 2016.

Knappertsbusch, M. W., Binggeli, D., Herzig, A., Schmutz, L., Stapfer, S., Schneider, C., Eisenecker, J., and Widmer, L.: AMOR – A NEW SYSTEM FOR AUTOMATED IMAGING OF MICROFOSSILS FOR MORPHOMETRIC ANALYSES, Palaeontologia Electronica, 12, http://palaeo-electronica.org/2009_2/165/index.html, 2009.

Knappertsbusch, M. and Eisenecker, J.: Towards a Fleet of Robots for Orientation, Imaging, and Morphometric Analyses of Planktonic Foraminifera, Frontiers in Marine Science, 9, https://doi.org/10.3389/fmars.2022.798002, 2022.

Layout of thesis

Chapter 1 Introduction

Chapter 2 Test-size evolution of the planktonic foraminifer *Globorotalia menardii* in the eastern tropical Atlantic since the Late Miocene

This chapter investigates the test-size evolution of the *G. menardii*-*G. limbata*-*G. multicamerata* lineage in the eastern equatorial Atlantic ODP Hole 667A. The observed pattern in size evolution in *G. menardii* is discussed considering the Agulhas leakage hypothesis and the hypothesis of a punctuated evolutionary event in the early Pleistocene. It also introduces the AMOC and thermocline hypothesis, which may explain the overall pattern in size evolution of menardiform globorotaliids.

Chapter 3 Morphometric measurements of the planktonic foraminifer *Globorotalia menardii* from the Mozambique Channel provide new evidence for the Agulhas leakage hypothesis

In this chapter, the test-size evolution of the *G. menardii*-*G. limbata*-*G. multicamerata* lineage is described at IODP Hole U1476A in the Mozambique Chanel, Indian Ocean. The results are discussed in terms of the Agulhas leakage hypothesis and the thermocline hypothesis.

Chapter 4 Geometric morphometrics do not indicate speciation in the planktonic foraminifer *Globorotalia menardii* since the late Miocene

Form and shape variation of *G. menardii* is analysed in the eastern tropical Atlantic Ocean Hole 667A, the Indian Ocean Hole U1476A and the western tropical Pacific Ocean Hole 806C since the late Miocene. The chapter tests if the proposed new, giant morphotype can be distinguished from its ancestor by form and shape differences.

Chapter 5 Synopsis, Conclusion and Outlook

Chapter 1: Introduction

Charles Darwin's hypothesis about the evolution of species in "On the origin of Species", first published in 1859, (Darwin, 2003) drastically increased our understanding and knowledge of organisms and life history. Evolution of organisms is defined as the continuous change of species-specific characteristics in populations through time. It is driven by natural selection, which favours the survival of that specimens within a population, whose characteristics fit best to the changing environment.

Evolution cannot be directly observed in nature as the process is beyond the scope of a human life and takes geological timespans.

Nowadays, there are two approaches to investigate evolution and relationships among a group of organisms. Molecular studies analyse genes to determine species and the degree of relationship. However, this kind of analysis is restricted to (semi-) extant organisms and does not allow to recognise the tempo of evolution and involved processes. The study of the fossil record provides an alternative method for the study of evolution as it allows the investigation of the tempo and mode of evolution.

An example for an exceptional fossil record, which provides great potential for evolutionary studies, is that of planktonic foraminifera (PF). PF are marine protists which build a calcitic shell, i.e. test. Species of this group show a wide range of test morphology. The size of adult PF typically ranges from 50 to 1000 µm (de Vargas et al., 2004), but was occasionally observed to reach up to 1400 µm (Knappertsbusch, 2016, 2022). Due to their numerous occurrences, they contribute greatly to the marine calcareous flux and the deep-sea carbonate deposition (Schmidt et al., 2006).

About 50 extant morphospecies are known, which occur in five biogeographic zones: the polar, sub-polar, transitional, sub-tropical and tropical zone. The lowest diversity is exhibited in polar regions, while the highest is observed in the subtropics (Schiebel and Hemleben, 2017a). Within these zones, species are considered to be cosmopolitan, with the exception of three species (Kucera, 2007).

The numerous, worldwide occurrence since the Lower Cretaceous (Schiebel and Hemleben, 2017b) left an exceptional fossil record in marine areas of carbonate preservation. The evolution of species-specific morphological characteristics allows the identification on species level in case tests are well preserved (Bolli and Saunders, 1985). Thus, PF are ideal candidates for biostratigraphical studies, the investigation of palaeoenvironmental and oceanographic changes by stable isotopic measurements (e.g. Chaisson and Ravelo, 2000; Number, 2020) and faunal

composition (e.g. Wright and Thunell, 1988), and for evolutionary studies (e.g. Malmgren et al., 1983; Kucera and Malmgren, 1996; Pearson and Ezard, 2014; Knappertsbusch, 2007, 2016). The exceptional record of PF allows the investigation of temporal and spatial processes of speciation events. There are different concepts and models about mode and tempo of speciation, from which the most important will be introduced in the following sections.

1.1 Modes of speciation

Several hypotheses about the mode of evolution and speciation exist. They are based on the biological species concept and suggest that two populations are considered as different species, if interbreeding between the populations is not possible anymore due to genetic distinction.

Allopatric speciation suggests that the development of an extrinsic (external) barrier causes a physical isolation of two populations, which prohibits geneflow between them (Fig. 1.1 A). The geographical isolation has to maintain the genetically intrinsic isolation of the two populations until the two populations are no longer able to interbreed in case the barrier breaks.

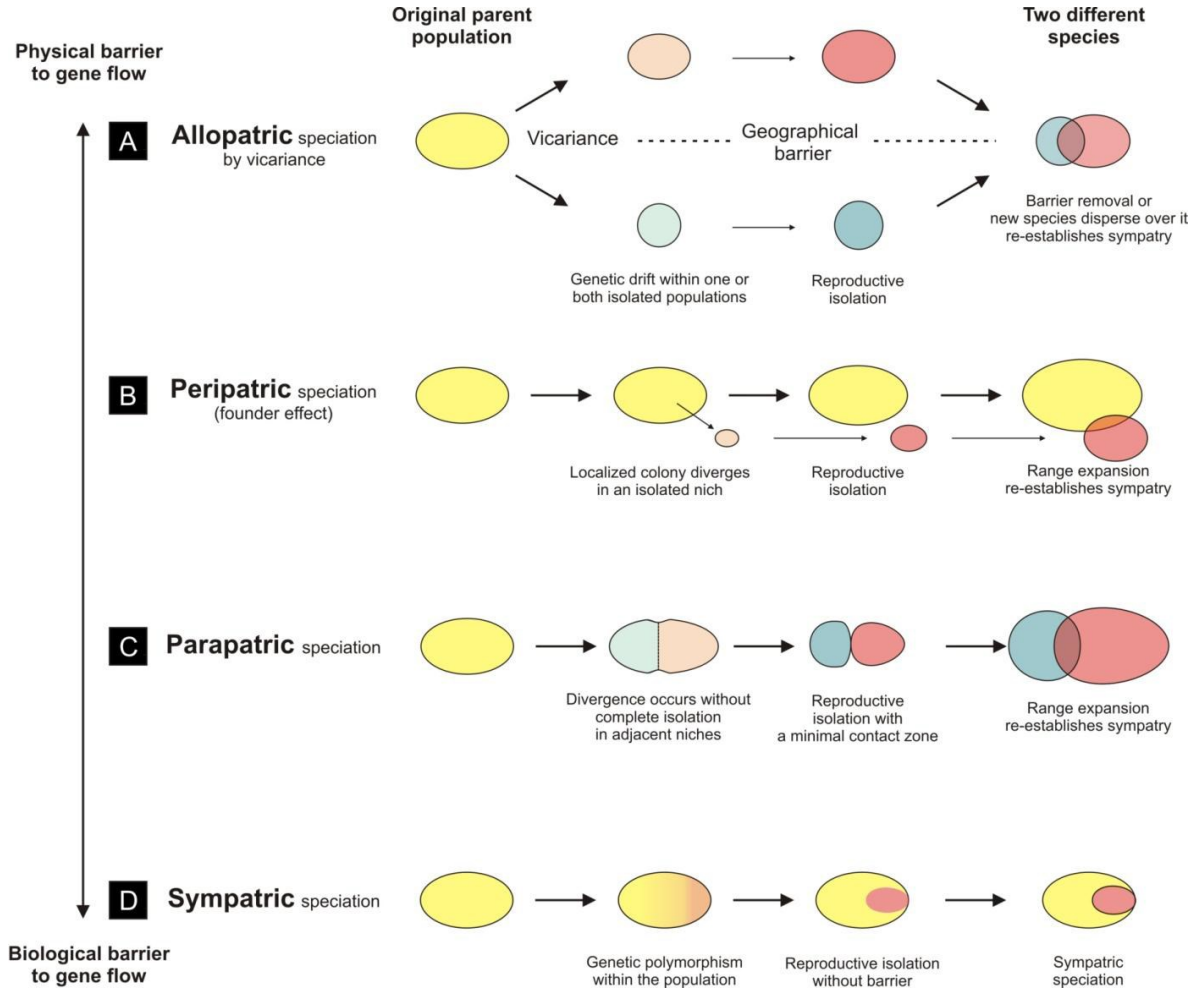

Figure 1.1: Scheme of the hypothesis about modes of evolution and speciation. **A**) Allopatric speciation. **B**) Peripatric speciation. **C**) Parapatric speciation. **D**) Sympatric speciation. Figure 1.1 in Mary (2013).

The peripatric speciation model (Fig. 1.1B) proposes that a small, peripheral population is isolated by an extrinsic barrier which causes an intrinsic isolation similar to the allopatric speciation.

In the parapatric speciation mode, the reproductive isolation is caused by the entrance of a population into a new niche or habitat, which is peripheral, but still attached to the parent species' niche or habitat (Fig. 1.1C). The shift in the niche or habitat occurs when the environment of the original species is drastically changed. Exchange of individuals between the populations and thus gene flow is not restricted by an extrinsic barrier, but by the chance of mating: the chance of an individual to mate with a geographic neighbour is higher than mating with a distant individuum of the population.

Speciation in the sympatric model is caused by a reproductive isolation due to genetic polymorphism within a population. The new species evolves in the same geographical region as its ancestor (Fig. 1.1D)

1.2 Models for the tempo of evolution and speciation

The fossil record allows to define different models for the tempo of evolution and speciation, for which Hohenegger (2014) provides an overview.

1.2.1 Phyletic gradualism (Simpson, 1944; Fig. 1.2a)

Phyletic gradualism proposes that the adaptive Zone 1, stable and occupied by species A, rapidly transforms into zones 2 and 3, which become stable again after the transition. The population of species A transforms within the new zones 2 and 3 towards the genotype, which is favourable for this zone. The adaptive zone is defined as the "complex of environmental conditions determining the type of adaptations of a given group of organisms" (Hohenegger, 2017).

1.2.2 Gradualistic speciation (Fig. 1.2b)

The adaptive zone inhabited by species 1 changes continuously, which triggers a steady transformation and adaptation of species A. When a new adaptive zone starts to develop, it causes a part of the population of species A to adapt to the new zone and evolves into species B. During diverging evolution, there is a time, in which the population still belongs to a single species, but is genetically already inhomogeneous.

1.2.3 Punctuated equilibrium (Eldredge & Gould, 1972; Fig. 1.2C)

Within a stable adaptive zone 1, occupied by species A, a new, stable adaptive zone B opens within a short geological time. A peripheral part of the population in the adaptive zone 2 is able to rapidly transform into a new species B, which has the preferred genotype for this zone.

1.2.4 Steady quantum speciation / Punctuated gradualism (Simpson, 1944; Malmgren et al., 1983; Fig. 1.2D)

A stable adaptive zone A abruptly collapses. During a, geologically short time interval at the end of the existence of adaptive zone A, the stable zone B appears. Both zones simultaneously coexist for a short time, during which a species A rapidly transforms into species B, which has the preferred genotype for this zone. With the end of zone 1, the mother species A becomes extinct.

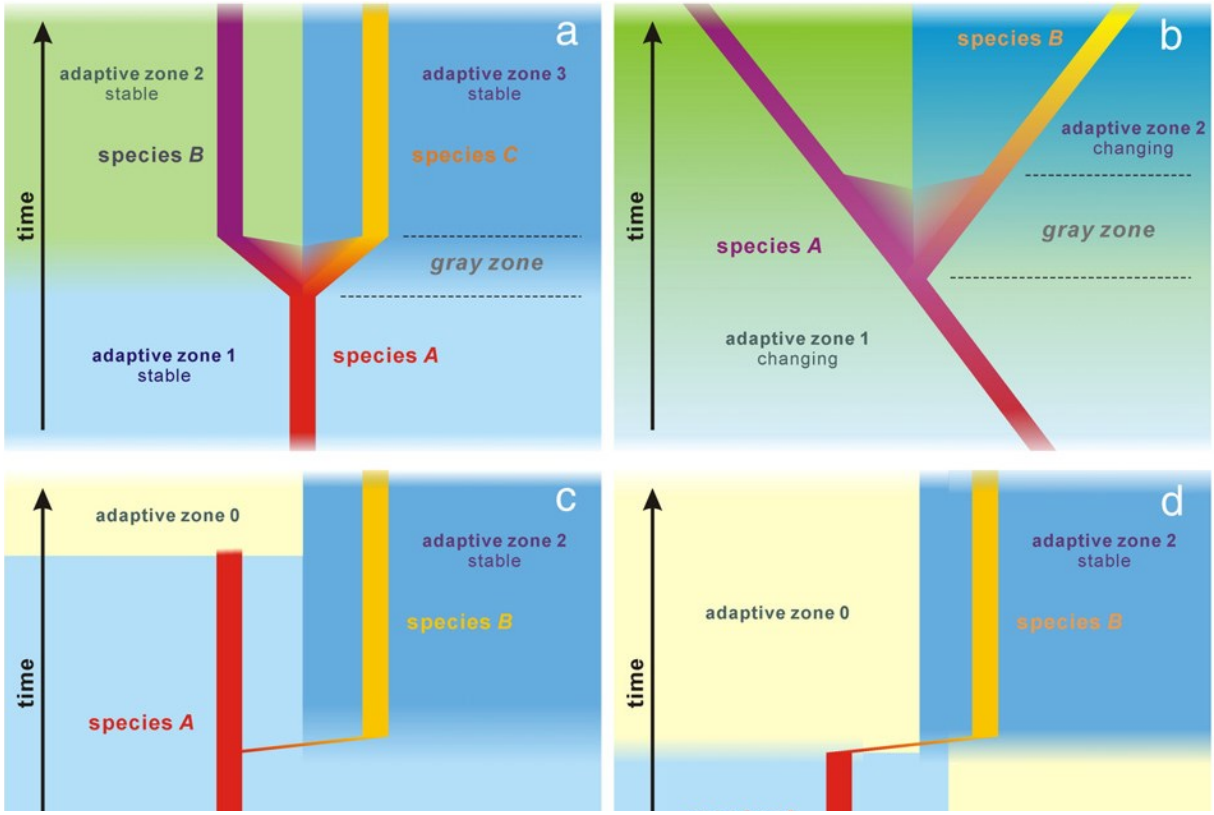

Figure 1.2: Hypotheses of models in evolution. **a**) Phyletic gradualism (Simpson, 1944). **b**) Gradualistic speciation. **c**) Punctuated equilibrium (Eldredge & Gould, 1972). **d**) Steady quantum speciation (Simpson, 1944) / Punctuated Gradualism (Malmgren et al., 1983). Grey Zone: within this transitional phase, genetical and/or morphological variation in species A increases. Specimens within a population still belong to species A, as they are able to interbreed with each other. (Hohenegger, 2014)

1.3 Challenges for evolutionary studies using the fossil record

Recognising the mode of speciation in the fossil record is often challenging. In palaeontology, species are the smallest unit, which can be recognised by their "characteristic, distinctive skeletal morphology, geographic distribution, and temporal range" (Lazarus, 1983). Molecular studies in recent PF revealed that morphospecies, which is a group of individuals that exhibit the same distinctive skeletal morphology, contain several different genotypes (e.g. de Vargas et al., 2001; Darling et al., 2007; Darling and Wade, 2008; Ujiié et al., 2010; Morard et al., 2011; Seears et al., 2012; André et al.., 2014). Those "cryptic species" often show distinct ecologies (e.g. Darling and Wade, 2008). However, molecular taxonomy is limited to recent organisms, so that species diversity in the fossil record can be underestimated: within the 50 extent morphospecies of PF, about 250 genotypes were discovered (Schiebel and Hemleben, 2017b). Contrary, molecular data revealed that morphologically distinct specimens, considered as distinct morphospecies, lack genetic differences (Ujiié et al., 2010; André et al., 2018). Those observations complicate the recognition of the underlying mode of a speciation event, as the actual speciation event stays undetected in the fossil record.

Determination of the tempo of speciation in the fossil record also remains a challenge. Speciation events following the different models can leave similar signals in the fossil record (Fig. 1.3). For example, the sudden occurrence of a new morphospecies in the fossil record of a specific area could fit the model of a punctuated evolutionary event, similar to punctuated equilibrium or quantum evolution. However, this pattern could also be caused by the dispersal of the new morphospecies from a distinct geographic area, which evolved in a gradual speciation event.

A field, which could benefit from evolutionary studies, is biostratigraphy. Biostratigraphy is the recognition and mapping of fossil units in rocks to be able to compare age and facies (environmental conditions during the time of sedimentation) of a formation (Ludvigsen, et al., 1986). Biostratigraphic data are often used to calibrate Age-Depth plots for bore holes. Due to the lack of spatial occurrence data, first and last occurrence dates of morphospecies are often assumed to be isochronal within an ocean basin (e.g. Berggren et al., 1995; Gradstein et al., 2012). However, this assumption can induce an error in the determination of a sediment sample, if a morphospecies shows diachronic occurrence or disappearance dates within an ocean basin (e.g. Weaver and Raymo, 1989; Spencer-Cervato and Thierstein, 2000; Knappertsbusch, 2007, 2016; Brombacher et al., 2021).

The collection of additional, spatial occurrence data through time could increase the precision of age determination based on biostratigraphic data.

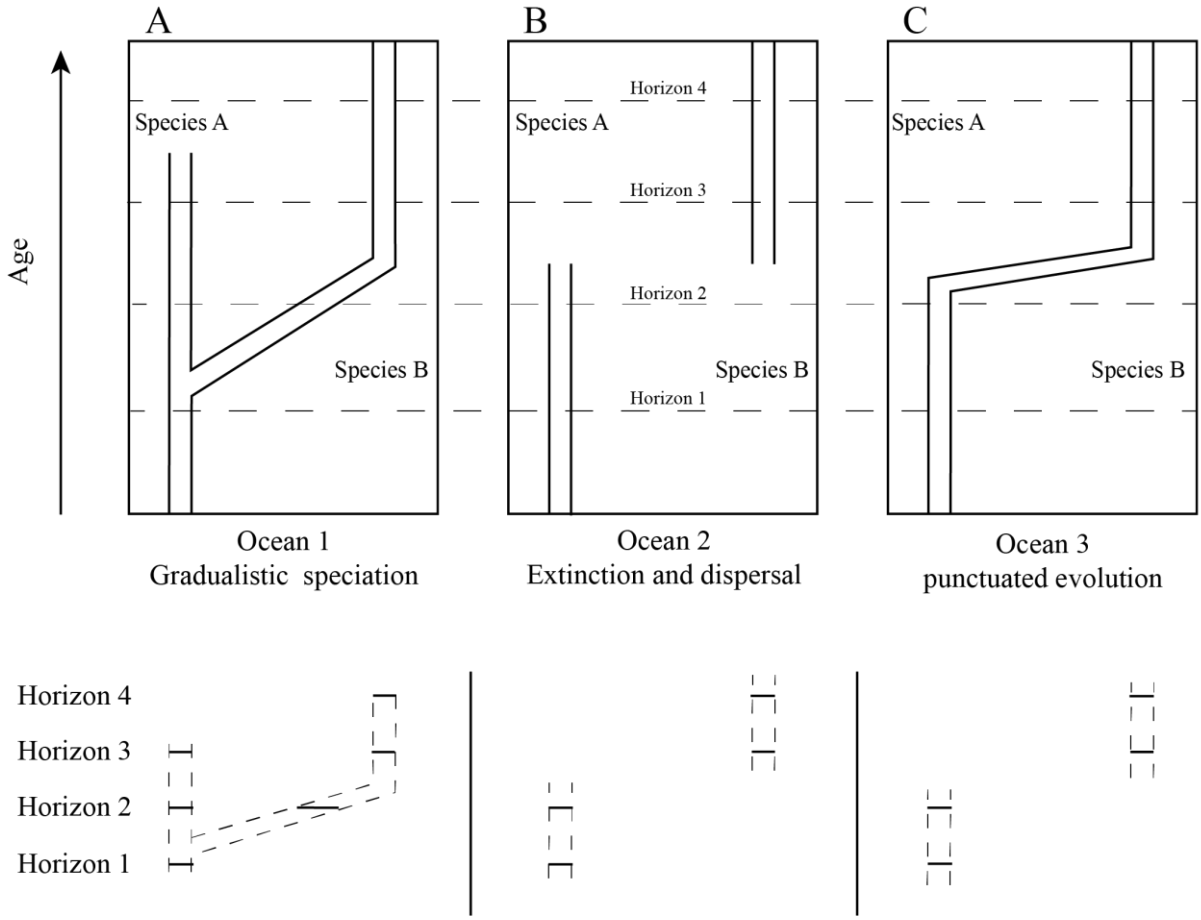

Figure 1.3: Example for different evolutionary processes at different locations and which pattern they leave in the fossil record. (**A**) In Ocean 1, species B evolves gradually from species A through time (cladogenesis). If the sediment record is investigated at the shown horizons 1 to 4, a transitional form between species A and B can be recognised in Horizon 2. (**B**) In Ocean 2, species A becomes extinct between horizon 2 and 3. Due to a dispersal event, species B occurs at the location. In the fossil record, species A disappears, and B occurs. (**C**) In Ocean 3, species B evolves from species A in a punctuated evolutionary event. In the fossil record, species B occurs while species A disappears between horizon 2 and 3. When comparing the fossil record of Ocean 2 and 3, the same pattern in the fossil record is observed. Thus, the processes involved in the evolution of species A and B cannot be reconstructed with data from one site but need further spatial investigation. This strategy of mapping morphological changes through time at different locations is called "Evolutionary prospection" (Knappertsbusch, 2011).

1.4 Thesis objectives

The main objective of this study is the investigation of the tempo and mode of evolution and their drivers of the pelagic planktonic foraminifer *Globorotalia menardii* since the late Miocene (8 Ma to present), by applying the strategy of evolutionary prospection. This strategy is defined as the systematical documentation of morphological trends through time at different localities of a species or a group of organisms (Knappertsbusch, 2011).

1.4.1 *Globorotalia menardii* and menardiform globorotaliids

Globorotalia menardii is a pelagic planktonic foraminifer which is known to dwell in the thermocline of the tropical and subtropical oceans (Caley et al., 2012; Schiebel and Hemleben, 2017b). Its test has a low trochospiral, large discoidal morphology with a narrow umbilical-extraumbilical aperture and the prominent keel is very characteristic. Those morphological characteristics make *G. menardii* easy to distinguish from other (extinct) foraminiferal species. The test is relatively resistant to (dis-)solution (Kucera, 2007) and its morphology allows a good orientation for morphometric measurements (Brown, 2007; Knappertsbusch 2007, 2016; Mary, 2013).

In the tropical zones of the world's oceans, this group shows a high abundance in the fossil record since the mid Miocene (Kennett and Srinivasan, 1983; Bolli and Saunders, 1985; Caley et al., 2012). The continuous fossil record of *G. menardii* allows to track its evolution in high resolution through time. The high number of fossil specimens enables a statistically significant determination of the species' morphological end members of populations through time.

The extant species *Globorotalia menardii* (Parker, Jones & Brady, 1865), after which this group of menardiform globorotaliids is named, is thought to be the ancestor of several species (e.g. Kennett and Srinivasan, 1983; Bolli and Saunders, 1985; Fig. 1.5), like *Globorotalia limbata* (Fornsanini, 1902) and *Globorotalia multicamerata* CUSHMAN & JARVIS, 1930. The evolution of closely related morphospecies can be directly observed and allows to investigate the tempo of inter- and intraspecific evolution as well as the mode of speciation.

1.4.2 Background and objectives of the study

The focus of this thesis is put on the investigation of evolutionary processes which are involved in a drastic increase in the test size of *G. menardii* in the Atlantic Ocean in the early Pleistocene: The maximum axial test length more than doubles from 500 µm at 2.3 Ma to 1150 µm at 1.95 Ma in the western tropical Atlantic Ocean (Knappertsbusch, 2016, Fig. 1.4C) and to 1300 µm at 1.7 Ma in the Caribbean Sea (Knappertsbusch, 2007; Fig. 1.4B).

As the observed maximum test size is a novelty for *G. menardii* populations in the Atlantic Ocean, this event was interpreted to mark the occurrence of a new, giant morphotype (Knappertsbusch, 2016). Specimens with a size of >1000 µm were previously observed in the eastern equatorial Pacific Ocean at 3.39 Ma (Knappertsbusch, 2007). However, as the giant morphotype was first observed in the Atlantic Ocean after the closure of the Panamanian Isthmus (O'Dea et al., 2016), it could not have derived from the eastern tropical Pacific Ocean.

Two hypotheses are considered to explain the rapid test-size increase observed in the fossil record in the tropical Atlantic Ocean: the Agulhas leakage hypothesis (chapter 1.4.3) and the hypothesis of a punctuated evolutionary event (chapter 1.4.4).

These hypotheses will be tested by comparing the morphological evolution of *G. menardii* in the Atlantic Ocean and the Indian Ocean during the past 8 Myr, following the strategy of evolutionary prospection. A previous occurrence of the giant type in the Indian Ocean in comparison to the Atlantic Ocean would corroborate the Agulhas leakage hypothesis, as the giant form could have been dispersed into the Atlantic Ocean. If the giant type is not observed in the Indian Ocean or shows a later occurrence compared to the Atlantic Ocean, it would rather support the idea of a punctuated evolutionary event.

The extensive dataset of morphometric measurements through time obtained by this dissertation will be used to search for further environmental processes and tectonic and palaeoceanographic drivers, which could have influenced the test-size evolution of menardiform globorotaliids. Between 8 Ma and ca. 2 Ma, the evolution exhibits different patterns in the Pacific Ocean (Fig. 1.4A), where a gradual test-size increase over time is observed, and the Atlantic Ocean (Fig. 1.4.B, C), in which time intervals of test size increase and decrease alternate.

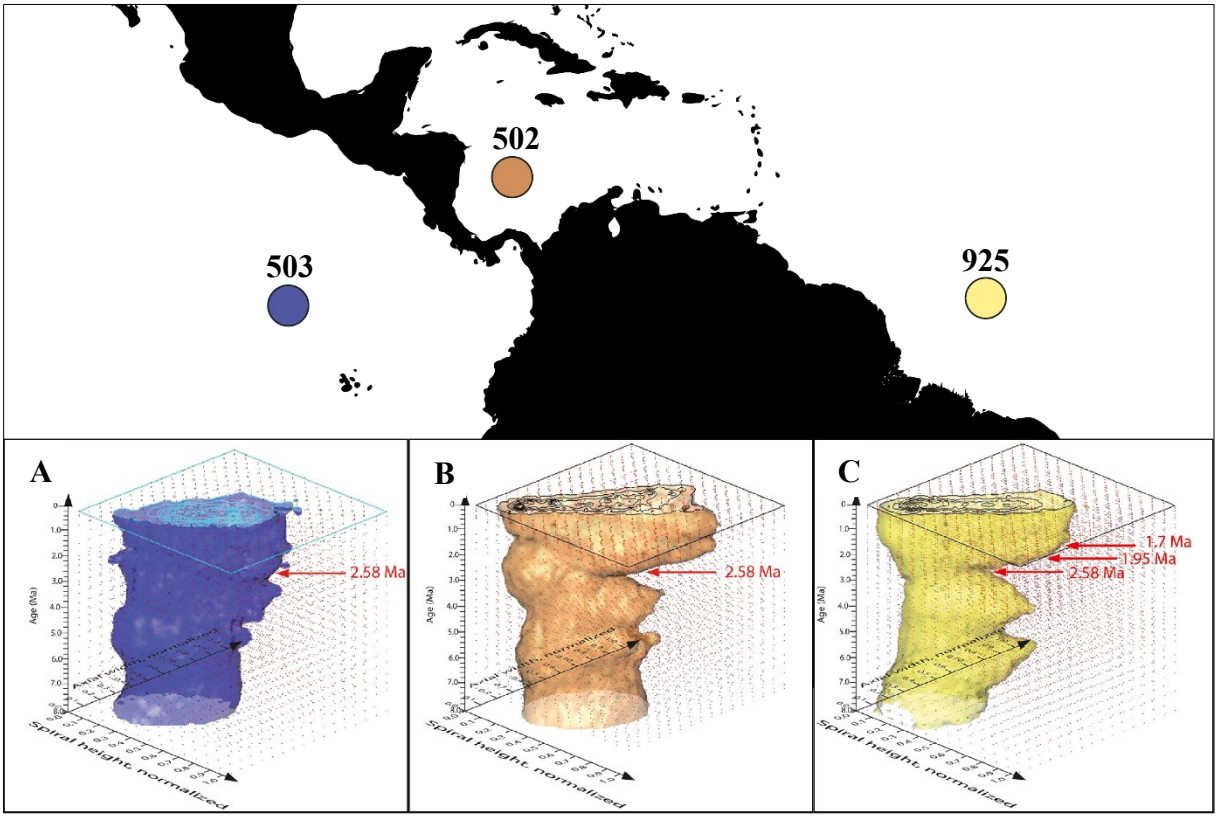

Figure 1.4: Test-size evolution of *G. menardii* at (**A**) the eastern tropical Pacific Ocean Site 503 (blue point), (**B**) the Caribbean Sea Site 502 (orange point) and (**C**) the western tropical Atlantic Ocean Site 925 (yellow point). The volume density diagrams (VDD) plot the normalised spiral height (x-axis) versus axial length (y-axis) and age (Ma). The VDDs images are taken from Knappertsbusch (2016).

Another objective is the observation of interspecific morphological trends within the *G. menardii-Globorotalia limbata-Globorotalia multicamerata* lineage. *Globorotalia limbata* and *G. multicamerata* are considered as descendants of *G. menardii* (e.g. Kennett and Srinivasan, 1983; Fig. 1.5). While *Globorotalia limbata* evolved in the late mid Miocene (Kennett and Srinivasan, 1983) and became extinct in the early Pleistocene (Wade et al., 2011), *Globorotalia multicamerata* occurred in the late Miocene (Kennett and Srinivasan, 1983) and became extinct in the Pliocene (Berggren et al., 1995).

The species of this lineage exhibit a high degree of morphological similarity (Knappertsbusch, 2007, 2016, 2022; Mary, 2013; Mary and Knappertsbusch, 2015). Adult specimens of *G. limbata* differ from *G. menardii* by an eponymous limbation of sutures of the chamber walls

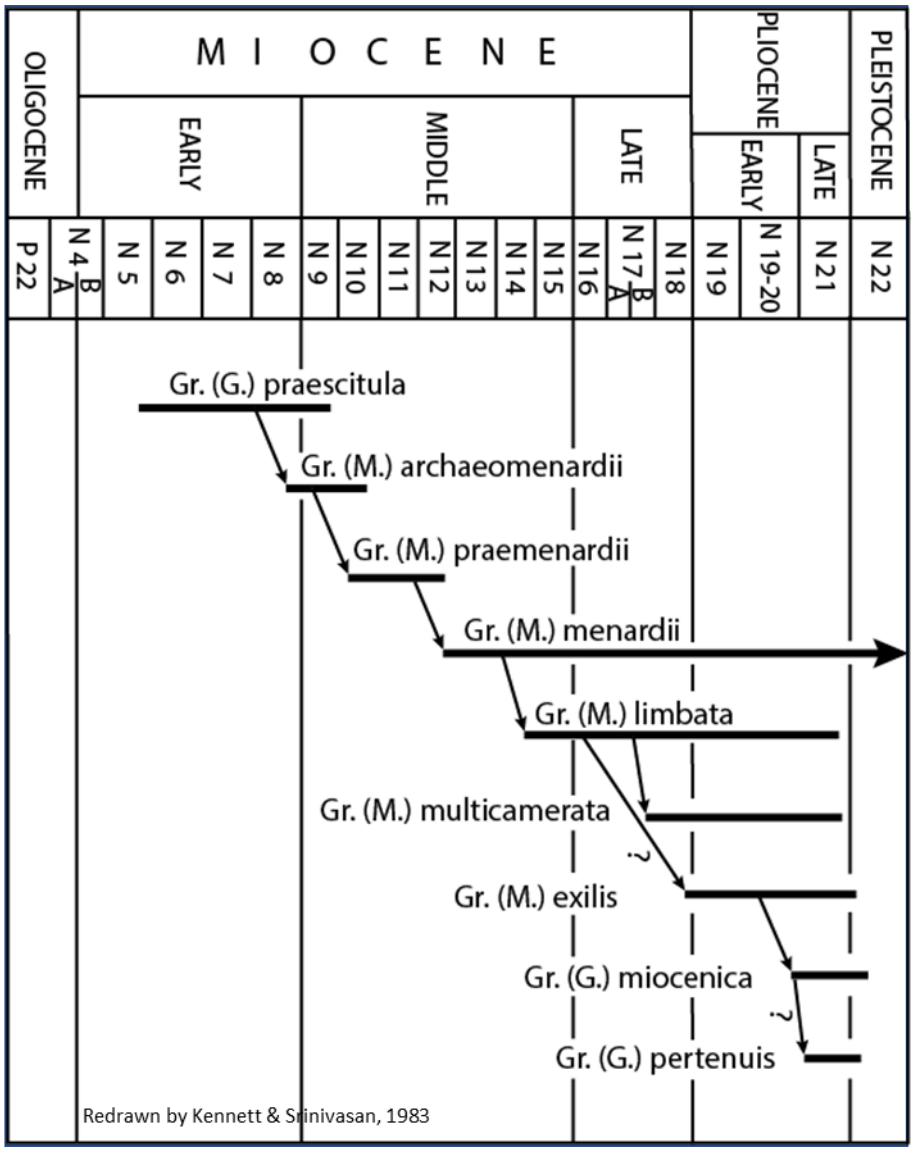

Figure 1.5: Systematic model of the phylogeny of menardiform globorotaliids by Kennett and Srinivasan (1983). Modified from Fig. 14 in Kennett and Srinivasan (1983).

on the spiral side. The number of chambers in the last whorl (6-8) is increased in comparison to *G. menardii*, which has up to 6 chambers (Kennett and Srinivasan, 1983).

Globorotalia multicamerata is distinguished from *G. menardii* and *G. limbata* by its higher number of chambers in the last whorl (8-10) and a wide, circular and deep umbilicus (Kennett and Srinivasan, 1983). Those criteria only account for adult specimens, although they do not seem to be sufficient, as, for example, the limbation of chamber sutures on the spiral side of *G. limbata* is also observed in extant *G. menardii* specimens (Knappertsbusch, personal communication; personal observation).

It will be investigated if interspecific trends in morphological characteristics indicate a continuous diverging trend through time between the three species after the morphotypes evolved. The observation of diverging trends would indicate that those morphotypes are different species and do not represent ecophenotypic variations of one species.

The identification of interspecific trends might also help to identify a morphological characteristic, which allows a distinct discrimination of adult and/or juvenile/neanic forms of the three species.

1.4.3 Agulhas leakage hypothesis

The Agulhas Leakage hypothesis proposes the dispersal of a giant *G. menardii* morphotype from the tropical Indian Ocean via the Agulhas Leakage into the tropical Atlantic Ocean during the early Pleistocene between 2.3 Ma and 1.95 Ma (Knappertsbusch, 2016).

The Agulhas leakage describes the separation of ring-shaped water masses from the Agulhas Current south of the tip of Africa at the retroflection point of the Agulhas Current (Biastoch et al., 2009; Beal et al., 2011; Laxenaire et al., 2018; Fig. 1.6). In this way, warm tropical Indian Ocean surface water is transported into the Atlantic Ocean, influencing the salt and heat budget of the Atlantic and thus the thermohaline circulation of the Atlantic (Beal et al., 2011). The giant eddies are also known to disperse tropical Indian Ocean biota into the Atlantic (Peeters et al., 2004; Caley et al., 2012; André et al., 2013; Villar et al., 2015). The Agulhas leakage system exists since at least 1.3 Ma (Caley et al., 2012).

1.4.4 Punctuated evolutionary event

The hypothesis of a punctuated evolutionary event proposes the regional and fast evolution of the giant type in the Atlantic Ocean between 2.3 Ma and 2 Ma in the early Pleistocene (Knappertsbusch, 2016; similar to the process shown in Fig. 1.3C), resembling the pattern known as punctuated equilibrium (Eldredge/Gould, 1972; Fig. 1.2c) or punctuated gradualism

(Malmgren et al., 1983; Fig. 1.2d). Several studies in different planktonic foraminiferal species (Malmgren et al., 1983; Hull and Norris, 2009; Pearson and Coxall, 2014; Bicknell et al., 2018) indicate that new morphospecies can evolve relatively fast within 44 kyr to 600 kyrs.

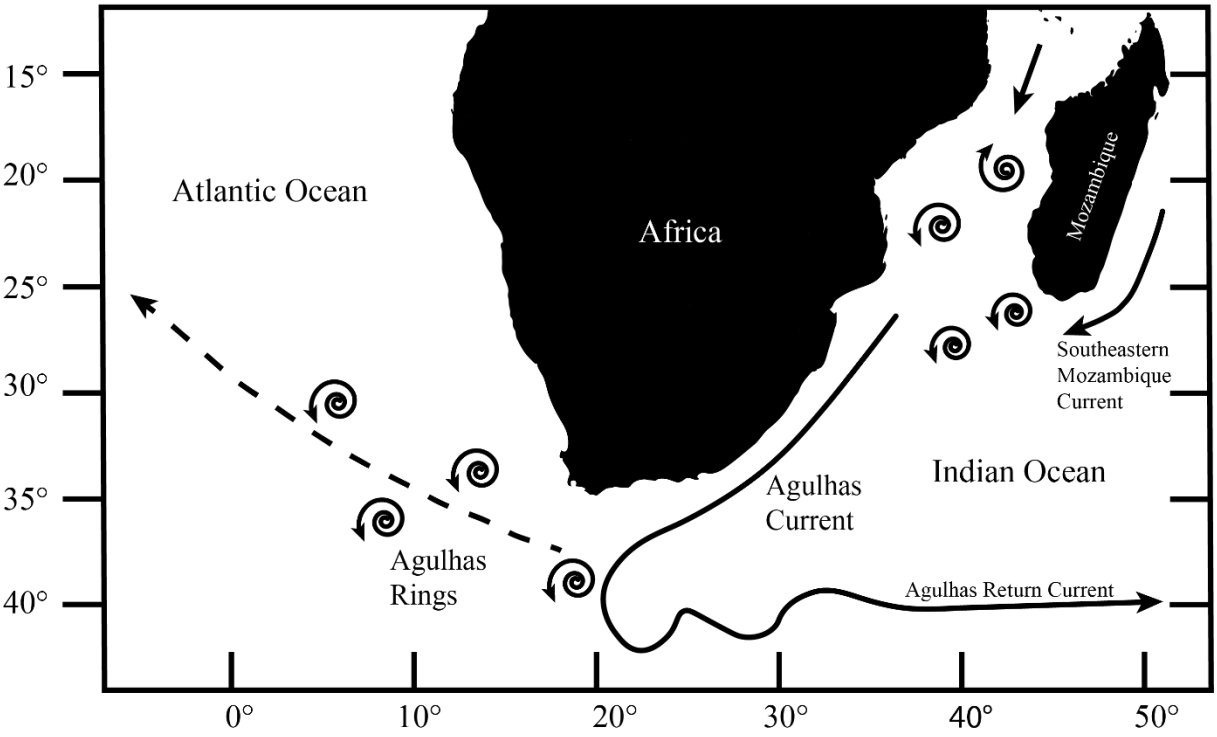

Figure 1.6: Oceanographic map of the southern Indian Ocean and South Atlantic Ocean in the area of southern Africa. The Agulhas current flows southwards along the south-eastern coast of Africa and transports tropical waters from the south-eastern Mozambique Current and from waters of the Mozambique Channel. At the southern tip of Africa, the Agulhas Current is retroflected back into the Indian Ocean as a result of meeting cooler South Atlantic water masses. Ring shaped water masses part from the Agulhas Current at the point of retroflection, which drift north-west wards into the Atlantic Ocean. This mechanism is called Agulhas leakage.

1.5 Methodology

A number of studies showed that separation of morphospecies in menardiform globorotaliids is possible by statistical analysis (Brown, 2007; Knappertsbusch, 2007, 2016, 2022; Mary, 2013). Quantitative measurements of morphological characteristics of a high quantity of individuals are used to show morphological variability and plasticity within the population of different menardiform globorotaliid species. The following approach is applied in this dissertation to identify speciation processes within the investigated population.

(1) Specimens in the periphery of the observed morphological variation are defined as end members or extreme forms. Identification of end members through time provides information about the evolution in the variance of a characteristic within a population. Temporal changes

in the variation of those morphological characteristics might be related to evolution of the gene pool. However, variability of morphological characteristics could also be related to changes in the environmental conditions within the actual range of the gene pool.

(2) Variability of a morphological characteristic in a population at a specific age can be illustrated in a diagram of frequency. By plotting the measured values against the number of individuals (Fig. 1.7A, C, E), the numerical range of the observed variability in the considered characteristic is shown and provides a quantification of the distribution, the frequency, of the measured values across the population. The distribution of a population belonging to a single species is considered to be unimodal (Peeters et al. 1999; Mary, 2013; Fig. 1.7A, B). Therefore, two or more modal centres in the distribution curve are indicative for the presence of two or several (sub)populations (Brown, 2007; Knappertsbusch, 2007, 2016, 2022; Mary, 2013; Mary and Knappertsbusch, 2015; Fig. 1.7C, D, E, F), probably indicating different morphospecies or an evolutionary splitting process within the observed population.

The combination of frequency plots of two measured morphological characteristics allows to assess the quantified distribution of the two investigated morphological characteristic in a two-dimensional manner (Fig. 1.7B, D, F). By stacking those frequency diagrams through time, potential temporal changes in the variability of the considered morphological characteristics and the number of modal centres can be studied (Fig. 1.7G). The detection of changes in the maximum variability range and in the modality (branching) can be indicative for evolutionary events or processes, such as cladogenesis (Knappertsbusch, 2016).

(3) A further approach to investigate tempo and mode of evolution in *G. menardii* is to analyse potential changes in the test form and shape by applying geometric morphometrics of outline coordinates. Form is defined as the combination of shape and size (Klingenberg, 2016), which includes the allometric signal. Allometry is the covariation of the shape and size (Klingenberg, 1996). As PF are known to change shape throughout ontogeny (Brown, 2007; Mary, 2013; Schmidt et al., 2013; Caromel et al., 2016; Knappertsbusch et al., 2016), evolution of form is expected to covary with the size evolution.

As the evolutionary component of the form and shape evolution is of interest, the dataset is corrected for size, i.e. the ontogenetic signal. Indicative for the occurrence of a new morphospecies would be a permanent change in the test shape.

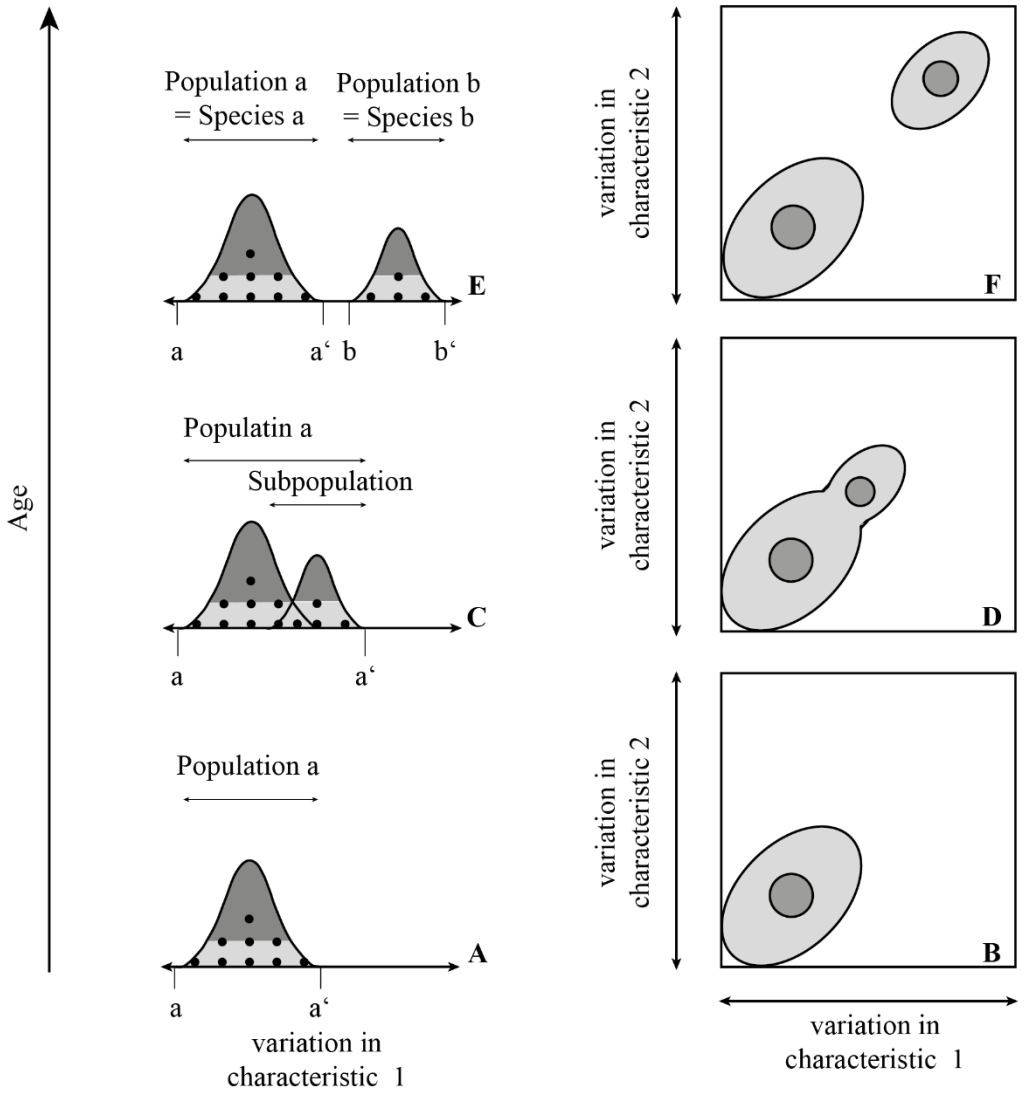
Age
Population a
= Species a
Population b
= Species b
E
a
a‘
b
b‘
Populatin a
Subpopulation
C
a
a‘
Population a
A
a
a‘
variation in
characteristic 1
variation in
characteristic 2
F
variation in
characteristic 2
D
variation in
characteristic 2
B
variation in
characteristic 1

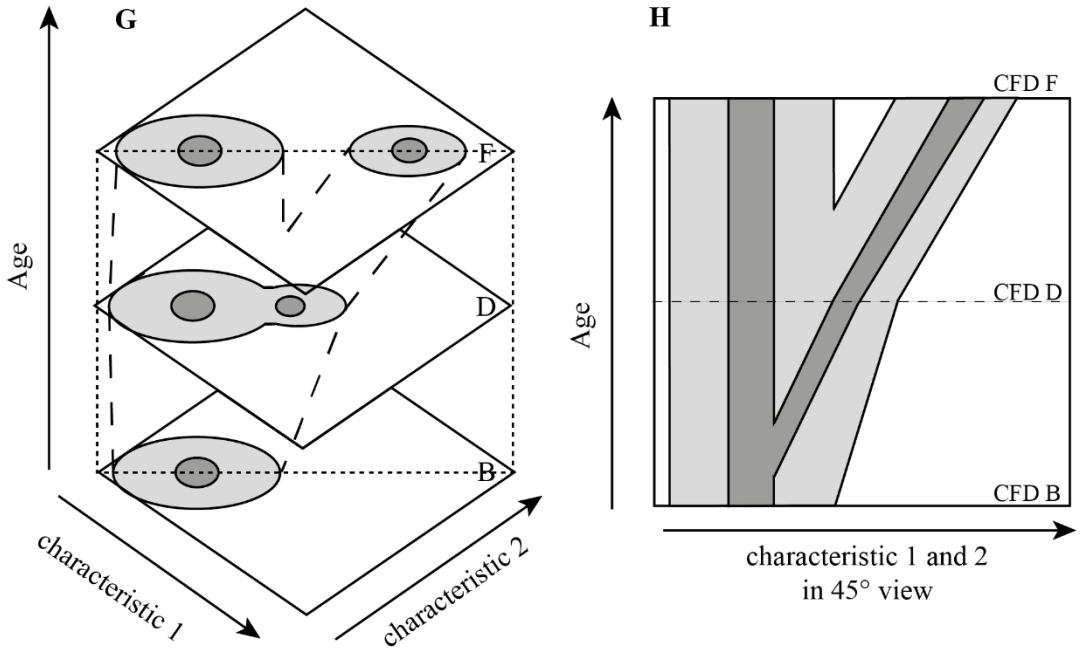
G
Age
F
D
B
characteristic 1
characteristic 2
H
CFD F
CFD D
CFD B
Age
characteristic 1 and 2
in 45° view

Figure 1.7: Methodological approach to investigate tempo and mode of evolution through time. In the first step (**A**, **C**, **E**), the observed variation of a characteristic 1 within the population a is plotted against the number of individuals, represented by dots. It allows to investigate the distribution of the individuals of a population across the observed variation, i.e. frequency. Changes in the number and position of the centres of frequency is indicative for morphological evolution, while the number of modal centres within a population is used to identify subpopulations. The presence of subpopulations might be indicative for a speciation process. Permanent changes in the observed variation, illustrated by the arrow above the curve, give evidence for genetic evolution. Rare specimens at the periphery, the "end members" (a, a', b, b'), allow the determination of the total variation within a population.
Plotting the frequency of characteristic 1 versus characteristic 2 and contouring the frequency allows to investigate variation of morphological characteristics in two dimensions (Fig. **B**, **D**, **F**). Those diagrams are called "contoured frequency diagram" (CFD). The stack of CFDs through time (Fig. **G**) illustrates changes in variation and evolution of modal centres through time. This diagram is a Volume Density Diagram (Knappertsbusch and Mary, 2012).(**H**): A vertical cross section though the stack (dotted line in Fig. **G**) facilitates the detection of continuous evolutionary trends in modal centres. They can form branches, which are indicative for the tempo and mode of evolution in the investigated morphospecies. The here shown example resembles a gradualistic speciation event.

Variation in test form and shape is investigated by applying a principal component analysis (PCA). A PCA is a mathematical algorithm which reduces the dimensionality of a dataset while it preserves most of the variation of the dataset (Ringnér, 2008).

1.6 AMOR

In this thesis, morphometric measurements of selected characteristics are based on images of menardiform globorotaliids. Those images were taken with the "Automated Measurment system for shell mORphology" (AMOR; Knappertsbusch et al., 2009; Knappertsbusch and Eisenecker, 2022; Fig. 1.8), which was realised by a cooperation between the Natural History Museum Basel and the Fachhochschule Nordwestschweiz (FHNW). The system was optimised for automatically orientating and imaging tests of menardiform globorotaliids in keel view and used in several studies (Knappertsbusch, 2016, 2022; Mary, 2013; Mary and Knappertbusch, 2013, 2015). It is also capable of orientating and imaging specimens from other, similar shaped PF like the *Truncorotalia* genus (Bicknell et al., 2018).

The AMOR system was constructed to facilitate the handling of large numbers of individuals, which are required to build up statistically significant datasets of morphometric measurements for studies applying the approach of evolutionary prospection project. The derived images show individual specimens in a homologous and standardised position, which maximises the comparability between each image as it minimises human error (Knappertsbusch et al., 2009).

The first system, AMOR 1, was realised in 2009 (Knappertsbusch et al., 2009; Fig. 1.8A). It is a modified and motorised Leica MZ6 standard microscope. The images of the specimens are taken with analogue 3CCD colour camera from Sony (DXP 390P). Test of specimens, which were previously mounted on P.A.S.I. Plummer cells in keel view, are placed on a motorised stage, which tilts and rotate the Plummer cell into a position, which represents the optimal test

orientation. The software version AMOR 3.28, which was used to image specimens of Hole 667A, was programmed in LabView 8.5 environment. Automatic orientation and imaging of a specimen takes ca. 4 minutes. The standard error for precision and repeatability was determined to be 0.233 % and 3.438 %, respectively.

System AMOR 2, which is also a modified and motorised Leica MZ6 standard microscope, is an improved version of the AMOR 1 system, which uses new hardware and improved software (Knappertsbusch and Eisenecker, 2022; Fig. 1.8B). New motor systems provide a smoother and more precise movement of the components. The analogue camera of AMOR system 1 was replaced by the digital camera KY-F75 from JVC, which needs no more frame grabber. Imaging of specimens from IODP Hole U1476A were made with the AMOR 2 system using the software AMOR 4.2, which was programmed in the commercial application LabView 14.

Intercalibration tests for precision and comparability between the AMOR 1 and AMOR 2 system showed a deviation of ±2.44 µm (0.69%) of mean radius R of specimen for the outline deviation and ±2.76 µm (average deviation of 0.79%) from the mean radius of the test specimen for repeatability (Knappertsbusch & Eisenecker, 2022).

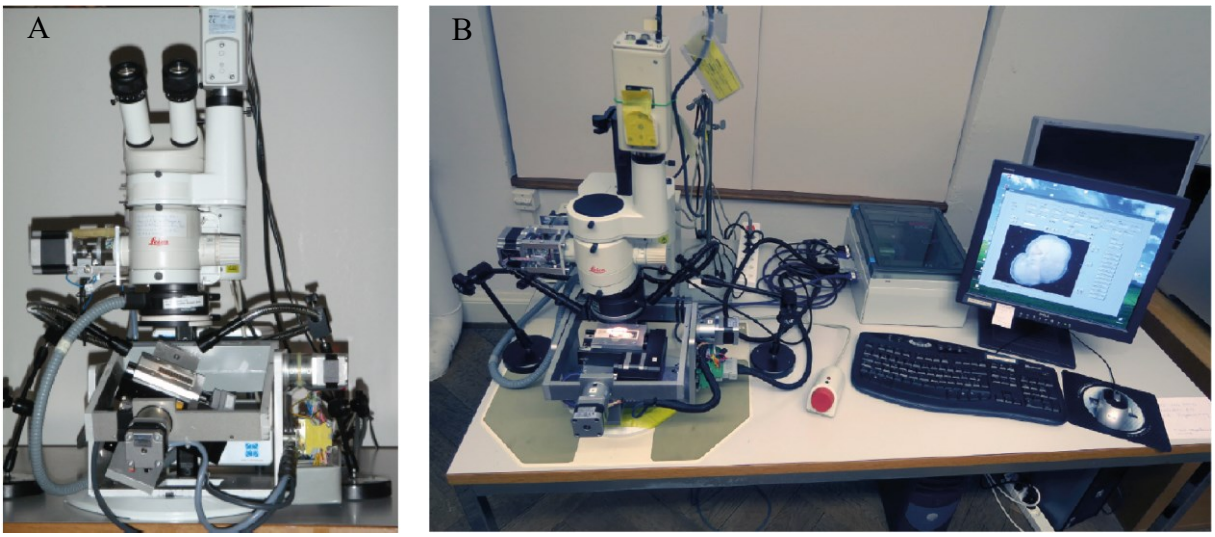

Figure 1.8: System AMOR 1 (**A**; image from Knappertsbusch et al., 2009) and System AMOR 2 (**B**; modified from Knappertsbusch & Eisenecker, 2022).

References

André, A., Weiner, A., Quillévéré, F., Aurahs, R., Morard, R., Douady, C. J., de Garidel-Thoron, T., Escarguel, G., de Vargas, C., and Kucera, M.: The cryptic and the apparent reversed: lack of genetic differentiation within the morphologically diverse plexus of the planktonic foraminifer Globigerinoides sacculifer, Paleobiology, 39, 21–39, https://doi.org/10.5061/dryad.rb06j, 2013.

Beal, L. M., De Ruijter, W. P. M., Biastoch, A., and Zahn, R.: On the role of the Agulhas system in ocean circulation and climate, Nature, 472, 429–436, https://doi.org/10.1038/nature09983, 2011.

Berggren, W. A., Kent, D. V., Swisher, C. C., and Aubry, M.-P.: Geochronology, time scales and global stratigraphic correlation, vol. 54, chap. A Revised Cenozoic Geochronology and Chronostratigraphy, pp. 129–212, SEPM (Society for Sedimentary Geology), https://doi.org/10.2110/pec.95.04.0129, 1995.

Biastoch, A., Böning, C. W., Schwarzkopf, F. U., and Lutjeharms, J. R. E.: Increase in Agulhas leakage due to poleward shift of Southern Hemisphere westerlies, Nature, 462, 495–498, https://doi.org/10.1038/nature08519, 2009.

Bicknell, R. D. C., Collins, K. S., Crundwell, M., Hannah, M., Crampton, J. S., and Campione, N. E.: Evolutionary Transition in the Late Neogene Planktonic Foraminiferal Genus Truncorotalia, iScience, https://doi.org/10.1016/ j.isci.2018.09.013, 2018.

Bolli, H. M. and Saunders, J. B.: Plankton Stratigraphy, vol. 1, chap. 6. Oligocene to Holocene low latitude planktic foraminifera, pp. 155–262, Cambridge University Press, 1985.

Brombacher, A., Wilson, P. A., Bailey, I., and Ezard, T. H. G.: The Dynamics of Diachronous Extinction Associated With Climatic Deterioration Near the Neogene/Quaternary Boundary, Paleoceanography and Paleoclimatology, 36, e2020PA004205, https://doi.org/10.1029/2020pa004205, 2021.

Brown, K. R.: Biogeographic and morphological variation in late Pleistocene to Holocene globorotalid foraminifera, PhD-Thesis, University of Basel, https://edoc.unibas.ch/780/, 2007.

Caley, T., Jiraudeau, J., Malaizé, B., Rossignol, L., and Pierre, C.: Agulhas leakage as a key process in the modes of Quaternary climate changes, PNAS, 109, 6835–6839, https://doi.org/10.1073/pnas.1115545109, 2012.

Caromel, A. G. M., Schmidt, D. N., Fletcher, I., and Rayfield, E. J.: Morphological Change During The Ontogeny Of The Planktic Foraminifera, Journal of Micropalaeontology, 35, 2–19, https://doi.org/10.1144/jmpaleo2014-017, 2016.

Chaisson, W. P. and Ravelo, A. C.: Pliocene development of the east-west hydrographic gradient in the equatorial Pacific, Paleoceanography and Paleoclimatology, 15, 497–505, https://doi.org/10.1029/1999PA000442, 2000.

Cushman, J. A. and Jarvis, P. W.: Miocene foraminifera from Buff Bay, Jamaica., Journal of Paleontology, 4, 353–368, https://www.jstor.org/stable/1298001, 1930.

Darling, K. F. and Wade, C. M.: The genetic diversity of planktic foraminifera and the global distribution of ribosomal RNA genotypes, Marine Micropaleontology, 67, 216–238, https://doi.org/10.1016/j.marmicro.2008.01.009, 2008.

Darling, K. F., Kucera, M., and Wade, C. M.: Global molecular phylogeography reveals persistent Arctic circumpolar isolation in a marine planktonic protist, Proceedings of the National Academy of Sciences, 104, 5002–5007, https://doi.org/10.1073/pnas.0700520104, 2007.

Darwin, C.: On the Origin of Species, 1859, Routledge, 1 edn., https://doi.org/10.4324/9780203509104, 2003.

de Vargas, C., Renaud, S., Hilbrecht, H., and Pawlowski, J.: Pleistocene adaptive radiation in Globorotalia truncatulinoides: genetic, morphologic, and environmental evidence, Paleobiology, 27, 104–125, https://doi.org/10.1666/0094-8373(2001)027<0104:parigt>2.0.co;2, 2001.

de Vargas, C., Sáez, A. G., Medlin, L. K., and Thierstein, H. R.: Super-Species in the calcareous plankton, in: Coccolithophores, edited by Thierstein, H. R. and Young, J. R., vol. 1, pp. 271–298, Springer, Berlin, Heidelberg, https://doi.org/10.1007/978-3-662-06278-4_11, 2004.

Eldredge, N. and Gould, S. J.: Puncutated equilibria: an alternative to phyletic gradualism, chap. Models of Paleobiology, pp. 82–115, Freeman Cooper and Company, https://doi.org/10.1515/9781400860296.193, 1972.

Fornasini, C.: Sinossi metodica dei foraminiferi sin qui rinvenuti nella sabbia del Lido di Rimini, Academia de la scienze di Bologna., pp. 1–68, 1902.

Gradstein, F. M., Ogg, J. G. Schmitz, M. D., and Hilgen, F. J.: The Geologic Time Scale 2012, 2-Volume Set, Elsevier LTD, Oxford, 2012.

Hohenegger, J.: Species as the basic units in evolution and biodiversity: Recognition of species in the Recent and geological past as exemplified by larger foraminifera, Gondwana Research, 25, 707–728, https://doi.org/10.1016/j.gr.2013.09.009, 2014.

Hull, P. M. and Norris, R. D.: Evidence for abrupt speciation in a classic case of gradual evolution, PNAS, 106, 21224–21229, https://doi.org/10.1073/pnas.0902887106, 2009.

Kennett, J. P. and Srinivasan, M. S.: Neogene planktonic foraminifera. A phylogenetic atlas, Hutchinson Ross Publishing Company, Stroudsburg, Pa. New York, NY, ISBN: 0879330708, 1983.

Klingenberg, C. P.: Multivariate Allometry, in: Advances in Morphometrics, pp. 23–49, Springer US, https://doi.org/10.1007/978-1-4757-9083-2_3, 1996.

Klingenberg, C. P.: Size, shape, and form: concepts of allometry in geometric morphometrics, Development Genes and Evolution, 226, 113–137, https://doi.org/10.1007/s00427-016-0539-2, 2016.

Knappertsbusch, M.: Morphological evolution of menardiform globorotalids at Western Pacific Warm Pool ODP Hole 806C (Ontong-Java Plateau) Evolution morphologique du groupe de Globorotalia menardii au Site ODP 806C (Ontong-Java Plateau, Pacifique tropical occidental), Revue de Micropaléontologie, 74, 100608, https://doi.org/10.1016/j.revmic.2022.100608, 2022.

Knappertsbusch, M. and Eisenecker, J.: Towards a Fleet of Robots for Orientation, Imaging, and Morphometric Analyses of Planktonic Foraminifera, Frontiers in Marine Science, 9, https://doi.org/10.3389/fmars.2022.798002, 2022.

Knappertsbusch, M. W.: Morphological variability of Globorotalia menardii (planktonic foraminifera) in two DSDP cores from the Caribbean Sea and the Eastern Equatorial Pacific, Carnets de Geologie, CG2007, 1–34, hal-00164930, 2007.

Knappertsbusch, M. W.: Evolution im marinen Plankton, Mitteilungen der Naturforschenden Gesellschaften beider Basel, pp. 3–14, https://doi.org/10.5169/seals-676589, 2011.

Knappertsbusch, M. W.: Evolutionary prospection in the Neogene planktic foraminifer Globorotalia menardii and related forms from ODP Hole 925B (Ceara Rise, western tropical Atlantic): evidence for gradual evolution superimposed by long distance dispersal?, Swiss Journal of Palaeontology, 135, 205–248, https://doi.org/10.1007/s13358-016-0113-6, 2016.

Knappertsbusch, M. W. and Mary, Y.: Mining morphological evolution in microfossils using volume density diagrams, Palaeontologica Electronica, 15, 1–29, https://doi.org/10.26879/278, 2012.

Knappertsbusch, M. W., Binggeli, D., Herzig, A., Schmutz, L., Stapfer, S., Schneider, C., Eisenecker, J., and Widmer, L.: AMOR – A NEW SYSTEM FOR AUTOMATED IMAGING OF MICROFOSSILS FOR MORPHOMETRIC ANALYSES, Palaeontologia Electronica, 12, http://palaeo-electronica.org/2009_2/165/index.html, 2009.

Kucera, M.: Proxies in Late Cenozoic Paleoceanography, vol. 1, chap. Chapter six planktonic foraminifera as tracers of past oceanic environments, pp. 213–262, Elsevier, https://doi.org/10.1016/S1572-5480(07)01011-1, 2007.

Kucera, M. and Malmgren, B. A.: Latitudinal variation in the planktic foraminifer Contusotruncana contusa in the terminal Cretaceous ocean, Marine Micropaleontology, 28, 31–52, https://doi.org/10.1016/0377-8398(95)00078-x, 1996.

Laxenaire, R., Speich, S., Blanke, B., Chaigneau, A., Pegliasco, C., and Stegner, A.: Anticyclonic Eddies Connecting the Western Boundaries of Indian and Atlantic Oceans, Journal of Geophysical Research: Oceans, 123, 7651–7677, https://doi.org/10.1029/2018JC014270, 2018.

Lazarus, D.: Speciation in pelagic Protista and its study in the planktonic microfossil record: a review, Paleobiology, 9, 327–340, https://doi.org/ 10.1017/s0094837300007806, 1983.

Ludvigsen, R., Westrop, S. R., Pratt, B. R., Tuffnell, P. A., and Young, G. A.: Paleoscene #3. Dual Biostratigraphy: Zones and biofacies, Geoscience Canada, 13, 139–154, https://-journals.lib.unb.ca/index.php/GC/article/view/3461, 1986.

Malmgren, B. A., Berggren, W. A., and Lohmann, G. P.: Evidence for punctuated gradualism in the Late Neogene Globorotalia tumida lineage of planktonic foraminifera, Paleobiology, 9, 377–389, https://doi.org/10.1017/s0094837300007843, 1983.

Mary, Y.: Morphologic, biogeographic and ontogenetic investigation of Mid-Pliocene menardellids (planktonic foraminifera), PhD Thesis, University of Basel, https://doi.org/10.5451/unibas-006194467, 2013.

Mary, Y. and Knappertsbusch, M. W.: Worldwide morphological variability in Mid-Pliocene menardellid globorotalids, Marine Micropaleontology, 121, 1–15, https://doi.org/10.1016/j.marmicro.2015.09.001, 2015.

Morard, R., Quill´ev´er´e, F., Douady, C. J., de Vargas, C., de Garidel-Thoron, T., and Escarguel, G.: Worldwide Genotyping in the Planktonic Foraminifer Globoconella inflata: Implications for Life History and Paleoceanography, PLoS, 6, https://doi.org/10.1371/journal.pone.0026665, 2011.

Nuber, S.: Atmospheric CO2 across the Plio-Pleistocene, PhD-Thesis, Cardiff University, http://orca.cf.ac.uk/134264/, 2020.

O'Dea, A., Lessios, H. A., Coates, A. G., Eytan, R. I., Restrepo-Moreno, S. A., Cione, A. L., Collins, L. S., de Queiroz, A., Farris, D. W., Norris, R. D., Stallard, R. F., Woodburne, M. O., Aguilera, O., Aubry, M.-P., Berggren, W. A., Budd, A. F., Cozzuol, M. A., Coppard, S. E., Duque-Caro, H., Finnegan, S., Gasparini, G. M., Grossman, E. L., Johnson, K. G.,

Keigwin, L. D., Knowlton, N., Leigh, E. G., Leonard-Pingel, J. S., Marko, P. B., Pyenson, N. D., Rachello-Dolmen, P. G., Soibelzon, E., Soibelzon, L., Todd, J. A., Vermeij, G. J., and Jackson, J. B. C.: Formation of the Isthmus of Panama, Science Advances, 2, https://doi.org/10.1126/sciadv.1600883, 2016.

Pearson, P. N. and Coxall, H. K.: Origin of the Eocene Planktonic Foraminifer Hantkenina by Gradual Evolution, Palaeontology, 57, 243–267, https://doi.org/10.1111/pala.12064, 2014.

Peeters, F., Ivanova, E., Conan, S., Brummer, G.-J., Ganssen, G., Troelstra, S., and van Hinte, J.: A size analysis of planktic foraminifera from the Arabian Sea, Marine Micropaleontology, 36, 31–63, https://doi.org/10.1016/s0377-8398(98)00026-7, 1999.

Peeters, F. J. C., Acheson, R., Brummer, G.-J. A., de Ruijter, W. P. M., Schneider, R. R., Ganssen, G. M., Ufkes, E., and Kroon, D.: Vigorous exchange between the Indian and Atlantic oceans at the end of the past five glacial periods, Nature, 430, 661–665, https://doi.org/10.1038/nature02785, 2004.

Ringnér, M.: What is principal component analysis?, Nature Biotechnology, 26, 303–304, https://doi.org/10.1038/nbt0308-303, 2008.

Schiebel, R. and Hemleben, C.: Ecology, in: Planktic Foraminifers in the Modern Ocean, chap. 7, pp. 209–230, Springer Berlin Heidelberg, https://doi.org/10.1007/978-3-662-50297-6_7, 2017a.

Schiebel, R. and Hemleben, C.: Introduction, in: Planktic Foraminifers in the Modern Ocean, chap. 1, pp. 1–9, Springer Berlin Heidelberg, https://doi.org/10.1007/978-3-662-50297-6_1, 2017b.

Schiebel, R. and Hemleben, C.: Classification and Taxonomy of Extant Planktic Foraminifers, in: Planktic Foraminifers in the Modern Ocean, chap. 2, pp. 11–110, Springer Berlin Heidelberg, https://doi.org/10.1007/978-3-662-50297-6_2, 2017c.

Schmidt, D. N., Lazarus, D., Young, J. R., and Kucera, M.: Biogeography and evolution of body size in marine plankton, Earth-Science Reviews, 78, 239–266, https://doi.org/10.1016/j.earscirev.2006.05.004, 2006.

Schmidt, D. N., Rayfield, E. J., Cocking, A., and Marone, F.: Linking evolution and development: Synchrotron Radiation Xray tomographic microscopy of planktic foraminifers, Palaeontology, 56, 741–749, https://doi.org/10.1111/pala.12013, 2013.

Seears, H. A., Darling, K. F., and Wade, C. M.: Ecological partitioning and diversity in tropical planktonic foraminifera, BMC Evolutionary Biology, 12, 54, https://doi.org/10.1186/1471-2148-12-54, 2012.

Simpson, G. G.: Tempo and Mode in Evolution, Columbia University Press, https://doi.org/10.7312/simp93040, 1944.

Spencer-Cervato, C. and Thierstein, H. R.: First appearance of Globorotalia truncatulinoides: cladogenesis and immigration, Marine Micropaleontology, 30, 267–291, https://doi.org/10.1016/s0377-8398(97)00004-2, 1997.

Ujiié, Y., de Garidel-Thoron, T., Watanabe, S., Wiebe, P., and de Vargas, C.: Coiling dimorphism within a genetic type of the planktonic foraminifer Globorotalia truncatulinoides, Marine Micropaleontology, 77, 145–153, https://doi.org/10.1016/j.marmicro.2010.09.001, 2010.

Villar, E., Farrant, G. K., Follows, M., Garczarek, L., Speich, S., Audic, S., Bittner, L., Blanke, B., Brum, J. R., Brunet, C., Casotti, R., Chase, A., Dolan, J. R., d'Ortenzio, F., Gattuso, J.-P., Grima, N., Guidi, L., Hill, C. N., Jahn, O., Jamet, J.-L., Le Goff, H., Lepoivre, C., Malviya, S., Pelletier, E., Romagnan, J.-B., Roux, S., Santini, S., Scalco, E., Schwenck, S. M., Tanaka, A., Testor, P., Vannier, T., Vincent, F., Zingone, A., Dimier, C., Picheral, M., Searson, S., Kandels-Lewis, S., Oceanscoordinators, T., Acinas, S. G., Bork, P., Boss, E., de Vargas, C., Gorsky, G., Ogata, H., Pesant, S., Sullivan, M. B., Sunagawa, S., Wincker, P., Karsenti, E., Bowler, C., Not, F., Hingamp, P., and Iudicone, D.: Environmental characteristics of Agulhas rings affect interocean plankton transport, Science, 348, 1261447, https://doi.org/10.1126/science.1261447, 2015.

Wade, B. S., Pearson, P. N., Berggren, W. A., and Pälike, H.: Review and revision of Cenozoic tropical planktonic foraminiferal biostratigraphy and calibration to the geomagnetic polarity and astronomical time scale, Earth-Science Reviews, 104, 111–142, https://doi.org/10.1016/j.earscirev.2010.09.003, 2011.

Weaver, P. P. E. and Raymo, M. E.: Late Miocene to Holocene planktonic foraminifers from the equatorial Atlantic, Leg 108, in: Proc. ODP, Sci. Results 108, edited by Baldauf, J., Heath, G. R., Ruddiman, W. F., and Sarnthein, M., vol. 108, chap. 5, pp. 71–91, College Station, TX (Ocean Drilling Program), https://doi.org/10.2973/odp.proc.sr.108.130.1989, 1989.

Wright, J. D. and Thunell, R. C.: Neogene Planktonic Foraminiferal Biogeography and Paleoceanography of the Indian Ocean, Micropaleontology, 34, 193, https://doi.org/10.2307/1485752, 1988.

Chapter 2: Test-size evolution of the planktonic foraminifer *Globorotalia menardii* in the eastern tropical Atlantic since the Late Miocene

Thore Friesenhagen[1,2]

[1]Natural History Museum Basel, Augustinergasse 2, 4001 Basel, Switzerland

[2] Department Umweltwissenschaften, University of Basel, Bernoullistrasse 32, CH-4056 Basel

This chapter is published as:

Friesenhagen, T.: Test-size evolution of the planktonic foraminifer *Globorotalia menardii* in the eastern tropical Atlantic since the Late Miocene, Biogeosciences, 19, 777–805, https://doi.org/10.5194/bg-19-777-2022, 2022.

Abstract

The mean test size of planktonic foraminifera (PF) is known to have increased especially during the last 12 Myr, probably in terms of an adaptive response to an intensification of the surface-water stratification. On geologically short timescales, the test size in PF is related to environmental conditions. In an optimal species-specific environment, individuals exhibit a greater maximum and average test size, while the size decreases the more unfavourable the environment becomes.

An interesting case was observed in the late Neogene and Quaternary size evolution of *Globorotalia menardii*, which seems to be too extreme to be only explained by changes in environmental conditions. In the western tropical Atlantic Ocean (WTAO) and the Caribbean Sea, the test size more than doubles from 2.6 Ma to 1.95 Ma and 1.7 Ma, respectively, following an almost uninterrupted and successive phase of test-size decrease from 4 Ma. Two hypotheses have been suggested to explain the sudden occurrence of a giant *G. menardii* form: it was triggered by either (1) a punctuated, regional evolutionary event or (2) the immigration of specimens from the Indian Ocean via the Agulhas Leakage.

Morphometric measurements of tests from sediment samples of the Ocean Drilling Program (ODP) Leg 108 Hole 667A in the eastern tropical Atlantic Ocean (ETAO) show that the giant type already appears 0.1 Myrs earlier at this location than in the WTAO, which indicates that the extreme size increase in the early Pleistocene was a tropical-Atlantic-Ocean-wide event. A coinciding change in the predominant coiling direction likely suggests that a new morphotype occurred. If the giant size and the uniform change in the predominant coiling direction are an indicator for this new type, the form already occurred in the eastern tropical Pacific Ocean at the Pliocene–Pleistocene boundary at 2.58 Ma. This finding supports the Agulhas leakage hypothesis. However, the hypothesis of a regional, punctuated evolutionary event cannot be dismissed due to missing data from the Indian Ocean.

This paper presents the Atlantic Meridional Overturning Circulation (AMOC) and thermocline hypothesis in the ETAO, which possibly can be extrapolated for explaining the test-size evolution of the whole tropical Atlantic Ocean and the Caribbean Sea for the time interval between 2 and 8 Ma. The test-size evolution shows a similar trend with indicators for changes in the AMOC strength. The mechanism behind this might be that changes in the AMOC strength have a major influence on the thermal stratification of the upper water column and hence the thermocline, which is known to be the habitat of *G. menardii*.

2.1 Introduction

While short-term changes in the size of planktonic foraminifera (PF) calcareous skeletons, so-called "tests", are thought to be related to changes in environmental conditions (Hecht, 1976; Ortiz et al., 1995; Schmidt et al., 2006; Woodhouse et al., 2021), macroevolutionary increase in the test size is primarily associated with evolutionary adaptation to new ecological niches, for example surface-water stratification (Schmidt et al., 2004; Wade et al., 2016).

Knappertsbusch (2007a; 2016) observed interesting long-term test-size evolution of PF in studies of the *G. menardii–G. limbata–G. multicamerata* lineage from the late Miocene until the present. His studies revealed a striking size increase in *G. menardii* in the tropical Atlantic Ocean and the Caribbean Sea in the early Pleistocene from 2.6 Ma to 1.95 Ma and 1.7 Ma, respectively. The size more than doubled within this time interval.

Although the maximum average test size of a species is reached in regions which provide optimal species-specific temperatures and salinities on geologically short time intervals (Hecht, 1976; Schmidt et al., 2004), this event seemed to be too pronounced and incisive to only be related to even a drastic improvement of environmental conditions. Therefore, Knappertsbusch argued that this relatively sudden and pronounced increase had been caused by the occurrence of a new giant *G. menardii* form in the Atlantic Ocean that may be passively entrained from the Indian Ocean, possibly via an intensified "palaeo- Agulhas" leakage after the onset of the Northern Hemisphere Glaciation (NHG). The Agulhas Leakage is mediated by the transport of ring-shaped water masses from the Indian Ocean into the Atlantic Ocean, which separates from the Agulhas Current at its retroflection point at the southernmost tip of Africa (Biastoch et al., 2009; Beal et al., 2011; Laxenaire et al., 2018). These Agulhas Rings are known to transport tropical Indian Ocean biota into the Atlantic Ocean (Norris, 1999; Caley et al., 2012; Villar et al., 2012). A similar mechanism has been proposed for the dispersal of giant menardiform specimens ca. 2 Myr ago (Knappertsbusch, 2016).

During the NHG, permanent ice sheets were established in the Northern Hemisphere. The NHG started ca. 2.7 Myr ago, intensified until 1.8 Ma, and has had a major influence on the global climate and environmental conditions (Raymo, 1994; Tiedemann et al., 1994). The closure of the Isthmus of Panama probably triggered and/or intensified the NHG (Haug and Tiedemann, 1998; Bartoli et al., 2005; O'Dea et al., 2016).

Punctuated gradualism (Malmgren et al., 1983), i.e. rapid test-size evolution, comes to mind as an alternative mechanism to explain the observed patterns. It proposes a regional in situ size evolution under changed niche, nutritional or growth conditions of *G. menardii* after the onset

of the NHG and a simultaneously rapid spread within the entire tropical to subtropical Atlantic Ocean.

The present study documents the associated morphological changes. Particularly, it investigates if the pronounced test-size increase in *G. menardii* observed in the Caribbean Sea (Knappertsbusch, 2007) and the western tropical Atlantic Ocean (WTAO; Knappertsbusch, 2016) in the early Pleistocene occurs also in the eastern tropical Atlantic Ocean (ETAO). It seeks new insight for the underlying evolutionary processes. The new data from the ETAO will be discussed against the background of the Agulhas leakage hypothesis and the punctuated gradualism hypothesis while acknowledging the fact that neither the location nor the sampling resolution can unequivocally prove the mentioned hypotheses. The data rather give evidence for the likelihood of these hypotheses by extending the morphological dataset of menardiform globorotallids.

This study follows the strategy of "evolutionary prospection" (Knappertsbusch, 2011). Here, the concept of evolutionary prospection is to map morphological variations of tests of the *G. menardii* lineage within its entire biogeographic range at several different localities through

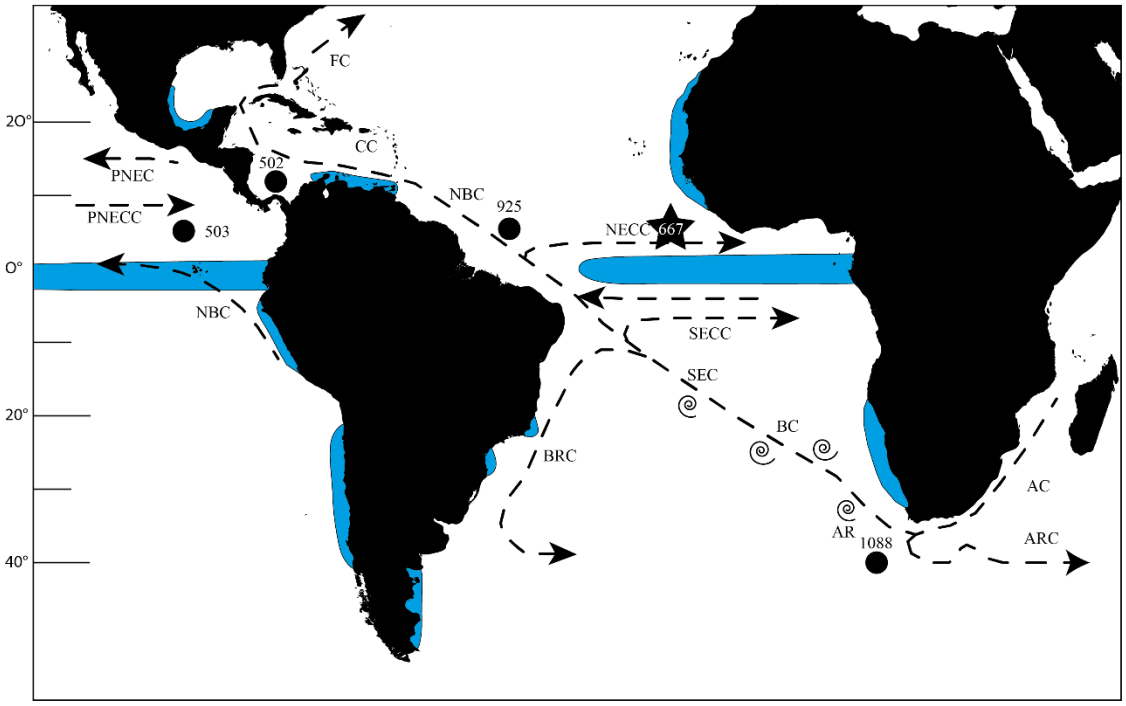

Figure 2.1: Map of the southern and tropical Atlantic Ocean showing the investigated and other important sites, as well as the most important currents. The star marks Site 667 and the black dots Sites 502, 503 and 925, which were investigated by Knappertsbusch (2007a; 2016), as well as ODP Site 1088, which was used by Dausmann et al. (2017) for a reconstruction of the AMOC strength using εNd isotopes. Blue areas show regions of upwelling (Shipboard Scientific Party, 1998; Shipboard Scientific Party, 2003; Merino and Monreal-Gómez, 2009; Clyde-Brockway, 2014; Pelegrí and Benazzouz, 2015; Kämpf and Chapman, 2016). Currents following Shipboard Scientific Party (1998). AC = Agulhas Current, AR = Agulhas Rings, ARC = Agulhas Return Current, BC = Benguela Current, BRC = Brazil Current, CC = Caribbean Current, FC = Florida Current, NBC = North Brazil Current, NECC = North Equatorial Counter Current, PNEC = Pacific North Equatorial Current, PNECC = Pacific North Equatorial Counter Current, SEC = South Equatorial Current, SECC = South Equatorial Counter Current

geological time. This global approach and increasing datasets of test-size measurements of menardiform globorotallids for the last 8 Myr hopefully allow us to disentangle and understand the evolutionary processes behind the observed pattern and general environmental processes influencing test-size evolution.

In this context, a new Atlantic Meridional Overturning Circulation (AMOC) and thermocline hypothesis is proposed, which may explain the evolutionary pattern of the size evolution in the tropical Atlantic during the time interval lasting from 8 Ma to 2 Ma.

2.2 Materials and methods

2.2.1 ODP Hole 667A

Ocean Drilling Program (ODP) Hole 667A was visited during Leg 108 and is located at the Sierra Leone Rise in the eastern equatorial Atlantic Ocean (4°34.15' N, 21°54.68' W; Fig. 2.1). Several characteristics qualify this site for being investigated in terms of the test-size increase event of *G. menardii* in the early Pleistocene:

(1) This area is located within tropical waters, the known habitat for *G. menardii* (Caley et al., 2012). Surface sediments show that *G. menardii* has a high Holocene occurrence at this site. Throughout the studied interval, sediments contain an adequate number of *G. menardii* and related forms (Manivit, 1989). The core location is outside or within the peripheral northwest African upwelling system (Fig. 2.1) and therefore, only marginally affected by the system for the investigated time interval of the last 8 Myr (Weaver and Raymo, 1989). Thus, there is a relatively long-term water-column stability on the geological timescale at ODP Site 667. (2) This area is within the range of water masses which are affected by the Agulhas leakage (Biastoch et al., 2009; Rühs et al., 2013), so that biota originating in the Indian Ocean are transported by currents up to this location. (3) The preservation of the fossils is good to moderate (Manivit, 1989). It is partly attributed to a sediment deposition depth (present:
3529.3 m water depth below sea level) above the carbonate compensation depth, i.e. the water depth in the ocean, at which the rate of calcium carbonate supply equals the rate of calcium carbonate dissolution and below which no calcite is preserved. (4) For the studied interval from 8 Ma until the present, sedimentation has most likely been continuous. The sediment sequence is only disturbed by a small slump (Shipboard Scientific Party, 1988), which was avoided for sampling.

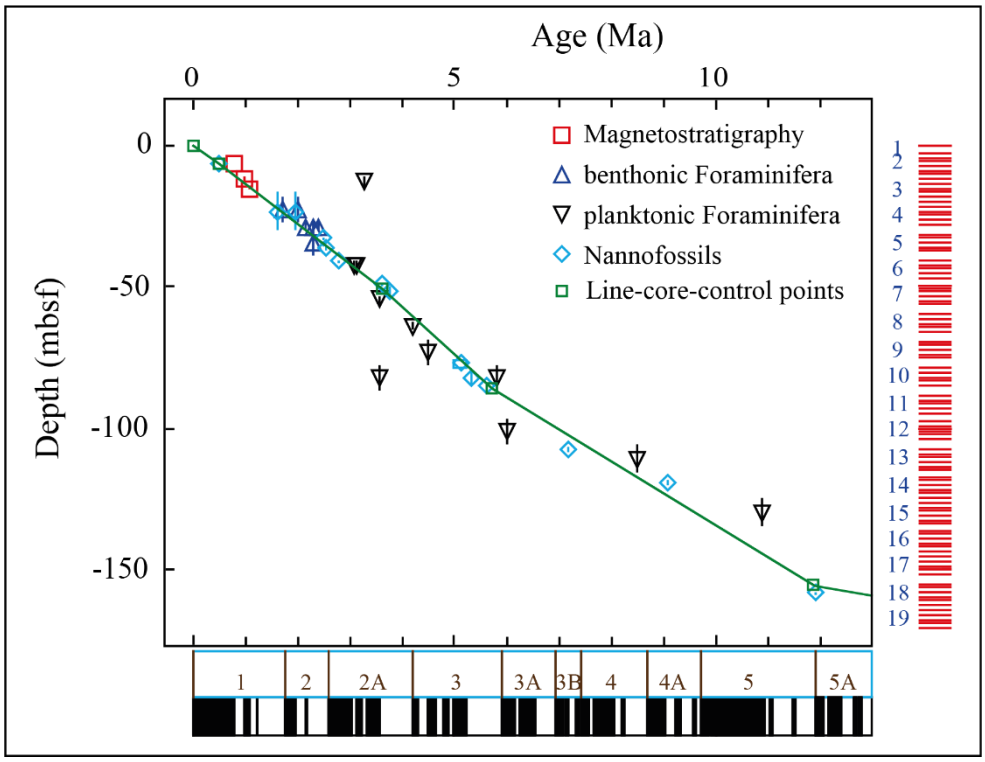

Figure 2.2: Age (Ma) versus depth (m.b.s.f. – metre below seafloor) plot for ODP Leg 108 Hole 667A, modified from Michael Knappertsbusch (personal communication, 2021). The green line represents the NEPTUNE Age Model. Biostratigraphic data were taken from Weaver et al. (1989) and from Weaver and Raymo (1989). Magnetostratigraphic data were taken from Shipboard Scientific Party (1988). The vertical bars within the symbols illustrate the depth range in which this event took place. The data for the palaeomagnetic reversals below the x axis are taken from Berggren et al. (1995). The red bars on the right side indicate cores and core recovery.

2.2.2 Sample selection

The samples were chosen from interglacial periods with a similar age as the investigated samples of the studies of Knappertsbusch (2007a; 2016) (Table 1). The working hypothesis presumes *G. menardii* to reach its maximum test size during interglacials, inferred from the observation of an overall decrease in population size or even complete absence during glacial intervals in the Atlantic Ocean (Ericson and Wollin, 1956; Sexton and Norris, 2011 and references therein; Portilho-Ramos er al., 2014).

Due to the lack of stable isotopic data for this site, the age–depth plot uses biostratigraphic data of PF and nannoplankton (Weaver and Raymo, 1989) as well as magnetostratigraphic events (Shipboard Scientific Party, 1988; Fig. 2.2). The "Age Depth Plot" program by Lazarus (1992) was used to manually draw a line of correlation (loc) through recognised bio- and magnetostratigraphic events (Fig. 2.2). Using the loc's control points numerical ages were computed by linear interpolation with the help of the "Age Maker" (Lazarus, 1992) (NEPTUNE Age Model; see supplementary materials file "667A.loc95.txt"). The age–depth plot is based

on published core-depth information from Hole 667A (Shipboard Scientific Party, 1988) and biostratigraphic occurrences of first and last occurrence dates of nannofossils, planktonic and benthonic foraminifera, and magnetostratigraphic polarity reversals given in the initial reports and scientific results of that leg. The time chronology of Berggren et al. (1995) was applied to allow direct comparison to previous studies of Knappertsbusch (2007; 2016).

2.2.3 Sample preparation and parameter measurement

The procedure for the treatment of the samples follows that of Knappertsbusch (2016). Approximately 2-3 cm^3 bulk sediment per sample were dried at 40°C over night and weighed. In a following step, the samples were gently boiled with water, containing soda as an additive, and wet-sieved with a 63 µm net. The fraction <63 µm was decanted, dried and preserved. The >63 µm fraction was dried at 40°C for 24 h and weighed afterwards. A microsplitter was used to split the >63 µm fraction until at least 200 menardiform specimens could be picked from the sample. This number of specimens was judged to be a reasonable compromise between efforts for picking and manual mounting, imaging, analytical and statistical steps and the limited amount of time for this project. The specimens were mounted on standard faunal Plummer cells from Prodotti e Apparecchiature Scienze e Industria (P.A.S.I.) srl in keel view. The preference was given to keel view because it allows a better orientation into (semi-) homologous positions than the umbilical or spiral views. In *G. menardii*'s sister lineage *Globorotalia tumida*, morphological variation in keel view has proven useful for the detection of evolutionary change (Malmgren et al., 1983). Intact specimens showing a menardiform morphology were picked from the sample splits. They include the whole *G. menardii* lineage as well as members of the *G. tumida* lineage. In total, 4482 *G. menardii*, 764 *G. limbata* and 228 *G. multicamerata* specimens were picked from samples at 33 stratigraphic levels back to 8 Ma (Table 1). All study material is stored in the collections of the Natural History Museum Basel.

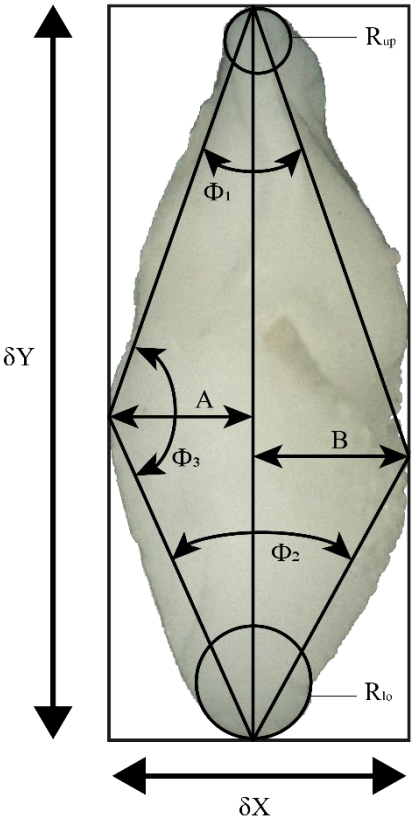

Figure 2.3: Investigated morphometric parameters. δX: spiral height; δY: axial length; Φ_1: upper keel angle; Φ_2: lower keel angle; Φ_3: angle at the apex; A: spiral convexity; B: umbilical convexity; R_{up}: radius of the osculating circle in upper keel region; R_{lo}: radius of the osculating circle in lower keel region.

Digital images of the menardiforms were collected with the Automated Measurement System for Shell Morphology

(AMOR), software version 3.28 (Knappertsbusch et al., 2009). This system automatically orientates and photographs tests in keel view to achieve orientation for outline analysis (Knappertsbusch et al., 2009). Repeated orientation tests with AMOR have shown that precision was 11.4 µm (3.2 % of mean radius of a specimen), when magnification was changing, and 6.7 µm (1.9 % of mean radius of the test) at constant magnification (MorphCol supplement #29 by Knappertsbusch, June 2021). In addition, the programme "AutoIt" (Mary, 2013) was used for an automated processing of the imaging. The free software ImageJ 1.52i of the National Institute of Health was used to clean and pre-process images for outline coordinate extraction. Processing steps include removal of adhering particles, smoothing, enhancement of contrast, binarization and closing of single pixel embayments before storing the processed pictures as 640 x 480 pixel and 8 bit grey-level Tiff files. Adapted MorphCol software programmed in Fortran 77 from Absoft by Knappertsbusch (2007a; 2016) were used (Appendix Fig. A2.1) to extract cartesian outline coordinates and to derive morphometric measurements. These applications were converted to Fortran 95 versions and adapted for usage on Windows operating systems. The adapted MorphCol programmes and codes are deposited on the internal media server of the Natural History Museum Basel and will also be available on the PANGAEA repository.

These programmes considerably accelerate the process of measuring several different morphometric parameters from the images. Derived parameters include the spiral height (δX) and the axial length (δY), the aspect ratio (R = δX / δY), the area of the specimen in keel view (Ar), the convexities of the spiral (A) and the umbilical (B) side, the ratio of the convexities ($R_{A/B}$), the upper (Φ_1) and the lower (Φ_2) keel angles, the angle at the apex (Φ_3), and the radii of the osculating circles in the upper (R_{up}) and the lower (R_{lo}) keel regions (see Fig 2.3). This study focuses on the test-size parameter δX, δY and Ar. In order to compare specimens with dextral and sinistral coiling, dextral specimens were vertically mirrored using the adapted "DexFlip_win" programme, modified from Knappertsbusch (2016).

2.2.4 *Globorotalia menardii* lineage–species discrimination

The identification on species level of picked menardiform specimens is based on illustrations in Kennett and Srinivasan (1983) and Bolli et al. (1985), as well as comparison with the reference collection to "49 Cenozoic planktonic foraminiferal zones and subzones prepared by Bolli in 1985 – 1987", which is deposited at the Natural History Museum Basel. This includes the species *G. menardii, Globorotalia limbata, Globorotalia multicamerata, Globorotalia exilis*, *Globorotalia pertenuis*, *Globorotalia miocenica*, *Globorotalia pseudomiocenica*,

Globorotalia tumida, *Globorotalia merotumida*, *Globorotalia plesiotumida* and *Globorotalia ungulata*. Diagnostic features included the size, the outer wall structure (shiny surface due to finer perforation), number of chambers in the last whorl and the δX and δY ratio. After species determination, forms like *G. exilis*, *G. pertenuis*, *G. miocenica*, *G. pseudomiocenica* and the *G. tumida* group, as well as the *G. menardii* subspecies *G. m. cultrata* and *G. m. fimbriata*, *G. m. gibberula* and *G. m. neoflexuosa*, were sorted out and not included in the present morphometric study. Thus, the dataset presented herein only contains specimens of *G. menardii menardii* (in the following referred to as *G. menardii*), *G. limbata* and *G. multicamerata*.

Globorotalia menardii is discriminated from its extinct descendants *G. limbata* and *G. multicamerata* by the number of chambers in the last whorl (Fig. 2.4). This pragmatic approach was applied because the apparently most distinctive morphological character of *G. limbata*, its limbation of the chamber sutures on the spiral side (Kennett and Srinivasan, 1983), is difficult to recognise and is also observed in *G. menardii* and *G. multicamerata* (Knappertsbusch, personal communication; personal observation). In order to solidify a possible cladogenetic pattern between *G. menardii* and *G. limbata*, the present study experimented with the pragmatic discrimination that *G. limbata,* which became extinct during the early Pleistocene at 2.39 Ma (Wade et al., 2011), has only seven chambers in its last whorl. Menardiform specimens with six or fewer chambers were determined as *G. menardii*. *Globorotalia multicamerata* has more than seven

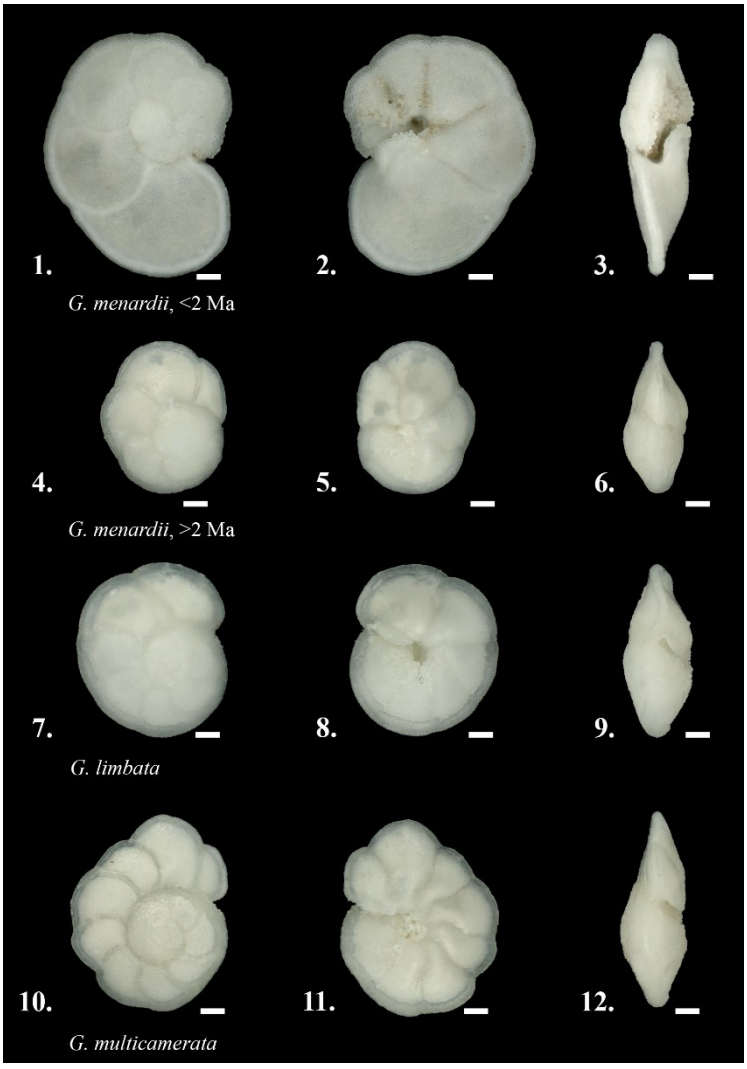

Figure 2.4: The investigated species in spiral, umbilical and keel view. 1–3: *Globorotalia menardii*, typically found during the past 2 Myr in the Atlantic Ocean, sample 667A-1H-1, 3–4cm, specimen 667011004aK2501. 4–6: *Globorotalia menardii*, preferentially found in samples older than 2 Ma, sample 667A-6H-4, 113–114cm, specimen 667064114bK0301. 7–9: *Globorotalia limbata*, sample 667A-6H-4, 113–114cm, specimen 667064114aK5701. 10-12: *Globorotalia multicamerata*, sample 667A-6H-4, 113–114cm, specimen 667064114aK5201. Scale bar: 100 µm. Images were produced with Keyence VHX-6000 microscope.

chambers in its last whorl and became extinct in the Pliocene at 3.09 Ma (Berggren et al., 1995). Knappertsbusch (2016) refers to the disappearance of *G. limbata* as a possible pseudoextinction because of the sporadic occurrence of specimens of menardiforms with seven chambers in the last whorl after 2.39 Ma.

2.2.5 Univariate and contoured frequency diagrams

Statistical analysis and univariate parameter-versus-age plots were prepared with RStudio (V. 3.5.3; RStudio Team, 2020), using the packages psych (Revelle, 2018), readxl (Wickham and Bryan, 2019), ggplot2 (Wickham, 2016), pacman (Rinker and Kurkiewicz, 2018) and rio (Chan et al., 2018). For the generation of contour frequency diagrams (CFDs) the commercial software applications Origin 2018 and Origin 2019 by OriginLab Corporation were used. CFDs per species help to detect shifts in the dominant test size of populations throughout time. The same method was applied in Knappertsbusch (2007a; 2016) and enables a direct comparison of evolutionary change in Hole 667A with previous studies. Emergence and divergence of new frequency peaks between subsequent samples may help to empirically identify signs of cladogenetic splitting or anagenetic evolution in the lineage of *G. menardii–G. limbata–G. multicamerata*. The CFDs were constructed from so-called "gridded files", obtained by plotting δX versus δY, superposing a grid with grid-cell sizes of ΔX = 50 µm and ΔY = 100 µm (see Knappertsbusch 2007a; 2016) and then counting the number of specimens per grid cell. This gridding procedure was performed with programme "Grid2.2_win" (adapted MorphCol software by Knappertsbsuch, 2007; 2016), and the result was a two-dimensional matrix of absolute frequencies of specimens per grid cell. No smoothing of frequencies was applied, because experiments revealed an increasing loss of frequency variation with increasing size of bin width. However, in contrast to Knappertsbusch and Mary (2012) and Knappertsbusch (2016), local absolute specimen frequencies were used throughout instead of relative frequencies.

Different contour intervals were used for the CFDs, because the number of *G. menardii* specimens per sample varies from 1 (667A-5H-2, 105–106 cm) to 273 (667A-4H-3, 120–121 cm). This approach increases the legibility of the single CFDs because setting a high contour interval in a sample with few specimens would have levelled out the CFD. Conversely, choosing a low contour interval would lead to exaggerated contour line densities in CFDs when the number of specimens is high.

2.2.6 Volume Density Diagrams

Volume density diagrams (VDDs) were made with the commercial software Voxler 4 by Golden Software. This method was shown to be useful to illustrate and visualise evolutionary tendencies in coccolithophores, but also in menardiform globorotallids (Knappertsbusch and Mary, 2012). Conceptually, they are constructed by stacking the contour frequency diagrams from different time levels. In this way, the grid cells of plane bivariate contour frequency diagrams expand to include time as the third dimension, e.g. spiral height, axial length and time. The local frequency is the fourth dimension (F). In this manner, a four-dimensional unit (X, Y, time, F) called "voxel" is generated. The component F of a voxel (local frequency) can then be represented as the iso-surface, which is done using Voxler. In other words, the iso-surface of the VDD represents the distribution of a constant local frequency through time (Knappertsbusch, 2016). High iso-values form the core of a VDD and represent abundant specimens. They allow the main evolutionary path through time to be investigated. Low iso-values illustrate rare specimens and show the extremes of test size. They are often related to innovation caused by evolution or represent extreme forms introduced by dispersal.

The protocol for constructing a VDD developed by Knappertsbusch (2007a; 2016) and Knappertsbusch and Mary (2012) was modified to improve the level of coincidence between the plane CFDs and VDDs. The most important changes concern (1) the usage of absolute instead of normalised frequencies in the input files, (2) a different set-up in the gridder option and (3) the modification of the iso-value. A detailed list of the adjustments used is given in the supplementary material (File "VDD_set-ups.txt").

The commercial software PDF3D ReportGen by Visual Technology Services Ltd was used to create the three-dimensional model from the Open Inventor (.iv) file format of a VDD when exported from Voxler.

2.3 Results

In a first step of analysis, the test-size evolution of *G. menardii* at Hole 667A was investigated by plotting δX and δY versus the age. This is the simplest analysis for evolutionary change and allows a direct comparison with previous data from Knappertsbusch (2007a; 2016). At Hole 667A, this test-size variation shows different phases of evolution through time: these two parameters serve as a primary measure for the intraspecific variability in the *G. menardii* lineage.

2.3.1 Morphological parameters through time

The comparison of the test size of *G. menardii* during times of co-occurrence with its sister taxa *G. limbata* and *G. multicamerata* and the size after the extinction of *G. limbata* and *G. multicamerata* may give evidence about possible shifts in the ecology of *G. menardii*. Major changes in the size of *G. menardii* before and after the extinction of its sister taxa probably point to an adaption to a different, new niche, e.g. in terms of "incumbency replacement" (Rosenzweig and McCord, 1991). Between 7.96 and 2.58 Ma, the evolution of δX in *G. menardii* shows three peaks at 7.11 Ma, 5.78 Ma and 3.99 Ma in the mean and median values (Fig. 2.5). Except for the sample 667A-10H-1, 97–98 cm at 5.26 Ma, at which the maximum size of *G. menardii* does not decrease as the mean and median do, the maxima of δX follow the

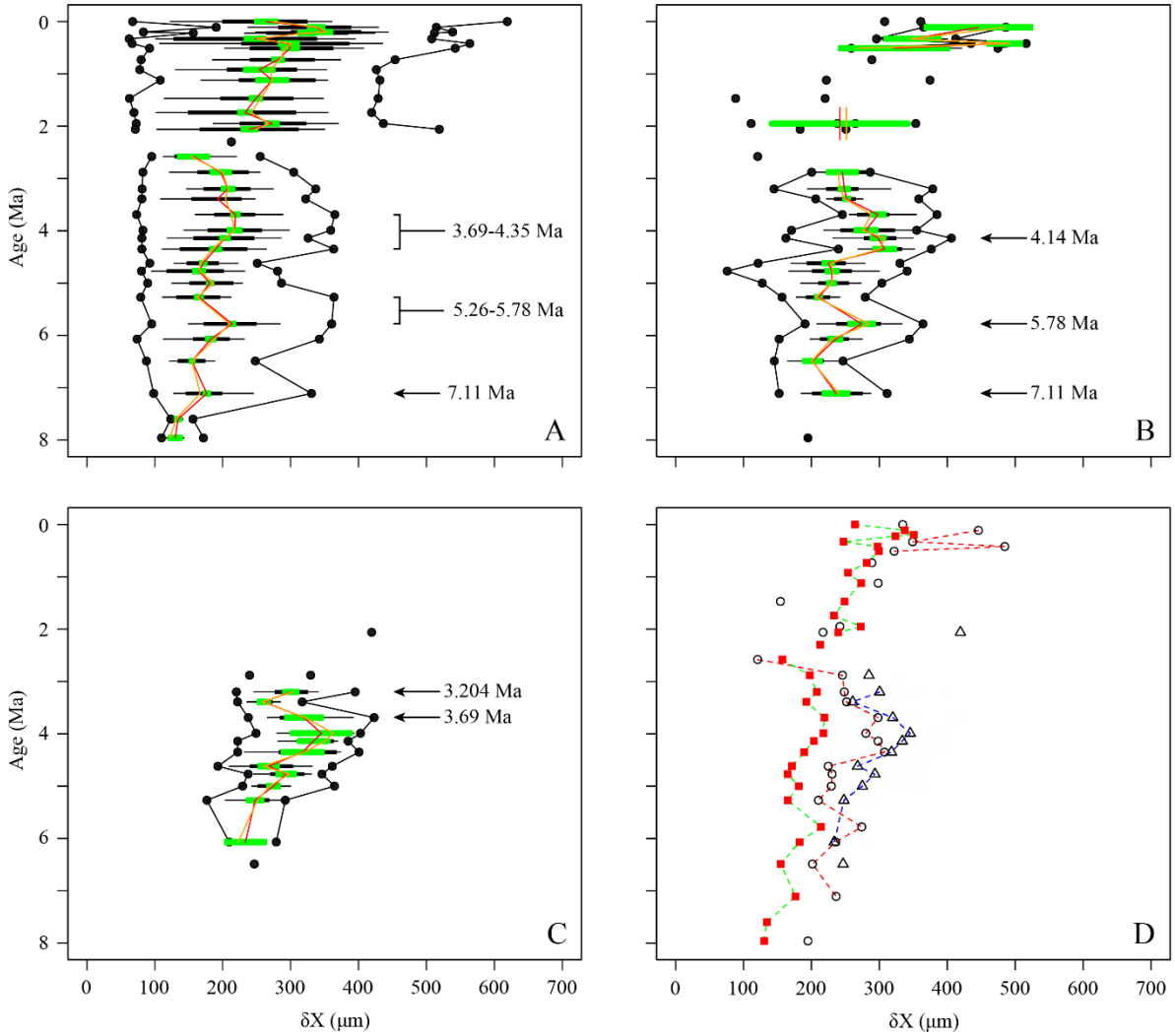

Figure 2.5: Spiral height (δX) in keel view (in µm) versus time (Ma) at ODP Hole 667A for (**A**) *G. menardii*, (**B**) *G. limbata*, (**C**) *G. multicamerata* and (**D**) the mean values of the three species. In A–C, black dots represent minimum and maximum values. The thin horizontal black bars represent the 10 to 90 % sample percentiles and thick black bar bars the lower and the upper quartiles, and the green horizontal bar shows the confidence interval of the mean. Means are illustrated as a vertical red line and median values by a vertical orange line. In D, mean δX of *G. menardii* are shown as red squares, those of *G. limbata* by black circles and means of *G. multicamerata* by black triangles. Samples containing fewer than three specimens of the corresponding species are shown as isolated symbols because this number does not allow reasonable statistical analysis.

trends of the corresponding mean and median values. The maximum values exhibit one peak at 7.11 Ma and two "peak plateaus" from 5.78 Ma to 5.26 Ma and 4.35 Ma to 3.69 Ma. In samples from 2.3 Ma and younger, δX of *G. menardii* increases to a maximum value of 619 µm in the youngest sample, (667A-1H-1, 3–4 cm; 0.003 Ma), which is almost a doubling of the size reached between 7.96 and 2.58 Ma (maximum value 365 µm at 3.69 Ma). Prior to its extinction, *G. limbata* shows similar maximum (Fig. 2.5b) and mean δX peaks (Fig. 2.5d) as *G. menardii* at 7.11 Ma, 5.78 Ma and 4.14 Ma. On average, populations of *G. limbata* are slightly larger in size than those of *G. menardii*. Specimens with seven chambers in the last whorl, which are considered as *G. limbata*, still occur after 2.58 Ma, but only sporadically and in low numbers and no statistically significant statements are possible for those times.

Globorotalia multicamerata attains the largest size of the three species at times before 3 Ma (Fig. 2.5c). It surpasses *G. menardii* and *G. limbata* in test-size mean and maximum values in

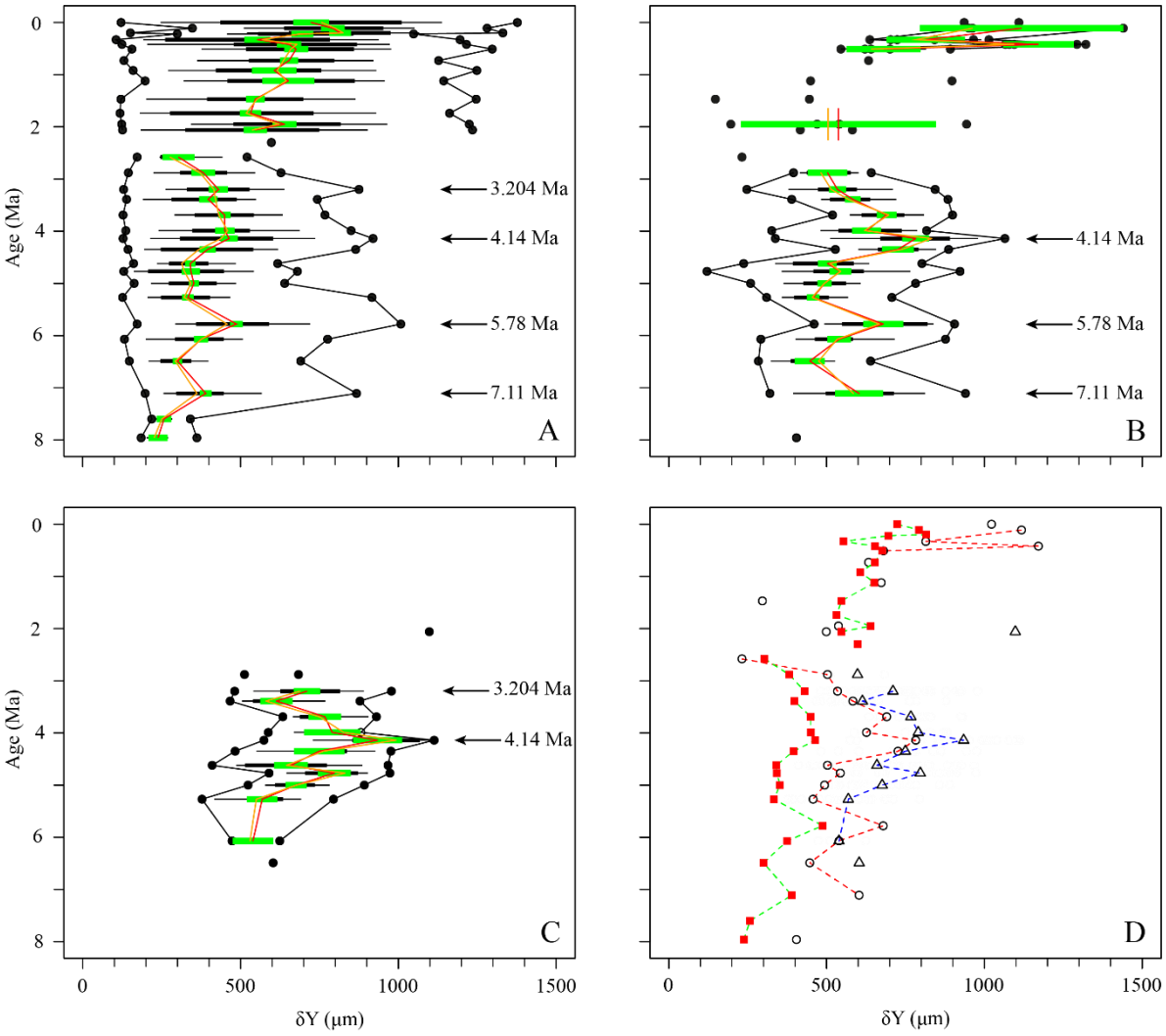

Figure 2.6: Axial length (δY) in keel view (in µm) versus time (Ma) at ODP Hole 667A for (**A**) *G. menardii*, (**B**) *G. limbata*, (**C**) *G. multicamerata* and (**D**) the mean values of the three species. See Fig. 2.5 for the explanation of the symbols.

all samples in which it occurs (Fig. 2.5d). Exceptions are the samples at 6.07 Ma, which have the same mean value as *G. limbata*, and at 2.057 Ma. No specimen was found at 5.78 Ma. Thus, *G. multicamerata* only exhibit one major peak in the maximum values at 3.69 Ma and in the mean values at 3.99 Ma.

Similar to δX, the mean and median values of δY also show three major peaks (7.11 Ma, 5.78 Ma, 4.14 Ma) for *G. menardii* and *G. limbata* between 7.96 Ma and 2.58 Ma (Fig. 2.6, 2.7). Maxima of δY exhibit similar peaks, but note a fourth peak in δY at 3.204 Ma for *G. menardii* (Fig. 2.6a). Measurements of Ar are shown in Fig. 2.7. Between 7.96 Ma and 2.58 Ma the Ar of *G. menardii* reveals three peaks at 7.11 Ma, 5.78 Ma and 3.204 Ma and a plateau from 4.35 Ma to 3.99 Ma. The data also show a peak in Ar for *G. limbata* at 4.14 Ma. Between 2.58 Ma

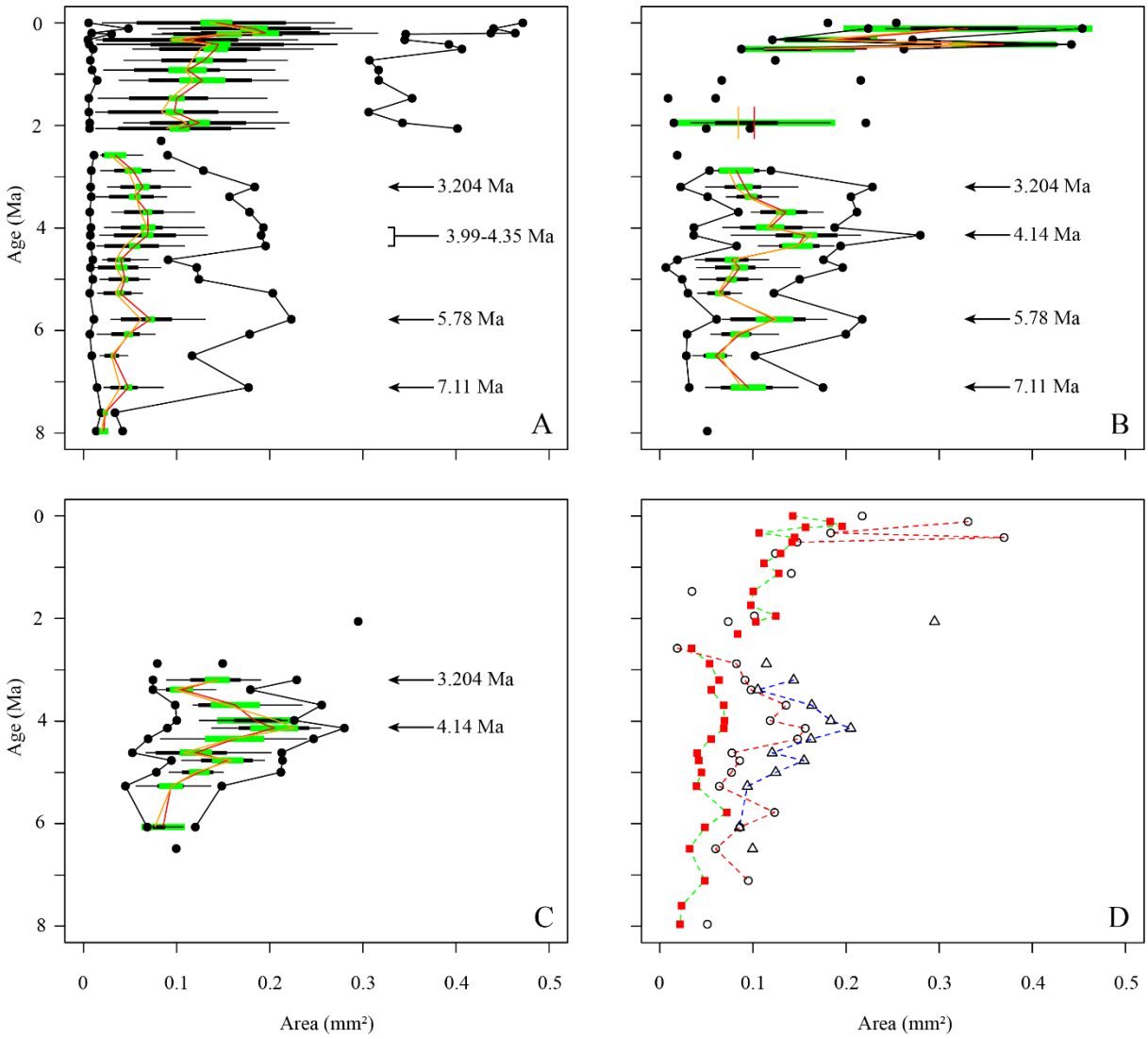

Figure 2.7: Test area (Ar) in keel view (in mm²) versus time (Ma) at ODP Hole 667A for (**A**) *G. menardii*, (**B**) *G. limbata*, (**C**) *G. multicamerata* and (**D**) the mean values of the three species. See Fig. 2.5 for the explanation of the symbols.

and 2.057 Ma, the maximum values of δY (Fig.2. 6a) of *G. menardii* more than double from 520 µm to 1235 µm, while Ar increases 5-fold from ca. 0.08 mm² to 0.4 mm² (Fig. 2.7).

For *G. multicamerata*, the maximum and mean δY and Ar values show a similar pattern as δX (Fig. 2.6c, 2.7c) but with a major peak at 4.14 Ma. This species exhibits the largest size in these two parameters in comparison to the other two species.

The three parameters show a high degree of overlap between the three species. However, morphological overlap between these species point to strong interspecific size variation. *Globorotalia multicamerata* exhibited the largest mean population test size and *G. menardii* the smallest mean size, while *G. limbata* was intermediate.

2.3.2 Contour frequency diagrams of spiral height and axial length

As already mentioned in the "Materials and methods" section (Sect. 2.5.), CFDs may help to detect patterns of cladogenetic splitting or anagenetic evolution by identifying shifts in the dominant test size of populations through time. The underlying grid-cell size for CFDs (and VDDs in the next section) is 50 µm in δX direction and 100 µm in δY direction.

In general, the contour frequency plots of *G. menardii* (Fig. 2.8) show that size measurements vary almost linearly by a diagonal semi-continuous morphocline in the δX and δY morphospace. This trend is due to a flattening of the test during the ontogenetic growth of the

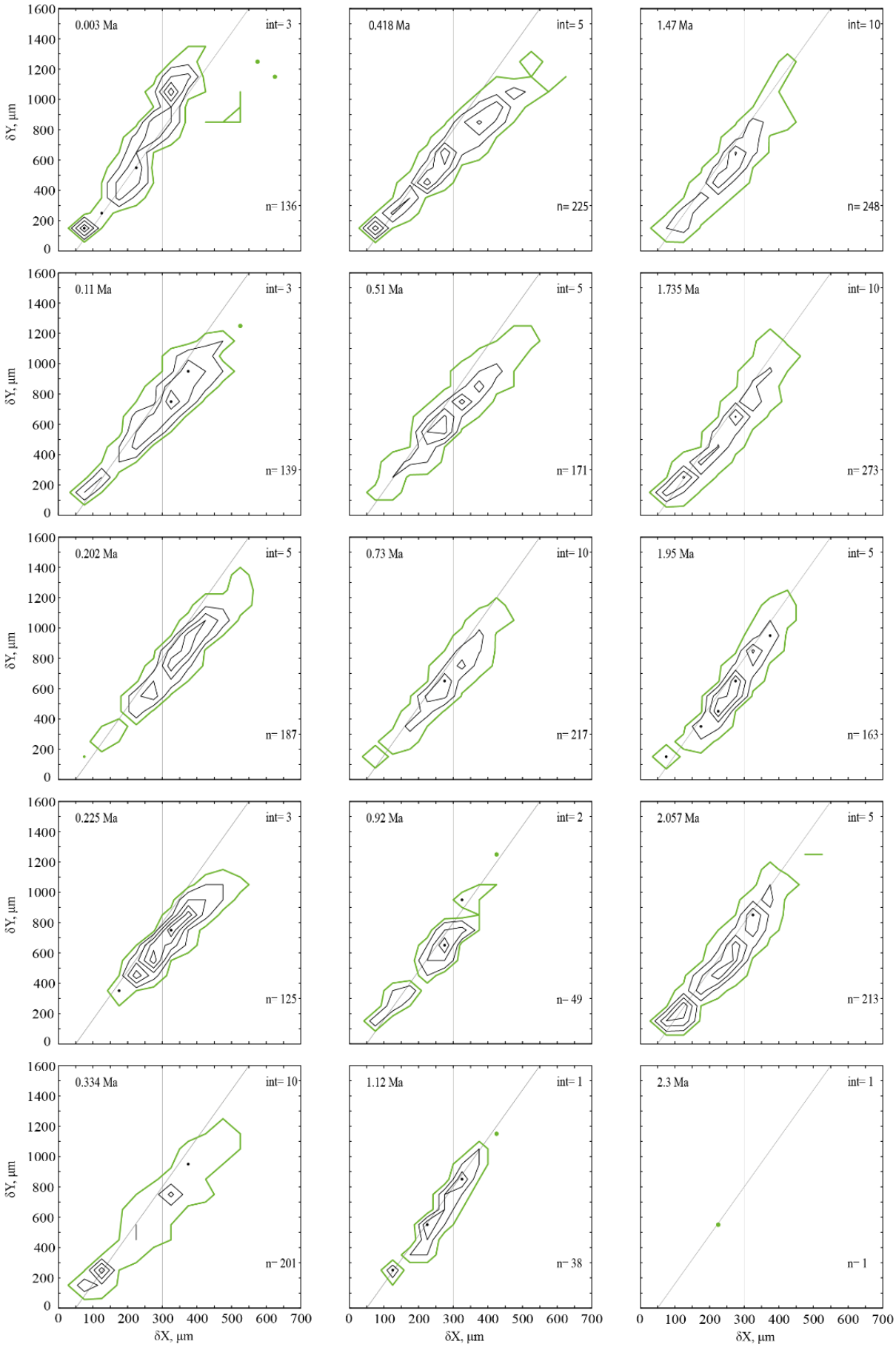
0.003 Ma
int= 3
n= 136
0.418 Ma
int= 5
n= 225
1.47 Ma
int= 10
n= 248
0.11 Ma
int= 3
n= 139
0.51 Ma
int= 5
n= 171
1.735 Ma
int= 10
n= 273
0.202 Ma
int= 5
n= 187
0.73 Ma
int= 10
n= 217
1.95 Ma
int= 5
n= 163
0.225 Ma
int= 3
n= 125
0.92 Ma
int= 2
n= 49
2.057 Ma
int= 5
n= 213
0.334 Ma
int= 10
n= 201
1.12 Ma
int= 1
n= 38
2.3 Ma
int= 1
n= 1
δY, µm
δX, µm
0
200
400
600
800
1000
1200
1400
1600
100
300
500
700

Fig. 2.8A

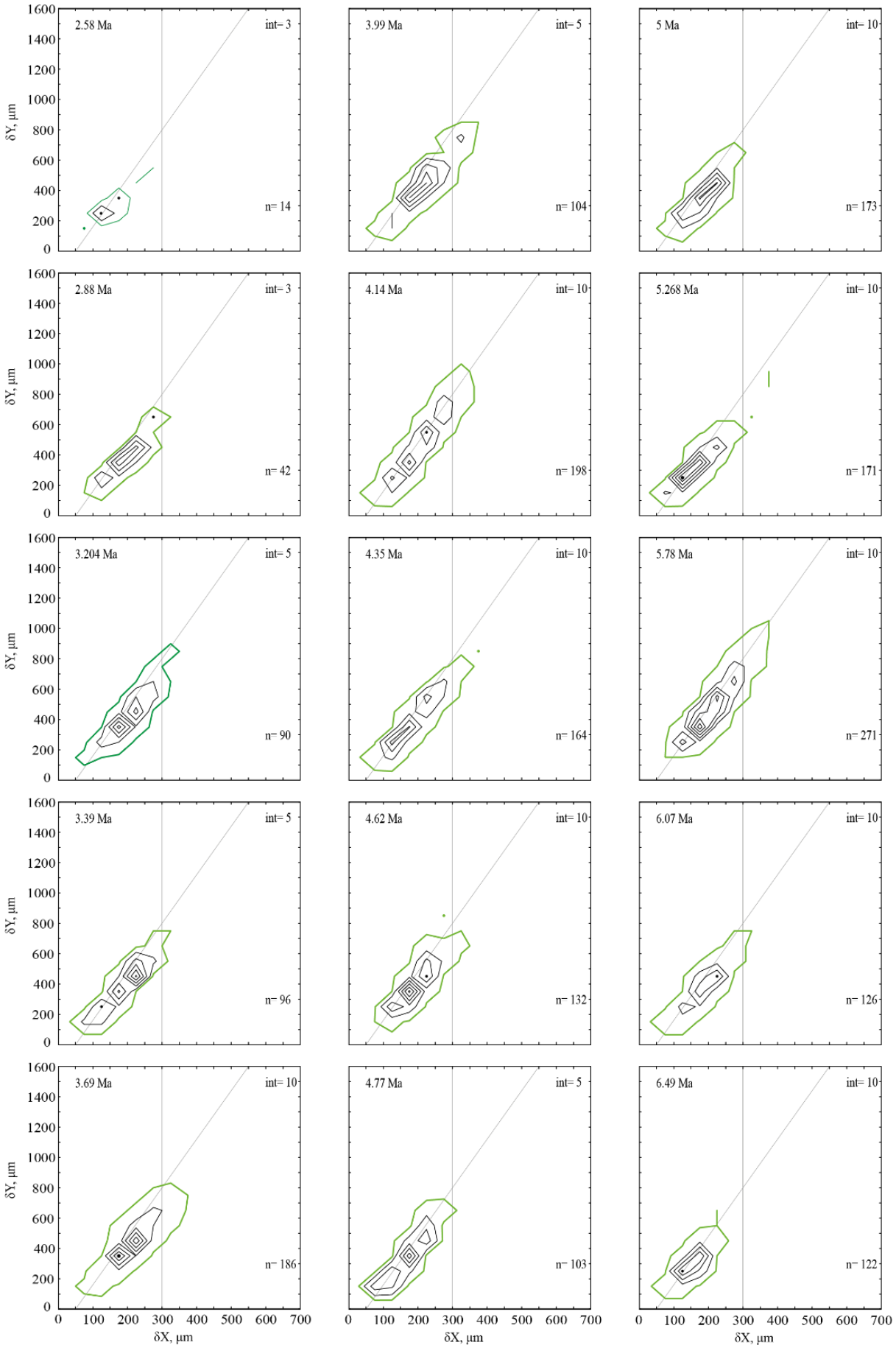
2.58 Ma
int= 3
n= 14
3.99 Ma
int= 5
n= 104
5 Ma
int= 10
n= 173
2.88 Ma
int= 3
n= 42
4.14 Ma
int= 10
n= 198
5.268 Ma
int= 10
n= 171
3.204 Ma
int= 5
n= 90
4.35 Ma
int= 10
n= 164
5.78 Ma
int= 10
n= 271
3.39 Ma
int= 5
n= 96
4.62 Ma
int= 10
n= 132
6.07 Ma
int= 10
n= 126
3.69 Ma
int= 10
n= 186
4.77 Ma
int= 5
n= 103
6.49 Ma
int= 10
n= 122
δY, µm
δX, µm
0
200
400
600
800
1000
1200
1400
1600
100
300
500
700

Fig. 2.8B

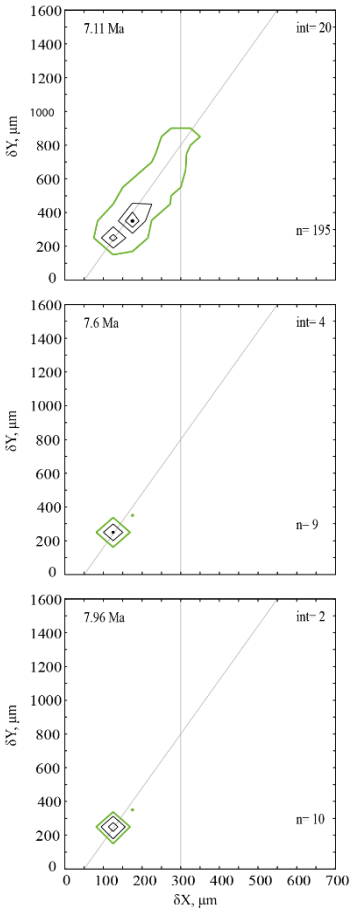

Fig. 2.8C

Figure 2.8: (**A**, **B**, **C**) Contoured frequency plots of spiral height on the x axis (δX) versus the axial length (δY) on the y axis of *Globorotalia menardii* in keel view at ODP 108 Site 667 from 0.003 to 7.96 Ma. The upper-left corner shows the age (Ma). "int" indicates the contour interval in the number of specimens per grid cell. The grid-cell size is 50 µm x 100 µm in direction of δX and δY, respectively. "n" in the lower-right corner gives the number of specimens represented in the diagram. Green-coloured contour lines and dots represent the contour interval from 0 to 1. The diagonal grey line is drawn to separate the morphotype of *G. menardii menardii* (area below the line) and *G. menardii cultrata* (area above of the line) proposed by Knappertsbusch (2007a). The vertical grey line at δX = 300 µm delimits the dominant population of *G. menardii* older than 2.88 Ma and is also drawn for comparison.

individuals (Caromel et al., 2016). As was already recognised in the univariate parameter-versus-time diagrams, two different phases of shell size development can be distinguished in the CFDs. The first phase ranges from 7.96 Ma until about 2.88 Ma and is characterised by populations with a dominant test size smaller than 300 µm in δX and smaller than 600 µm for δY for *G. menardii*, as well as predominantly unimodal distributions of the population size (Fig. 2.8). The only sample in this first phase showing bimodality is at 4.35 Ma. At 2.58 Ma and 2.3 Ma, the *G. menardii* population is very reduced and small or almost completely vanished. A different pattern appeared from 2 Ma until the present. In that younger interval, several samples exhibit visually distinct bimodal distributions along the δX versus δY morphocline (2.057 Ma, 1.95 Ma, 1.735 Ma, 1.12 Ma, 0.92 Ma,0.418 Ma, 0.334 Ma, 0.11 Ma and 0.003 Ma). The smaller mode is limited to a range of 200 µm (δX) and 300 µm (δY), while the larger surpasses 250 µm (δX) and 600 µm (δY) in each case. There is a noteworthy change in the youngest sample (0.003 Ma), where the majority of specimens occur above the diagonal separation line (see. Fig. 2.8), while specimens of older samples are mostly distributed below that line. This is also visible in the VDD in chapter 3.4.

2.3.3 Bimodal patterns in contour frequency diagrams

Several samples younger than 2.057 Ma (2.057 Ma, 1.95 Ma, 1.735 Ma, 1.12 Ma, 0.92 Ma, 0.418 Ma, 0.334 Ma, 0.11 Ma and 0.003 Ma) and the sample from 4.35 Ma visually display a bimodal distribution, in which the peaks are separated either at ca. δX = 200 µm or at δX = 300 µm (Fig. 2.8). If the described bimodality patterns were to indicate speciation within *G. menardii*, modal centres would connect into continuous branches that diverge for the last 2 Myr. Populations can be more closely inspected through vertical stacking of CFDs via a volume density diagram (see next chapter 3.4).

2.3.4 Volume density diagrams

The iso-surface of Fig. 2.9 illustrates the test size of rare, often innovative specimens, which either evolved within the Atlantic Ocean or intruded by dispersal. As the VDD is basically a stacking of the individual CFDs, it shows the same peaks at 7.11 Ma, 5.78 Ma and 4.14 Ma for *G. menardii*. The VDD clearly illustrates the size decrease during the interval from 4.14 Ma until 2.58 Ma, and the striking size increase from 2.58 Ma to 2.057 Ma (Fig. 2.9a). The size reached at 2.057 Ma is unprecedented.

Of special note is the aberrant steeper slope of the youngest CFD (0.003 Ma; Fig. 2.8), which is displayed with respect to the rest of the VDD towards elongated and flattened specimens. Such a trend to flat specimens was also observed in the uppermost Quaternary of DSDP Site 502 (Knappertsbusch, 2007). In the present case specimens have developed a strong keel and so are presumably not classified as *G. m. cultrata*.

An interactive version of the VDD can be found in the 3D-PDF file "VDD_3D_PDF.pdf" (see supplementary materials).

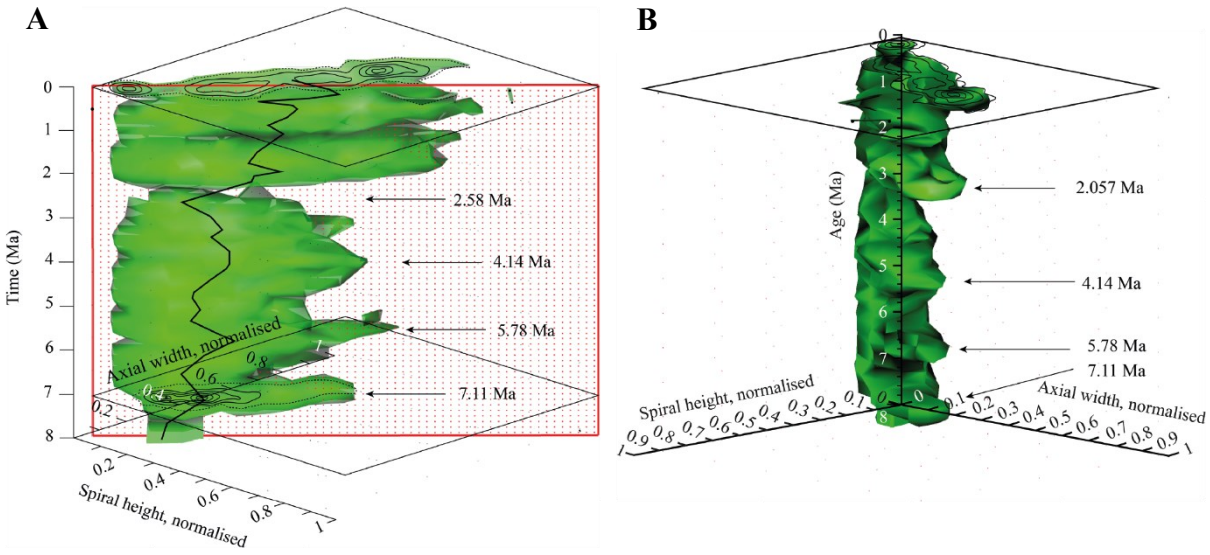

Figure 2.9: Volume density diagrams (VDD) of the normalised spiral height (δX) versus the normalised axial width (δY) over the past 8 Myr for *G. menardii* at the eastern tropical Atlantic Hole 667A. The shown iso-surface has a value of 0.89447168, which equals the frequency of one specimen. Thus, it represents rare, innovative specimens. (**A**) VDD in side view. The red, dotted plain represents the section shown in Fig. **2.**10. The CFDs of the samples from 0.003 Ma and 7.11 Ma are displayed. The black line represents the mean values. (**B**) VDD in front view. The CFD of the sample from 0.003 Ma is displayed as an example. The arrows at 7.11 Ma, 5.78 Ma and 4.14 Ma point to size peaks and the arrow at 2.58 Ma marks the sample with the smallest observed test size. The settings for the VDD construction are given in the supplementary material (file "VDD_set-up_data.txt").

2.3.5 Longitudinal section of frequencies of spiral height and axial length through time

A longitudinal section through the VDD, as shown in Fig. 2.10, allows us to check for and identify changes and shifts in the frequencies and to investigate whether modal centres in size distribution arrange along continuous and diverging branches through time. The occurrence of multiple, distinct density peaks in the CFD may indicate the occurrence of populations with different test sizes. If these density peaks combine to continuous morphological clades through time, diverging branches may point to morphological speciation within *G. menardii*. A clear split into robust branches that separate through time cannot be recognised in Fig.2.10.

During the time interval from 7.96 Ma to 2.58 Ma, one continuous clade consisting of two or more modes can be identified, which follows the mean value. Higher up in the core, a tendency to a bifurcation into two distinct clades is indicated around 1.735 Ma. This sample was already

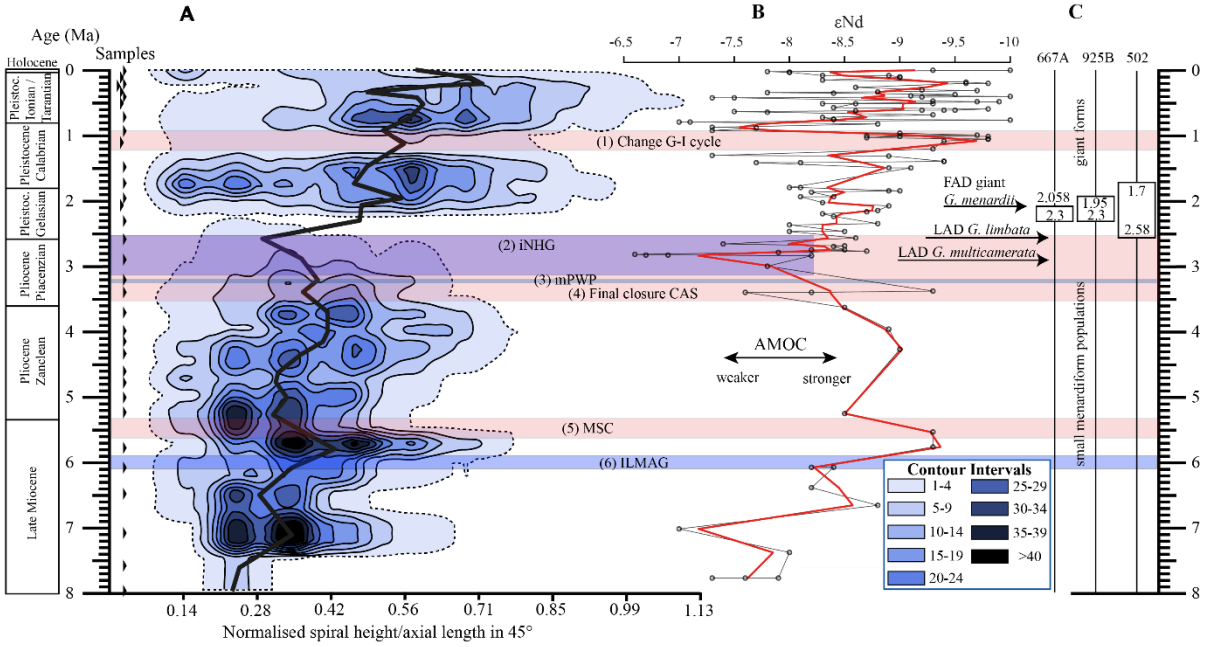

Figure 2.10: (**A**) Longitudinal section (offset value = 0) through the 45° view on the volume density diagram of Hole 667A in a palaeoceanographic context. The dotted line represents a density of one specimen per grid cell, and solid lines are contours at density intervals of five specimens per grid cell. The evolution of mean values through time is shown as a thick black line. (1) The time interval in which a shift to increased amplitude of glacial–interglacial cycles and a corresponding 100 Kyr fluctuation in ice sheets is observed (Clemens et al., 1996; Ivanova, 2009). (2) The cooling trend, which leads into the NHG (Chapman, 2000). (3) The mid-Pliocene warm period (mPWP; Haywood et al., 2016). (4) The time interval in which the final closure of the Central American Seaway (CAS) is supposed by Bartoli et al. (2005), Jackson and O`Dea (2013), and O'Dea et al. (2016). (5) The time interval of the Mediterranean salinity crisis (Krijgsman et al., 1999). (6) The intensification of the Late Miocene Antarctic Glaciation (ILMAG) (Chaisson and Ravelo, 1997). (**B**) The right side shows εNd isotopic curve at Site 1088 in the South Atlantic taken from Dausmann et al. (2017), a proxy for the AMOC strength. The black line with circles represents the original data from Dausmann et al. (2017) and the red line a smoothed version, produced with the RStudios' command 'smooth.spline' at the value of 0.35. (**C**) The black triangles on the left side display the investigated samples. The boxes on the right side show the time intervals in which the giant *G. menardii* specimens occurred at Sites 667, 925 and 502 and in which the size increase is presumed to have taken place. The arrows show the first appearance date (FAD) of giant *G. menardii* specimens and the last appearance date (LAD; more than one specimen per sample split) of *G. limbata* and *G. multicamerata* at Site 667.

mentioned to develop bimodality in CFDs (Fig. 2.8). In the youngest part of the core this bifurcation is no longer observed, despite the presence of distinct modal centres in individual CFDs, during which *G. menardii* tends to gradually increase its test size. The complexity of the size evolution of *G. menardii* through time is further illustrated in two parallel sections in 45° orientation with different offsets and three orthogonal sections at 135° (Appendix Fig. A2.2-A2.7). The different perspectives of the VDD show other density peak trends. An "ideal" description of maximal evolutionary trends would require a flexural vertical section plain at 45°.

Figure 2.10 indicates that the test-size evolution may be directly or indirectly affected by major palaeoceanographic events. The overall decrease from ca. 4 Ma to 2.5 Ma follows the closure of the Isthmus of Panama and the intensification of the NHG. The figure also indicates a potential influence of the AMOC strength on the test size (see chapter 4.1.3).

2.3.6 Changes in coiling direction in *G. menardii*

The data also show changes in the coiling direction of *G. menardii*, which may be related to understand evolutionary changes (see, for example, Bolli, 1950).

In the ETAO, three different phases in the predominant coiling direction of *G. menardii* were observed, in which patterns in the predominant coiling direction change (Fig. 2.11a). In the first phase from 7.96 Ma until 5.268 Ma, coiling seems to frequently swing between sinistral and

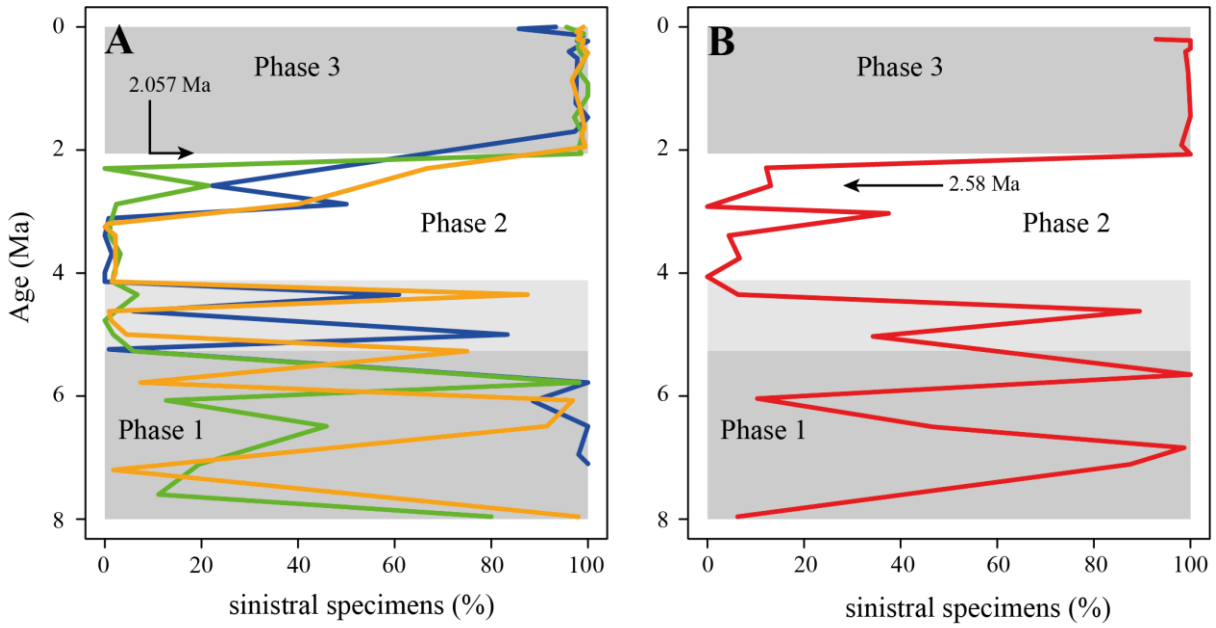

Figure 2.11: Percentage of sinistral specimens within the *G. menardii* population through time. (**A**) Tropical Atlantic Ocean Site 667 (green; this study), 502 (blue; Knappertsbusch, 2007b) and 925 (orange; Knappertsbusch, 2015). (**B**) Eastern tropical Pacific Ocean Site 503 (Knappertsbusch, 2007c). The grey areas represent the recognised phases as mentioned in the text. The lighter grey bar from 5.3 Ma until ca. 4 Ma shows the extended phase 1 for Sites 502, 503 and 925.

dextral. During the second phase from 5.268 Ma to 2.057 Ma dextrally coiled specimens dominated (>90 %, except at 2.58 Ma with 78.5 %). In the youngest phase, lasting from 2.057 Ma to present, sinistral coiling prevailed strongly (>95 %). These phase are in agreement with Bolli and Saunders (1985) and references therein (Bolli, 1950; Bermúdez and Bolli, 1969; Robinson, 1969; Bolli, 1970; Lamb and Beard, 1972; Bolli and Premoli Silva, 1973). It is interesting that sites from the WTAO (925B), the Caribbean Sea (502) and the eastern tropical Pacific Ocean (503) exhibit a similar history of changes in the coiling direction in menardiforms (Fig. 2.11), although phase 1 extends at in these sites until ca. 4.15 Ma and the stratigraphic resolution for trans-oceanic correlation remains rather low.

Nevertheless, the reversal in the preferential coiling direction from dextral (phase 2) to sinistral (phase 3) at ca. 2 Ma is nearly synchronous at all of the above-mentioned sites and coincides with the stratigraphic entry of giant *G. menardii* forms in the Atlantic Ocean.

2.4. Discussion

2.4.1. Size variation in *Globorotalia menardii*

A substantial test-size increase in *G. menardii* is observed at Hole 667A. Within the short time interval from 2.58 to 2.057 Ma, the size more than doubles (Fig. 2.5, 2.6, 2.7, 2.8). Knappertsbusch (2007a; 2016) observed a similar expansion in test-size evolution in western Atlantic ODP Hole 925B and at the Caribbean Sea DSDP Site 502 between 2.58 Ma and 1.95 Ma and 1.7 Ma, respectively. He considered two hypotheses which could explain this observation: a rapid faunal immigration via Agulhas leakage or rapid evolutionary test-size increase by punctuated evolution.

The new data from Hole 667A are discussed in the context of these two hypotheses. Although the results of this site cannot prove or reject one of the hypotheses, they may reveal evidence for their likelihood. A third hypothesis is introduced which proposes the AMOC strength as a possible (palae-)oceanographic influencer on the test size of *G. menardii* and could explain the size evolution during the time interval from 8 Ma to ca. 2 Ma.

2.4.1.1. Agulhas leakage hypothesis

In the Agulhas leakage hypothesis, *G. menardii* is assumed to have been entrained from the subtropical Indian Ocean into the tropical Atlantic Ocean by episodic and especially strong Agulhas faunal leakage events (Knappertsbusch, 2016).

The Agulhas leakage is known to disperse Indian Ocean biota into the Atlantic Ocean on a large scale via giant eddies (Peeters et al., 2004; Caley et al., 2012; André et al., 2013; Villar et al.,

2015). These eddies form when water masses of the Agulhas Current separate from the retroflection point off South Africa (e.g. Lutjeharms and Van Ballegooyen, 1988; Norris, 1999; Bard and Rickaby, 2009; Biastoch et al., 2009; Beal et al., 2011; Fig. 2.1). At ODP Site 1087, which is located in the southern Benguela region, the Agulhas leakage has been found to exist since 1.3 Ma by presence/absence of *G. menardii* (Caley et al., 2012).

Globorotalia menardii is a well-known tropical dweller (Caley et al., 2012; Schiebel and Hemleben, 2017, and references therein). Over the southern tip of Africa, the tropical provinces of the Atlantic and Indian oceans are disconnected by strong fronts from the transitional province of the Southern Ocean. These frontal barriers are rather difficult to surpass for tropical species like *G. menardii* and so prevent continuous genetical exchange. The Agulhas leakage mechanism and its probable changes in strength and intensity allow tropical plankton faunas to surmount oceanographic barriers and to transport them from the tropical Indian Ocean into the southern Atlantic and further into the tropical Atlantic (Caley et al., 2012). The relatively sudden appearance of giant *G. menardii* in the Atlantic Ocean might thus be explained by such a large distance dispersal of tropical populations at a time when the Agulhas leakage became possibly intensified between ca. 2.58 and 2.057 Ma. If true, this would pre-date the existence of the Agulhas leakage by at least 0.7 Myr.

Interestingly, giant menardiforms occurred ca. 0.1 Myr earlier at the ETAO Site 667 than at the WTAO Site 925. Under present oceanographic conditions, simulations showed that Agulhas rings follow predominantly the South Equatorial Current rather than the Benguela Current along the southwest African continent (Biastoch et al., 2009; van Sebille et al., 2011; Rühs et al., 2013; Laxenaire et al., 2018; Fig. 2.1). With this scenario in mind, one would expect the giant forms to first be transported into the WTAO, which on first sight would contradict the Agulhas hypothesis. However, an eastward meandering and fluctuation in strength of the Agulhas leakage ring pathway during different climatic conditions than today could explain the observed pattern. Instead of traversing the South Atlantic, rings may have drifted closer to the coast of southwest Africa. In such a scenario, the giant *G. menardii* type dispersing from in the Indian Ocean would have reached the ETAO first.

An alternative idea is proposed by Norris (1999), according to which unfavourable environmental conditions in the WTAO prevented *G. menardii* from stabilising viable populations, which could explain the size differences during 2.58–1.95 Ma at Hole 925B. The Indian-Ocean-influenced water masses were perhaps further transported to the ETAO via the North Equatorial Countercurrent (Fig. 2.1), where more favourable conditions prevailed, allowing *G. menardii* to thrive. A similar hypothesis of presence and absence of suitable

environmental conditions was already considered to explain a distinct short pulse of *Globorotalia truncatulinoides* in the southern Atlantic Ocean at 2.54 Ma (Spencer-Cervato and Thierstein, 1997; Sexton and Norris, 2008).

According to Chaisson and Ravelo (1997), a trade-wind see-saw between the ETAO and the WTAO prevailed, which possibly resulted in unfavourable environmental conditions for *G. menardii* at Site 925B between 2.5 and 1.95 Ma. These authors argue that trade winds influence the thermocline depth at each side of the equatorial Atlantic Ocean in a reverse way: increased trade winds in the WTAO pile up warm surface waters, leading to a massive thermocline layer and a deeper thermocline. At the same time in the ETAO, increased trade winds shoal the thermocline by inducing upwelling and hence cool the sea surface temperature. This is in agreement with reconstructions (Billups et al., 1999), observations (Niemitz and Billups, 2005) and models (Merle, 1983; Ravelo et al., 1990) about seasonal latitudinal shifts in the position of the trade winds and the Intertropical Convergence Zone (ITCZ). Both influence the depth of the thermocline layer in the eastern and the western tropical Atlantic Ocean in an alternating reversed way.

Globorotalia menardii is a typical thermocline dweller (Fairbanks et al., 1982; Curry et al., 1983; Thunell and Reynolds, 1984; Keller, 1985; Savin et al., 1985; Ravelo et al., 1990; Schweitzer and Lohmann, 1991; Gasperi and Kennett, 1992; Ravelo and Fairbanks, 1992; Gasperi and Kennett, 1993; Hilbrecht and Thierstein, 1996; Stewart, 2003; Steph et al., 2006; Mohtadi et al., 2009; Regenberg et al., 2010; Wejnert et al., 2010; Sexton and Norris, 2011; Davis et al., 2019) and may react sensitively in reproduction, abundance and morphology to vertical shifts of the regional thermal surface-water stratification.

The observed changes in the predominant coiling direction (Fig. 2.11) also support the Agulhas leakage hypothesis and may point to the establishment of a new Atlantic *G. menardii* clade past 2 Ma in the Atlantic Ocean. The giant and sinistrally coiling *G. menardii* form was first observed at the eastern tropical Pacific Ocean Site 503 at 2.58 Ma, while it occurred at the Atlantic Ocean Site 667 ca. 0.5 Myr later. Since the final closure of the Isthmus of Panama between 4 Ma and 2.8 Ma (Chaisson, 2003; Bartoli et al., 2005; O'Dea et al., 2018) prohibited a direct water exchange between the tropical Pacific Ocean and the tropical Atlantic Ocean, the coiling evidence potentially suggests spreading of the giant type from the Pacific Ocean into the Atlantic Ocean via the Indian Ocean and the Agulhas leakage route within 500 Kyr. A study within the Indian Ocean is currently in progress to further test the Agulhas leakage hypothesis.

2.4.1.2. Punctuated gradualism by local evolution and/or environmental adaptation

A regional, more punctuated evolution of *G. menardii* into giant forms is another possible process to explain the observed test-size pattern in the tropical Atlantic at ca. 2 Ma.

In PF and other planktonic microfossils, speciation is sometimes observed to happen within short time periods. Examples include the speciation of *G. tumida* from *G. plesiotumida* within only 600 Kyr during the late Miocene and early Pliocene at DSDP Site 214 in the southern Indian Ocean (Malmgren et al., 1983). Hull and Norris (2009) suggest an even more rapid speciation for this group in the western tropical Pacific (ODP Hole 806C), where *G. tumida* was observed to evolve from its ancestor *G. plesiotumida* in the late Miocene and early Pliocene within 44 Kyr. Pearson and Coxall (2014) observed transitions in the *Hantkenina* genus from a normal-spined to a tubulospined form within only 300 Kyr. In the case of the Pliocene radiolarian *Pterocanium prismatium* cladogenetic speciation from its ancestor *P. charybdeum* was reported to occur within 50 Kyr (Lazarus, 1986).

The mentioned cases show that the giant menardiform morphotype may have evolved rapidly within the 242 Kyr from 2.3 Ma to 2.057 Ma in the ETAO. With the ETAO as "founder area", a further dispersal into the WTAO within only ca. 100 Kyr and then into the Caribbean Sea within another 250 Kyr cannot be excluded but would require more biogeographic, high-resolution mapping of test-size patterns through time.

A persistent question remains, however: why did such rapid evolutionary change take place especially and only at the time between 2.3 and 2.057 Ma? Answers may be sought in the final closure of the Central American Seaway from ca. 4 Ma until 2.58 Ma–2.057 Ma (Chaisson, 2003, O'Dea et al., 2016) and associated environmental changes, as was suggested by Schmidt et al. (2016), Todd et al. (2020) and Woodhouse et al. (2021) for other PF species. Perhaps mainly the establishment of Northern Hemisphere ice sheets (Raymo, 1994; Tiedemann et al., 1994; Bartoli et al., 2005) and the initiation of the NHG were important drivers for such rapid evolutionary events. The global climate cooling caused fundamental changes in the stratification of the upper water column (Chapman, 2000) and undoubtedly led to unfavourable environmental conditions for species like menardiform globorotallids in the Atlantic Ocean (see chapter 4.2). An ongoing deterioration in viability under environmental pressure of the NHG presumably caused first the extinction of *G. multicamerata* after 2.88 Ma and then the (pseudo-)extinction of *G. limbata* after 2.58 Ma at Site 667, which is the same time interval in which the thermocline-dwelling *Globoconella puncticulata* showed a decreasing trend in test size and finally went extinct at 2.41 Ma (Brombacher et al., 2017; 2021). Isotopic measurements (Keller, 1985; Gasperi and Kennett, 1993; Pfuhl and Shackleton, 2004) suggest that also *G. limbata* and

G. multicamerata were thermocline dwellers, with *G. multicamerata* living at the top, *G. limbata* in the centre and *G. menardii* at the bottom of the thermocline.

These ecological niches were occupied during relatively rapid adaption and evolution from the ancestral *G. menardii* sensu the "incumbency replacement" process of Rosenzweig and McCord (1991). Support for such a process is also given by consideration of the maximal test growth values attained by the involved species. After extinction of *G. multicamerata* and *G. limbata* in the course of the NHG, their niches in the upper to middle thermocline became liberated and could be re-occupied by *G. menardii*. The settlement of the latter species at higher levels in the water column may have led to optimum growth and development of larger tests. However, isotopic data are required to further test this hypothesis.

Unfortunately, the temporal sampling resolution of this study is too coarse to prove the hypothesis of a punctuated or gradual evolutionary event but could be resolved as soon as higher temporal and spatial sampling intervals are investigated at Hole 667A, Hole 925B and Site 502 in the period between 2.3 and 2.057 Ma.

2.4.2 Possible influence of the AMOC strength on the test size of *G. menardii*

Unexpectedly, the measured variations in test-size maxima of *G. menardii* show a similar trend with the dissolved radiogenic isotope composition of Neodymium (εNd), which is an indicator for the relative long-term strength of the AMOC (Dausmann et al., 2017; see Fig. 2.10, 2.12) from the Late Miocene until the early Pleistocene. During time intervals of increasing test size, εNd, and thus the strength of the AMOC, appeared to generally increase as well. In contrast, a decrease in the test size is on average accompanied by a decreasing trend in εNd, the latter suggesting a weak AMOC. The AMOC is the Atlantic part of the global ocean conveyor belt, which causes a redistribution of heat within the global oceans. At the surface, warm and salty water is transported from the South Atlantic Ocean via the Caribbean Sea into the North Atlantic. There, it sinks down, caused by a loss of buoyancy due to the release of heat, and flows southward at depth as the North Atlantic Deep Water. The release of heat in the North Atlantic influences the climate of northeastern Europe, leading to relatively mild winter temperatures. (McCarthy et al., 2017)

The εNd isotope is used as a tracer for ocean circulation (Dausmann et al., 2017; Blaser et al., 2019). Erosion and weathering of continental crust, which displays characteristic isotopic signatures from the samarium-neodymium decay system for different continents, is the source of dissolved Nd in the ocean water. After entry to the sea, convection of the characteristic εNd

signature to deep waters allows this tracer to reconstruct large-scale patterns in ocean circulation (Blaser et al., 2019).

Water originating in the North Atlantic is known to develop more negative εNd values in comparison to waters of other origin (Dausmann et al., 2017; Blaser et al., 2019). In the study of Dausmann et al. (2017) a continuous high-resolution record for εNd at ODP Site 1088 in the South Atlantic (Fig. 2.1) was generated and used for the reconstruction of the AMOC strength, where the more negative the εNd values are, the higher the admixture of North Atlantic Deep Water at Site 1088 is, and the stronger the AMOC is. To the best of the authors knowledge this is so far the only εNd record which covers the investigated time interval and larger regional settings of the present study.

Although very preliminary, the present empirical observation of a possible relationship between *G. menardii* size trends and εNd suggests that a connection between menardiform test size and AMOC strength may exist. A possible linkage between the North Atlantic Deep Water production, and thus the AMOC strength, and the abundance of *G. menardii* in the Atlantic Ocean was already proposed by Berger & Wefer (1996) and can be derived from Fig. 2.10 in Sexton and Norris (2011).

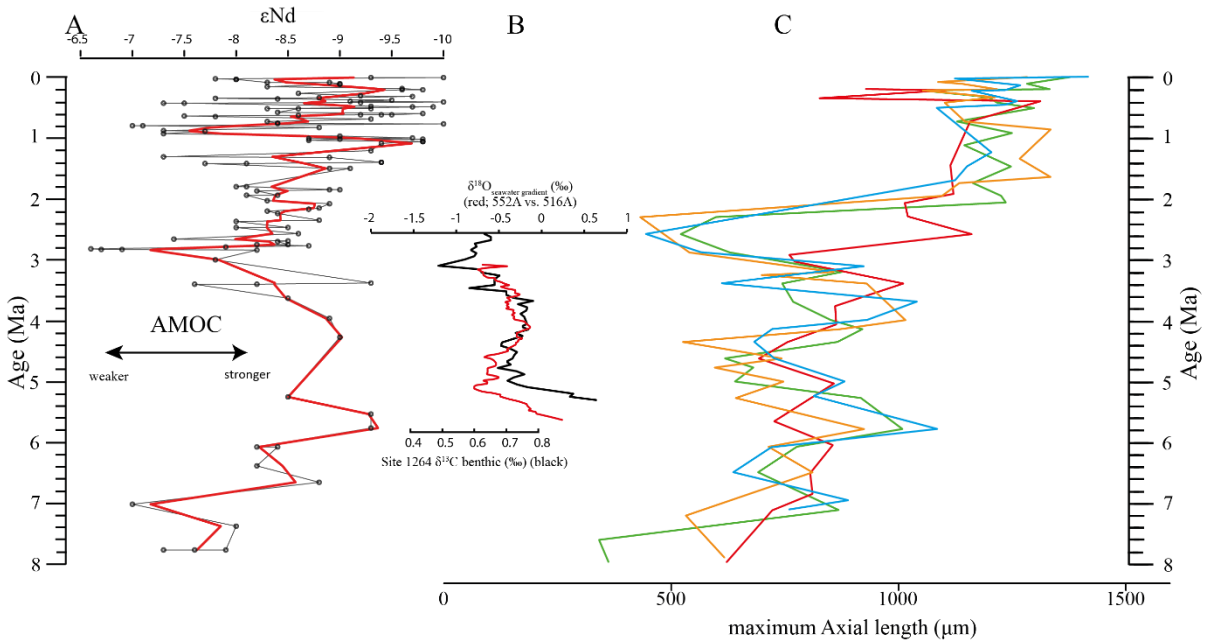

Figure 2.12: Comparison of seawater Neodymium isotope evolution (εNd), a proxy for the strength of the AMOC, and the maximum axial length of *Globorotalia menardii*. (A) Dausmann et al. (2017): εNd at Site 1088 in the southern Atlantic Ocean. The thin black line shows the original data and the red line a smoothed version, produced with the RStudios' command 'smooth.spline' at the value of 0.35. (B) AMOC strength reconstruction by Karas et al. (2017): the red line represents the $\delta^{18}O$ seawater gradient of Sites 552A and 516A, while the black one is the benthic $\delta^{13}C$ curve from Site 1264. (C) Maximum axial length (δY) versus age (Ma). The green line represents the size evolution of Hole 667A (eastern tropical Atlantic; this study), orange of Hole 925B (western tropical Atlantic; Knappertsbusch, 2016), blue of Site 502 (Caribbean Sea) and red of Site 503 (eastern tropical Pacific) (Knappertsbusch, 2007).

Although the maximum test size for Hole 667A also shows a similar trend to the AMOC strength reconstruction of Karas et al. (2017) for the Pliocene (Fig. 2.12b), the overall correlation between the maximum test size and the linear interpolation of εNd values by Dausmann et al. (2017) remains poor ($R^2 = 0.1477$, Appendix Fig. A2.8). In the authors opinion, this result is not surprising. The system is most likely not strictly mechanistic, and there are a multitude of subtle interrelationships between ecology and the test size of *G. menardii*. In order to explain the missing strict, linear and cause-and-effect relationship, one may reason the following hypotheses:

(1) The younger giant *G. menardii* form (0-2 Ma) may have occupied a (slightly) different ecology (ecological niche) in comparison to the ancestral Miocene–Pliocene form (2-8 Ma). The younger type thus might not have been affected in the same way by changes in the AMOC strength than the older form. Evidence for this explanation is given by Fig. A2.8a in the Appendix. It shows the correlation between linearly interpolated εNd values and the maximum size from Hole 667A for the time interval from 0 to 2 Ma (black points) and 2 to 8 Ma (red points), which fall into two groups. A similar observation is made in the WTAO Hole 925B, where the data allow a clear grouping into the new giant form (0-2 Ma, black dots) and the ancestral form (2-8 Ma, red dots; Fig. A2.8b in the Appendix).

(2) Due to the closure of the Central American Seaway, the Atlantic's hydrography and oceanography altered and the AMOC strength changed significantly (Haug and Tiedemann, 1998; Haug et al., 2001; Bartoli et al., 2005). The alterations maybe affected the way the AMOC strength influenced the environmental conditions within the Atlantic Ocean so that the AMOC had no major influence on the test size of *G. menardii* anymore.

The rough parallel trend between *G. menardii* test size and εNd between 2 Ma and 8 Ma suggests a direct or indirect influence of the AMOC strength on the vertical thermal structure (Haarsma et al., 2008; dos Santos et al., 2010) of the upper ocean water column in the tropical Atlantic Ocean.

Thus, changes in the strength of the AMOC may be invoked, which shifted the position of the ITCZ and associated trade winds (Billups et al., 1999; Timmermann et al., 2007), and which in turn affect the thermocline strength (Merle, 1983; Chaisson and Ravelo, 1997; Wolff et al., 1999). It is, for example, known that the ETAO thermocline reacts sensitively to variations in the AMOC strength (Haarsma et al., 2008; dos Santos et al., 2010). In this manner, the habitat of *G. menardii* would have been altered as well. A model for the response of test size of *G. menardii* under a changing thermocline is presented in the next section.

2.4.3 A thermocline model for size variation in *G. menardii*

A number of stable isotopic studies (Curry et al., 1983; Keller, 1985; Savin et al., 1985; Schweitzer and Lohmann, 1991; Gasperi and Kennett, 1992; Ravelo and Fairbanks, 1992; Gasperi and Kennett, 1993; Stewart, 2003; Steph et al., 2006; Mohtadi et al., 2009; Regenberg et al., 2010; Wejnert et al., 2010; Davis et al., 2019), plankton tows (Fairbanks et al., 1982; Thunell and Reynolds, 1984; Ravelo et al., 1990), census data from sediments (Sexton and Norris, 2011), and in situ observation (Hilbrecht and Thierstein, 1996) showed that *G. menardii* preferably dwells in the thermocline. According to Sexton and Norris (2011) and references therein, this coincides often with vertical habitats of increasing organic particle concentration and segregation, a zone in the thermocline where oxygen consumption due to particle degradation is high and where oxygen content becomes lowered.

Changes in the test size of PF are thought to be related to changes in the environmental conditions (Hecht, 1976; Malmgren and Kennett, 1976; Naidu and Malmgren, 1995; Schmidt et al., 2004; André et al., 2018), assuming that under optimum conditions, test size of species increases to its maximum, while under non-optimum conditions, the size is reduced, although detailed physiological processes at individual levels are still not entirely understood. However, Rillo et al. (2018) argued against the general validity of this hypothesis.

Assuming the "optimum-condition" hypothesis, Fig. 2.13 presents a model of how the thermocline strength could have influenced the test size of *G. menardii*: A strong thermocline

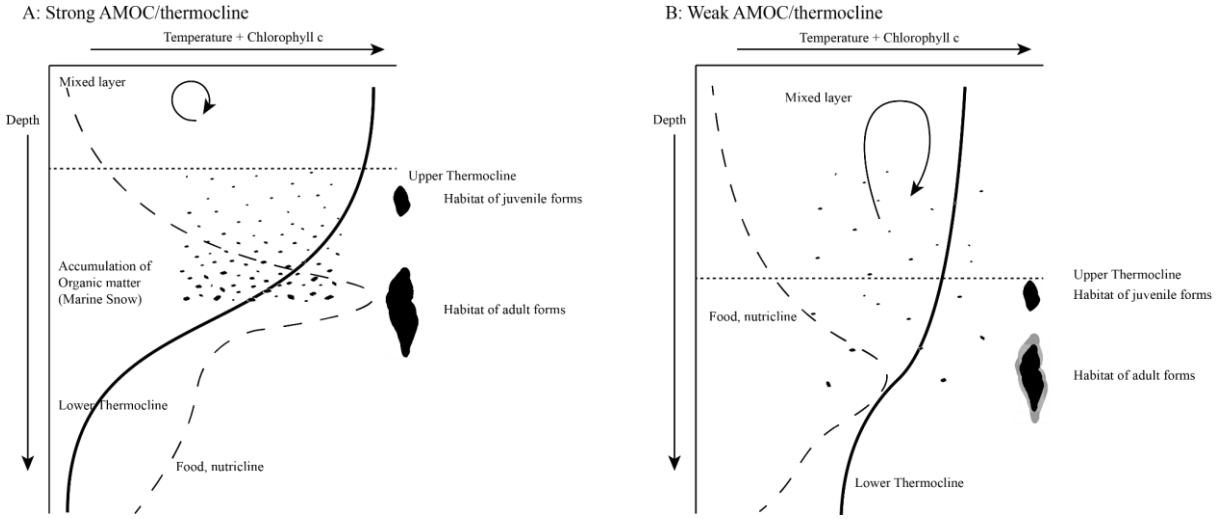

Figure 2.13: Schematic illustration of the AMOC–thermocline hypothesis. Environmental conditions are expressed as changes in the relative temperature (solid line) and the chlorophyll concentration (dashed line) with increasing depth. (A): Relatively strong AMOC–thermocline. A thin mixed layer consists of relatively warm water, while the subsurface layer is cooler. It causes a strong temperature gradient and thus a strong thermocline. This results in an increased accumulation of organic matter (marine snow) and a high concentration of chlorophyll within the thermocline. The concentration of food and the physical conditions may favour the test growth of *G. menardii*. (B): A relatively cool and deep mixed layer and a warm subsurface layer develop a weak thermocline. In comparison to strong thermocline conditions, the accumulation of chlorophyll and organic matter is low. The physical conditions may also contribute to a reduction in the test growth of *G. menardii*. Illustration modified by Brown (2007).

leads to a stronger density gradient between the surface and the subsurface layer. Often the chlorophyll maximum zone is located at this boundary (Fairbanks et al., 1982; Ravelo and Fairbanks, 1992; Steph et al., 2006), where marine snow accumulates (Möller et al., 2012; Prairie et al., 2015). The increased concentration of degrading particulate organic matter enhances nutritional conditions and favours the test growth of *G. menardii*. It is, for example, known that nutrient-rich conditions facilitate test-size increase in the PF species *Globigerinoides sacculifer* (Bé et al., 1981), *Globigerinoides ruber*, *Globigerinita glutinata*, *Globigerina bulloides* and *Neogloboquadrina dutertrei* (Naidu and Malmgren, 1995). The thermocline may play a crucial role in other aspects of *G. menardii'*s life cycle as well. A strong thermocline and the corresponding high-density contrast are thought to concentrate its gametes and food particles at a narrower zone and thus increases their chance to survive (Norris, 1999; Broecker and Pena, 2014).

This model of ecological factors within the regional thermocline influencing the phenotypic expression of *G. menardii* fits with Sexton and Norris' (2011) deglaciation proliferation model modulating the stratigraphic distribution of *G. menardii*. They suggest that *G. menardii* tracks thermoclines in areas with a moderately low oxygen concentration of ~50–100 µmol kg^{-1}, probably reduced by the degradation of organic matter.

Furthermore, Sexton and Norris (2011) postulate the reduction or vanishing of *G. menardii* populations during glacial times due to better-ventilated surface water masses, i.e. a weaker thermocline. Weakening of the AMOC during glacial times (Broecker, 1991; Berger and Wefer, 1996; Buizert and Schmittner, 2015) and associated changes in the position of the ITCZ led to a weakening and/or re-positioning of the thermocline, so that ambient conditions became less suitable for growth and proliferation of *G. menardii*.

The proposed thermocline hypothesis (Fig. 2.13) offers a possible way to explain the test-size evolution of the *G. menardii* lineage between 7.96 Ma and 2.057 Ma within the tropical Atlantic Ocean, the Caribbean Sea and the Pacific Ocean, assuming analogous conditions.

A causal chain of physiological processes in order to explain the empirical similarity between the AMOC strength and the evolution of test size of *G. menardii*, however, still remains elusive and needs further investigation.

2.5 Conclusions

1. Test-size measurements of the planktonic foraminifer *Globorotalia menardii* from the eastern tropical Atlantic Ocean ODP Hole 667A show a striking size increase in the early Pleistocene and a test-size evolution during the past 8 Myr similar to observations done in the tropical Atlantic and Caribbean Sea (Knappertsbusch, 2007; 2016). The giant forms of *G. menardii* occurred at ca. 2.06 Ma at Hole 667A, approximately 100 Kyr earlier than its occurrence in the western tropical Atlantic.
2. The coincidence of the relatively sudden size increase and the prominent change to sinistral coiling during the last 2 Myr give reason to suspect a new, giant *G. menardii* population in the Atlantic Ocean that is different from ancestral smaller forms. If true, this new menardiform would have appeared already in the eastern tropical Pacific since at least 2.58 Ma. It cannot be excluded that they have been dispersed from there throughout the Pacific and Indian Ocean, and then via Agulhas leakage into the Atlantic Ocean.
3. The test-size evolution within the time interval from ca. 8 Ma to 2 Ma in the tropical Atlantic Ocean and Caribbean Sea shows a rough parallel trend with the isotopic εNd proxy for AMOC strength. It suggests that the stronger the AMOC becomes, the larger *G. menardii* grow. This empirical and so far preliminary observation suggests a causal relationship between menardiform test size, thermal upper-water stratification in the habitat of *G. menardii* and AMOC strength. Further studies are needed to confirm this hypothesis.
4. A combination of the Agulhas leakage hypothesis and the AMOC–thermocline hypothesis probably provides the most reasonable explanation for the observed Atlantic test-size evolution since the late Miocene, assuming that both models are related to each other. While the size evolution seemed to be influenced by the strength of the AMOC from 8 Ma to ca. 2 Ma, the Agulhasl leakage could have dispersed a new giant, sinistrally coiling *G. menardii* form from the Pacific Ocean via the Indian Ocean into the Atlantic Ocean within the time interval from 2.58 Ma and 2.057 Ma. The establishment of a new giant form is probably related to a rapid improvement of the environmental conditions for *G. menardii*, such as a strengthening of the thermocline after the onset of the Northern Hemisphere Glaciation in the tropical Atlantic Ocean.
5. At present, the alternative hypothesis of a regional and punctuated evolutionary event cannot be dismissed until more palaeobiogeographic data are available at higher geographic resolution, especially from the Indian Ocean realm.

6. The results of this paper show that for an improvement of a taxonomic distinction between closely related species with high morphological overlap, it is strongly necessary to better include temporal measurements of morphological divergence.

Table 2.1: Studied samples, their depths in metres below seafloor (m.b.s.f.) and age (Ma; Neptune model 0667A.loc95 (using magnetostratigraphic, planktonic foraminiferal and calcareous nannofossil data)) of Hole 667A, following the age depth plot of Fig. 2.2.

Sample	Depth (m.b.s.f.)	Age (Ma)
667A-1H-1, 4.4 cm	0.044	0.003
667A-2H-1, 31 cm	1.61	0.11
667A-2H-2, 16 cm	2.96	0.202
667A-2H-2, 50 cm	3.3	0.225
667A-2H-3, 60 cm	4.9	0.334
667A-2H-4, 33 cm	6.13	0.418
667A-2H-5, 15 cm	7.45	0.51
667A-2H-CC, 2 cm	ca. 10.51	ca. 0.73
667A-3H-2, 85 cm	13.15	0.92
667H-3H-4, 64 cm	15.94	1.12
667A-4H-1, 51 cm	20.81	1.47
667A-4H-3, 120 cm	24.5	1.735
667A-4H-5, 119 cm	27.49	1.95
667A-4H-6, 118 cm	28.98	2.057
667A-5H-2, 106 cm	32.36	2.3
667A-5H-5, 46 cm	36.26	2.58
667A-6H-1, 113 cm	40.43	2.88
667A-6H-4, 115 cm	44.95	3.204
667A-6H-6, 73 cm	47.53	3.39
667A-7H-3, 13 cm	51.93	3.69
667A-7H-6, 40 cm	ca. 56.94	ca.3.99
667A-8H-1, 114 cm	59.44	4.14
667A-8H-4, 15 cm	62.95	4.35
667A-8H-CC, 16 cm	67.46	4.62
667A-9H-2, 66 cm	69.96	4.77
667A-9H-5, 1 cm	73.81	5
667A-10H-1, 98 cm	78.28	5.268
667A-10H-CC, 16 cm	86.46	5.78
667A-11H-2, 142 cm	89.72	6.07
667A-11H-6, 15 cm	94.45	6.49
667A-12H-4, 63 cm	101.43	7.11
667A-13H-1, 114 cm	106.94	7.60
667A-13H-4, 69 cm	110.99	7.96

Code

The modified MorphCol programmes, which were used to process the raw data, as well as their codes, are available at PANGAEA Data Repository (Friesenhagen, 2022) and stored atinternal servers of the Natural History Museum Basel.

Data availability

The full set of derived and raw data and images are deposited at PANGAEA Data Repository (Friesenhagen, 2022) and at internal servers of the Natural History Museum Basel.
The supplied zip archive Supplementary_Material.zip is an extract of all data and contains the necessary data to reproduce the illustrated figures.

Sample availability

The sample material is deposited in the collections of the Natural History Museum Basel, Switzerland.

Competing interests

The author declare that he has no conflict of interest.

Acknowledgements

Thanks go to the Swiss National Science Foundation (SNF) for funding of this project (SNF-No.: 200021_169048/1 and 200021_169048/2).
The International Ocean Discovery Program is greatly acknowledged for providing the sample material used in this study (IODP request #047348IODP from 06 December 2016).
Without the excellent collaboration with the staff of the Natural History Museum Basel and especially Michael Knappertsbusch, curator in the Geoscience-department and initiator and supervisor of this project, this study would not have been possible.
Special thanks go to the three anonymous reviewers and the commentator, Nisan Sariaslan for giving valuable feedback and their help to improve this paper.
I would like to thank Stefanie Schumacher of the PANGAEA Editoral Team for her effort.
Last but not least, I am especially obliged to Loïc Costeur, Christian De Capitani, Thomas Kuhn, Bastien Mennecart, Johannes Pietsch, Diana Isabel Rendon Mera, Anja Studer and Alexandra Viertler for feedback, discussions, corrections and support.

Appendix

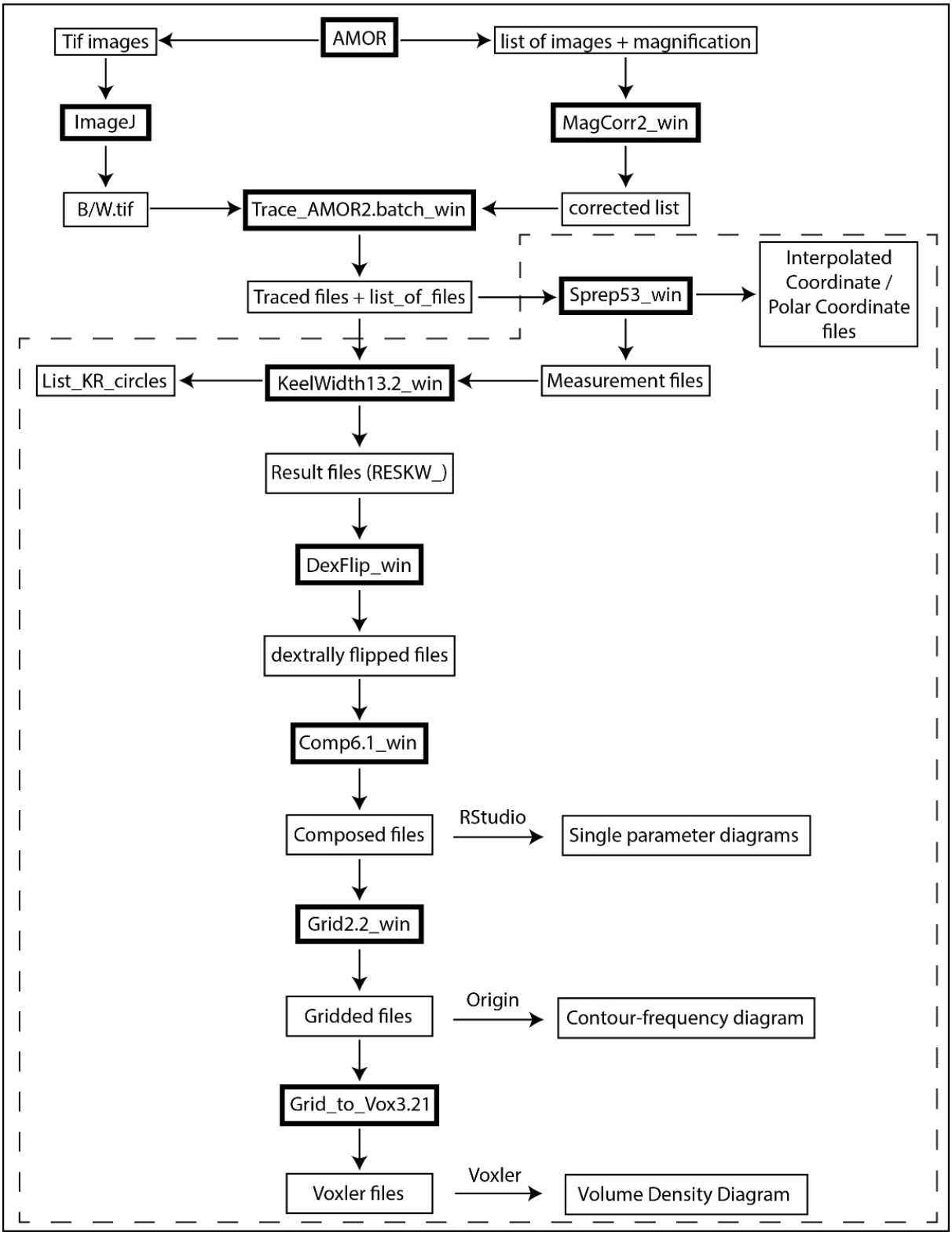

Figure A2.1: Flow chart of MorphCol programmes used. The dashed frame indicates processing steps after sorting of files with respect to species, number of chambers in the final whorl and coiling direction.

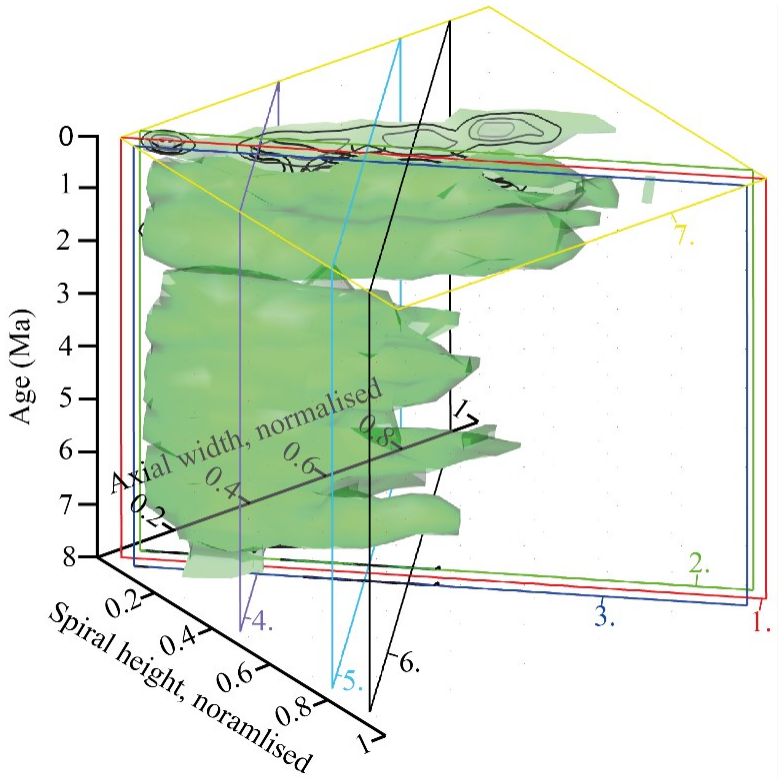

Figure A2.2: VDD of normalised spiral height (δX) versus normalised axial length (δY) during the past 8 Myr for *G. menardii*. The position of the vertical frontal and sagittal sections shown in Fig. 2.10 and Fig. A2.3 - A2.7 are indicated as coloured planes. The iso-surface (value = 0.89447168) represents the density of one specimen per grid cell. The red frontal section (1) is that of Fig. 2.10. Frontal section 2 (green) has an offset value of -0.05 (away from the reader; see Fig. A2.3). Frontal section 3 (blue) has an offset value of +0.05 (towards the reader; see Fig. A2.4). Sagittal section 4 (violet, offset = -0.55; Fig. A2.5), sagittal section 5 (light blue, offset value = -0.23; Fig. A2.6) and sagittal section 6 (black, offset = -0.1; Fig. A2.7) are orthogonally positioned in comparison to sections 1, 2 and 3. The yellow transversal plain at 0.003 Ma (7.) shows the aberrant orientation of the contour frequency diagram in sample 667A-1H-1, 3-4cm (see text). The black lines represent contour intervals of 3.

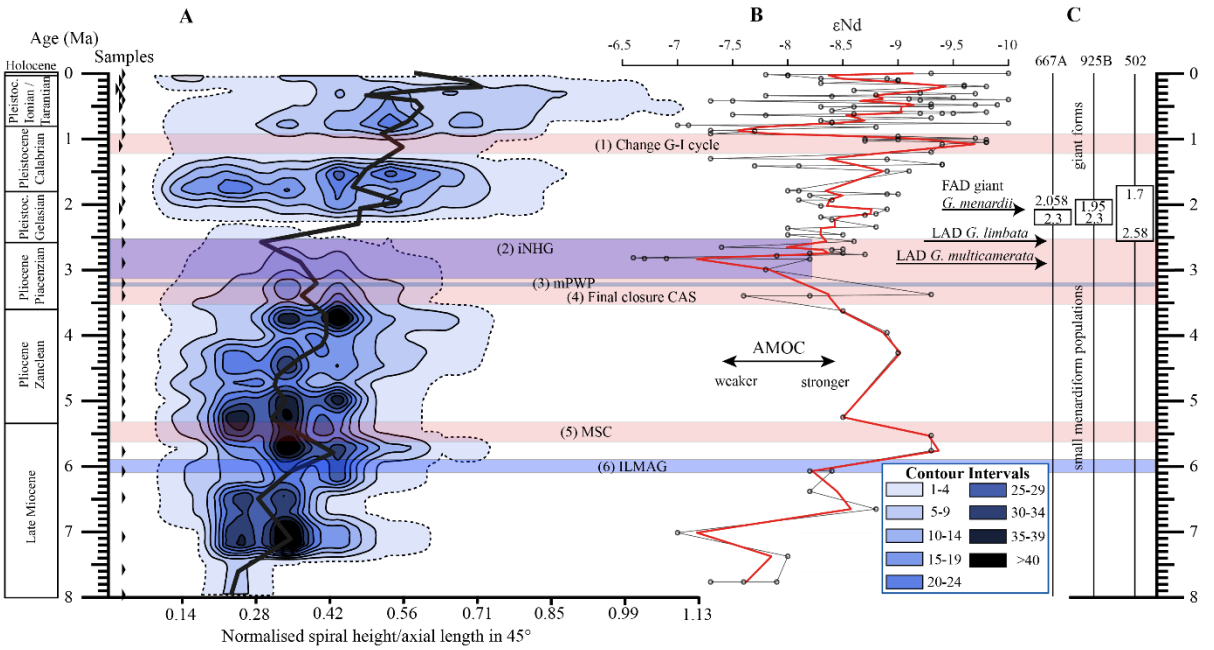

Figure A2.3: Frontal section (offset value = -0.05, away from the reader) through the 45° view on VDD of Hole 667A in a palaeoceanographic context. The dotted line represents the interval line 1, and the solid lines show the contours with an interval of 5. The position of this section within the VDD is plotted in Fig. A2.2. For further explanation, see Fig. 2.10 in the text.

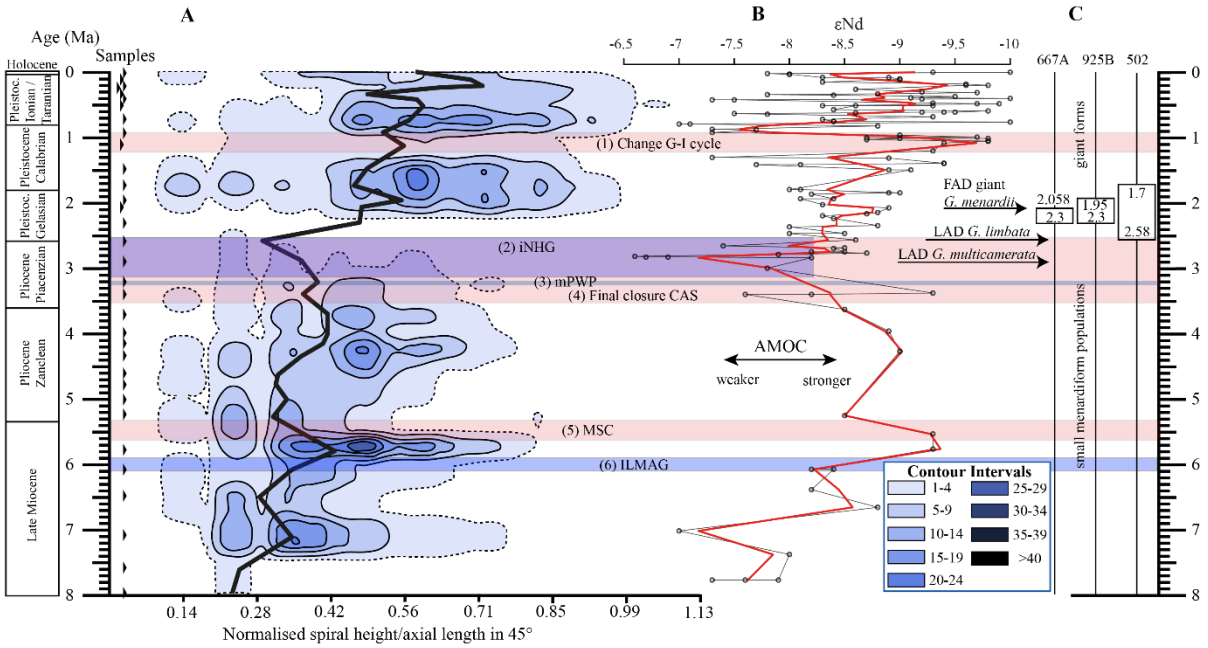

Figure A2.4: Frontal section (offset value = +0.05, towards the reader) through the 45° view on VDD of Hole 667A in a palaeoceanographic context. The dotted line represents the interval line 1, and the solid lines show the contours with an interval of 5. The position of this section within the VDD is plotted in Fig. A2.2. For further explanation, see Fig. 2.10 in the text.

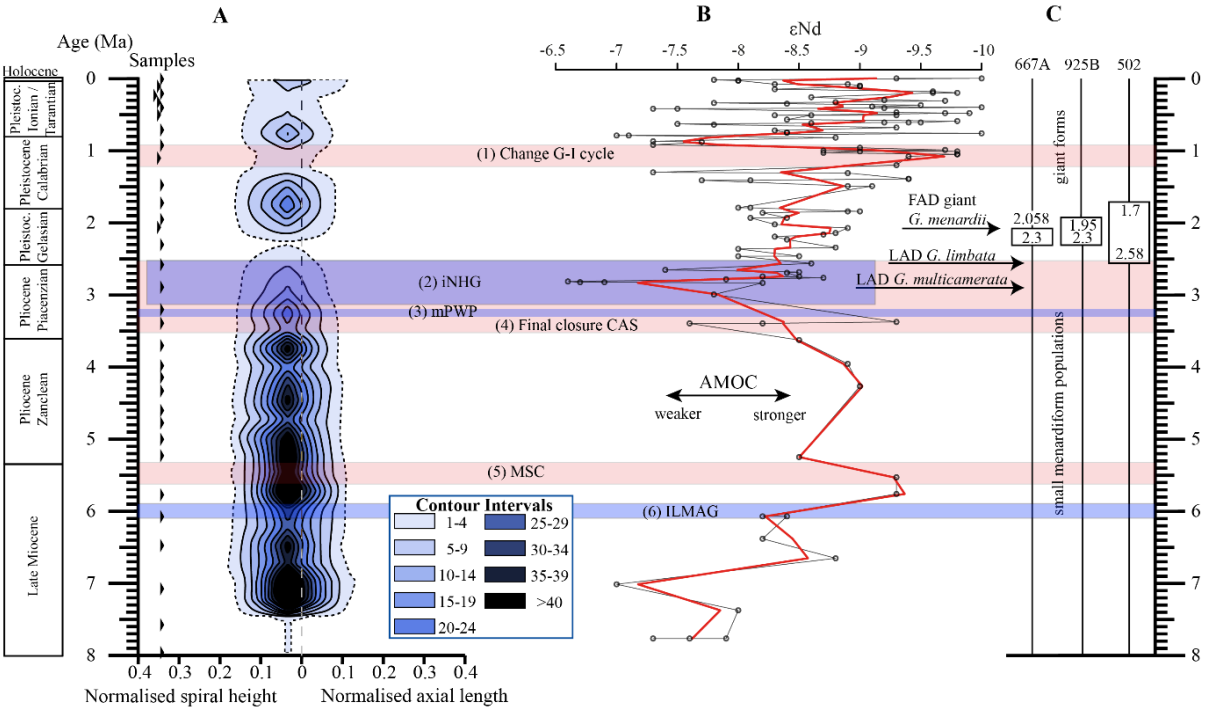

Figure A2.5: Sagittal section with an offset value of -0.55 through the 135° view on the VDD of Hole 667A in a palaeoceanographic context. The dotted line represents the interval line 1, and the solid lines show the contours with an interval of 5. The vertical dashed line at $x = 0$ symbolises the position of the z axis, which is hidden behind the contour plot. The position of this section within the VDD is plotted in Fig. A2.2. For further explanation, see Fig. 2.10 in the text.

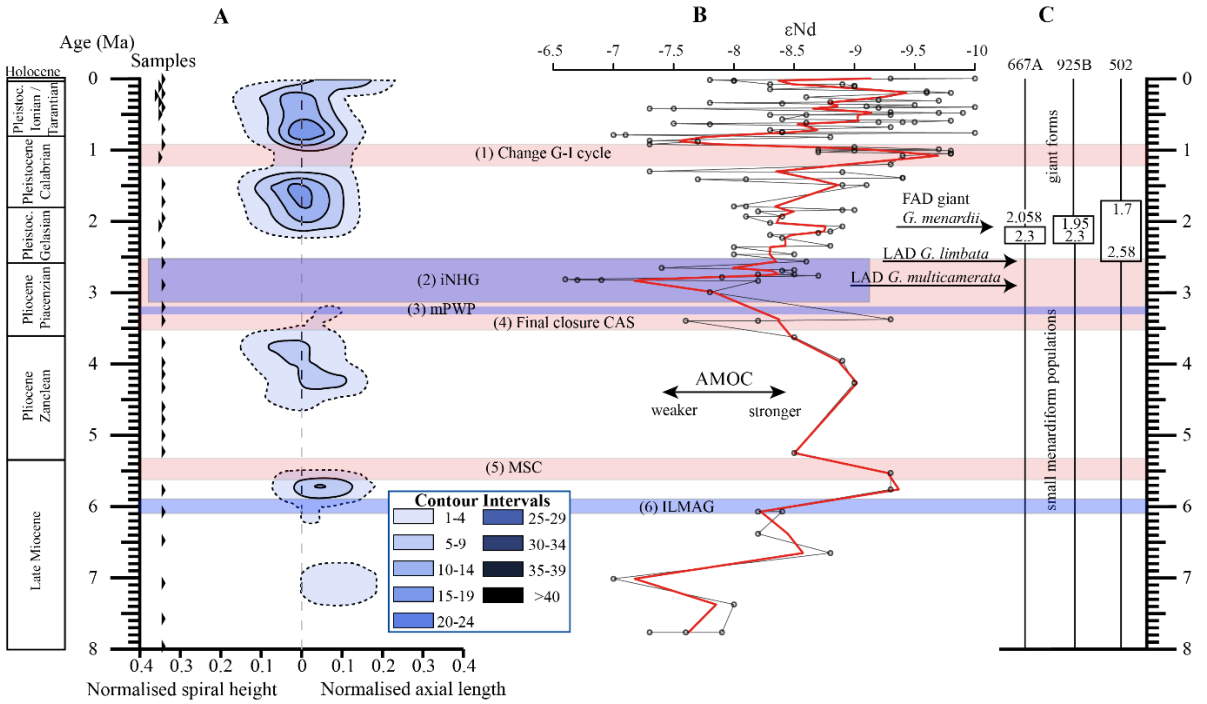

Figure A2.6: Sagittal section with an offset value of -0.23 through the 135° view on the VDD of Hole 667A in a palaeoceanographic context. The dotted line represents the interval line 1, and the solid lines show the contours with an interval of 5. The vertical dashed line at x = 0 symbolises the position of the z-axis, which is hidden behind the contour plot. The position of this section within the VDD is plotted in Fig. A2.2. For further explanation, see Fig. 2.10 in the text.

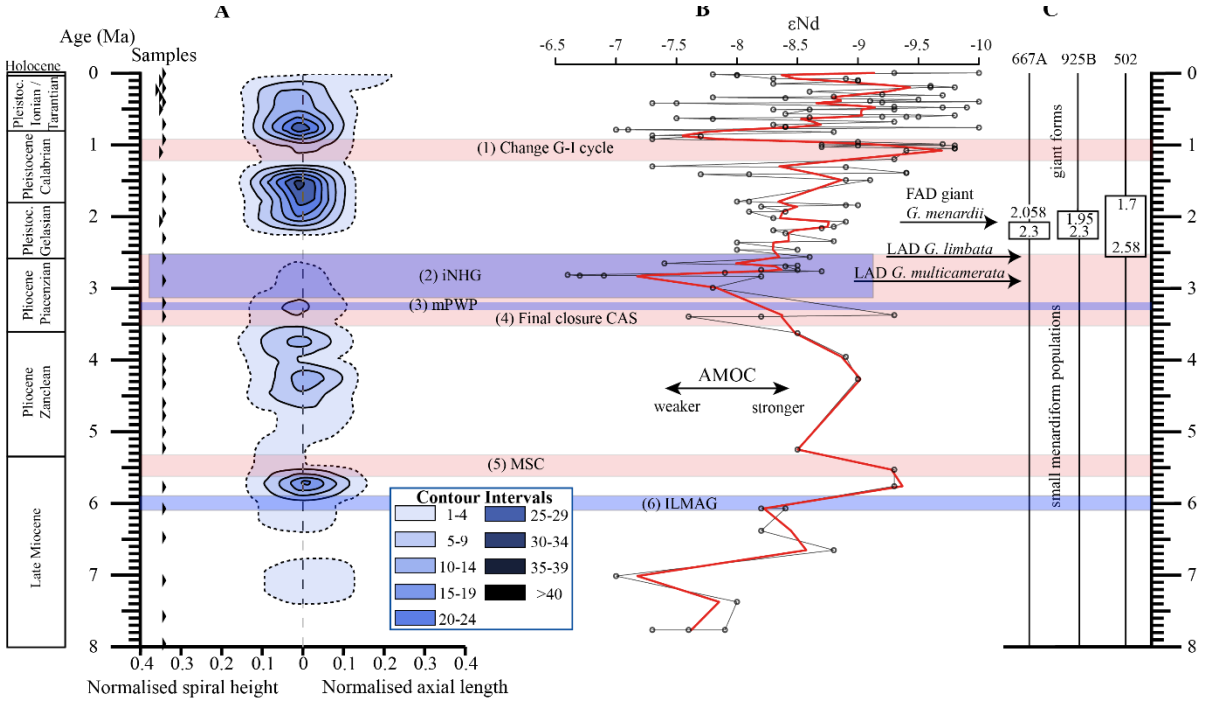

Figure A2.7: Sagittal section with an offset value of -0.1 through the 135° view on the VDD of Hole 667A in a palaeoceanographic context. The dotted line represents the interval line 1, and the solid lines show the contours with an interval of 5. The vertical dashed line at x = 0 symbolises the position of the z axis, which is hidden behind the contour plot. The position of this section within the VDD is plotted in Fig. A2.3. For further explanation, see Fig. 2.10 in the text.

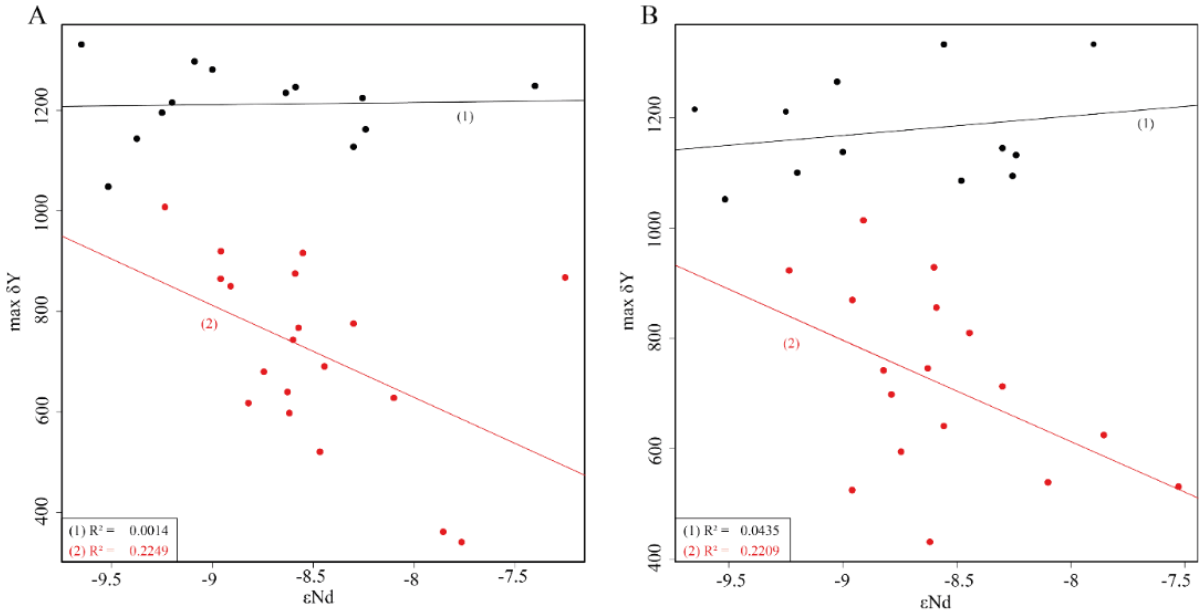

Figure A2.8: Linearly interpolated εNd values derived from Dausmann et al. (2017) plotted versus the maximum axial length (δY) of *G. menardii* from 33 sediment samples from Hole 667A and 29 samples from Hole 925B. The samples have an age of up to 8 Ma (Table 1, this study; Knappertsbusch 2016, respectively). (**A**) Correlation between εNd and δY for all samples of Hole 667A. Black points represent samples with an age between 0 Ma and 2 Ma and red dots samples with an age between 2 Ma and 8 Ma. The black line (1) is the coefficient of determination (R^2) for samples with an age of 0–2 Ma and the red one (2) for samples from 2 to 8 Ma. (**B**) Correlation between εNd and δY for samples of Hole 925B. Red dots represent samples from time intervals 8 Ma to 2 Ma. The left-bottom corner shows the corresponding R^2 and p values.

References

André, A., Weiner, A., Quillévéré, F., Aurahs, R., Morard, R., Douady, C. J., de Garidel-Thoron, T., Escarguel, G., de Vargas, C., and Kucera, M.: The cryptic and the apparent reversed: lack of genetic differentiation within the morphologically diverse plexus of the planktonic foraminifer Globigerinoides sacculifer, Paleobiology, 39, 21–39, doi: https://doi.org/10.5061/dryad.rb06j, 2013.

André, A., Quillévéré, F., Schiebel, R., Morard, R., Howa, H., Meilland, J., and Douady, C. J.: Disconnection between genetic and morphological diversity in the planktonic foraminifer Neogloboquadrina pachyderma from the Indian sector of the Southern Ocean, Marine Micropaleontology, 144, 14–24, doi: https://doi.org/10.1016/j.marmicro.2018.10.001, 2018.

Bard, E. and Rickaby, R. E. M.: Migration of the subtropical front as a modulator of glacial climate, Nature, 460, 380–383, doi: https://doi.org/10.1038/nature08189, 2009.

Bartoli, G., Sarnthein, M., Weinelt, M., Erlenkeuser, H., Garbe-Schönberg, D., and Lea, D. W.: Final closure of Panama and the onset of northern hemisphere glaciation, Earth and Planetary Science Letters, 237, 33–44, doi: https://doi.org/10.1016/j.epsl.2005.06.020, 2005.

Bé, A. W. H., Caron, D. A., and Anderson, O. R.: Effects of feeding frequency on life processes of the planktonic foraminifer Globigerinoides sacculifer in laboratory culture, Journal of the Marine Biological Association of the United Kingdom, 61, 257–277, doi: https://doi.org/10.1017/s002531540004604x, 1981.

Beal, L. M., De Ruijter, W. P. M., Biastoch, A., and Zahn, R.: On the role of the Agulhas system in ocean circulation and climate, Nature, 472, 429–436, doi: https://doi.org/10.1038/nature09983, 2011.

Berger, W. H. and Wefer, G.: Expeditions into the Past: Paleoceanographic Studies in the South Atlantic, in: The South Atlantic, 363–410, Springer Berlin Heidelberg, https://doi.org/10.1007/978-3-642-80353-6_21, 1996.

Berggren, W. A., Kent, D. V., Swisher, C. C. and Aubry, M.-P.: A Revised Cenozoic Geochronology and Chronostratigraphy, in: Geochronology, time scales and global stratigraphic correlation, edited by Aubry, M. P. and Hardenbol, J.,SEPM (Society for Sedimentary Geology), 54, 129–212, https://doi.org/10.2110/pec.95.04.0129, 1995.

Bermúdez, P. J. and Bolli, H. M.: Consideraciones sobre los sedimentos del Mioceno medio al Reciente de las costas central y oriental de Venezuela, Boletin de Geologia, Ministerio de Minas e Hidrocarburos, 10, 137-223, 1969.

Biastoch, A., Böning, C. W., Schwarzkopf, F. U., and Lutjeharms, J. R. E.: Increase in Agulhas leakage due to poleward shift of Southern Hemisphere westerlies, Nature, 462, 495–498, doi: https://doi.org/10.1038/nature08519, 2009.

Billups, K., Ravelo, A. C., Zachos, J. C., and Norris, R. D.: Link between oceanic heat transport, thermohaline circulation, and the Intertropical Convergence Zone in the early Pliocene Atlantic, Geology, 27, 319–322, doi: https://doi.org/10.1130/0091-7613(1999)027<0319:lbohtt>2.3.co;2, 1999.

Blaser, P., Frank, M., and van der Flierdt, T.: Revealing past ocean circulation with neodymium isotopes, Past Global Changes Magazine, 27, 54–55, doi: https://doi.org/10.22498/pages.27.2.54, 2019.

Bolli, H. M.: The direction of coiling in the evolution of some Globorotaliidae, Contributions from the Cushman Foundation for Foraminiferal Research, 1, 82–89, 1950.

Bolli, H. M.: Initial Reports of the Deep Sea Drilling Project, vol. IV, chap. 25. The Foraminifera of Sites 23-31, LEG 4, pp. 577–644, U.S. Government Printing Office, doi: https://doi.org/10.2973/dsdp.proc.4.125.1970, 1970.

Bolli, H. M. and Premoli Silva, I.: Oligocene to Recent Planktonic Foraminifera and Stratigraphy of the Leg 15 Sites in the Caribbean Sea, in: Initial Reports of the Deep Sea Drilling Project, 15, edited by Edgar, N. T. and Kaneps, A. G. andHerring, J. R., vol. 15, pp. 475–497, U.S. Government Printing Office, doi: https://doi.org/10.2973/dsdp.proc.15.110.1973, 1973.

Bolli, H. M. and Saunders, J. B.: Oligocene to Holocene low latitude planktic foraminifera. in: Plankton Stratigraphy, edited by Bolli, H. M., Saunders, J. B. and Perch-Nielsen, K., Cambridge University Press, 1, 155–262, ISBN: 0521235766, 1985.

Broecker, W. S.: The Great Ocean Conveyor. Oceanography, 4, 79–89, https://doi.org/10.5670/oceanog.1991.07, 1991.

Broecker, W. S. and Pena, L. D.: Delayed Holocene reappearance of G. menardii, Paleoceanography and Paleoclimatology, 29, 291–295, doi: https://doi.org/10.1002/2013PA002590, 2014.

Brombacher, A., Wilson, P. A., Bailey, I. and Ezard, T. H. G.: The Breakdown of Static and Evolutionary Allometries during Climatic Upheaval, The American Naturalist, 190, 350–362, doi: https://doi.org/10.1086/692570, 2017.

Brombacher, A., Wilson, P. A., Bailey, I. and Ezard, T. H. G.: The Dynamics of Diachronous Extinction Associated With Climatic Deterioration Near the Neogene/Quaternary Boundary,

Paleoceanography and Paleoclimatology, 36, e2020PA004205, https://doi.org/10.1029/2020PA004205, 2021.

Brown, K. R.: Biogeographic and morphological variation in late Pleistocene to Holocene globorotalid foraminifera, Ph.D. thesis, University of Basel, https://edoc.unibas.ch/780/, 2007.

Buizert, C. and Schmittner, A.: Southern Ocean control of glacial AMOC stability and Dansgaard-Oeschger interstadial duration, Paleoceanography, 30, 1595–1612, doi: https://doi.org/10.1002/2015pa002795, 2015.

Caley, T., Jiraudeau, J., Malaizé, B., Rossignol, L., and Pierre, C.: Agulhas leakage as a key process in the modes of Quaternary climate changes, PNAS, 109, 6835–6839, doi: https://doi.org/10.1073/pnas.1115545109, 2012.

Caromel, A. G. M., Schmidt, D. N., Fletcher, I., and Rayfield, E. J.: Morphological Change During The Ontogeny Of The Planktic Foraminifera, Journal of Micropalaeontology, doi: https://doi.org/10.1144/jmpaleo2014-017, 2016.

Chaisson, W. P.: Vicarious living: Pliocene menardellids between an isthmus and an ice sheet, Geology, 31, 1085–1088, doi: https://doi.org/10.1130/G19834.1, 2003.

Chaisson, W. P. and Ravelo, A. C.: Changes in upper water-column structure at Site 925, late Miocene-Pleistocene: planktonic foraminifer assemblage and isotopic evidence, in: Proceedings of the Ocean Drilling Program, edited by Shackleton, N. J., Curry, W. B., Richter, C., and Bralower, T. J., 154, 255–268, College Station, TX (Ocean Drilling Program), doi: https://doi.org/10.2973/odp.proc.sr.154.105.1997, 1997.

Chan, C.-H., Chan, G. C. H., Leeper, T. J., and Becker, J.: rio: A Swiss-army knife for data file I/O, R package version 0.5.16, https://cran.r-project.org/src/contrib/Archive/rio/ (last access: 07 September 2021), 2018.

Chapman, M. R.: Biotic Response to Global Changes: The Last 145 Million Years, chap. The response of planktonic foraminifera to the Late Pliocene intensification of Northern Hemisphere glaciation, pp. 79–96, 115, Cambridge University Press, https://doi.org/10.1017/CBO9780511535505.007, 2000.

Clemens, S. C., Murray, D. W., and Prell, W. L.: Nonstationary Phase of the Plio-Pleistocene Asian Monsoon, Science, 274, 943–948, doi: https://doi.org/10.1126/science.274.5289.943, 1996.

Clyde-Brockway, C. E.: Inter-Nesting and Post-Nesting Movements and Behavior of East Pacific Green Turtles (Cheloniamydas agassizii) from Playa Cabuyal, Guanacaste, Costa

Rica, Masterthesis, Indiana University - Purdue University Fort Wayne, ProQuest Dissertations Publishing, 2014.

Curry, W. B., Thunell, R. C., and Honjo, S.: Seasonal changes in the isotopic composition of planktonic foraminifera collected in Panama Basin sediment traps, Earth and Planetary Science Letters, 64, 33–43, doi: https://doi.org/10.1016/0012-821x(83)90050-x, 1983.

Dausmann, V., Frank, M., Gutjahr, M., and Rickli, J.: Glacial reduction of AMOC strength and long–term transition in weathering inputs into the Southern Ocean since the mid–Miocene: Evidence from radiogenic Nd and Hf isotopes, Paleoceanography, 32, 265–283, doi: https://doi.org/10.1002/2016PA003056, 2017.

Davis, C. V., Fuqua, L., Pride, C., and Thunell, R.: Seasonal and interannual changes in planktic foraminiferal fluxes and species composition in Guaymas Basin, Gulf of California, Marine Micropaleontology, 149, 78–88, doi: https://doi.org/10.1016/j.marmicro.2019.05.001, 2019.

dos Santos, R. A. L., Prange, M., Castañeda, I. S., Schefuß, E., Mulitza, S., Schulz, M., Niedermeyer, E. M., Damsté, J. S. S., and Schouten, S.: Glacial-interglacial variability in Atlantic meridional overturning circulation and thermocline adjustments in the tropical North Atlantic, Earth and Planetary Science Letters, 300, 407–414, doi: https://doi.org/10.1016/j.epsl.2010.10.030, 2010.

Ericson, D. B. and Wollin, G.: Micropaleontological and isotopical determinations of Pleistocene climates, Micropaleontology, 2, 257–270, doi: https://doi.org/10.2307/1484180, 1956.

Fairbanks, R. G., Sverdlove, M., Free, R., Wiebe, H. P., and Bé, A. W. H.: Vertical distribution and isotopic fractionation of living planktonic foraminifera from the Panama Basin, Nature, 298, 841–844, doi: https://doi.org/10.1038/298841a0, 1982.

Friesenhagen, T.: Archive to the evolutionary study about menardiform globorotallids planktonic foraminifer in the eastern tropical Atlantic ocean ODP Hole 667A, PANGAEA, https://doi.pangaea.de/10.1594/PANGAEA.940563, 2022.

Gasperi, J. T. and Kennett, J. P.: Isotopic evidence for depth stratification and paleoecology of Miocene Planktonic foraminifera-Western equatorial Pacific DSDP site 289, in: Pacific Neogene-Environment, Evolution, and Events, edited by Tsuchi, R. and Ingle, J. C., Tokyo: University of Tokyo Press, 117–147, 1992.

Gasperi, J. T. and Kennett, J. P.: Vertical thermal structure evolution of Miocene surface waters Western equatorial Pacific DSDP Site 289, Marine Micropaleontology, 22, 235–254, doi: https://doi.org/10.1016/0377-8398(93)90046-Z, 1993.

Haarsma, R. J., Campos, E., Hazeleger, W., and Severijns, C.: Influence of the Meridional Overturning Circulation on Tropical Atlantic Climate and Variability, Journal of Climate, 21, 1403–1416, doi: https://doi.org/10.1175/2007JCLI1930.1, 2008.

Haug, G. H. and Tiedemann, R.: Effect of the formation of the Isthmus of Panama on Atlantic Ocean thermohaline circulation, Nature, 393, 673–676, doi: https://doi.org/10.1038/31447, 1998.

Haug, G. H., Tiedemann, R., Zahn, R., and Ravelo, A. C.: Role of Panama uplift on oceanic freshwater balance, Geology, 29, 207–210, doi: https://doi.org/10.1130/0091-7613(2001)029<0207:ROPUOO>2.0.CO;2, 2001.

Haywood, A. M., Dowsett, H. J., and Dolan, A. M.: Integrating geological archives and climate models for the mid-Pliocene warm period, Nature Communications, 7, 10646(2016), doi: https://doi.org/10.1038/ncomms10646, 2016.

Hecht, A. D.: An ecologic model for test size variation in Recent planktonic foraminifera; applications to the fossil record, The Journal of Foraminiferal Research, 6, 295–311, doi: https://doi.org/10.2113/gsjfr.6.4.295, 1976.

Hilbrecht, H. and Thierstein, H. R.: Benthic behavior of planktic foraminifera, Geology, 24, 200–202, doi: https://doi.org/10.1130/0091-7613(1996)024<0200:BBOPF>2.3.CO;2, 1996.

Hull, P. M. and Norris, R. D.: Evidence for abrupt speciation in a classic case of gradual evolution, PNAS, 106, 21224–21229, doi: https://doi.org/10.1073/pnas.0902887106, 2009.

Ivanova, E. V.: Paleoceanography of the Northern Indian Ocean: Linkages to Monsoon and Global Thermohaline Paleocirculation, in: The Global Thermohaline Paleocirculation, pp. 107–145, Springer Netherlands, doi: https://doi.org/10.1007/978-90-481-2415-2_5, 2009.

Karas, C., Nürnberg, D., Bahr, A., Groeneveld, J., Herrle, J. O., Tiedemann, R., and deMenocal, P. B.: Pliocene oceanic seaways and global climate, Scientific Reports, 7, 39842 (2017), doi: https://doi.org/10.1038/srep39842, 2017.

Jackson, J. B. C. and O'Dea, A.: Timing of the oceanographic and biological isolation of the Caribbean Sea from the tropical eastern Pacific Ocean, Bulletin of Marine Science, 89, 779–800, doi: http://dx.doi.org/10.5343/bms.2012.1096, 2013.

Kämpf, J. and Chapman, P.: The Peruvian-Chilean Coastal Upwelling System, in: Upwelling Systems of the World, Springer International Publishing, 161-202, https://doi.org/10.1007/978-3-319-42524-5_5, 2016.

Keller, G.: Depth stratification of planktonic foraminifers in the Miocene ocean, in: Geological Society of America Memoirs, pp. 177–196, Geological Society of America, doi: https://doi.org/10.1130/mem163-p177, 1985.

Kennett, J. P. and Srinivasan, M. S.: Neogene planktonic foraminifera. A phylogenetic atlas, Hutchinson Ross Publishing Company, Stroudsburg, Pa. New York, NY, ISBN: 0879330708, 1983.

Knappertsbusch, M. W.: Morphological variability of Globorotalia menardii (planktonic foraminifera) in two DSDP cores from the Caribbean Sea and the Eastern Equatorial Pacific, Carnets de Geologie, CG2007, hal-00164930, 2007.

Knappertsbusch, M. W.: Morphometric data and processing steps of planktonic foraminifera from DSDP Site 68-502. PANGAEA, https://doi.pangaea.de/10.1594/PANGAEA.863573, 2007b

Knappertsbusch, M. W.: Morphometric data and processing steps of planktonic foraminifera from DSDP Site 68-503. PANGAEA, https://doi.pangaea.de/10.1594/PANGAEA.863575, 2007c

Knappertsbusch, M. W.: Evolution im marinen Plankton, Mitteilungen der Naturforschenden Gesellschaften beider Basel, 13, 3–14, doi: https://doi.org/10.5169/seals-676589, 2011.

Knappertsbusch, M. W., 2015. Raw-data to morphometric investigations about the Neogene planktonic foraminifer Globorotalia menardii and related forms from ODP Hole 154-925B (Céara Rise, western tropical Atlantic). PANGAEA, https://doi.pangaea.de/10.1594/PANGAEA.855900, 2015.

Knappertsbusch, M. W.: Evolutionary prospection in the Neogene planktic foraminifer Globorotalia menardii and related forms from ODP Hole 925B (Ceara Rise, western tropical Atlantic): evidence for gradual evolution superimposed by long distance dispersal?, Swiss Journal of Palaeontology, 135, 205–248, https://doi.org/10.1007/s13358-016-0113-6, 2016.

Knappertsbusch, M. W. and Mary, Y.: Mining morphological evolution in microfossils using volume density diagrams, Palaeontologica Electronica, 15, 1–29, https://doi.org/10.26879/278, 2012.

Knappertsbusch, M. W., Binggeli, D., Herzig, A., Schmutz, L., Stapfer, S., Schneider, C., Eisenecker, J., and Widmer, L.: AMOR – A New System For Automated Imaging Of Microfossils For Morphometric Analyses, Palaeontologia Electronica, 121, 12.2.2T, 2009.

Krijgsman, W., Hilgen, F. J., Raffi, I., Sierro, F. J., and Wilson, D. S.: Chronology, causes and progression of the Messinian salinity crisis, Nature, 400, 652–655, doi: https://doi.org/10.1038/23231, 1999.

Lamb, J. L. and Beard, J. H.: Late Neogene planktonic foraminifers in the Caribbean, Gulf of Mexico and Italian stratotypes, Harold Norman Fisk Memorial Papers, The University of Kansas Paleontological Contributions, 57, 128921806, 1972.

Laxenaire, R., Speich, S., Blanke, B., Chaigneau, A., Pegliasco, C., and Stegner, A.: Anticyclonic Eddies Connecting the Western Boundaries of Indian and Atlantic Oceans, Journal of Geophysical Research: Oceans, 123, 7651–7677, https://doi.org/10.1029/2018JC014270, 2018.

Lazarus, D.: Tempo and mode of morphologic evolution near the origin of the radiolarian lineage Pterocanium prismatium, Paleobiology, 12, 175–189, doi: https://doi.org/10.1017/s0094837300013646, 1986.

Lazarus, D.: Age Depth Plot and Age Maker: Age Modeling of Stratigraphic Sections on the Macintosh Series of Computers, Geobyte, 7(1), 7–14, 5425155, 1992.

Lutjeharms, J. R. E. and Van Ballegooyen, R. C.: The Retroflection of the Agulhas Current, Journal of Physical Oceanography, 18, 1570–1583, doi: https://doi.org/10.1175/1520-0485(1988)018<1570:TROTAC>2.0.CO;2, 1988.

Malmgren, B. A. and Kennett, J. P.: Biometric analysis of phenotypic variation in Recent Globigerina bulloides d'Orbigny in the southern Indian Ocean, Marine Micropaleontology, 1, 3–25, https://doi.org/10.1016/0377-8398(76)90003-7, 1976.

Malmgren, B. A., Berggren, W. A., and Lohmann, G. P.: Evidence for punctuated gradualism in the Late Neogene Globorotalia tumida lineage of planktonic foraminifera, Paleobiology, 9, 377–389, https://doi.org/10.1017/s0094837300007843, 1983.

Manivit, H.: Calcareous Nannofossil Biostratigraphy in Leg 108 Sediments, in: Proc. ODP, Sci. Results 108, edited by Baldauf, J., Heath, G. R., Ruddiman, W. F., and Sarnthein, M., 108, 35–69, College Station, TX (Ocean Drilling Program), https://doi.org/10.2973/odp.proc.sr.108.126.1989, 1989.

Mary, Y.: Morphologic, biogeographic and ontogenetic investigation of Mid-Pliocene menardellids (planktonic foraminifera), Ph.D. thesis, University of Basel, https://doi.org/10.5451/unibas-006194467, 2013.

McCarthy, G., Smeed, D., Cunningham, S., and Roberts, C.: Atlantic Meridional Overturning Circulation, MCCIP Science Review 2017, MCCIP, Lowestoft, UK, 15–21, https://doi.org/10.14465/2017.ARC10.002-ATL, 2017.

Merino, M. and Monreal-Gómez, M. A.: Ocean Currents and Their Impact on Marine Life, in: Marine Ecology, edited by Duarte, C. M. and Helgueras, A. L., Eolss Publishers Co. Ltd., Oxford, 52–74, ISBN: 978-1-84826-464-9, 2009.

Merle, J.: Seasonal Variability of Subsurface Thermal Structure in the Tropical Atlantic Ocean, in: Hydrodynamics of The Equatorial Ocean, Proceedings of The 14th International Liege

Colloquium on Ocean Hydrodynamics, 31–49, Elsevier, https://doi.org/10.1016/s0422-9894(08)70626-3, 1983.

Mohtadi, M., Steinke, S., Groeneveld, J., Fink, H. G., Rixen, T., Hebbeln, D., Donner, B., and Herunadi, B.: Low-latitude control on seasonal and interannual changes in planktonic foraminiferal flux and shell geochemistry off south Java: A sediment trap study, Paleoceanography, 24, PA1201, https://doi.org/10.1029/2008pa001636, 2009.

Möller, K. O., John, M. S., Temming, A., Floeter, J., Sell, A. F., Herrmann, J.-P., and Möllmann, C.: Marine snow, zooplankton and thin layers: indications of a trophic link from small-scale sampling with the Video Plankton Recorder, Marine Ecology Progress Series, 468, 57–69, https://doi.org/10.3354/meps09984, 2012.

Naidu, P. D. and Malmgren, B. A.: Monsoon upwelling effects on test size of some planktonic foraminiferal species from the Oman Margin, Arabian Sea, Paleoceanography, 10, 117–122, https://doi.org/10.1029/94pa02682, 1995.

Niemitz, M. D. and Billups, K.: Millennial-scale variability in western tropical Atlantic surface ocean hydrography during the early Pliocene, Marine Micropaleontology, 54, 155–166, https://doi.org/10.1016/j.marmicro.2004.10.001, 2005.

Norris, R. D.: Hydrographic and tectonic control of plankton distribution and evolution, in: Reconstruction Ocean History, edited by Abrantes, F. and Mix, A., Springer US, 173–193, https://doi.org/10.1007/978-1-4615-4197-4, 1999.

O'Dea, A., Lessios, H. A., Coates, A. G., Eytan, R. I., Restrepo-Moreno, S. A., Cione, A. L., Collins, L. S., de Queiroz, A., Farris, D. W., Norris, R. D., Stallard, R. F., Woodburne, M. O., Aguilera, O., Aubry, M.-P., Berggren, W. A., Budd, A. F., Cozzuol, M. A., Coppard, S. E., Duque-Caro, H., Finnegan, S., Gasparini, G. M., Grossman, E. L., Johnson, K. G., Keigwin, L. D., Knowlton, N., Leigh, E. G., Leonard-Pingel, J. S., Marko, P. B., Pyenson, N. D., Rachello-Dolmen, P. G., Soibelzon, E., Soibelzon, L., Todd, J. A., Vermeij, G. J. and Jackson, J. B. C.: Formation of the Isthmus of Panama, Science Advances, 2, e160088, https://doi.org/10.1126/sciadv.1600883, 2016.

Ortiz, J. D., Mix, A. C., and Collier, R. W.: Environmental control of living symbiotic and asymbiotic foraminifera of the California Current, Paleoceanography, 10, 987–1009, 10.1029/95pa02088, 1995.

Pearson, P. N. and Coxall, H. K.: Origin of the Eocene Planktonic Foraminifer Hantkenina by Gradual Evolution, Palaeontology, 57, 243–267, https://doi.org/10.1111/pala.12064, 2014.

Peeters, F. J. C., Acheson, R., Brummer, G.-J. A., de Ruijter, W. P. M., Schneider, R. R., Ganssen, G. M., Ufkes, E., and Kroon, D.: Vigorous exchange between the Indian and

Atlantic oceans at the end of the past five glacial periods, Nature, 430, 661–665, https://doi.org/10.1038/nature02785, 2004.

Pelegrí, J. L. and Benazzouz, A.: Oceanographic and biological features in the Canary Current Large Marine Ecosystem, Vol. 115, chap. 3.4, Coastal upwelling off North–West Africa, IOC–UNESCO, Paris, IOC Technical Series Technical Series, 93–103, IOC/2015/TS/115 REV, http://hdl.handle.net/10261/128554TS4 (last access: 09 October 2019), 2015.

Pfuhl, H. A. and Shackleton, N. J.: Changes in coiling direction, habitat depth and abundance in two menardellid species, Marine Micropaleontology, 50, 3–20, https://doi.org/10.1016/s0377-8398(03)00063-x, 2004.

Portilho-Ramos, R. D. C., Barbosa, C. F., and Rios-Netto, A. M.: Planktonic foraminiferal variations in the southwestern Atlantic since the last glacial-interglacial cycle, Palaios, 29, 38–44, http://dx.doi.org/10.2110/palo.2012.104, 2014.

Prairie, J. C., Ziervogel, K., Camassa, R., McLaughlin, R. M., White, B. L., Dewald, C., and Arnosti, C.: Delayed settling of marine snow: Effects of density gradient and particle properties and implications for carbon cycling, Marine Chemistry, 175, 28–38, https://doi.org/10.1016/j.marchem.2015.04.006, 2015.

Ravelo, A. C. and Fairbanks, R. G.: Oxygen Isotopic Composition of Multiple Species of Planktonic Foraminifera: Recorders of the Modern Photic Zone Temperature Gradient, Paleoceanography, 7, 815–831, https://doi.org/10.1029/92pa02092,1992.

Ravelo, A. C., Fairbanks, R. G., and Philander, S. G. H.: Reconstructing tropical Atlantic hydrography using planktonic foraminifera and an ocean model, Paleoceanography, 5, 409–431, https://doi.org/10.1029/pa005i003p00409, 1990.

Raymo, M. E.: The Initiation of Northern Hemisphere Glaciation, Annual Review of Earth and Planetary Sciences, 22, 353–383, https://doi.org/10.1146/annurev.ea.22.050194.002033, 1994.

Regenberg, M., Nielsen, S. N., Kuhnt, W., Holbourn, A., Garbe-Schönberg, D., and Andersen, N.: Morphological, geochemical, and ecological differences of the extant menardiform planktonic foraminifera Globorotalia menardii and Globorotalia cultrata, Marine Micropaleontology, 74, 96–107, https://doi.org/10.1016/j.marmicro.2010.01.002, 2010.

Revelle, W.: psych: Procedures for Psychological, Psychometric, and Personality Research, Northwestern University, Evanston, Illinois, https://CRAN.R-project.org/package=psych, R package version 1.8.12, 2018.

Rinker, T. W. and Kurkiewicz, D.: pacman: Package Management for R, Buffalo, New York, http://github.com/trinker/pacman, R. package version 0.5.0, 2018.

Rillo, M. C., Miller, C. G., Kucera, M. and Ezard, T. H. G.: Predictability of intraspecific size variation in extant planktonic foraminifera, bioRxiv, https://doi.org/10.1101/468165, 2018.

Robinson, R.: Coiling Directions in Planktonic Foraminifera from the Coastal Group of Jamaica, Gulf Coast Association of Geological Societies Transactions, 19, 555–558, 1969.

Rosenzweig, M. L. and McCord, R. D.: Incumbent replacement: evidence for long-term evolutionary progress, Paleobiology, 17, 202–213, https://doi.org/10.1017/s0094837300010563, 1991.

RStudio Team: RStudio: Integrated Development Environment for R, RStudio, PBC., Boston, MA, https://www.rstudio.com/ (last access: 25 May 2021), 2020.

Rühs, S., Durgadoo, J. V., Behrens, E., and Biastoch, A.: Advective timescales and pathways of Agulhas leakage, Geophysical Research Letters, 40, 3997–4000, https://doi.org/10.1002/grl.50782, 2013.

Savin, S. M., Abel, L., Barrera, E., Hodell, D., Kennett, J. P., Murphy, M., Keller, G., Killingley, J., and Vincent, E.: The evolution of Miocene surface and near-surface marine temperatures: Oxygen isotopic evidence, in: Geological Society of America Memoirs, Geol. Soc. Am., 163, 49–82, https://doi.org/10.1130/mem163-p49, 1985.

Schiebel, R. and Hemleben, C.: Classification and Taxonomy of Extant Planktic Foraminifers. In: *Planktic Foraminifers in the Modern Ocean*. Springer Berlin Heidelberg, 11–110, doi: https://doi.org/10.1007/978-3-662-50297-6, 2017

Schmidt, D. N., Thierstein, H. R., Bollmann, J., and Schiebel, R.: Abiotic Forcing of Plankton Evolution in the Cenozoic, Science, 303, 207–210, https://doi.org/10.1126/science.1090592, 2004.

Schmidt, D. N., Lazarus, D., Young, J. R., and Kucera, M.: Biogeography and evolution of body size in marine plankton, Earth-Science Reviews, 78, 239–266, https://doi.org/10.1016/j.earscirev.2006.05.004, 2006.

Schweitzer, P. N. and Lohmann, G. P.: Ontogeny and habitat of modern menardiiform planktonic foraminifera, The Journal of Foraminiferal Research, 21, 332–346, https://doi.org/10.2113/gsjfr.21.4.332, 1991.

Sexton, P. F. and Norris, R. D.: Dispersal and biogeography of marine plankton: Long-distance dispersal of the foraminifer Truncorotalia truncatulinoides, Geology, 36, 899–902, https://doi.org/10.1130/G25232A.1, 2008.

Sexton, P. F. and Norris, R. D.: High latitude regulation of low latitude thermocline ventilation and planktic foraminifer populations across glacial-interglacial cycles, Elsevier, 311, 69–81, https://doi.org/10.1016/j.epsl.2011.08.044, 2011.

Shipboard Scientific Party: Site 667, in: Ruddiman, W. and Sarnthein, M. and Baldauf, J. et al, Proc. ODP, Init. Repts. (Pt. B), edited by Stewart, S. K. and Rose, W. D., 108, 833–930, College Station, TX (Ocean Drilling Program), https://doi.org/10.2973/odp.proc.ir.108.112.1988, 1988.

Shipboard Scientific Party: Facies Patterns and Authigenic Minerals of Upwelling Deposits off Southwest Africa, in: Proceedings of the Ocean Drilling Program 175 Initial Reports, edited by Baez, L. A. and Scroggs, J. M., 175, 7–25, College Station, TX (Ocean Drilling Program), Ocean Drilling Program, https://doi.org/10.2973/odp.proc.ir.175.116.1998, 1998.

Shipboard Scientific Party: Site 1237, in: Proc. ODP, Init. Repts., 202, edited by Tiedemann, R., Mix, A. C., Richter, C., and Ruddiman, W. F., 202, 1–107, College Station, TX (Ocean Drillng Program), https://doi.org/10.2973/odp.proc.ir.202.108.2003, 2003.

Spencer-Cervato, C. and Thierstein, H. R.: First appearance of Globorotalia truncatulinoides: cladogenesis and immigration, Marine Micropaleontology, 30, 267–291, https://doi.org/10.1016/s0377-8398(97)00004-2, 1997.

Steph, S., Tiedemann, R., Groeneveld, J., Sturm, A., and Nürnberg, D.: 12. Pliocene Changes in Tropical East Pacific Upper Ocean Stratification: Response to Tropical Gateways?, in: Proc. ODP, Sci. Results, 202, 1–51, College Station, TX (Ocean Drilling Program), https://doi.org/10.2973/odp.proc.sr.202.211.2006, 2006.

Stewart, D. R. M.: Evolution of Neogene globorotaliid foraminifera and Miocene climate change, Doctoral dissertation, University of Bristol, https://ethos.bl.uk/OrderDetails.do?uin=uk.bl.ethos.288306 (last access: 09 December 2014), 2003.

Thunell, R. C. and Reynolds, L. A.: Sedimentation of planktonic foraminifera: Seasonal changes in species flux in the Panama Basin, Micropaleontoloty, 30, 243–262, https://doi.org/10.2307/1485688, 1984.

Tiedemann, R., Sarnthein, M., and Shackleton, N. J.: Astronomic timescale for the Pliocene Atlantic 18O and dust flux records of Ocean Drilling Program Site 659, Paleoceanography, 9, 619–638, https://doi.org/10.1029/94pa00208, 1994.

Timmermann, A., Okumura, Y., Clement, A., Dong, B., Guilyardi, E., Hu, A., Jungclaus, J. H., Renold, M., Stocker, T. F., Stouffer, R. J., Sutton, R., Xie, S.-P., and Yin, J.: The Influence of a Weakening of the Atlantic Meridional Overturning Circulation on ENSO, Journal of Climate, 20, 4899–4919, https://doi.org/10.1175/JCLI4283.1, 2007.

Todd, C. L., Schmidt, D. N., Robinson, M. M. and De Schepper, S.: Planktic Foraminiferal Test Size and Weight Response to the Late Pliocene Environment, Paleoceanography and Paleoclimatology, 35, e2019PA003738, https://doi.org/10.1029/2019PA003738, 2020.

van Sebille, E., Beal, L. M., and Johns, W. E.: Advective Time Scales of Agulhas Leakage to the North Atlantic in Surface Drifter Observations and the 3D OFES Model, Journal of Physical Oceanography, 41, 1026–1034, https://doi.org/10.1175/2011JPO4602.1, 2011.

Villar, E., Farrant, G. K., Follows, M., Garczarek, L., Speich, S., Audic, S., Bittner, L., Blanke, B., Brum, J. R., Brunet, C., Casotti, R., Chase, A., Dolan, J. R., d'Ortenzio, F., Gattuso, J.-P., Grima, N., Guidi, L., Hill, C. N., Jahn, O., Jamet, J.-L., Le Goff, H., Lepoivre, C., Malviya, S., Pelletier, E., Romagnan, J.-B., Roux, S., Santini, S., Scalco, E., Schwenck, S. M., Tanaka, A., Testor, P., Vannier, T., Vincent, F., Zingone, A., Dimier, C., Picheral, M., Searson, S., Kandels-Lewis, S., Oceanscoordinators, T., Acinas, S. G., Bork, P., Boss, E., de Vargas, C., Gorsky, G., Ogata, H., Pesant, S., Sullivan, M. B., Sunagawa, S., Wincker, P., Karsenti, E., Bowler, C., Not, F., Hingamp, P., and Iudicone, D.: Environmental characteristics of Agulhas rings affect interocean plankton transport, Science, 348, 1261447, https://doi.org/10.1126/science.1261447, 2015.

Wade, B. S., Pearson, P. N., Berggren, W. A., and Pälike, H.: Review and revision of Cenozoic tropical planktonic foraminiferal biostratigraphy and calibration to the geomagnetic polarity and astronomical time scale, Earth-Science Reviews, 104, 111–142, https://doi.org/10.1016/j.earscirev.2010.09.003, 2011.

Wade, B. S., Poole, C. R. and Boyd, J. L.: Giantism in Oligocene planktonic foraminifera Paragloborotalia opima: Morphometric constraints from the equatorial Pacific Ocean, Newsletters on Stratigraphy, 49, 421–444, https://doi.org/10.1127/nos/2016/0270, 2016.

Weaver, P. P. E. and Raymo, M. E.: Late Miocene to Holocene planktonic foraminifers from the equatorial Atlantic, Leg 108, in: Proc. ODP, Sci. Results 108, edited by Baldauf, J., Heath, G. R., Ruddiman, W. F., and Sarnthein, M., 108, 71–91, College Station, TX (Ocean Drilling Program), https://doi.org/10.2973/odp.proc.sr.108.130.1989, 1989.

Wejnert, K. E., Pride, C. J., and Thunell, R. C.: The oxygen isotope composition of planktonic foraminifera from the Guaymas Basin, Gulf of California: Seasonal, annual, and interspecies variability, Marine Micropaleontology, 74, 29–37, https://doi.org/10.1016/j.marmicro.2009.11.002, 2010.

Wickham, H.: ggplot2: Elegant Graphics for Data Analysis, Springer-Verlag New York, https://doi.org/10.1007/978-3-319-24277-4, 2016.

Wickham, H. and Bryan, J.: readxl: Read Excel Files, https://CRAN.R-project.org/-package=readxl, R package version 1.3.1, 2019.

Wolff, T., Mulitza, S., Rühlemann, C., and Wefer, G.: Response of the tropical Atlantic thermocline to late Quaternary trade wind changes, Paleoceanography, 14, 374–383, https://doi.org/10.1029/1999PA900011, 1999.

Woodhouse, A., Jackson, S. L., Jamieson, R. A., Newton, R. J., Sexton, P. F. and Aze, T.: Adaptive ecological niche migration does not negate extinction susceptibility, Research Square, 11, 15411, https://doi.org/10.1038/s41598-021-94140-5, 2021.

Chapter 3: Morphometric measurements of the planktonic foraminifer *Globorotalia menardii* from the Mozambique Channel provide new evidence for the Agulhas leakage hypothesis

Thore Friesenhagen[1,2]

Michael Knappertsbusch[1]

[1]Natural History Museum Basel, Augustinergasse 2, 4001 Basel, Switzerland

[2] Department Umweltwissenschaften, University of Basel, Bernoullistrasse 32, CH-4056 Basel

Abstract

This study presents a new dataset of morphometric measurements of the planktonic foraminiferal *G. menardii-G. limbata-G. multicamerata* lineage from Hole U1476A in the Mozambique Channel (western Indian Ocean) for the last 6.5 Myr, for which an improved version of the 'Automated Measurement System for Shell Morphology' (System AMOR 2) was used. The dataset was collected in order to discuss the possibility of the Agulhas Leakage hypothesis. In this hypothesis the prominent test-size increase of *G. menardii*, observed in the early Pleistocene of the tropical Atlantic Ocean and the Caribbean Sea, is explained by episodic dispersal of *G. menardii* from the Indian Ocean into the Atlantic Ocean via a hypothesized strengthening phase of the Agulhas Leakage after the initiation of the Northern Hemisphere Glaciation. Simultaneously, the size increase in the Atlantic Ocean came along with a permanent change to predominant sinistral coiling of tests of *G. menardii* populations and probably marks the appearance of a new, giant *G. menardii* form (axial length >1000 µm). Therefore, an indication in favour to the Agulhas Leakage hypothesis would be, that the first appearance of this sinistral type in the Indian Ocean leads the first appearance in the Atlantic Ocean. Indeed, the first specimen of the giant form is already observed at 2.95 Ma, ca. 0.9 Myr earlier than its first appearance in the Atlantic Ocean. Hence, the Agulhas Leakage hypothesis for *G. menardii* is a reasonable explanation for the enigmatic sudden size increase in the Atlantic Ocean around ca. 2 Ma.

Superposed to this pattern is the size evolution of the Indian Ocean *G. menardii* populations, which presumably happened in concert with major changes of the Indian Monsoon system.

3.1 Introduction

Planktonic foraminifera (PF) are ideal candidates for evolutionary studies (e.g. Lohmann and Malmgren, 1983; Malmgren et al., 1983; Leckie, 1983; Norris, 1999; Majewski, 2002; Schmidt et al., 2004; Hull and Norris, 2009) and palaeoceanographic reconstructions (e.g. Poore, 1981; Keller, 1985; Ravelo et al., 1990; Wolff et al., 1999; Chaisson and Ravelo, 1997; Caley et al., 2012; Caley et al., 2014). However, the detailed forces and processes that lead to morphological changes, as for example the test size, are still poorly known. Traditionally, the increase in the long-term mean test size in PF is attributed to adaptations to new environmental niches, such as for example during a general increase in water column stratification within the last 12 Ma (Schmidt et al., 2004; Schmidt et a., 2006). On a shorter timescale, shifts in season lengths can

lead to shifts in reproduction as well as growth and can also influence variations in the maximum test sizes in PF (Hecht, 1976; Ortiz et al., 1995; Schmidt et al., 2006).

An interesting case is the test-size evolution of the PF *Globorotalia menardii* in the Atlantic Ocean during the early Pleistocene (Knappertsbusch, 2016; Friesenhagen, 2022a): It shows a relatively rapid increase of maximum test sizes, that more than doubles within 0.5 Myr from 2.5 Ma to 2 Ma. These observations raise the question for the precise cause and mechanism behind that pattern.

Knappertsbusch (2016) proposed two possible explanations:

Hypothesis (I) proposes the dispersal of specimens of a new *G. menardii* type during the Gelasian, that previously developed in the Indian-Pacific realm and entered the Atlantic via an episodically strengthened Agulhas Leakage after the initiation of the Northern Hemisphere Glaciation (NHG). In the modern South Atlantic, giant eddies shed off from the Agulhas main current in the cape region off Africa and further drift west to northwest. Agulhas rings are known to transport (sub-)tropical Indian Ocean biota into the Atlantic Ocean (Berger and Wefer, 1996; Norris, 1999; Peeters et al., 2004; Villar et al., 2015) along the south-eastern coast of Africa, which otherwise would not be able to surpass the transitional zone. Modern *G. menardii* is strongly limited to tropical and subtropical waters and usually not known to be viable in waters south of 30°S (Berger and Wefer, 1996; Caley et al., 2012; Schiebel and Hemleben, 2017 and references therein). Its tropical preference makes it a perfect tracer for reconstructing the initiation, path, and strength of the Agulhas Leakage (Wright and Thunell, 1988; Rau et al., 2002; Caley et al., 2012; Santos et al., 2014).

Hypothesis (II) proposes a sudden increase in the evolutionary rate of regional *G. menardii* populations, which is limited to the Atlantic Ocean. Under the influence of the NHG, severe changes in water stratification and rapid establishment of a new ecological niche for *G. menardii* would have triggered the enigmatic and relatively rapid morphological size increase in the Atlantic Ocean, thereby leaving behind a pattern of punctuated gradualism in the underlying sediments (Malmgren et al., 1983). Such rapid morphological patterns were observed in other PF species (Wei and Kennett, 1988; Malmgren et al., 1983; Hull and Norris, 2009; Pearson and Coxall, 2014) and Radiolaria (Lazarus, 1986), which were always attributed to rapid changes of evolutionary rate.

Such rapid evolution may be considered as morphological responses after the “bottle-neck” effect of the NHG, where extreme conditions prevailed in periods of cold chills (Raymo, 1994; Tiedemann, 1994). But are these extreme conditions sufficient to explain the unique nature of this sudden size increase, that seemingly were restricted to the Atlantic?

This study at first documents the pattern of test-size evolution of *G. menardii* from an Indian Ocean source, e.g. right way in the source area of the Agulhas current system. International Ocean Discovery Program (IODP) Hole U1476A is located northwest of the Mozambique Channel, an area known of intense formation of the Agulhas current and siphoning tropical waters from the western Indian Ocean. The expectation is that giant *G. menardii* with sinistral coiling preference can be observed at Site U1476 prior to large forms on the Atlantic Site 667 at 2.058 Ma (Friesenhagen, 2022a).

The investigation of Indian Ocean populations may also serve as a test for the idea that the long-term size-evolution trends of *G. menardii* are modulated by more regional or local changes of environmental conditions, also in a large ocean (Friesenhagen, 2022a). For example, in the Atlantic Ocean, the strength of the Atlantic Meridional Overturning Circulation (AMOC) was proposed to modulate test-size evolution over longer geological time. In the present case this role is taken by the Indian Monsoon variability modulating size evolution. In the modern Indian Monsoon system the seasonal signature is driven by shifts of pressure cells, which themselves are caused by changes in the solar radiation (Ivanova, 2009). During summer, the pressure gradient between the Southern Indian Ocean High and the continental South Asian Low induces strong winds from SW to NE leading to precipitations overland (Summer monsoon). Off Somalia and in the Arabian Sea, upwelling is caused by the Findlater Jet, that blows northwards and strongly influences the northern Indian Ocean surface circulation. During winter, the South Asian Low is replaced by the Tibetan High and establishes the North Western or Indian Winter monsoon (IWM) (Ivanova, 2009).

The related large-scale changes in seasonal turnover and re-structuring of the vertical water masses should also be visible in the test-size trend of *G. menardii*, the study of which remains challenging but interesting.

3.2 Material and Methods

3.2.1 IODP Hole U1476A and Oceanographic Setting

Hole U1476A is located on Davie Ridge in the northern part of the Mozambique Channel (15°49.25′S, 41°46.12′E; Fig. 3.1) at a water depth of 2166 m.b.s.l. and was drilled during IODP LEG 361 (Hall et al., 2017a). Several strategic advantages make this site a suitable study location for this project:

(1) it is in the middle of the Mozambique Channel in subtropical waters, close to source area of the Agulhas Current (Schouten et al., 2003; Tew-Kai and Marsac, 2009; Ivanova, 2009). If the adjacent subtropical IO is the origin of the giant *G. menardii* type, populations were transported

along the route of the Agulhas Current (AC) into waters off South Africa and in the South Atlantic. (2) The sedimentary recovery is complete and of high quality, with a continuous record until 7 Ma. There are no indications of reworking, hiatuses or turbidites (Hall et al., 2017b; Tangunan et al., 2018), site chapter to U1476). (3) Sediments were deposited above the CCD and show mostly an excellent preservation of PF (Hall et al., 2017b).

A challenge is the rather complex oceanic setting as "one of the most turbulent areas in the world ocean" (Ternon et al., 2014). Seasonal changes in the sea surface temperature (SST) (Tew-Kai and Marsac, 2009) and productivity (Ternon et al., 2014) are induced by the alternation of the Indian summer monsoon (ISM) and the Indian winter monsoon (IWM). Southward drifting cyclonic and anticyclonic eddies further increase the complexity of the oceanographic setting (Boebel et al., 2003; Schouten et al., 2003; Fallet et al., 2010; Lebourges-Dhaussy et al., 2014). These eddies lead to strong fluctuations in nutrients, productivity (Lebourges-Dhaussy et al., 2014; Ternon et al., 2014) and vertical position of the seasonal mixed layer depth (Lebourges-Dhaussy et al., 2014). Furthermore, a local reduction in the

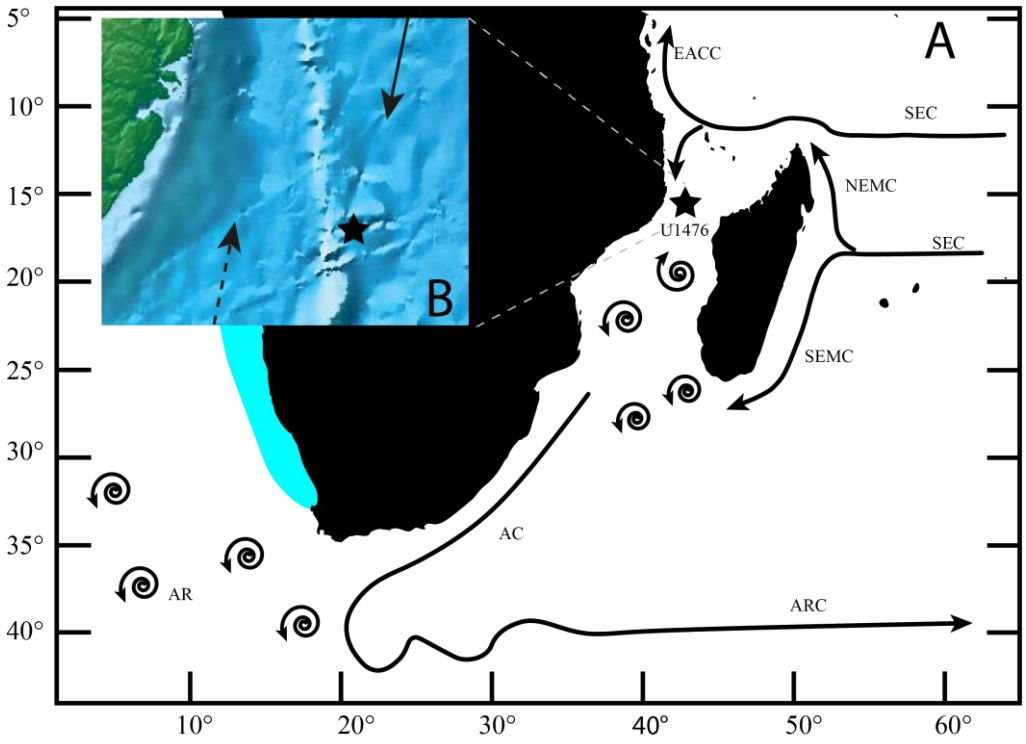

Figure 3.1: (**A**) Map of the south-western Indian Ocean and the eastern South Atlantic Ocean, showing the location of IODP Site U1476 and major oceanographic features of this area, modified after Fig. F1 in Hall et al. (2017b). The star marks the location of Site U1476, while the arrows symbolise the most important surface currents following Beal et al. (2011) and Tangunan et al. (2018). Cyclonic and anticyclonic gyres are represented by clockwise and anticlockwise helices. The Benguela Upwelling is located along the south-western coast of Africa (blue area; Shipboard Scientific Party, 1998). AC = Agulhas Current, AR = Agulhas Rings, ARC = Agulhas Retroflection Current, EACC = East African Coastal Current, NEMC = North East Madagascar Current, SEC = South Equatorial Current, SEMC = South Eastern Madagascar Current. (**B**) Position of Site U1476 at Davis Ridge. The dotted arrow shows the bottom current, the solid arrow the surface current. Figure modified by Hall et al. (2017b).

gradient between the surface and the thermocline is observed (Steinhardt et al., 2014). This highly variable environment favours a great diversity of marine organisms (Ternon et al., 2014). In the Indian Ocean, the monsoon has a strong influence on the seasonal and long-term stability of the thermocline. The cycles of ISM and IWM cause profound seasonal changes in the hydrographic/oceanographic conditions, also in the Mozambique Channel. From season to season, differences in the SST of 4°C to 5°C (Tew-Kai and Marsac, 2009; Fallet et al., 2010) and changes in the mixed layer depth (Fallet et al., 2010) are observed. Primary productivity in the Mozambique Channel was modelled to show highest concentrations during the ISM and a second peak during winter (Lévy et al., 2007). Seasonality in hydrography strongly affects the abundances of the surface-dwelling warm-water PF *Globigerinoides trilobus* and *G. sacculifer* (Fallet et al., 2010).

3.2.2 Sample-Selection and Age Model

G. menardii is known to occur at its greatest abundance and test size during interglacial times (Ericson and Wollin, 1956; Sarkar and Guha, 1997; Sexton and Norris, 2011; Portilho-Ramos et al., 2014; table A1, Appendix). Since a stable isotope record was not available at the time of this study, the magnetic susceptibility (MS) record was applied to identify, at least, the youngest few interglacials. The MS at Hole U1476 is nearly continuous and shows good correlation with the $\delta^{18}O$ stack from Lisiecki & Raymo (2005) for the past 800 ka. Hall et al. (2016) noted that "ideal coring conditions and good signal in the magnetic susceptibility allowed for near-real time correlation at Site U1476." Berger et al. (1998) has shown that MS and oxygen isotope records can sometimes exhibit a good correlation.

The mechanism behind the idea of identifying glacial and interglacial intervals via the MS record is the change in the primary production between glacials and interglacials. During interglacials, a relatively high primary production causes a higher sedimentation rate of non-magnetic material, i.e. calcareous and silicious particles of biogenic origin. This material dilutes the magnetic signal produced by the deposition of magnetic minerals like magnetite (Hall et al., 2017b). During glacials, primary production decreases in comparison to interglacial times, resulting in a relative enrichment of magnetic minerals in the sediment and an increase in the MS signal.

To test the accuracy of interglacial and glacial sample selection via the MS record, the depths of the selected samples (table A3.1) were plotted against the recently published benthic isotopic record of van der Lubbe et al. (2021). The translation of core depth below seafloor (CSF-A) for all used depths in this study, including the MS record and the age-depth plot, into core

composite depth below seafloor (CCSF-A) was calculated by linear interpolation using the depth data given in the tables 10 and 12 in Hall et al. (2017b).

The comparison of the sample depths with the benthic isotopic record (Fig. A3.1) shows that from the seven interglacial samples (sample 1, 2, 3, 4, 5, 6 and 7 in table A3.1) selected via the MS record, two samples (sample 4 and 5) did not coincide with the peak of the interglacials in the stable isotopic record (Fig. A3.1). The three supposed glacial samples (sample 1.5, 3.5 and 5.5) are located close to the negative peak (Fig. A3.1).

Amplitudes in the MS record weaken after 800 ky (ca. 18 m CCSF-A), so that a distinct correlation with a corresponding marine isotope stage is not possible (Fig. A3.1).

In the time interval from 0.8 Ma to ca. 5.5 Ma, the $\delta^{18}O$ stack from Lisiecki & Raymo (2005; LR05 stack) was projected on the available age model. It means that the ages of selected interglacials, similar to those ages of previous studies, were projected on the age model (Fig. 3.2) to determine the corresponding sediment depth in Hole U1476A. The age model for Hole U1476A is based on the combination of PF and calcareous nannofossils datums, given in Hall et al. (2017a, b; see also Fig. A3.2).

For direct comparison of the results of this study with previous studies (Knappertsbusch, 2007; Knappertsbusch, 2016; Knappertsbusch, 2022; Friesenhagen, 2022a), the biostratigraphic dates used for the age model given in Hall et al. (2017b) were back-converted to the Berggren et al. (1995) time-scale (Table A3.2).

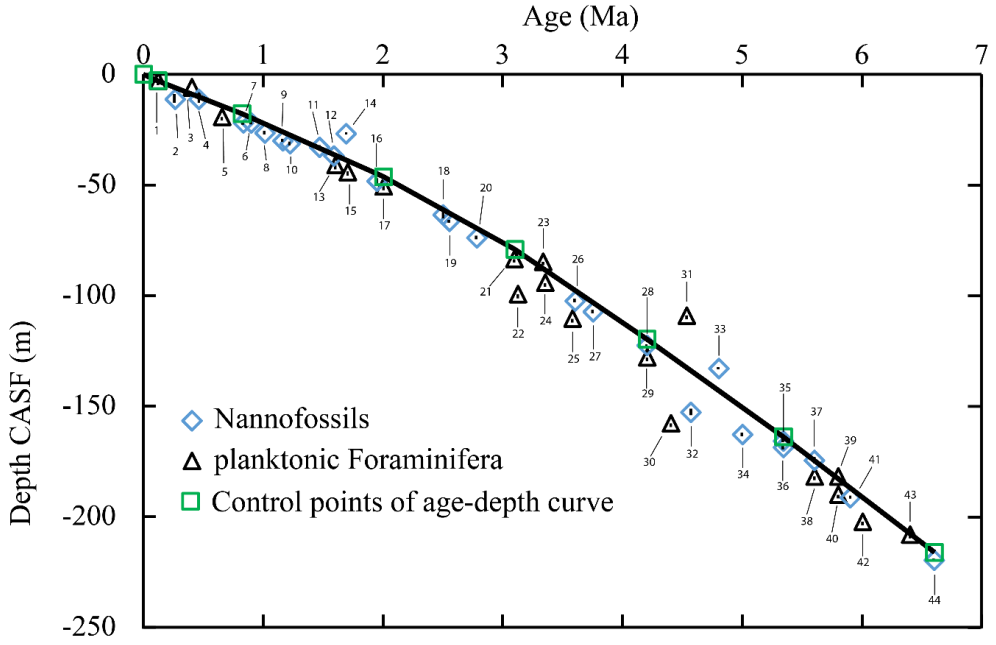

Figure 3.2: Age (Ma) versus Depth [CASF (m)] plot for Hole U1476A. The black line represents the age model based on biostratigraphic data of Hall et al. (2017b), which were re-converted to the timescale of Berggren et al. (1995). Bars inside the symbols indicate depth ranges for stratigraphic events. The event numbers are explained in Table A2.

The line of correlation was manually constructed with the "Age Depth Plot" software by Lazarus (1992). The control points of this line were used for linear interpolation of sample ages in the time interval from 0.8 Ma to 6.5 Ma, which are given in table A3.3.

The comparison of the applied age model with the isotopic record by van der Lubbe et al. (2021) reveals a discrepancy of up to 2 m within the time interval from ca. 1 Ma to 2 Ma (ca. 20 m CCSF-A to 45 m CCSF-A, see Fig. A3.2). The discrepancy is explained by the high temporal resolution of the isotopic measurements, which provides a detailed age-depth estimation. This accuracy cannot be achieved with a model based on fossil datums. Thus, chosen samples within the respective interval were corrected by up to 0.078 Myr (Table A3.1).

Currently, the accuracy of sample dates older than 2.027 Myr, which are based on the LR05 stack, cannot be tested as a stable isotope record for this time interval is not available for Hole U1476A.

The last three samples are out of range of the LR05 stack and were chosen by applying along the mircopalaeontological age model at similar ages as were investigated in previous studies of the authors (Knappertsbusch, 2016, Friesenhagen, 2022a).

3.2.3 Sample Preparation and Parameter Measurement

31 samples from different time horizons were investigated from IODP Hole U1476A, from which 28 were taken from interglacials and 3 from glacials (table 1, Appendix).

The sample preparation follows the processing scheme of Knappertsbusch (2007; 2016; 2022) and Friesenhagen (2022a). A volume of 2-3 cm^3 of the bulk sediment were dried at 50°C over night, weighted and gently boiled in water with soda as an additive. After wet sieving over 63 µm, the <63 µm fraction was decanted, dried and stored along with the remaining sample material in the micropalaeontological collections of the Natural History Museum Basel. The >63 µm fraction of each sample was split with a microsplitter into binary aliquots so that ca. 200 menardiform specimens could easily been picked from a split. This number of specimens is a good compromise between statistical relevancy and analytical effort to follow picking, mounting, imaging, and data processing within the limited time for this project. Specimens were mounted in keel view with the spiral side on the left side and the primary aperture facing up on standard faunal Plummer cells from Prodotti e Apparecchiature Scienze e Industria (P.A.S.I. srl). Malmgren et al. (1983) and other studies have demonstrated that the morphological information gained in keel view are useful to detect evolutionary changes.

In total, 4978 specimens of *G. menardii*, 460 specimens of *G. limbata* and 68 specimens of *G. multicamerata* were picked and mounted in this way.

3.2.4 Imaging methods

Digital images of the specimens were produced with the system AMOR 2, a twin of AMOR, that was especially re-built and improved for this project (Knappertsbusch & Eisenecker, 2022). While software version of the older AMOR (from Automated Measurement system for shell mORphology, see Knappertsbusch et al., 2009), is AMOR 2.8, which was developed under LabView 8.5 from National Instruments, the new software is called AMOR 4.2, which was developed under LabView 14. An intercalibration experiment between the two systems revealed an average deviation of outlines of ±2.44 µm (0.69% of the mean radius) from the same specimen. Repeatability between old AMOR and System AMOR 2 was ±2.76µm or an average deviation of 0.79% from the mean radius of the test specimen (Knappertsbusch & Eisenecker, 2022). These errors have to be kept in mind if one comes to direct, detailed specimen-to-specimen comparisons of this study with the previous ones from Knappertsbusch (2007, 2016, 2022) and Friesenhagen (2022a).

For the extraction of outline coordinates, images were transformed in black/white images and prepared for further processing steps with the public domain software ImageJ 1.52i from National Institute of Health (Rasband, 1997-2018). Digital preprocessing of images includes the removal of adhering particles, smoothing, enhancement of contrast, binarization and closing of single pixel embayments. The processed images are stored as 640 x 480 pixel, 8 bit grey-level Tiff files. From these binary files, cartesian outline coordinates were extracted with modified MorphCol software. These programs were originally encoded in Fortran77 for Macintosh (Knappertsbusch, 2007; 2016), converted to Fortran95 under Windows by Friesenhagen (2022a) and adapted to AMOR 4.2 software, that drives System AMOR 2 (Fig. A3.4,

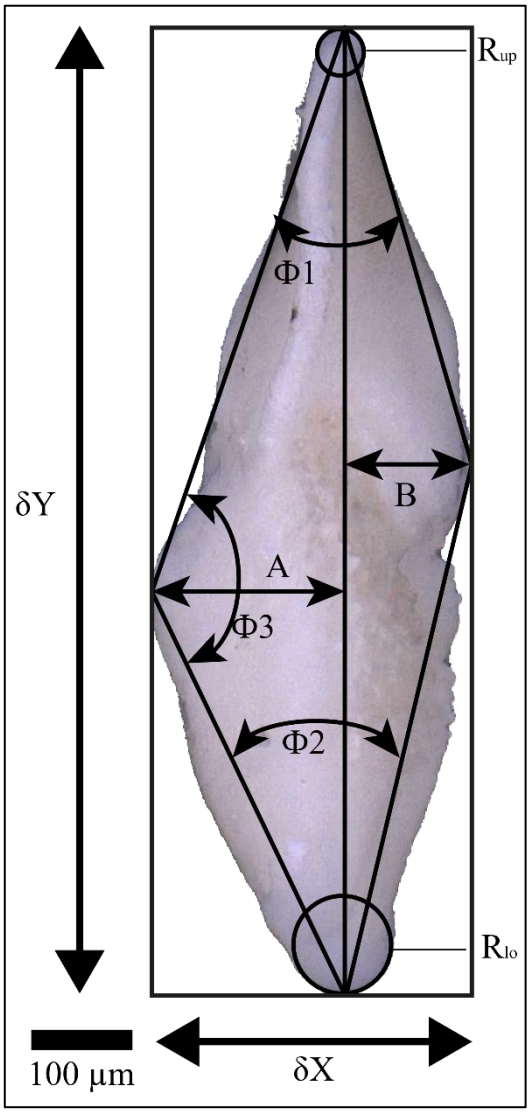

Figure 3.3: Investigated morphometric parameters. δX: spiral height; δY: axial length; Φ1: upper keel angle; Φ2: lower keel angle; Φ3: angle at the apex; A: spiral convexity; B: umbilical convexity; R_{up} (radius of the osculating circle in upper keel region); R_{lo} (radius of the osculating circle in lower keel region).
The illustrated specimen is the same as in Fig. 3.4.9.

see Appendix). In contrast to the earlier studies, which used the old AMOR running with AMOR 3.8 and older, System AMOR 2 employs different hardware, which allows to omit the magnification correction (MagCorr). It is to be used in combination with program Trace-AMOR3.1_batch_win, which is the windows version of program Trace_AMOR3_batch.out written by the senior author (Knappertsbusch, 2019: MorphCol Supplement #27).

The suite of MorphCol applications is used for the measurement of a variety of morphometric parameters. They include the spiral height (δX), the axial length (δY), the ratio of these two (R = δX / δY), the test area in keel view (Ar), the spiral (A) and the umbilical (B) sides' convexity, their ratio (RA/B), the upper (Φ_1) and the lower (Φ_2) keel angle, the angle of the apex (Φ_3) and the upper (R_{up}) and lower (R_{lo}) keel regions' and radii of the osculating circles (Fig. 3.3), and were already applied in Knappertsbusch (2016). These programs and updated versions are deposited in the Geological Archive of the NMB and are also available in the software container in Knappertsbusch (2021).

Dextrally coiling specimens were vertically mirrored using "DexFlip_win", another modified program by Knappertsbusch (2016), to enable direct comparison of these specimens with sinistrally coiling tests.

3.2.5 *G. menardii-G. limbata-G. multicamerata* lineage and Species Identification

Menardiform globorotaliids best qualify for morphometric studies for several reasons: They are exclusively (sub-) tropical dweller (Kennett and Srinivasan, 1983 and references therein; Berger and Wefer, 1996, Caley et al., 2012; Schiebel and Hemleben, 2017) and so minimize the biogeographic extend for the study. *Globorotalia menardii* evolved within the Middle Miocene (Kennett and Srinivasan, 1983; Bolli and Saunders, 1985) and is a long-lasting lineage, ideal for evolutionary studies over extended time. Their lenticular, simple outer low-trochospiral morphology makes them ideal for test-size studies (Tabachnick and Bookstein, 1990). Illustrations by Kennett and Srinivasan (1983), Bolli et al. (1985) as well as the reference collection "49 Cenozoic planktonic foraminiferal zones and subzones prepared by Bolli in 1985 – 1987", which is deposited at the Natural History Museum Basel, were used to recognise menardiform morphotypes. Specimens other than *G. menardii*, *G. limbata* and *G. multicamerata* were removed from the dataset.

3.2.5.1 Inter- and intraspecific variation of the *G. menardii-G. limbata-G. multicamerata* lineage

Specimens identified as members of the *G. menardii-G. limbata-G. multicamerata* lineage were further grouped by the number of chambers in the last whorl, a pragmatic approach that proved applicable in the other way confluent variation of tests in the group. Specimens of the *G. menardii-G. limbata-G. multicamerata* lineage with up to six chambers in their last whorl were considered as *G. menardii*, while specimens showing seven chambers were considered as *G. limbata*. *Globorotalia multicamerata* was characterised to show more than 7 chambers in its last whorl (Fig. 3.4).

Extant variants of *G. menardii* (*G. menardii cultrata, G. menardii fimbriata, G. menardii menardii*) never contain more than 6 chambers. *G. menardii neoflexuosa* and *G. menardii* gibberula furthermore exhibit different morphologies, making them easy to distinguish from

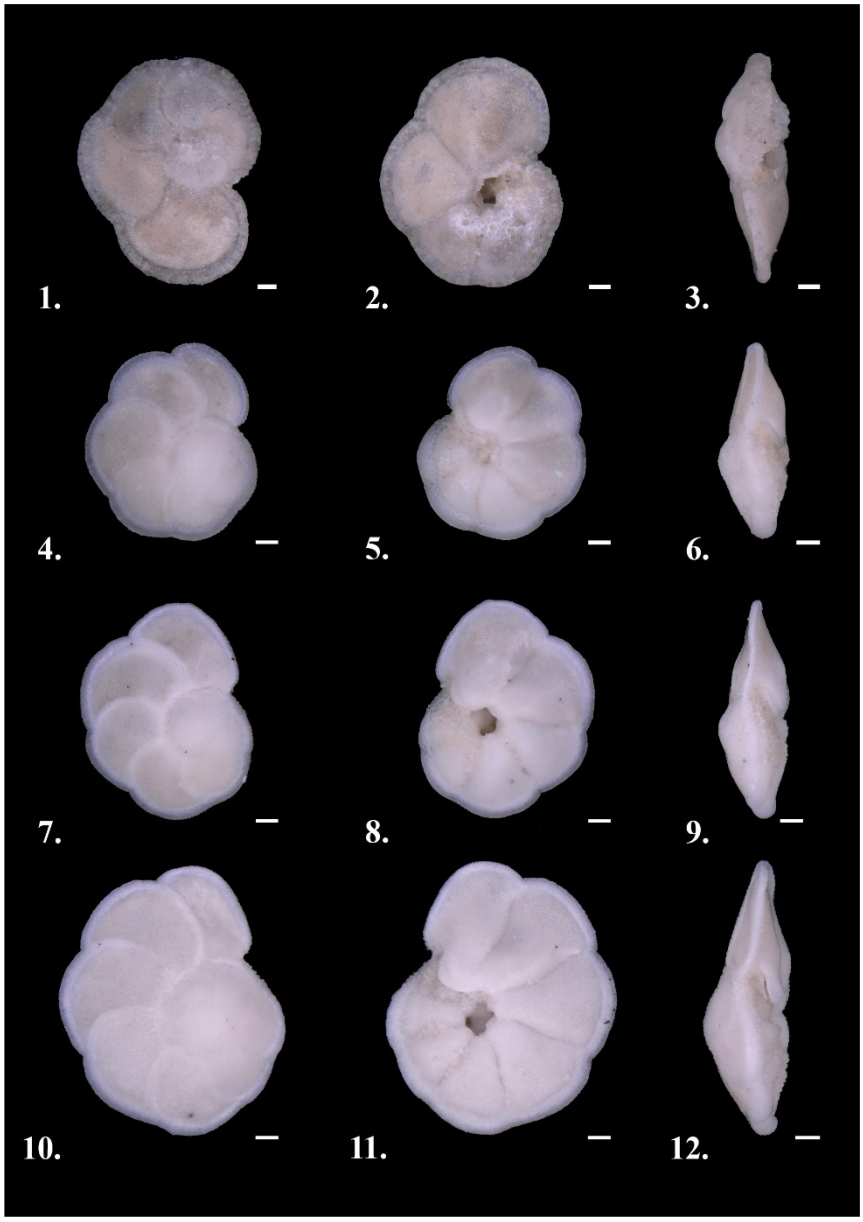

Figure 3.4: Plate of investigated species in spiral, umbilical and keel view. **1-3** *Globorotalia menardii*, typically found since the late Gelasian in the Mozambique Channel, Sample U1476A-2H-1, 99-100, cm, specimen 1476021100a2001; **4-6** *Globorotalia menardii*, typically found in samples older than 2.025 Ma, Sample U1476A-12H-2, 11-12 cm, specimen 1476122012a4601; **7-9** *Globorotalia limbata*, sample U1476A-12H-2, 11-12 cm, specimen 1476122012a2101; **10-12** *Globorotalia multicamerata*, sample U1476A-12H-2, 11-12 cm, specimen 1476122012a3301. Scale bar: 100 µm. A Keyence VHX-6000 digital microscope has been used to take images of the specimens.

G. menardii menardii (see Brown, 2007). In the present study only *G. menardii menardii* is included and is referenced as "*G. menardii*". Intermediate forms between *G. menardii* and *G. tumida* were also observed in several samples.

Some of these intermediate forms show an elongated, tumid chamber structure in umbilical view, characteristic for *G. tumida* (Kennett and Srinivasan, 1983; Bolli and Saunders, 1985) and have a *G. menardii*-like, low trochospiral and compressed test (= relatively small spiral height (δX)) in keel view. Other variations exhibit a more -in direct comparison- rounded, *G. menardii*-like chamber form in the umbilical and a biconvex, *G. tumida*-like shape in the keel view. Both forms can exhibit either a *G. tumida*-like heavy or a relatively more delicate, *G. menardii*-like keel.

Such transitions are a known phenomenon (Thompson, 1982; Schweitzer and Lohmann, 1982; Stewart, 2009; Hull & Norris, 2009: Knappertsbusch, 2022) and were excluded from for this study as well.

3.2.6 Univariate Plots, Contoured Frequency Diagrams and Histograms

Using the freeware packages psych (Revelle, 2018), readxl (Wickham and Bryan, 2019), ggplot2 (Wickham, 2016), pacman (Rinker and Kurkiewicz, 2018) and rio (Chan et al., 2018), statistical analyses, univariate plots and histograms were prepared with RStudio (V. 3.5.3; RStudio Team, 2020). For characterising test evolution, spiral height (δX) and axial length (δY) are combined to contour frequency diagrams (CFD). CFDs, which were created with the commercial software OriginPro 2020 from OriginLab Corporation, are very useful to detect changes in the dominant test size of a population. Tracking modal trends through time provide important signals of anagenetic evolution or cladogenetic splitting.

The CFDs are constructed from bivariate frequency matrices of δX and δY and subsequently are called gridded files. Uniform grid-cell sizes of $\Delta X = 50$ µm and $\Delta Y = 100$ µm were applied to construct these matrices from pairs of δX and δY (Knappertsbusch, 2007, 2016). These gridded files represent absolute specimen numbers per grid cell. They were generated using the modified MorphCol program "Grid2.2_win" (Fig. A3.2). During contour construction, frequencies were not smoothed.

Depending on the number of specimens per sample, contour intervals were adjusted as to increase readability of individual CFDs.

3.2.7 Volume Density Diagram

Volume Density Diagrams (VDDs) are a way to illustrate and visualise evolutionary tendencies in bivariate morphometric measurements through time (Knappertsbusch and Mary, 2012). These diagrams expand a stack of plane CFDs through time and add the local frequency F of specimens per grid-cell as the fourth dimension. The new created, four-dimensional (δX, δY, time, F) cell is called "voxel". The fourth component of the voxel, the local frequency F, can be illustrated by an iso-surface and represents a constant value of the local frequency through time (Knappertsbusch, 2016).

In the present study, the commercial software Voxler 4 by Golden Software was used to prepare the VDD. Low isovalues in the VDD represent rare specimens at the extreme test-size spectrum, and which can possibly be attributed to evolutionary innovation. A similar signal can also occur, however, if large forms are introduced by immigration into an otherwise smaller sized population.

In contrast, high iso-values illustrate abundant specimens, forming the "core" or main branch of the VDD. The core is supposed to represent the main evolutionary trend through time and is shown in a time-section through the VDD (section 3.3, 3.4, see further below).

VDDs were generated following the methods described in Friesenhagen (2022a) from ODP Hole 667A and Knappertsbusch (2022) from ODP Hole 806C. The calibrated VDDs illustrated herein display absolute frequencies at an iso-value of 0.738317757 per specimen per grid cell. Detailed information about adjustments in the VDD model is given in the supplementary material ("U1476_3D_PDF.pdf").

3.3 Results

This contribution concentrates on the evolution of δX, δY and Ar through time. These parameters proved best for the detection of inter- and intraspecific evolution within the *G. menardii-G. limbata-G. multicamerata* lineage and allow direct comparison to the previous, similar studies of Knappertsbsuch (2007; 2016; 2022) and Friesenhagen (2022a).

Globorotalia menardii occurs in large numbers in most of the investigated sediments, but became rare at 6.49 Ma and 6.07 Ma. *Globorotalia limbata* is continuously present from 6.49 Ma until its (pseudo-) extinction at 2.34 Ma. After 2.34 Ma, specimens with seven chambers in the last whorl and identified as *G. limbata* became rare, but were still sporadically present (Fig. 3.5, 3.6, 3.7). *Globorotalia multicamerata* was first detected in this study at 5.789 Ma and was last found at 2.34 Ma. It is absent in samples at 5.135 and 4.825 Ma.

In the following sections 3.1 through 3.4, test-size evaluation of the three species is presented in trends of individual parameters (3.1), bivariate frequency diagrams of δX vs. δY (3.2), volume-density diagrams (3.3) and a longitudinal section through the VDD (3.4). Chapter 3.5 describes changes in the coiling direction of *G. menardii* populations.

3.3.1 Evolution of δX, δY and Ar through Time

3.3.1.1 Spiral Height δX

The evolution of maximum δX values for *G. menardii* shows an overall gradual increase through time (Fig. 3.5a). The smallest maxima occurred in the two oldest samples at 6.49 Ma (213.5 µm) and 6.07 Ma (228.7 µm). Until 5.78 Ma, maxima steeply increased by ca. 150% to 347 µm and then gradually to 446.6 µm until 2.585 Ma. At 2.34Ma, a comparably large incursion in size occurred in short time (338.7 µm), but the general size continued until to increase 2.025 Ma to 497 µm. Although one major peak is observed at 1.072 Ma, the maximum δX values equilibrate in the samples younger than 1 Ma at around 480 µm.

Overall, the means and medians display only little net evolution (Fig. 3.5a, d). They fluctuate between 146 µm (1.436 Ma) and 234 µm (0.123 Ma) for the mean values and between 129 µm (2.025 Ma) to 260 µm (1.772 Ma) for the median.

Interestingly, the (normalised) differences of medians between neighbouring samples reveal four different temporal phases from bottom to top (Fig. A3.5a, d in the Appendix): Phase 1 shows only little variation, fluctuating between 30 % (increase) and -30 % (decrease) from 6.49 Ma to 3.19 Ma. Two exceptions are observed at 5.78 Ma and 4.13 Ma, where the rate exceeds (-)30 %. Phase 2 begins at 2.95 Ma, where the rate increases to almost -50 %. Until 1.44 Ma, the rate usually is greater than (-)30 %, except for 2.34 Ma (ca. 23 %). This phase shows the highest rates of median size changes. The maximum change (-100 % = -129µm) is observed between 1.77 Ma and 1.44 Ma. In Phase 3 from 1.44 Ma to 0.34 Ma, changes are low (<(-)30 %). Phase 4 is again characterised by relatively high rates of more than (-)30 %.

In contrast to *G. menardii*, the maximum δX values of *G. limbata* and *G. multicamerata* exhibit different trends. In *G. limbata* (Fig. 3.5b), after an initial increase from 263 µm (6.49Ma) to 326 µm (6.07 Ma), the maxima fluctuate between 297 µm (2.95 Ma) and 397 µm (3.935 Ma). The mean and median values of *G. limbata* vary between 291 µm (3.19 Ma) and 221 µm (2.59 Ma), the median between 293 µm (3.19 Ma) and 206 µm at 3.72 Ma (Fig. 3.5b).

The lowest maxima of δX of *G. multicamerata* are observed at 5.31 Ma (290 µm), the largest test was found at 3.93 Ma (390.7 µm; Fig. 3.5c). The means and medians fluctuate between

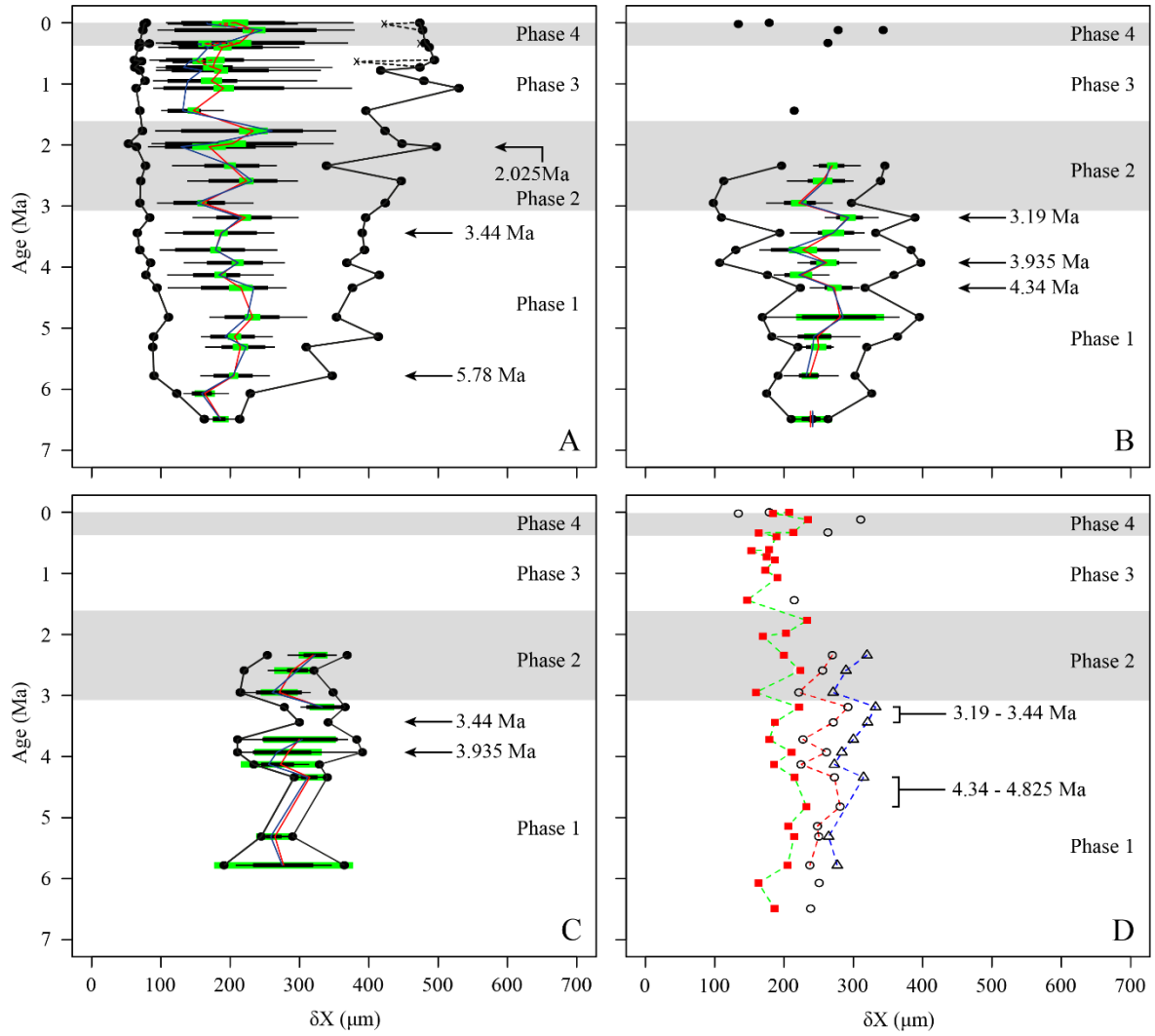

Figure 3.5: Spiral height (δX, in µm) versus time (Ma) at IODP Hole U1476A for (**A**) *G. menardii*, (**B**) *G. limbata*, (**C**) *G. multicamerata*, and (**D**) the mean values of the three species. In A–C, maxima and minima are represented by black dots. Horizontal thin bars represent the 10 to 90 % sample percentiles, thick black bars the upper and the lower quartiles about the median, and the green bars the confidence interval about the mean. The vertical red line illustrates means, the blue line the median. Dashed lines represent values for the glacial samples. In D, red squares symbolise the mean δX values of *G. menardii*, open, black circles those of *G. limbata* and blue triangles are *G. multicamerata*. Samples containing less than three specimen per species are shown as isolated symbols since a reasonable statistical analysis is not given. Recognised intervals in the evolution of the mean and median test size are marked with grey and white boxes. Phase 1 spans from 6.49 Ma to ca. 3.1 Ma, the second from 3.1 Ma to ca. 1.6 Ma, the third from ca 1.6 Ma to ca. 0.4 Ma and the last from ca. 0.4 Ma to present.

333 µm (3.19 Ma) and 258 µm (5.31 Ma) for the median and between 332 µm (3.19 Ma) and 264 µm at 5.31 Ma for the mean value.

Figure 3.5d shows that *G. multicamerata* exhibit the largest mean size of the three species, while *G. menardii* shows the smallest and *G. limbata* is always intermediate.

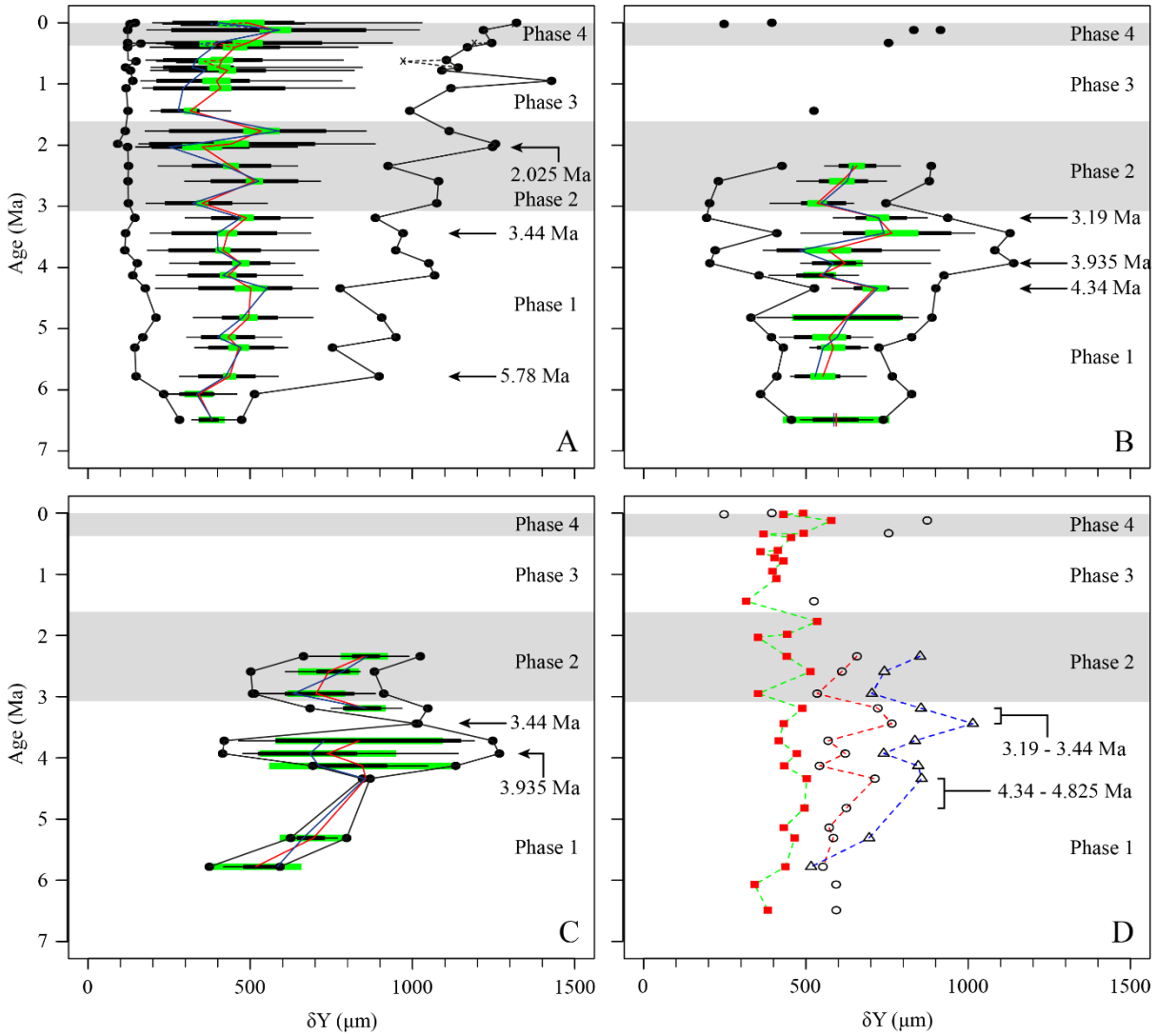

Figure 3.6: Axial length (δY in µm) versus time (Ma) at IODP Hole U1476A for (**A**) *G. menardii*, (**B**) *G. limbata*, (**C**) *G. multicamerata* and (**D**) the mean values of the three species. See Fig. 3.5 for explanation of the symbols.

3.3.1.2 Axial length (δY)

The δY values of *G. menardii* exhibit a similar gradual pattern as these of δX (Fig. 3.6a). In samples older than 6 Ma, the maximum size is relatively small (514 µm), but strongly increases until 5.78 Ma (898 µm) and show an overall gradual trend afterwards.

Samples at 2.34 Ma and 2.025 Ma are an exception: the observed decrease and the following test-size increase are, in relation, not as drastic in δY (1080 µm at 2.59 Ma, 925 µm at 2.34 Ma and 1247 µm at 2.025 Ma) as observed in the δX values. At 0.952 Ma, a second peak is located. The median values for δY fluctuate between 251 µm (2.025 Ma) and 591 mm (0.12 Ma). Maximum and minimum mean values are observed at 0.12 Ma (578 µm) and 1.44 Ma (316 µm). The four phases for the normalised differences of the median δX can also be observed for the normalised median differences of δY (Fig. A3.5b, d).

However, maximum δY values of *G. limbata* and *G. multicamerata* exhibit a different long-term pattern than those of δX. *Globorotalia limbata* shows a distinct test-size maximum of ca.

1100 µm from 3.93 until 3.44 Ma (Fig. 3.6b). The mean (median) values of *G. limbata* show no long-term trend at all and fluctuate between 534 µm (480 µm) and 764 µm (740 µm). Two peaks are observed at 4.34 Ma (mean = 712; median = 720 µm) and 3.44 Ma (mean = 764µm; median = 740µm).

The maximum values for *G. multicamerata* increase from 5.78 Ma (591µm) until 3.935 Ma (1276 µm) and decrease afterwards until 2.585 Ma (883µm) (Fig. 3.6c). Before its last occurrence at Hole U1476A at 2.34 Ma, the test size increases again from 882.7 µm to 1203.8 µm. Mean (median) values of *G. multicamerata* increase from 5.78 Ma to 4.34 Ma from 516 µm (582 µm) to 856 µm (854 µm). Two more peaks are observed at 3.77 Ma (mean = 1014 µm; median = 1014 µm) and 2.34Ma (mean = 852 µm; median = 860 µm). It has to be mentioned that only 2 specimens were found at 3.77 Ma.

Even clearer than with δX, *G. multicamerata* has the largest mean size in δY, *G. limbata* is intermediate and *G. menardii* exhibit the smallest size (Fig. 3.6d). An exception is found in 5.78 Ma, where *G. limbata* is minimally larger in mean δY than *G. multicamerata*.

3.1.3 Keel view area

The evolution of Ar shows the same trends as δX and δY for all of the three species.

For *G. menardii*, the maximum Ar increases from 0.068 mm² before 6 Ma to 0.209 mm² at 5.78 Ma (Fig. 3.7a). A gradual increasing pattern is observed afterwards, ending up at 0.376 mm² (0.004 Ma). Between 2.34 Ma to 2.025 Ma, the size more than doubles (0.194 mm² to 0.399 mm²). The mean values fluctuate between 0.02 mm² (2.025 Ma) and 0.95 mm² (0.12 Ma), while the medians range between 0.035 mm² (1.44 Ma) and 0.112 mm² (0.12 Ma). The four phases described in chapter 3.1.1 can be observed in the rates of change in the normalised medians (Fig. A3.5c, d in the Appendix).

The evolution of Ar of *G. limbata* shows no net trend (Fig. 3.7b). Four distinct peaks are developed, at 6.07 Ma (0.173 mm²), 4.82 Ma (0.229 mm²), 3.93 Ma (0.263 mm²) and at 2.34 Ma (0.205 mm²). Mean (median) values also show no trend and fluctuate between 0.14 mm² at 3.19Ma (0.139 µm at 3.19 Ma) and 0.079 µm at 2.95 Ma (0.067 µm at 3.72 Ma).

Maximum values of *G. multicamerata* show a trend of increased from 5.78 Ma (0.147 mm²; Fig. 3.7c) until 3.935 Ma (0.32 mm²), followed by a decreasing trend until 2.585 Ma (0.149 mm²). Ar increase again to 0.252 mm² until 2.025 Ma. Mean and median values of *G. multicamerata* covary strongly with δY. The mean/median values increase from 5.78 Ma (0.099 mm²/0.103 mm²) to 3.93 Ma (0.148 mm²/0.124 mm²) and show two distinct peaks at 3.44 Ma (0.214 mm²/0.214 mm²) and 2.34Ma (0.184 mm²/0.118 mm²).

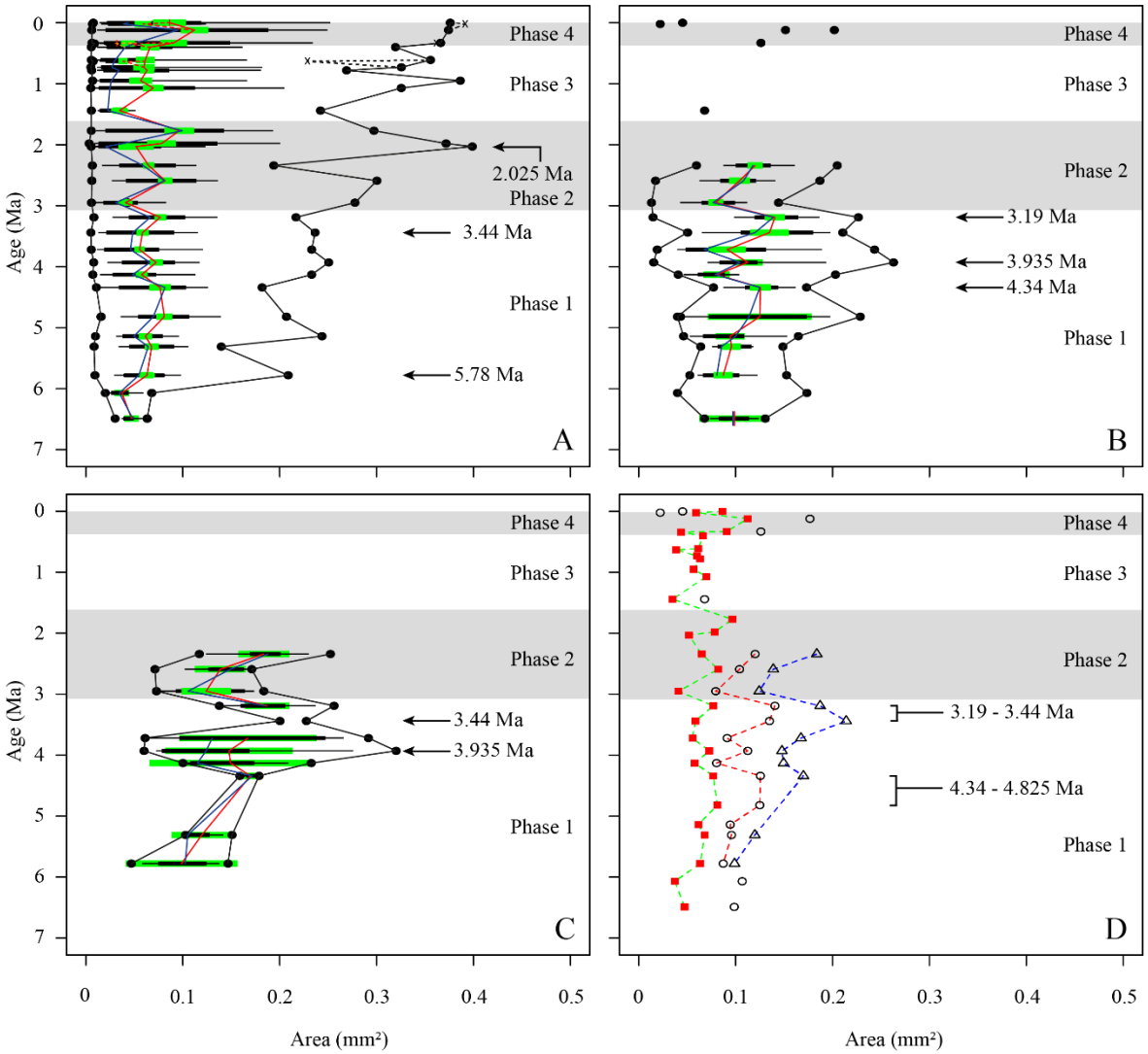

Figure 3.7: Test area (Ar in mm²) versus time (Ma) at IODP Hole U1476A for (**A**) *G. menardii*, (**B**) *G. limbata*, (**C**) *G. multicamerata* and (**D**) the mean values of the three species. See Fig. 5 for explanation of the symbols.

Overall, *G. menardii* exhibited the smallest mean test area, *G. multicamerata* had the largest Ar and *G. limbata* is again intermediate (Fig. 3.7d).

3.3.2 Contoured Frequency Diagrams of δX and δY

Presentation of the data in form of contoured size-frequency diagrams greatly facilitate detection of cladogenetic splitting or trends of anagenetic evolution. Directional modal shifts of populations indicate evolution of populations or even may point to splitting if trends divide up. In the present analysis, the grid-cell size was chosen at 50 µm for ΔX and 100 µm for ΔY, which is identical to previous such studies of Knappertsbusch (2007; 2016; 2022) and Friesenhagen (2022) (see section 2.6).

In general, measurements of δX and δY populate an almost linear, diagonal and semicontinuous morphocline in the δX and δY morphospace (Fig. 3.8). Flattening of the test during ontogenetic growth of individuals causes this trend (Caromel et al., 2016).

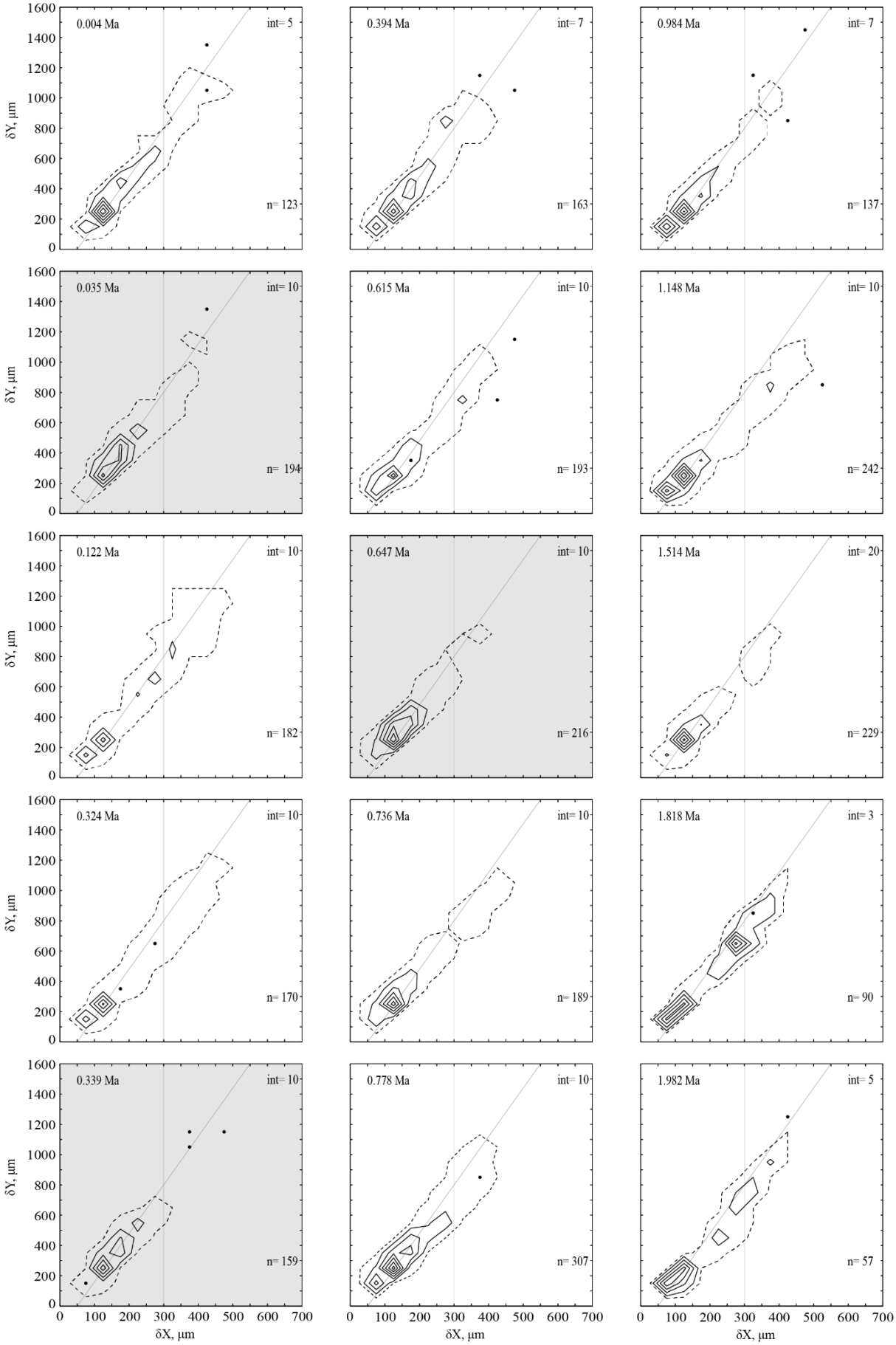
0.004 Ma
int= 5
n= 123
0.394 Ma
int= 7
n= 163
0.984 Ma
int= 7
n= 137
0.035 Ma
int= 10
n= 194
0.615 Ma
int= 10
n= 193
1.148 Ma
int= 10
n= 242
0.122 Ma
int= 10
n= 182
0.647 Ma
int= 10
n= 216
1.514 Ma
int= 20
n= 229
0.324 Ma
int= 10
n= 170
0.736 Ma
int= 10
n= 189
1.818 Ma
int= 3
n= 90
0.339 Ma
int= 10
n= 159
0.778 Ma
int= 10
n= 307
1.982 Ma
int= 5
n= 57
δY, µm
δX, µm
0
200
400
600
800
1000
1200
1400
1600
100
300
500
700

Figure 3.8A

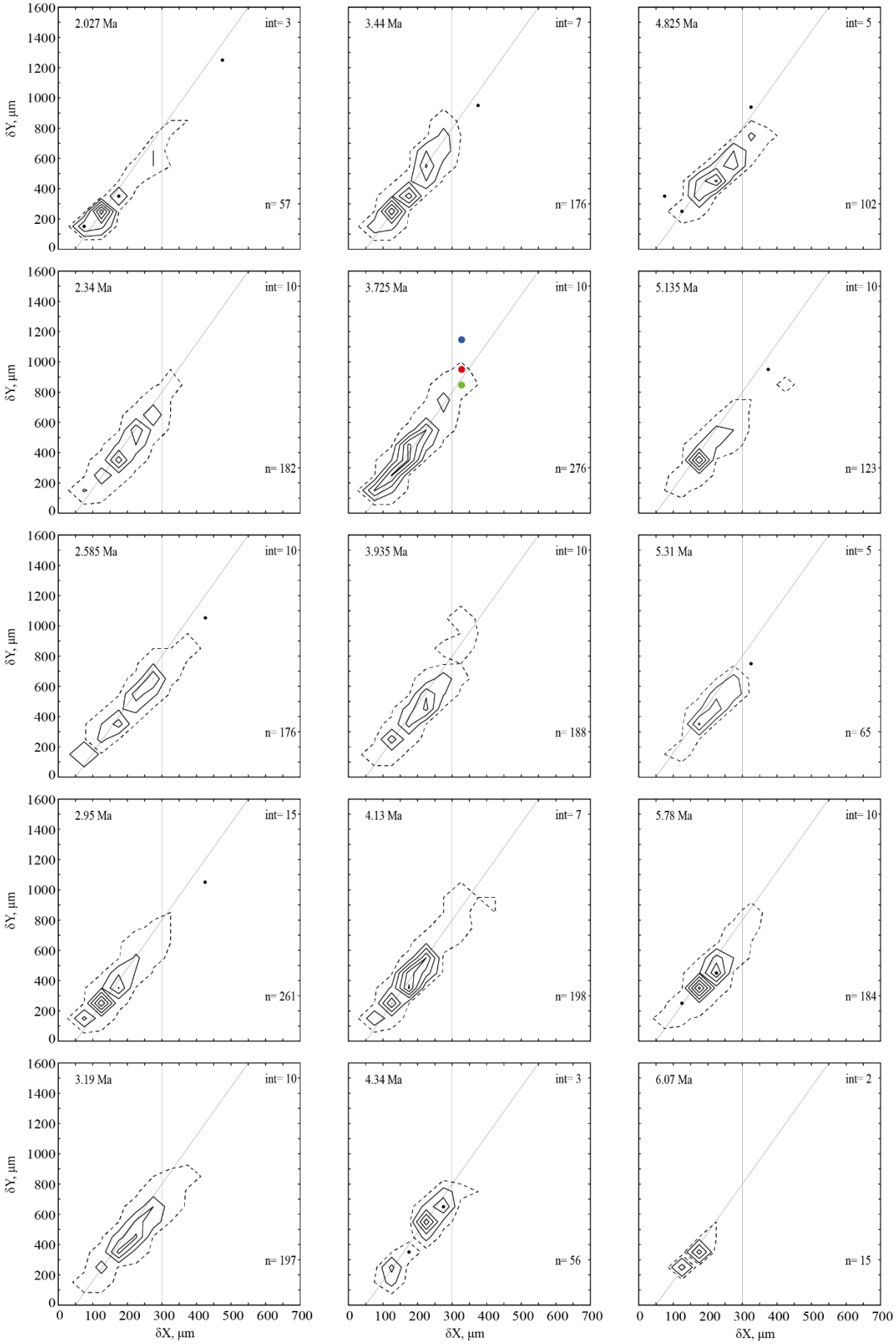
2.027 Ma
int= 3
n= 57
3.44 Ma
int= 7
n= 176
4.825 Ma
int= 5
n= 102
2.34 Ma
int= 10
n= 182
3.725 Ma
int= 10
n= 276
5.135 Ma
int= 10
n= 123
2.585 Ma
int= 10
n= 176
3.935 Ma
int= 10
n= 188
5.31 Ma
int= 5
n= 65
2.95 Ma
int= 15
n= 261
4.13 Ma
int= 7
n= 198
5.78 Ma
int= 10
n= 184
3.19 Ma
int= 10
n= 197
4.34 Ma
int= 3
n= 56
6.07 Ma
int= 2
n= 15
δY, µm
δX, µm
0
200
400
600
800
1000
1200
1400
1600
100
300
500
700

Figure 3.8B

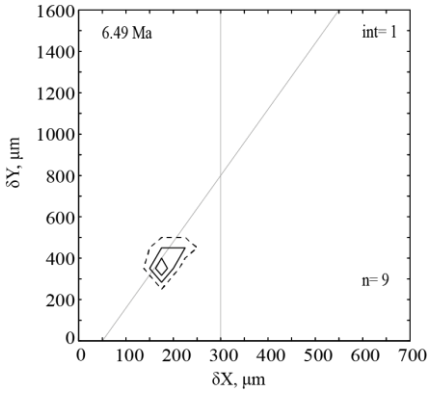

Figure 3.8C

Figure 3.8 (A, B, C): Contoured bivariate frequency diagrams (CFD) of the spiral height (δX) versus the axial length (δY) of *Globorotalia menardii* in keel view at IODP Leg 361 Hole U1476A from 0.004 Ma to 6.49 Ma. The age (Ma) is given in the left-upper corner. The 'int' number shows the contour interval by the number of specimens per grid cell. A gird cell has the size of 50 µm x 100 µm in the direction of δX and δY, respectively. The total number of specimens 'n', which are represented in the CFD, is shown in the lower right corner. The dashed line marks the contour interval from 0 to 1. The diagonal grey line is suggested to separate the modern morphotypes *G. menardii menardii* (area below the line) and G. menardii cultrata (area above the line) (Knappertsbusch, 2007). This and the vertical grey line at δX = 300 µm are drawn to facilitate direct comparison between single CFDs. In the diagram for 3.725 Ma in Fig. 3.8B, the green, red and blue point represents the position of the *G. menardii*, *G. limbata* and *G. multicamerata* specimen used for the figure 3.4, respectively.

Towards the larger side, distributions are tailored compared to juvenile specimens. Several samples exhibit bimodality, especially in samples younger than 2.025 Ma (Fig. 3.8, 3.9). The main peak represents a population with a size of up to 200 µm in δX and 400 µm in δY, the secondary peak represents populations with δX >200 µm and δY >500 µm (Fig. 3.8, 3.9a, b). Figures 3.9a and 3.9b are used here to better highlight this bimodality, while the contour plots in figure 3.8 illustrate the size-distribution in the bivariate morphospace of δX and δY. The graph reveals that adult specimens are often underrepresented compared to those of main peak, which represents juvenile-preadult forms. However, the univariate histograms of δX and δY bring the bimodal pattern to light (Fig. 3.9). The sample at 0.78 Ma is exceptional: it shows an unimodal, strongly skewed distribution with a strong shoulder towards larger forms.

Samples older than 2.025 Ma tend to be more unimodal in character, with an exception at 4.34 Ma.

The four samples (0.018 Ma, 0.343 Ma and 0.63 Ma, grey shaded in Fig. 3.8 and Fig. 3.9) are considered as unimodal, with rare large specimens.

3.3.3 VDD

A VDD (Fig. 13.0) was constructed from the above bivariate frequency distributions of δX and δY in order to obtain better insight into the morphological evolution of *G. menardii* and splitting off of close relatives. The VDD is basically a stack of CFDs from different times and should help to visualise the trends of evolution, speciation and splitting into groups that were already recognised in the CFDs and univariate plots (Figs. 3.5, 3.6, 3.7, 3.9). The VDD (Fig. 3.10) is calibrated for local frequency against the plane distributions shown in figure 3.8: The illustrated

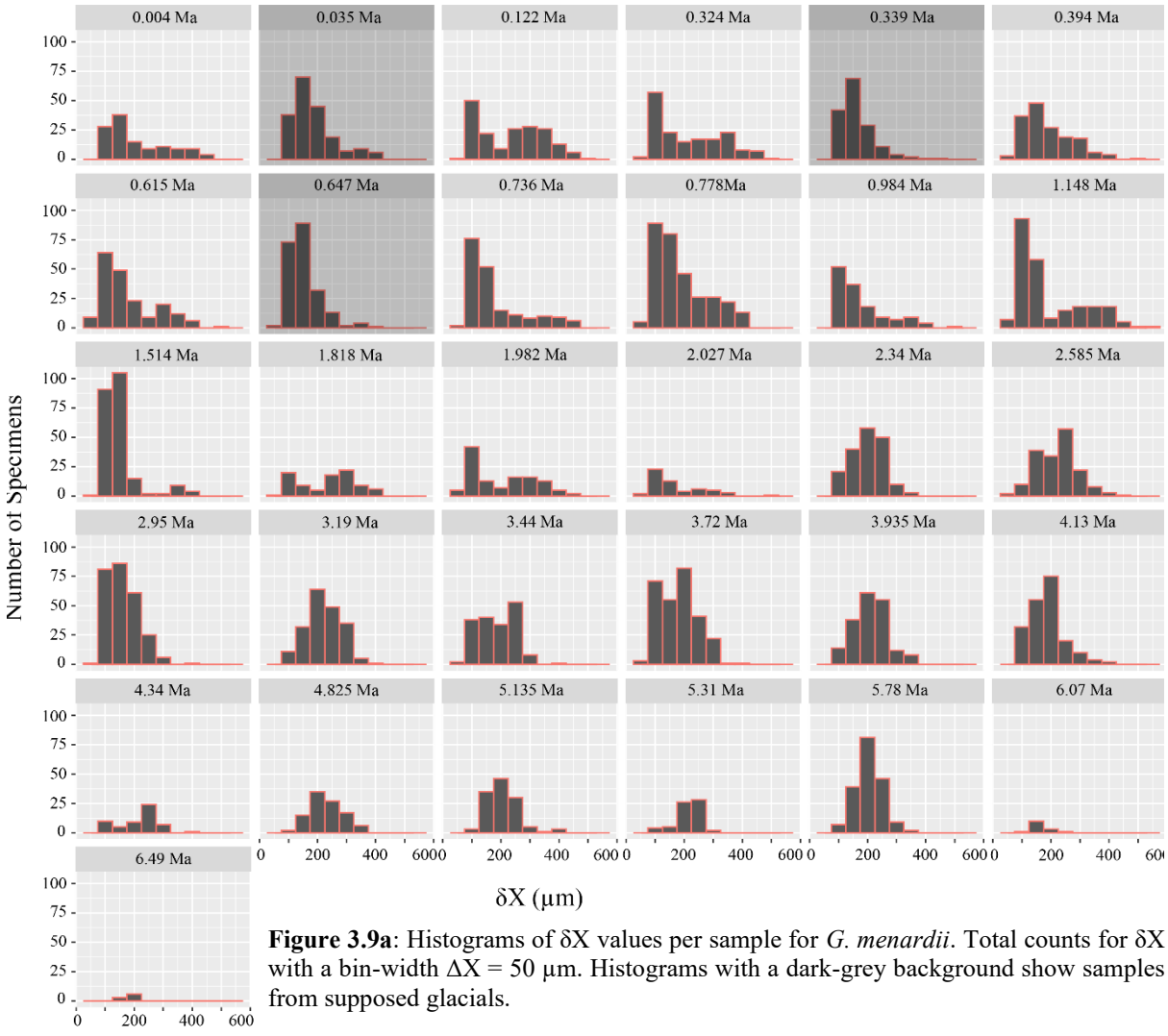

Figure 3.9a: Histograms of δX values per sample for *G. menardii*. Total counts for δX with a bin-width ΔX = 50 µm. Histograms with a dark-grey background show samples from supposed glacials.

isosurface value of 0.738317757 in Fig. 3.10 represents the local density of one specimen per grid cell and was selected to show rare specimens. Such extreme individuals may point to evolutionary innovations.

While the side view (parallel to the 45° plane in the δX, δY space) shows maximum variation (Fig. 3.10 a), the frontal view (perpendicular to side view) shows almost no net evolution during the last 6.5 Ma. Deviations at 3.935 Ma and 1.072 Ma illustrate forms with flattened or inflated adult tests, respectively.

3.3.4 Longitudinal Section through the VDD

In order to detect continuous morphological clades or splitting up of populations through time, a longitudinal section along the 45° plane through the VDD was constructed (Fig. 3.11). As mentioned before, a shift in bimodality through time points to the existence of two distinct populations and would be indicative for speciation. Seen through time, this pattern thus

Figure 3.9b: Histograms of δY values per sample for *G. menardii*. Total counts for δY with a bin-width ΔX = 100 µm. Histograms with a dark-grey background show samples from supposed glacials.

documents splitting and divergence of morphotypes, e.g. important signatures in the evolutionary history of the *G. menardii-limbata-multicamerata* complex.

In Fig. 3.11, one continuous branch pops out throughout the core in the VDD section. From 1.772 Ma onwards to present, a side branch towards larger sizes may have evolved but due to low frequency of large individuals, remains broken into single patches.

The complexity of the evolution of *G. menardii* through time is further illustrated in two sections in 45° and three sections in 135° view (Fig. A3.6-12).

3.3.5 Coiling Pattern

Changes in the coiling direction may bear additional information about the evolution of *G. menardii* (e.g. Bolli, 1950). Interestingly in context with the above results, the predominant coiling direction of *G. menardii* at Hole U1476A reveals several changes through time (Fig. 3.12).

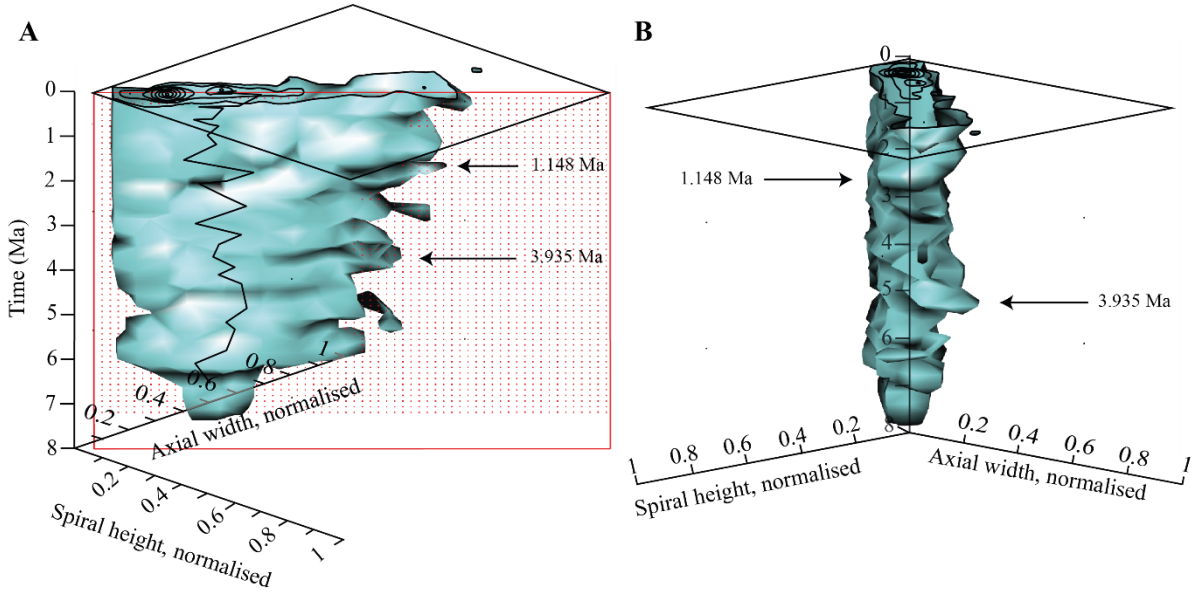

Figure 3.10: Volume Density Diagrams (VDD) of the normalised spiral height (δX) vs. the normalised axial length (δY) of *G. menardii* for the last 6.49 Ma at the Indian Ocean Hole U1476A. The iso-density surface represents the frequency of one specimen per gird-cell (iso-value = 0.738317757) to illustrate rare and probably innovative specimens. In (**A**), the VDD is shown in side view. The red dotted area represents the plain from which the section in Fig. 3.10 was extracted. The projection of the contour frequency diagram from 0.004 Ma enhances the three-dimensionality of this figure. (**B**) presents the frontal view of the VDD. To give an impression of the three-dimensionality of the figure, CFDs from the samples 0.004 Ma and 5.78 Ma are projected into the VDD. Arrows point to size peaks at 1.072 Ma and 3.935 Ma.
The tube-like outgrowth are artifacts generated by the iso-surface generation of the Voxler program when the isosurface calibration is made with 1 specimen per grid cell (value = 0.738317757). Artifacts vanish when the isosurface density is shifted by 0.22 to 1, representing 1.35 specimens per grid cell (not shown here).

At Hole U1476A, in the two oldest samples from 6.49 Ma and 6.07 Ma, 22.2 % and 26.6% of the specimens, respectively, coiled sinistrally. Sinistral coiling decreases to 3.3% at 5.78 Ma but then increases to 65.3 % until 5.135 Ma. The percentage of sinistral specimens remain low from 3.93 Ma (1.6 %) until 2.34 Ma (14.1 %). Thereafter, sinistral coiling became strongly dominant in all samples and only decreased below 90 % in the sample at 1.072 Ma (78.5 %).

The permanent change in the dominant coiling direction after 2.34 Ma suspects a new morphotype in the Indian Ocean.

3.4 Discussion

The sudden test-size increase observed between 2.3 Ma and 2 Ma in the tropical Atlantic Ocean (Knappertsbusch, 2007, 2016; Friesenhagen, 2022a) is supposed to be a result of invasion of Indian Ocean menardiform populations into the Atlantic Ocean during an episode of a strong Agulhas pulse or by an evolutionary event in the tropical Atlantic (Knappertsbusch, 2016). In the following sections, the new morphometric measurements of *G. menardii* from Site U1476 are discussed in light of these two alternative hypotheses.

3.4.1 Is there sufficient evidence given to support the Agulhas faunal leakage hypothesis for *G. menardii*?

The Agulhas Leakage hypothesis suggests the dispersal of giant *G. menardii* specimens from the Indian Ocean via the Agulhas Leakage into the Atlantic Ocean during the Gelasian.

The test-size increase observed in the tropical Atlantic Ocean between 2.057 Ma (Hole 667A) to 1.95-1.7 Ma (Site 925, 502) coincides with coeval change in the predominant coiling direction from dextral to sinistral (Fig. 3.12, Friesenhagen, 2022a). This observation may suggest the appearance of a new *G. menardii* type in this ocean because specimens of different coiling direction are considered in some planktonic foraminiferal species to represent different cryptic species (Pfuhl and Shackleton, 2004; Darling and Wade, 2008 for a review; Ujiié et al., 2010). A previous occurrence of this new giant (δY = >1000 µm), predominantly sinistral coiling type in the Indian Ocean would thus be expected for the Agulhas Leakage model. Although the observations from Hole U1476A do not show the drastic test-size increase seen in the Atlantic Ocean (Fig. 3.5, 3.6, 3.7), a permanent change in coiling direction is observed at almost the same time (2.027 Ma) as in the eastern Atlantic Ocean sites from 2.057 Ma onwards (Fig. 3.12). However, while in the Atlantic Ocean first giant forms were recorded at 2.057 Ma, the first *sinistral* giants in the Indian Ocean were encountered at 2.95 Ma (Fig. 3.11b, 3.12). These observations support the idea that the new, giant *G. menardii* had been present but was only rare in the Indian Ocean prior to 2.027 Ma. It therefore cannot be excluded that a strengthening of the Agulhas Leakage after the NHG had transported "early bird" giant *G. menardii* populations into the Atlantic, where these populations survived. With the current knowledge it remains unclear whether the Agulhas Leakage faunal exchange begun or intensified after the NHG, or whether the Agulhas Leakage continuously dispersed menardiform faunas into the Atlantic Ocean (Berger and Wefer, 1996). In the latter case, maintenance of viable populations would certainly have been reduced in population and test size by harsh glacial conditions in the tropical Atlantic Ocean. Interestingly, the occurrence of the sinistrally coiling, giant type can already be observed in the western Pacific Ocean at 3.19 Ma (Fig. 3.12). It may indicate that this giant type evolved in the Pacific Ocean and was dispersed along the surface currents into the Indian and the Atlantic Ocean.

This question can only be solved by higher resolved morphometric studies of menardiforms in the southern Mozambique Channel to Cape region between 3 and 2 Ma.

Another evidence supporting the idea of a giant morphospecies dominating the *G. menardii* population in samples younger than 2.34 Ma may be given in a tendency to develop bimodal test-size distributions of populations. "Bimodality" is expressed in main mode at smaller tests

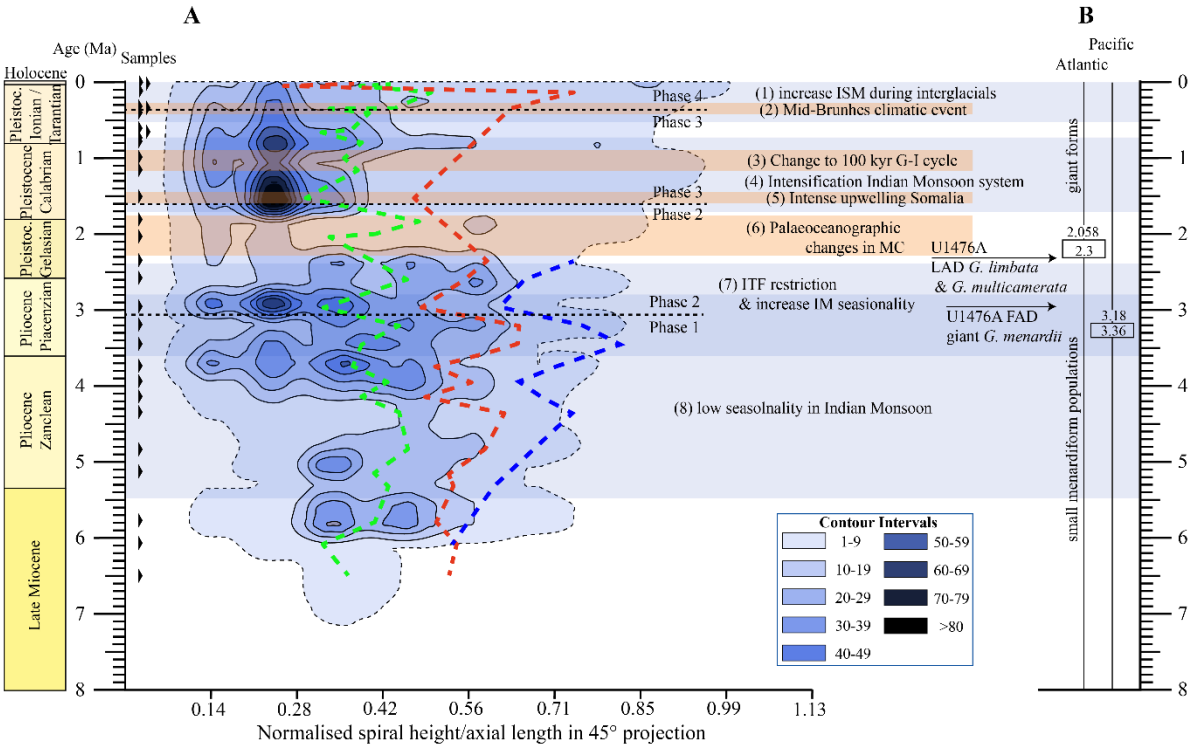

Figure 3.11: **(A)** Longitudinal section through the 45° view (offset-value = 0) of the VDD of Hole U1476A for *G. menardii* in a palaeoceanographical context. The solid lines represent contours at density intervals of ten specimens per grid-cell, the dotted line is the contour for a density of one specimen per grid-cell. The dashed green line illustrates the evolution of the mean size of *G. menardii*, the dashed red (blue) line the mean size evolution of *G. limbata* (*G. multicamerata*). (1) Increase in the Indian Summer Monsoon (ISM) (Petrick et al., 2019). (2) Mid-Brunhes climatic event (Jansen et al., 1986). (3) Shift towards an increased amplitude of glacial-interglacial cycles and a corresponding 100 ka fluctuation in global ice sheets (Clemens et al., 1996; Ivanova, 2009). (4) Intensification of the Indian Monsoon system (Gupta, 1999). (5) Intense upwelling in the Somalia Basin (Gupta, 1999). (6) Palaeoceanographic changes in the Mozambique Channel (Tangunan et al., 2018). (7) Tectonic restriction of the Indonesian Throughflow (De Vleeschouver et al., 2019, Auer et al., 2019) and increase in the Indian Monsoon seasonality (Gupta & Thomas, 2003; Ivanova, 2009; Chang et al., 2010). (8) Low seasonality of the Indian Monsoon, strong ISM, weaker Indian Winter monsoon (Gupta & Thomas, 2003). **(B)** shows the last appearance date (LAD) of *G. limbata* and *G. multicamerata* as well as the first appearance date of the giant G. menardii form at IODP Hole U1476A. Furthermore, it names the time intervals in which the giant form first occurred in the Atlantic Ocean (Friesenhagen, 2022a) and in the Pacific Ocean (Knappertsbusch, 2022).

and a subordinate secondary mode at larger test size (Fig. 3.8, 3.9). The underlying process may be the existence of vicariant dextrally and sinistrally coiling populations, possibly separated vertically or seasonally, developing different mean and median test sizes, as might be the case for *G. menardii-G. limbata-G. multicamerata* lineage.

The shift from an unimodal to a more bimodal distribution in samples younger than 2.34 Myr (Fig. 3.9 a, b) coincides with the change in dominance of coiling pattern from dextral to sinistral (Fig. 3.12). It possibly indicates an ecological replacement of the dominating, dextrally coiling incumbent by the new and larger growing, sinistrally coiling type. The time interval of this change-over occurred within a time of weaker water-column stratification in the Mozambique Channel (Tangunan et al., 2018) and during an interval of productivity changes in the western Indian Ocean (Curry et al., 1990).

In this context it is interesting to note that a unique bimodality in samples older than 2 Myr, at Site U1476 at 4.34 Ma (Fig. 3.8, 3.9), coincided with bimodality in the eastern tropical Atlantic Ocean Hole 667A (Friesenhagen, 2022a) at the same time.

All in all, the morphometric measurements of *G. menardii* from IODP Hole U1476A in the Mozambique Channel support the possibility of the dispersal of giant specimens from the Indian Ocean into the Atlantic Ocean via Agulhas leakage around 2 Ma. However, it does still not disprove the hypothesis of a punctuated-evolutionary event in the Atlantic Ocean as an explanation for the observed test-size increase.

3.4.2 Test-size evolution of *G. menardii*

In figure 3.5, 3.6 and 3.7, four different phases in the evolution of the mean and median test size of *G. menardii* were identified in δX, δY and Ar. If compared with palaeoceanographic reconstructions from the literature, transitions between the phases during the past 6.49 Ma seem to roughly coincide with major changes in the Indian and Asian monsoon system (Fig. 3.11a). The relatively stable values, exhibiting only minor changes, in the mean and median test-size in Phase 1 (Fig. A3.5 in the Appendix; ca. 6.49 to 3.19 Ma) go along with a reconstructed low seasonality in the Indian monsoon, in which a relatively strong ISM and a relatively weak IWM prevailed (Gupta and Thomas, 2003). From 3.19 Ma until 1.772 Ma (Phase 2), the mean and median size fluctuated strongly in short time (e.g. a doubling of median size between 2.025 and 1.772Ma). Records for the Indian monsoon show an increase in seasonality (Ivanova, 2009; Chang et al., 2010), which may be caused by a continuing constriction of the ITF (Auer et al., 2019]; De Vleeschouwer et al., 2018).

From 1.772 Ma until 0.4 Ma, the Indian monsoon index of Zhisheng et al. (2011) suggests an overall strengthened ISM and coincides with stable values of the mean and median δX and Ar (Fig. 3.5, 3.6, 3.7, A3.2). This phase ends with a strong increase in the δX, δY and Ar around 0.4 Ma, when the index indicates a weakening of the ISM during interglacials. The increase of the mean and median size also coincides with the Mid-Brunhes event, when climate shifted towards more glacial (interglacial) conditions in the Northern (Southern) Hemisphere 0.4 Ma ago (Jansen et al., 1986; Fig. 3.11a).

A possible explanation for the general coincidence of Indian monsoon and the size evolution of *G. menardii* may be found on the impact of long-term changes in the Indian Monsoon system on the (palaeo-)hydrography within the Mozambique Channel but needs to be investigated in high-resolution studies.

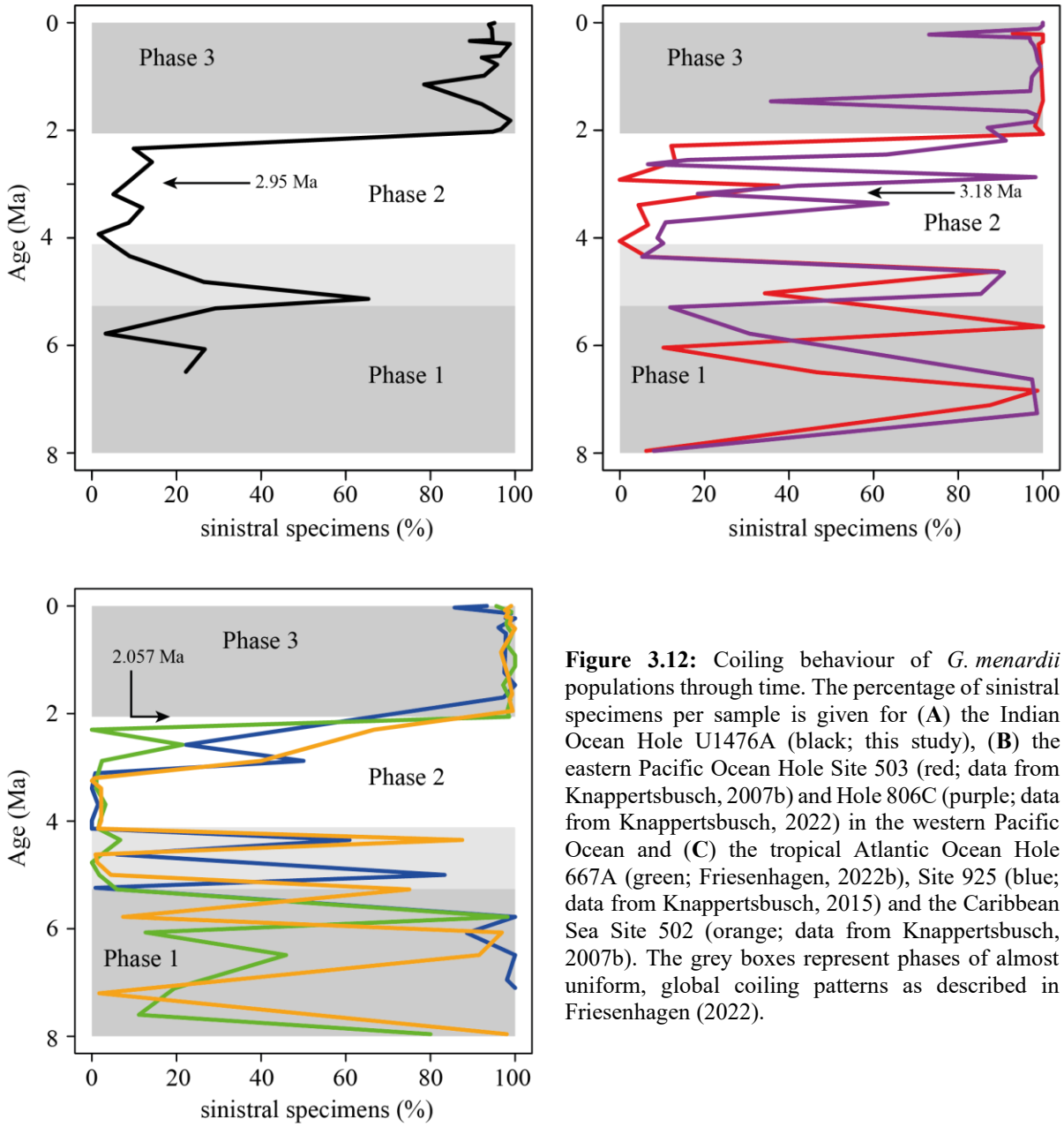

Figure 3.12: Coiling behaviour of *G. menardii* populations through time. The percentage of sinistral specimens per sample is given for (**A**) the Indian Ocean Hole U1476A (black; this study), (**B**) the eastern Pacific Ocean Hole Site 503 (red; data from Knappertsbusch, 2007b) and Hole 806C (purple; data from Knappertsbusch, 2022) in the western Pacific Ocean and (**C**) the tropical Atlantic Ocean Hole 667A (green; Friesenhagen, 2022b), Site 925 (blue; data from Knappertsbusch, 2015) and the Caribbean Sea Site 502 (orange; data from Knappertsbusch, 2007b). The grey boxes represent phases of almost uniform, global coiling patterns as described in Friesenhagen (2022).

In contrast to the mean and median size evolution, the long-term trend in maximum test-size evolution does not show any obvious coincidence with major palaeoceanographic changes but is gradual (Fig. 3.11). This gradual pattern in the evolution of the maximum test size (Fig. 3.5, 3.6, 3.7, 3.10) in the Indian Ocean is similar to the eastern and western tropical Pacific (Knappertsbusch, 2007a; 2022), but very different to the punctured pattern observed in the tropical Atlantic Ocean and Caribbean Sea (Knappertsbusch, 2007a; 2016; Friesenhagen, 2022a). The gradual size evolution of the larger test size extreme pattern might reflect Cope's rule, manifesting undistributed evolutionary trends towards increasing body sizes (Stanley, 1973; Brown and Maurer, 1973; Heim et al., 2015).

3.4.3 Morphometric Evolution of the *G. menardii*-*G. limbata*-*G. multicamerata*-lineage

A comparison of the evolution of the mean and median δX, δY and Ar in *G. menardii*, *G. limbata* and *G. multicamerata* shows that prior to 2.027 Myr *G. menardii* was rather static in size, *G. multicamerata* developed largest test size and *G. limbata* was intermediate in between the two (Fig. 3.5d, 3.6d, 3.7d). This observation is in agreement with results of former studies from the tropical Atlantic Ocean (Knappertsbusch, 2007a, 2016; Friesenhagen, 2022a) and the eastern and western equatorial Pacific Ocean (Knappertsbusch, 2007a, 2022).

The overall increasing trend in the means and medians of *G. limbata* and *G. multicamerata* differs from the more stable pattern in *G. menardii* and reveals a diverging trend: it starts at 3.935 Ma in the Indian Ocean, which is ca. 0.5 Myr later than in the Atlantic Ocean Site 667 (Friesenhagen, 2022a), and negated at ca. 3 Ma, similar to Site 667. Whether this trend is caused by evolution or is rooted in environmental effects has to be investigated in further, more detailed studies.

After 2 Ma, means and medians of the investigated parameters remain relatively stable in *G. menardii*. This contrasts the evolution observed in the Atlantic Ocean (Knappertsbusch, 2007; 2016; Friesenhagen, 2022a), where a discernible increase was interpreted as an evolutionary event sensu incumbency replacement (Rosenzweig and McCord, 1991) (Friesenhagen, 2022a).

Noteworthy is the last appearance date of *G. multicamerata* at 2.34 Ma for Hole U1476A. This is 750 kyr to 650 kyr later as it is described in Berggren et al. (1995) (3.09 Ma), Wade et al. (2011) (2.99 Ma), respectively, as well as in the tropical Atlantic Ocean in previous studies (2.88 Ma; Knappertsbusch, 2016; Friesenhagen, 2022a). This “delayed” extinction at Site U1476 was already noted in the planktonic foraminifer occurrence data in Hall et al. (2017b). Reworking of specimens is unlikely as an explanation because neither Hall et al. (2017b) nor Tangunan et al. (2018) could find evidence for (major) reworking in the sediment record between 2.85 Ma and 1.85 Ma. The visual core description of Site U1476 also does not indicate any signs for large-scale reworking, hiatuses, or drilling disturbances of sediments. Therefore, the results of this study confirm delayed (pseudo-) extinction of *G. multicamerata* in the Indian Ocean.

3.5 Conclusions

1. The new dataset of test-size measurements of the *G. menardii-G. limbata-G. multicamerata* lineage from the Indian Ocean IODP Hole U1476A for the last 6.5 Ma does not contradict the Agulhas Leakage hypothesis. Giant, sinistrally coiling *G. menardii* were first observed at 2.95 Ma preceding its Atlantic occurrence by 0.9 Myr. It can thus not be excluded that the giant form was dispersed into the Atlantic Ocean via the Agulhas Leakage between 2.3 Ma and 2.058 Ma, but a better geographic coverage at higher stratigraphic resolution is needed to further strengthen this conclusion.
2. Long-term changes of mean and median test-size show a coinciding trend with long-term changes in the Indian monsoon system. This might be explained by the alteration of the regional hydrography by the long-term changes in the monsoon system, which affect the thermocline habitat of *G. menardii*.
3. Investigated samples younger than 2.34 Ma reveal some bimodality in the size distribution. The beginning of bimodal distributions matches with the start to dominance of sinistrally coiling *G. menardii* populations. This pattern may indicate the establishment of vicariant populations. For further confirmation of these observations, a high-resolution dataset of size measurements for the time interval between 2.58 Ma and 2.058 Ma for the eastern tropical Atlantic Ocean would be required.
4. There is no evidence for rapid, punctured test-size evolution of Indian Ocean menardiforms, which stands in contrast to the situation in the Atlantic forms.
5. The interspecific comparison of the mean test size in the *G. menardii-G. limbata-G. multicamerata* lineage reveals similar pattern as observed in the Atlantic: *G. multicamerata* exhibit the largest size, *G. menardii* the smallest size and *G. limbata* is in between the two. However, *G. multicamerata* and *G. limbata* show a more divergent pattern in the size evolution in comparison to *G. menardii* than in the Atlantic Ocean.

Contributions

TF prepared the sample material, made measurements with the system AMOR 2, conducted the statistical evaluation, wrote the text and created the figures. MK critically reviewed the script and added the text passage about the comparability of the AMOR systems.

Code availability

The Fortran codes and programmes will be uploaded to the PANGAEA Data Repository and are stored at internal servers of the Natural History Museum Basel.

Data availability

The data will be uploaded to the PANGAEA Data Repository and are stored at internal servers of the Natural History Museum Basel.

Sample availability

All sample material and residuals are stored in the collection of the Natural History Museum Basel as the reference collection to the dissertation of Friesenhagen.

Acknowledgements

We are obligated to the International Ocean Discovery Program (IODP) for providing the investigated samples.

We thank An Zhisheng for providing data of the ISM Index.

Thank goes to the Natural History Museum Basel for excellent collaboration and all colleagues for discussions, feedback and support, in particular Daniel Burkhardt, Mark Charran, Christian de Capitani, Dominik Fleitmann, Thomas Kuhn, Sergio Kühni, Moritz Lehmann, David Marques, Bastien Mennecart, Johannes Pietsch, André Puschnig, Diana Rendon Mera, Tamara Spasojevic, Alexandra Viertler, and Andreas Wetzel.

Special thanks go to the Freiwillige Akademische Gesellschaft Basel (FAG) for financial support.

Financial support

The Swiss National Science Foundation (SNF) funded this project as well as the construction of system AMOR 2 (SNF-No.: 200021_169048/1 and 200021_169048/2).

References

Auer, G., De Vleeschouwer, D., Smith, R. A., Bogus, K., Groeneveld, J., Grunert, P., Castañeda, I. S., Petrick, B., Christensen, B., Fulthorpe, C., Gallagher, S. J., and Henderiks, J.: Timing and Pacing of Indonesian Throughflow Restriction and Its Connection to Late Pliocene Climate Shifts, Paleoceanography and Paleoclimatology, 34, 635–657, https://doi.org/10.1029/2018pa003512, 2019.

Beal, L. M., De Ruijter, W. P. M., Biastoch, A., and Zahn, R.: On the role of the Agulhas system in ocean circulation and climate, Nature, 472, 429–436, https://doi.org/10.1038/nature09983, 2011.

Berger, W. H. and Wefer, G.: Expeditions into the Past: Paleoceanographic Studies in the South Atlantic, in: The South Atlantic, pp. 363–410, Springer Berlin Heidelberg, https://doi.org/10.1007/978-3-642-80353-6_21, 1996.

Berggren, W. A., Kent, D. V., Swisher, C. C., and Aubry, M.-P.: Geochronology, time scales and global stratigraphic correlation, vol. 54, chap. A Revised Cenozoic Geochronology and Chronostratigraphy, pp. 129–212, SEPM (Society for Sedimentary Geology), https://doi.org/10.2110/pec.95.04.0129, 1995.

Boebel, O., Lutjeharms, J., Schmid, C., Zenk, W., Rossby, T., and Barron, C.: The Cape Cauldron: a regime of turbulent inter-ocean exchange, Deep Sea Research Part II: Topical Studies in Oceanography, 50, 57–86, https://doi.org/10.1016/s0967-0645(02)00379-x, 2003.

Bolli, H. M.: The direction of coiling in the evolution of some Globorotaliidae, Contributions from the Cushman Foundation for Foraminiferal Research, 1, 82–89, 1950.

Bolli, H. M. and Saunders, J. B.: Plankton Stratigraphy, chap. 6. Oligocene to Holocene low latitude planktic foraminifera, Cambridge University Press, 1, 155–262, ISBN 0521235766, 1985.

Brown, J. H. and Maurer, B. A.: Body size, ecological dominance and Cope' rule, Nature, 324, 248–250, https://doi.org/10.1038/324248a0, 1986.

Brown, K. R.: Biogeographic and morphological variation in late Pleistocene to Holocene globorotalid foraminifera, PhD-Thesis, University of Basel, https://edoc.unibas.ch/780/ (last access: 20 June 2012), 2007.

Caley, T., Jiraudeau, J., Malaizé, B., Rossignol, L., and Pierre, C.: Agulhas leakage as a key process in the modes of Quaternary climate changes, PNAS, 109, 6835–6839, https://doi.org/10.1073/pnas.1115545109, 2012.

Caley, T., Peeters, F. J., Biastoch, A., Rossignol, L., van Sebille, E., Durgadoo, J., Malaizé, B., Giradeau, J., Arthur, K., and Zahn, R.: Quantitative estimate of the paleo-Agulhas leakage,

Geophysical Research Letters, 41, 1238–1246, https://doi.org/10.1002/2014GL059278, 2014.

Caromel, A. G. M., Schmidt, D. N., Fletcher, I., and Rayfield, E. J.: Morphological Change During The Ontogeny Of The Planktic Foraminifera, Journal of Micropalaeontology, 35, 2–19, https://doi.org/10.1144/jmpaleo2014-017, 2016.

Chaisson, W. P. and Ravelo, A. C.: Changes in upper water-column structure at Site 925, late Miocene-Pleistocene: planktonic foraminifer assemblage and isotopic evidence, in: Proceedings of the Ocean Drilling Program, edited by Shackleton, N. J., Curry, W. B., Richter, C., and Bralower, T. J., vol. 154, pp. 255–268, Ocean Drilling Program, https://doi.org/10.2973/odp.proc.sr.154.105.1997, 1997.

Chan, C.-H., Chan, G. C. H., Leeper, T. J., and Becker, J.: rio: A Swiss-army knife for data file I/O, https://cran.r-project.org/web/packages/rio/, R package version 0.5.16, https://cran.r-roject.org/src/contrib/Archive/rio/ (last access: 7 September 2021), 2018.

Chang, Z., Xiao, J., Lü, L., and Yao, H.: Abrupt shifts in the Indian monsoon during the Pliocene marked by high-resolution terrestrial records from the Yuanmou Basin in southwest China, Journal of Asian Earth Sciences, 37, 166–175, https://doi.org/10.1016/j.jseaes.2009.08.005, 2010.

Clemens, S. C., Murray, D. W., and Prell, W. L.: Nonstationary Phase of the Plio-Pleistocene Asian Monsoon, Science, 274, 943–948, https://doi.org/10.1126/science.274.5289.943, 1996.

Curry, W. B., Cullen, J. L., and Backman, J.: Carbonate Accumulation in the Indian Ocean during the Pliocene: Evidence for a Change in Productivity and Preservation at about 2.4 Ma, in: Proceedings of the Ocean Drilling Program, 115 Scientific Results, vol. 115, chap. 26, pp. 509–518, Ocean Drilling Program, https://doi.org/10.2973/odp.proc.sr.115.164.1990, 1990.

Darling, K. F. and Wade, C. M.: The genetic diversity of planktic foraminifera and the global distribution of ribosomal RNA genotypes, Marine Micropaleontology, 67, 216–238, https://doi.org/10.1016/j.marmicro.2008.01.009, 2008.

de Vargas, C. and Pawlowski, J.: Molecular versus Taxonomic Rates of Evolution in Planktonic Foraminifera, Molecular Phylogenetics and Evolution, 9, 463–469, https://doi.org/10.1006/mpev.1998.0491, 1998.

De Vleeschouwer, D., Auer, G., Smith, R., Bogus, K., Christensen, B., Groeneveld, J., Petrick, B., Henderiks, J., Castañeda, I. S., O'Brien, E., Ellinghausen, M., Gallagher, S. J., Fulthorpe, C. S., and Pälike, H.: The amplifying effect of Indonesian Throughflow heat transport on

Late Pliocene Southern Hemisphere climate cooling, Earth and Planetary Science Letters, 500, 15–27, https://doi.org/10.1016/j.epsl.2018.07.035, 2018.

Ericson, D. B. and Wollin, G.: Micropaleontological and isotopical determinations of Pleistocene climates, Micropaleontology, 2, 257–270, https://doi.org/10.2307/1484180, 1956.

Fallet, U., Brummer, G.-J., Zinke, J., Vogels, S., and Ridderinkhof, H.: Contrasting seasonal fluxes of planktonic foraminifera and impacts on paleothermometry in the Mozambique Channel upstream of the Agulhas Current, Paleoceanography, 25, https://doi.org/10.1029/2010pa001942, 2010.

Friesenhagen, T.: Test-Size Evolution of the planktonic Foraminifera Globorotalia menardii in the Eastern Tropical Atlantic since the Late Miocene, Biogeosciences, 10.5194/bg-2021-67, 2022a

Friesenhagen, T.: Archive to the evolutionary study about menardiform globorotallids (planktonic foraminifer) in the eastern tropical Atlantic ocean ODP Hole 667A, PANGAEA Data Repository, https://doi.org/10.1594/PANGAEA.940563, 2022b

Gupta, A. K.: Latest Pliocene through Holocene paleoceanography of the eastern Indian Ocean: benthic foraminiferal evidence, Marine Geology, 161, 63–73, https://doi.org/10.1016/S0025-3227(99)00056-0, 1999.

Gupta, A. K. and Thomas, E.: Initiation of Northern Hemisphere glaciation and strengthening of the northeast Indian monsoon: Ocean Drilling Program Site 758, eastern equatorial Indian Ocean, Geology, 31, 47, https://doi.org/10.1130/0091-7613(2003)031<0047:ionhga>2.0.co;2, 2003.

Hall, I. R., Hemming, S. R., LeVay, L. J., and the Expedition 361 Scientists: Expedition 361 Scientific Prospectus: South African climates (Agulhas LGM density profile), International Ocean Discovery Program, http://dx.doi.org/10.14379/iodp.pr.361.2016, 2016.

Hall, I. R., Hemming, S. R., LeVay, L. J., Barker, S., Berke, M. A., Brentegani, L., Caley, T., Cartagena-Sierra, A., Charles, C. D., Coenen, J. J., Crespin, J. G., Franzese, A. M., Gruetzner, J., Han, X., Hines, S. K. V., Jimenez Espejo, F. J., Just, J., Koutsodendris, A., Kubota, K., Lathika, N., Norris, D. R., Periera dos Santos, T., Robinson, R., Rolinson, J. M., Simon, M. H., Tangunan, D., van der Lubbe, J. J. L., Yamane, M., and Zhang, H.: Expedition 361 summary, in: Proceedings of the International Ocean Discovery Program, International Ocean Discovery Program, http://dx.doi.org/10.14379/iodp.proc.361.101.2017, 2017.

Hall, I. R., Hemming, S. R., LeVay, L. J., Barker, S., Berke, M. A., Brentegani, L., Caley, T., Cartagena-Sierra, A., Charles, C. D., Coenen, J. J., Crespin, J. G., Franzese, A. M., Gruetzner, J., Han, X., Hines, S. K. V., Jimenez Espejo, F. J., Just, J., Koutsodendris, A., Kubota, K., Lathika, N., Norris, D. R., Periera dos Santos, T., Robinson, R., Rolinson, J. M., Simon, M. H., Tangunan, D., van der Lubbe, J. J. L., Yamane, M., and Zhang, H.: Site U1476, in: Proceedings of the International Ocean Discovery Program, International Ocean Discovery Program, http://dx.doi.org/10.14379/iodp.proc.361.105.2017, 2017.

Hecht, A. D.: An ecologic model for test size variation in Recent planktonic foraminifera; applications to the fossil record, The Journal of Foraminiferal Research, 6, 295–311, https://doi.org/10.2113/gsjfr.6.4.295, 1976.

Heim, N. A., Knope, M. L., Schaal, E. K., Wang, S. C., and Payne, J. L.: Cope's rule in the evolution of marine animals, Science, 347, 867–870, https://doi.org/10.1126/science.1260065, 2015.

Hull, P. M. and Norris, R. D.: Evidence for abrupt speciation in a classic case of gradual evolution, PNAS, 106, 21224–21229, https://doi.org/10.1073/pnas.0902887106, 2009.

Ivanova, E. V.: Paleoceanography of the Northern Indian Ocean: Linkages to Monsoon and Global Thermohaline Paleocirculation, in: The Global Thermohaline Paleocirculation, pp. 107–145, Springer Netherlands, https://doi.org/10.1007/978-90-481-2415-2_5, 2009.

Jansen, J. H. F., Kuijpers, A., and Troelstra, S. R.: A Mid-Brunhes Climatic Event: Long-Term Changes in Global Atmosphere and Ocean Circulation, Science, 232, 619–622, https://doi.org/10.1126/science.232.4750.619, 1986.

Keller, G.: Depth stratification of planktonic foraminifers in the Miocene ocean, in: Geological Society of America Memoirs, vol. 163, pp. 177–196, Geological Society of America, https://doi.org/10.1130/mem163-p177, 1985.

Kennett, J. P. and Srinivasan, M. S.: Neogene planktonic foraminifera. A phylogenetic atlas, Hutchinson Ross Publishing Company, Stroudsburg, Pa. New York, NY, ISBN 0879330708, 1983.

Knappertsbusch, M.: Morphological evolution of menardiform globorotalids at Western Pacific Warm Pool ODP Hole 806C (Ontong-Java Plateau) Evolution morphologique du groupe de Globorotalia menardii au Site ODP 806C (Ontong-Java Plateau, Pacifique tropical occidental), Revue de Micropaléontologie, 74, 100608, https://doi.org/10.1016/j.revmic.2022.100608, 2022.

Knappertsbusch, M. W.: Morphological variability of Globorotalia menardii (planktonic foraminifera) in two DSDP cores from the Caribbean Sea and the Eastern Equatorial Pacific, Carnets de Geologie, CG2007, 1–34, hal-00164930, 2007a

Knappertsbusch, M. W.: Morphological variability of Globorotalia menardii in DSDP Sites 68-502 and 68-503, supplement to: Knappertsbusch, Michael W (2007): Morphological variability of Globorotalia menardii (planktonic foraminifera) in two DSDP cores from the Caribbean Sea and the Eastern Equatorial Pacific. Carnets de Geologie, CG2007_A04, 10.1594/PANGAEA.863580, 2007.

Knappertsbusch, M. W.: Evolutionary prospection in the Neogene planktic foraminifer Globorotalia menardii and related forms from ODP Hole 925B (Ceara Rise, western tropical Atlantic): evidence for gradual evolution superimposed by long distance dispersal?, Swiss Journal of Palaeontology, 135, 205–248, https://doi.org/10.1007/s13358-016-0113-6, 2016.

Knappertsbusch, M. W.: Commented archive to studies about the morphological evolution of menardiform globorotalids at Western Pacific Warm Pool ODP Hole 806C (Ontong-Java Plateau), https://doi.org/10.1594/PANGAEA.932504, 2021.

Knappertsbusch, M. W. and Mary, Y.: Mining morphological evolution in microfossils using volume density diagrams, Palaeontologica Electronica, 15, 1–29, https://doi.org/10.26879/278, 2012.

Knappertsbusch, M. W., Binggeli, D., Herzig, A., Schmutz, L., Stapfer, S., Schneider, C., Eisenecker, J., and Widmer, L.: AMOR – A NEW SYSTEM FOR AUTOMATED IMAGING OF MICROFOSSILS FOR MORPHOMETRIC ANALYSES, Palaeontologia Electronica, 12, 12.2.2T, 2009.

Lazarus, D.: Tempo and mode of morphologic evolution near the origin of the radiolarian lineage Pterocanium prismatium, Paleobiology, 12, 175–189, https://doi.org/10.1017/s0094837300013646, 1986.

Lazarus, D.: Age Depth Plot and Age Maker: Age Modeling of Stratigraphic Sections on the Macintosh Series of Computers, Geobyte, 7:1, 7–14, 5425155,1992.

Lebourges-Dhaussy, A., Huggett, J., Ockhuis, S., Roudaut, G., Josse, E., and Verheye, H.: Zooplankton size and distribution within mesoscale structures in the Mozambique Channel: A comparative approach using the TAPS acoustic profiler, a multiple net sampler and ZooScan image analysis, Deep Sea Research Part II: Topical Studies in Oceanography, 100, 136–152, 10.1016/j.dsr2.2013.10.022, 2014.

Leckie, R. M.: A palaeoceanographic model for the early evolutionary history of planktonic foraminifera, Palaeogeography, Palaeoclimatology, Palaeoecology, 73, 107–138, https://doi.org/10.1016/0031-0182(89)90048-5, 1989.

Lévy, M., Shankar, D., André, J.-M., Shenoi, S. S. C., Durand, F., and de Boyer Montégut, C.: Basin-wide seasonal evolution of the Indian Oceans phytoplankton blooms, Journal of Geophysical Research, 112, https://doi.org/10.1029/2007jc004090, 2007.

Lisiecki, L. E. and Raymo, M.: A Pliocene-Pleistocene stack of 57 globally distributed benthic d18O records, Paleoceanography, 20, https://doi.org/10.1029/2004PA001071, 2005.

Lohmann, G. P. and Malmgren, B. A.: Equatorward migration of Globorotalia truncatulinoides ecophenotypes through the Late Pleistocene: Gradual evolution or ocean change?, Paleobiology, 9, 414–421, https://doi.org/10.1017/s0094837300007879, 1983.

Majewski, W.: Mid-Miocene invasion of ecological niches by planktonic foraminifera of the Kerguelen Plateau, Antarctica, Marine Micropaleontology, 46, 59–81, https://doi.org/10.1016/s0377-8398(02)00051-8, 2002.

Malmgren, B. A., Berggren, W. A., and Lohmann, G. P.: Evidence for punctuated gradualism in the Late Neogene Globorotalia tumida lineage of planktonic foraminifera, Paleobiology, 9, 377–389, https://doi.org/10.1017/s0094837300007843, 1983.

Norris, R. D.: Reconstruction Ocean History, chap. Hydrographic and tectonic control of plankton distribution and evolution, pp. 173–193, Springer US, https://doi.org/10.1007/978-1-4615-4197-4, 1999.

Nuber, S.: Atmospheric CO2 across the Plio-Pleistocene, PhD-Thesis, Cardiff University, http://orca.cf.ac.uk/134264/, 2020.

Ortiz, J. D., Mix, A. C., and Collier, R. W.: Environmental control of living symbiotic and asymbiotic foraminifera of the California Current, Paleoceanography, 10, 987–1009, https://doi.org/10.1029/95pa02088, 1995.

Pearson, P. N. and Coxall, H. K.: Origin of the Eocene Planktonic Foraminifer Hantkenina by Gradual Evolution, Palaeontology, 57, 243–267, https://doi.org/10.1111/pala.12064, 2014.

Peeters, F. J. C., Acheson, R., Brummer, G.-J. A., de Ruijter, W. P. M., Schneider, R. R., Ganssen, G. M., Ufkes, E., and Kroon, D.: Vigorous exchange between the Indian and Atlantic oceans at the end of the past five glacial periods, Nature, 430, 661–665, https://doi.org/10.1038/nature02785, 2004.

Petrick, B., Martnez-Garcá, A., Auer, G., Reuning, L., Auderset, A., Deik, H., Takayanagi, H., De Vleeschouwer, D., Iryu, Y., and Haug, G. H.: Glacial Indonesian Throughflow

weakening across the Mid-Pleistocene Climatic Transition, Scientific Reports, 9, https://doi.org/10.1038/s41598-019-53382-0, 2019.

Pfuhl, H. A. and Shackleton, N. J.: Changes in coiling direction, habitat depth and abundance in two menardellid species, Marine Micropaleontology, 50, 3–20, https://doi.org/10.1016/s0377-8398(03)00063-x, 2004.

Poore, R. Z.: Late Miocene biogeography and paleoclimatology of the central North Atlantic, Marine Micropaleontology, 6, 599–616, https://doi.org/10.1016/0377-8398(81)90023-2, 1981.

Portilho-Ramos, R. D. C., Barbosa, C. F., and Rios-Netto, A. M.: Planktonic foraminiferal variations in the southwestern Atlantic since the last glacial-interglacial cycle, Palaios, 29, 38–44, http://dx.doi.org/10.2110/palo.2012.104, 2014.

Railsback, L. B., Gibbard, P. L., Head, M. J., Voarintsoa, N. R. G., and Toucanne, S.: An optimized scheme of lettered marine isotope substages for the last 1.0 million years, and the climatostratigraphic nature of isotope stages and substages, Quaternary Science Reviews, 111, 94–106, 10.1016/j.quascirev.2015.01.012, 2015.

Rasband, W. S.: ImageJ, U.S. National Institute of Helath, https://imagej.nih.gov/ij/ (last access: 10 January 2019), version 1.8.0_172 (645-bit), 1997–2018.

Rau, A. J., Rogers, J., Lutjeharms, J. R. E., Giraudeau, J., Lee-Thorp, J. A., Chen, M.-T., and Waelbroeck, C.: A 450-kyr record of hydrological conditions on the western Agulhas Bank Slope, south of Africa, Marine Geology, 180, 183–201, https://doi.org/10.1016/s0025-3227(01)00213-4, 2002.

Ravelo, A. C., Fairbanks, R. G., and Philander, S. G. H.: Reconstructing tropical Atlantic hydrography using planktonic foraminifera and an ocean model, Paleoceanography, 5, 409–431, https://doi.org/10.1029/pa005i003p00409, 1990.

Raymo, M. E.: The Initiation of Northern Hemisphere Glaciation, Annual Review of Earth and Planetary Sciences, 22, 353–383, https://doi.org/10.1146/annurev.ea.22.050194.002033, 1994.

Revelle, W.: psych: Procedures for Psychological, Psychometric, and Personality Research, Northwestern University, Evanston, Illinois, https://CRAN.R-project.org/package=psych (last access: 28 September 2021), R package version 1.8.12, 2018.

Rinker, T. W. and Kurkiewicz, D.: pacman: Package Management for R, Buffalo, New York, http://github.com/trinker/pacman (last access: 17 September 2019), version 0.5.0, 2018.

Rosenzweig, M. L. and McCord, R. D.: Incumbent replacement: evidence for long-term evolutionary progress, Paleobiology, 17, 202–213, https://doi.org/10.1017/s0094837300010563, 1991.

RStudio Team: RStudio: Integrated Development Environment for R, RStudio, PBC., Boston, MA, http://www.rstudio.com/, https://www.rstudio.com/ (last access: 25 May 2021), 2020.

Santos, T. P., Belem, A. L., Barbosa, C. F., Dokken, T., & Albuquerque, A. L. S.: Paleoceanographic reconstruction of the western equatorial Atlantic during the last 40 kyr. Palaeogeography, palaeoclimatology, palaeoecology, 415, 14-20, http://dx.doi.org/10.1016/j.palaeo.2014.01.001, 2014

Sarkar, A. and Guha, A. K.: Pleistocene paleoclimatic zonation in northern Indian Ocean as revealed from Globorotalia menardii abundance, Indian Journal of Marine Sciences, 26, 84–87, http://nopr.niscair.res.in/handle/123456789/36152, 1997.

Schiebel, R. and Hemleben, C.: Classification and Taxonomy of Extant Planktic Foraminifers, in: Planktic Foraminifers in the Modern Ocean, e2019PA003738, chap. 2, pp. 11–110, Springer Berlin Heidelberg, 10.1007/978-3-662-50297-6_2, 2017.

Schmidt, D. N., Thierstein, H. R., Bollmann, J., and Schiebel, R.: Abiotic Forcing of Plankton Evolution in the Cenozoic, Science, 303, 207–210, https://doi.org/10.1126/science.1090592, 2004.

Schmidt, D. N., Lazarus, D., Young, J. R., and Kucera, M.: Biogeography and evolution of body size in marine plankton, Earth-Science Reviews, 78, 239–266, https://doi.org/10.1016/j.earscirev.2006.05.004, 2006.

Schouten, M. W., de Ruijter, W. P. M., van Leeuwen, P. J., and Ridderinkhof, H.: Eddies and variability in the Mozambique Channel, Deep Sea Research Part II: Topical Studies in Oceanography, 50, 1987–2003, https://doi.org/10.1016/s0967-0645(03)00042-0, 2003.

Schweitzer, P. N. and Lohmann, G. P.: Ontogeny and habitat of modern menardiiform planktonic foraminifera, The Journal of Foraminiferal Research, 21, 332–346, https://doi.org/10.2113/gsjfr.21.4.332, 1991.

Sexton, P. F. and Norris, R. D.: High latitude regulation of low latitude thermocline ventilation and planktic foraminifer populations across glacial-interglacial cycles, Elsevier, 311, 69–81, https://doi.org/10.1016/j.epsl.2011.08.044, 2011.

Shipboard Scientific Party: Facies Patterns and Authigenic Minerals of Upwelling Deposits off Southwest Africa, in: Proceedings of the Ocean Drilling Program 175 Initial Reports, edited by Baez, L. A. and Scroggs, J. M., vol. 175, pp. 7–25, Ocean Drilling Program, https://doi.org/10.2973/odp.proc.ir.175.116.1998, 1998.

Stanley, S. M.: An explanation for Cope's Rule, Evolution, 27, 1–26, https://doi.org/10.1111/j.1558-5646.1973.tb05912.x, 1973.

Steinhardt, J., Cléroux, C., Ullgren, J., de Nooijer, L., Durgadoo, J. V., Brummer, G.-J., and Reichart, G.-J.: Anti-cyclonic eddy imprint on calcite geochemistry of several planktonic foraminiferal species in the Mozambique Channel, Marine Micropaleontology, 113, 20–33, https://doi.org/10.1016/j.marmicro.2014.09.001, 2014.

Stewart, D. R. M.: Evolution of Neogene globorotaliid foraminifera and Miocene climate change, Doctoral dissertation, University of Bristol, https://ethos.bl.uk/OrderDetails.do?uin=uk.bl.ethos.288306 (last access: 9 December 2014), 2003.

Tabachnick, R. E. and Bookstein, F. L.: The structure of individual variation in Miocene Globorotalia, Evolution, 44, 416–434, https://doi.org/10.1111/j.1558-5646.1990.tb05209.x, 1990.

Tangunan, D. N., Baumann, K.-H., Just, J., LeVay, L. J., Barker, S., Brentegani, L., De Vleeschouwer, D., Hall, I. R., Hemming, S., and Norris, R.: The last 1 million years of the extinct genus Discoaster: Plio-Pleistocene environment and productivity at Site U1476 (Mozambique Cannel), Palaeogeography, Palaeoclimatology, Palaeoecology, 505, 187–197, https://doi.org/10.1016/j.palaeo.2018.05.043, 2018.

Ternon, J. F., Bach, P., Barlow, R., Huggett, J., Jaquemet, S., Marsac, F., Ménard, F., Penven, P., Potier, M., and Roberts, M. J.: The Mozambique Channel: From physics to upper trophic levels, Deep Sea Research Part II: Topical Studies in Oceanography, 100, 1–9, https://doi.org/10.1016/j.dsr2.2013.10.012, 2014.

Tew-Kai, E. and Marsac, F.: Patterns of variability of sea surface chlorophyll in the Mozambique Channel: A quantitative approach, Journal of Marine Systems, 77, 77–88, https://doi.org/10.1016/j.jmarsys.2008.11.007, 2009.

Thompson, P. R.: Foraminifers of the Middle America Trench, in: Initial Reports of the Deep Sea Drilling Project, 67, vol. 67, pp. 351–381, U.S. Government Printing Office, https://doi.org/10.2973/dsdp.proc.67.109.1982, 1982.

Tiedemann, R., Sarnthein, M., and Shackleton, N. J.: Astronomic timescale for the Pliocene Atlantic 18O and dust flux records of Ocean Drilling Program Site 659, Paleoceanography, 9, 619–638, https://doi.org/10.1029/94pa00208, 1994.

Ujiié, Y., de Garidel-Thoron, T., Watanabe, S., Wiebe, P., and de Vargas, C.: Coiling dimorphism within a genetic type of the planktonic foraminifer Globorotalia

truncatulinoides, Marine Micropaleontology, 77, https://doi.org/145–153, 10.1016/j.marmicro.2010.09.001, 2010.

van der Lubbe, H. J. L., Hall, I. R., Barker, S., Hemming, S. R., Baars, T. F., Starr, A., Just, J., Backeberg, B. C., and Joordens, J. C. A.: Indo-Pacific Walker circulation drove Pleistocene African aridification, 598, 618–623, https://doi.org/10.1038/s41586-021-03896-3, 2021.

Villar, E., Farrant, G. K., Follows, M., Garczarek, L., Speich, S., Audic, S., Bittner, L., Blanke, B., Brum, J. R., Brunet, C., Casotti, R., Chase, A., Dolan, J. R., d'Ortenzio, F., Gattuso, J.-P., Grima, N., Guidi, L., Hill, C. N., Jahn, O., Jamet, J.-L., Le Goff, H., Lepoivre, C., Malviya, S., Pelletier, E., Romagnan, J.-B., Roux, S., Santini, S., Scalco, E., Schwenck, S. M., Tanaka, A., Testor, P., Vannier, T., Vincent, F., Zingone, A., Dimier, C., Picheral, M., Searson, S., Kandels-Lewis, S., Oceanscoordinators, T., Acinas, S. G., Bork, P., Boss, E., de Vargas, C., Gorsky, G., Ogata, H., Pesant, S., Sullivan, M. B., Sunagawa, S., Wincker, P., Karsenti, E., Bowler, C., Not, F., Hingamp, P., and Iudicone, D.: Environmental characteristics of Agulhas rings affect interocean plankton transport, Science, 348, 1261447, https://doi.org/10.1126/science.1261447, 2015.

Wade, B. S., Pearson, P. N., Berggren, W. A., and Pälike, H.: Review and revision of Cenozoic tropical planktonic foraminiferal biostratigraphy and calibration to the geomagnetic polarity and astronomical time scale, Earth-Science Reviews, 104, 111–142, https://doi.org/10.1016/j.earscirev.2010.09.003, 2011.

Wei, K.-Y. and Kennett, J.-P.: Phyletic gradualism and punctuated equilibrium in the late Neogene planktonic foraminiferal clade Globoconella, Paleobiology, 14, 345–363, https://doi.org/10.1017/s0094837300012094, 1988.

Wickham, H.: ggplot2: Elegant Graphics for Data Analysis, Springer-Verlag New York, https://doi.org/10.1007/978-3-319-24277-4, 2016.

Wickham, H. and Bryan, J.: readxl: Read Excel Files, https://CRAN.R-project.org/-package=readxl, (last access: 16 September 2019), R package version 1.3.1, 2019.

Wolff, T., Mulitza, S., Rühlemann, C., and Wefer, G.: Response of the tropical Atlantic thermocline to late Quaternary trade wind changes, Paleoceanography, 14, 374–383, https://doi.org/10.1029/1999PA900011, 1999.

Wright, J. D. and Thunell, R. C.: Neogene Planktonic Foraminiferal Biogeography and Paleoceanography of the Indian Ocean, Micropaleontology, 34, 193, doi: 10.2307/1485752, 1988.

Zhisheng, A., Clemens, S. C., Shen, J., Qiang, X., Jin, Z., Sun, Y., Prell, W. L., Luo, J., Wang, S., Xu, H., Cai, Y., Zhou, W., Liu, X., Liu, W., Shi, Z., Yan, L., Xiao, X., Chang, H., Wu,

F., Ai, L., and Lu, F.: Glacial-Interglacial Indian Summer Monsoon Dynamics, Science, 333, 719–723, https://doi.org/10.1126/science.1203752, 2011.

Appendix

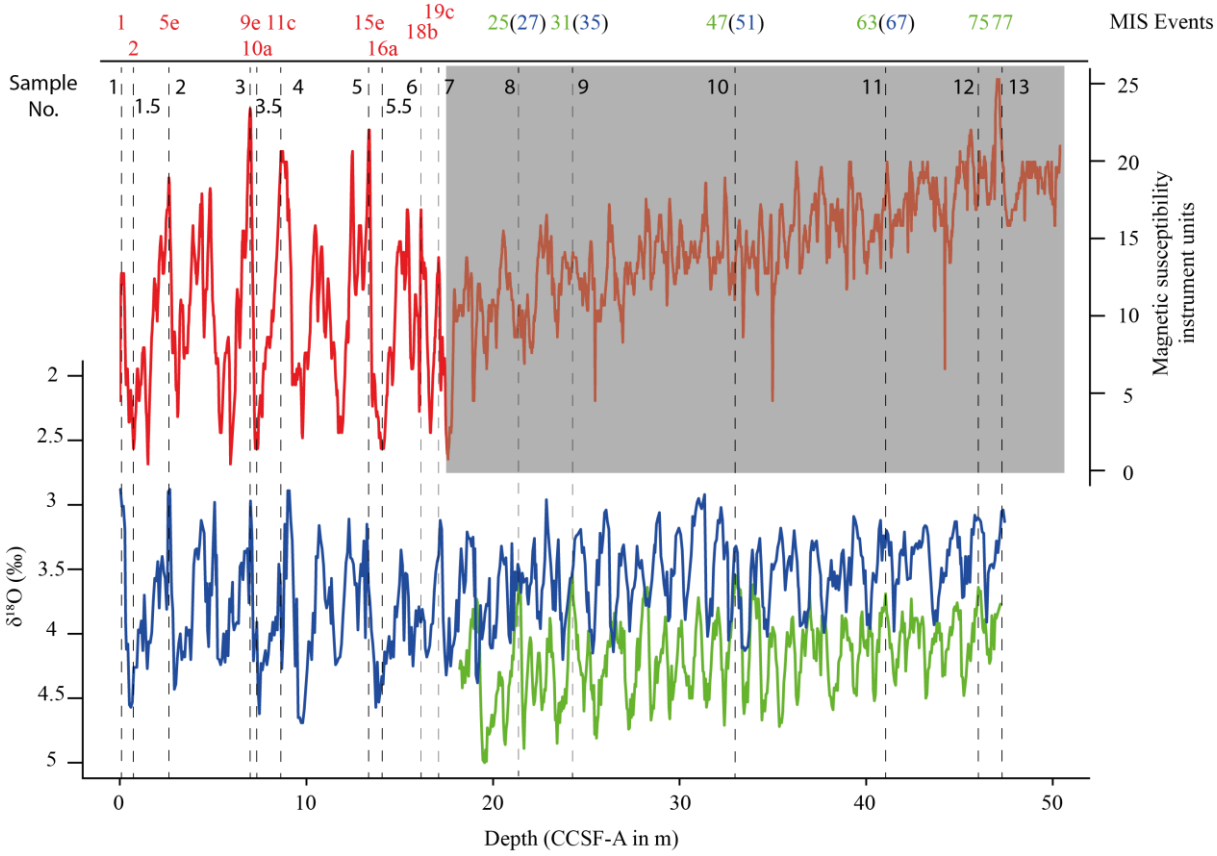

Figure A3.1: Illustration of sample selection process and temporal precision by comparison to the stable isotope record of van der Lubbe et al. (2021).
The red curve represents the record of magnetic susceptibility (MS) by Hall et al. (2017b), converted into CCSF-A (m) using table 10 and 12 in Hall et al. (2017b). That part of the curve which was not considered for samples selection is covered by a grey box, as the MS signal weakens and does not allow a distinctive correlation with the stable isotopic record. The blue line represents the $\delta^{18}O$ isotopic curve by van der Lubbe et al. (2021), the green line shows the $\delta^{18}O$ isotopic stack of Lisiecki and Raymo (2005; LR05). Sediment depths of the LR05 stack were converted to CCSF-A (m) by using table 10 and 12 in Hall et al. (2017b). The dashed lines indicate the depths of the investigated samples. The sample number refers to the number given in table 1. Red numbers of marine isotope stages (MIS) events indicate samples which were chosen based on the MS record, whereas MIS events with a green number represent samples, which were chosen by interglacial peaks in the LR05 stack. The number denotes the target MIS event. However, due to the discrepancy to the stable isotope record of van der Lubbe et al. (2021), the actual MIS event is given as a blue number in the brackets.

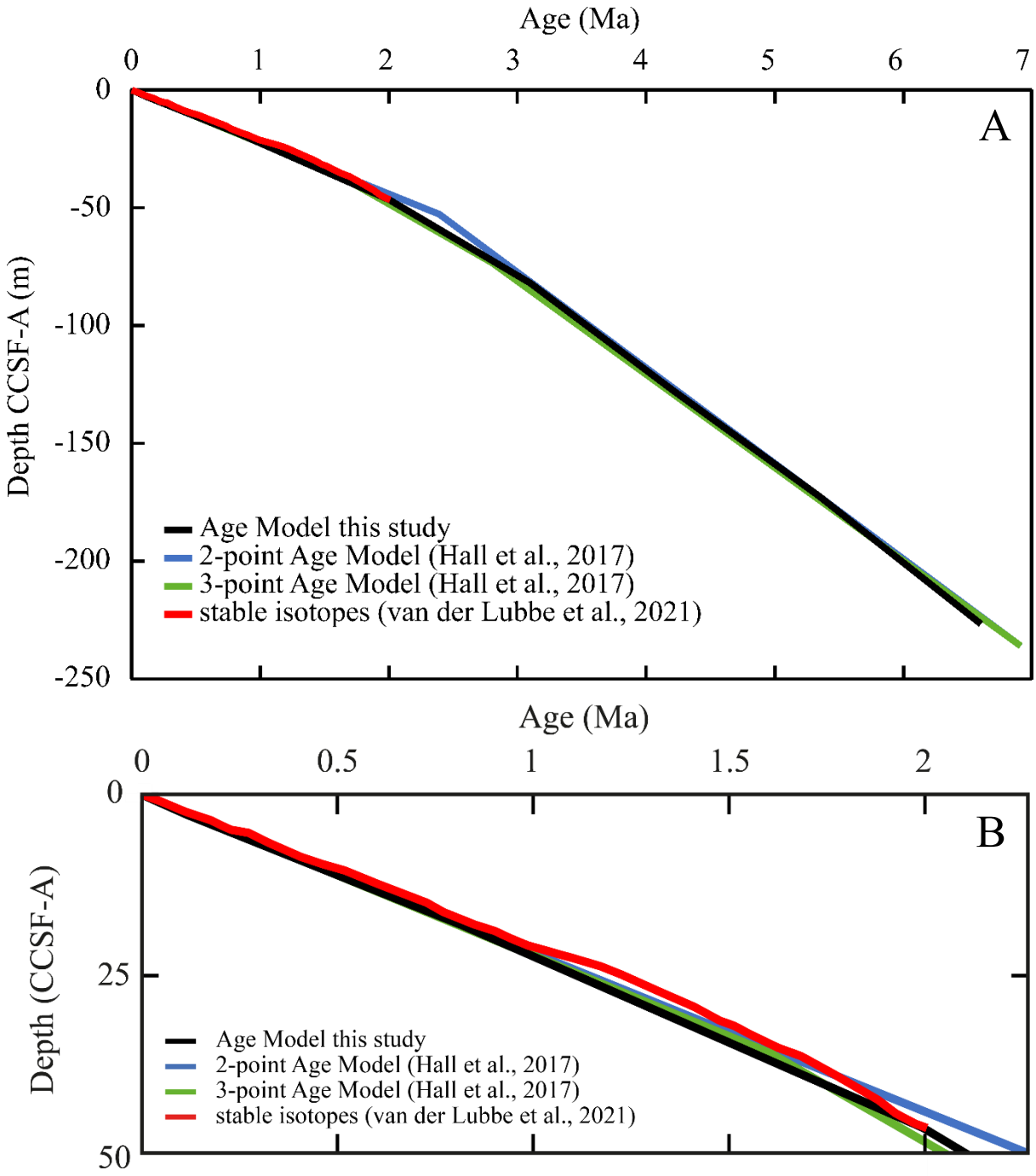

Figure A3.2: Comparison of the age models. The age (Ma) is plotted versus depth (CCSF-A in m). The black line represents the age model in this study (see also Fig. 3.2), the blue the two-point and green the three-point model by Hall et al. (2017b). The stable isotope record by van der Lubbe et al. (2021) is plotted as a red line. For conversion from CSF-A into CCSF-A for the age model of this study and that of Hall et al. (2017b), table 10 and 12 in Hall et al. (2017b) was used. (**A**) Comparison of the models along the entire core U1476A. (**B**) Extract of Fig. A3.2A.

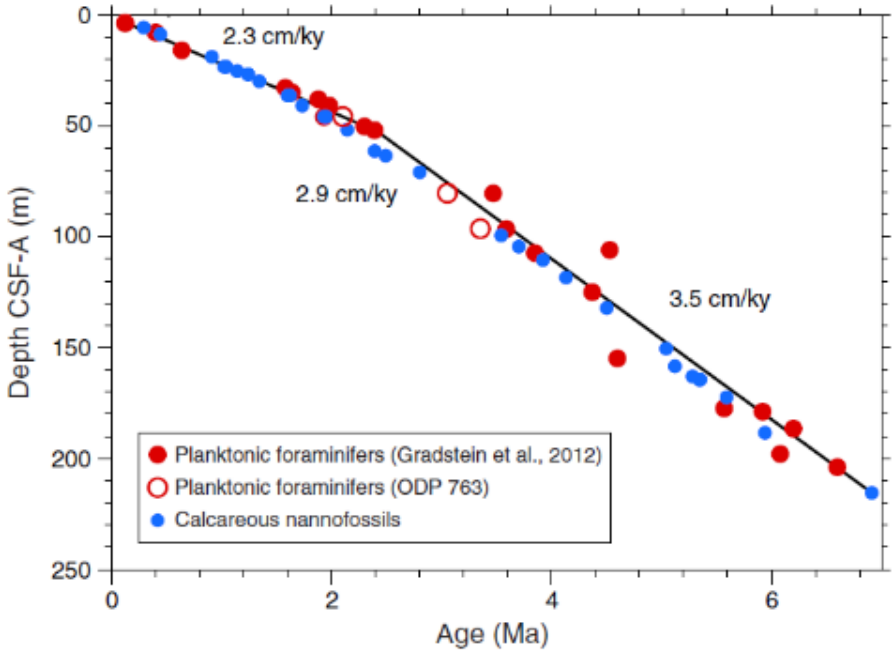

Figure A3.3: Age-Depth plot of Hole U1476A, based on the biochronology of calcareous nannofossils and planktonic foraminifers. Figure F38 in Hall et al. (2017b).

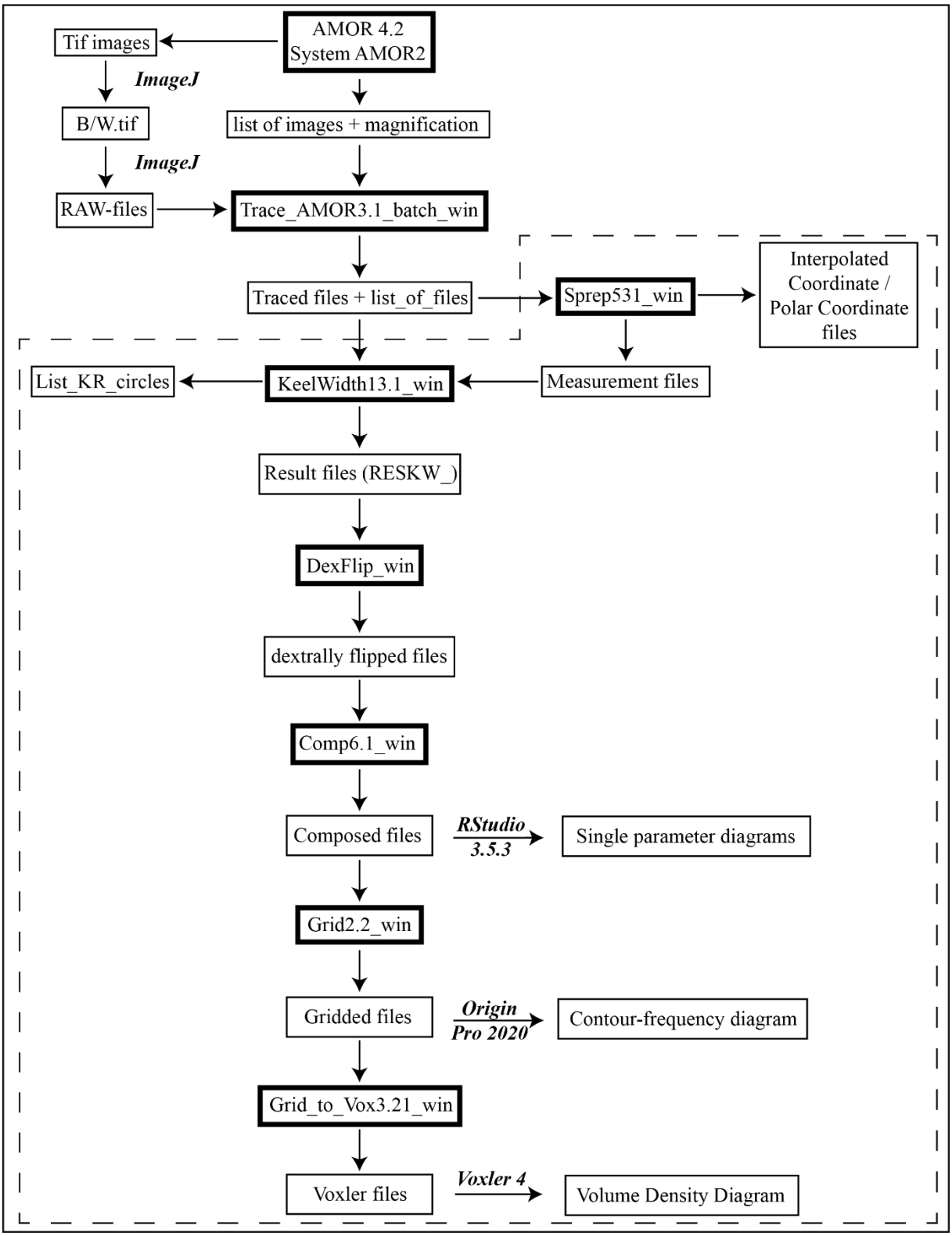

Figure A3.4: Flow chart of the used *MorphCol* programmes to process the data. Processing steps, which use sorted files in terms of species, number of chambers in the final whorl and the coiling direction, are indicated by the dashed frame. Applications are indicated by boxes with a thicker border. Output files are framed by thin lines. *RStudio (*V3.5.3*)* is public domain software, and *Origin* and *Voxler 4* are commercially available products.

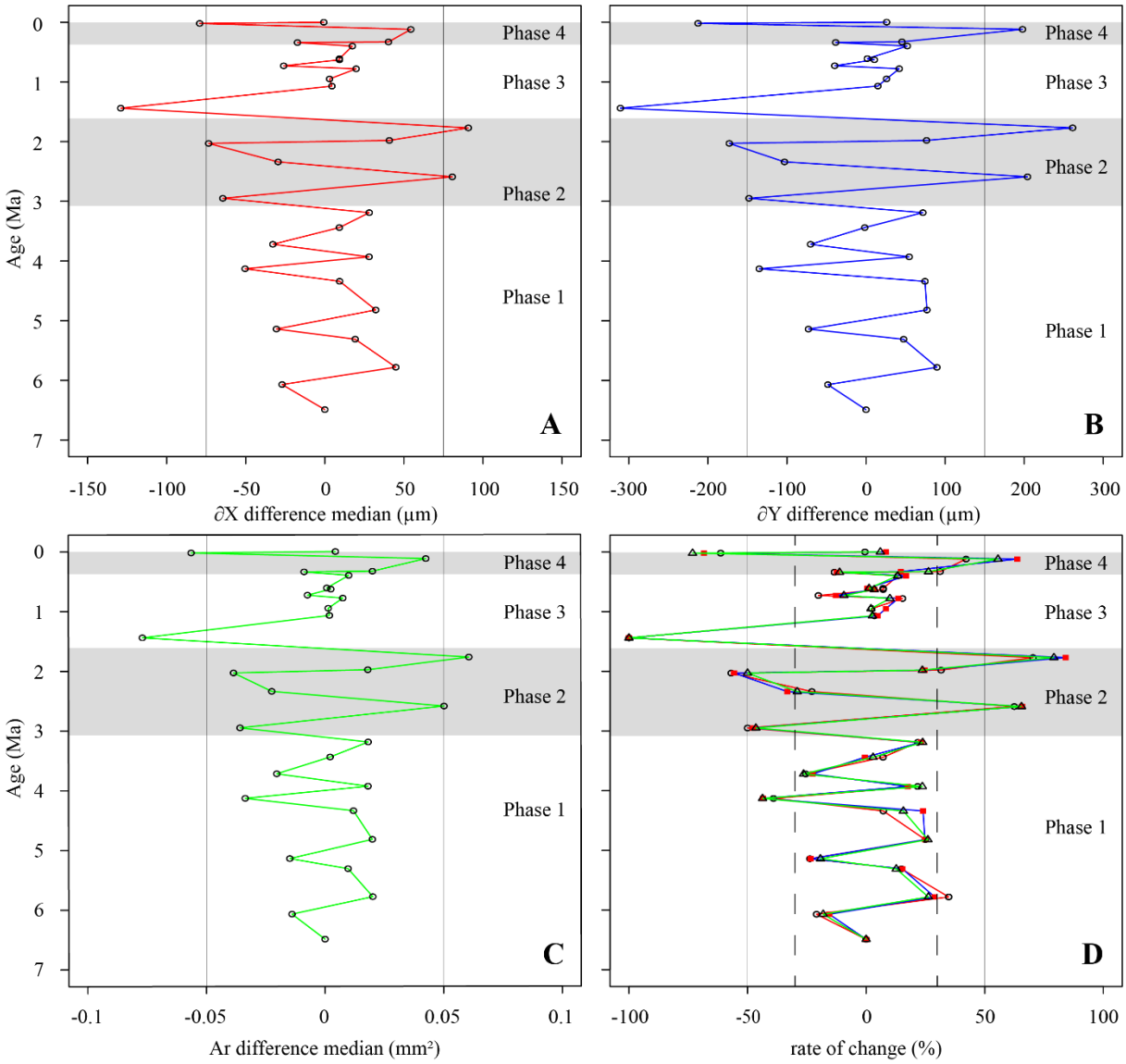

Figure A3.5: Absolute difference of the median values of δX (**A**), δX (**B**) and Ar (**C**) for *G. menardii*. (**D**) shows the normalized rate of change in % for δX (red line, open circles), δY (blue, red points) and Ar (green line, rectangles). The thin, vertical lines mark (-)75 µm in (**A**), (-)150 µm in (**B**), (-)0.05 mm² in (**C**) and (-)50 % in (**D**). For better visibility, Phase 2 and Phase 4 are highlighted in grey (see chapter 3.3.1.1).

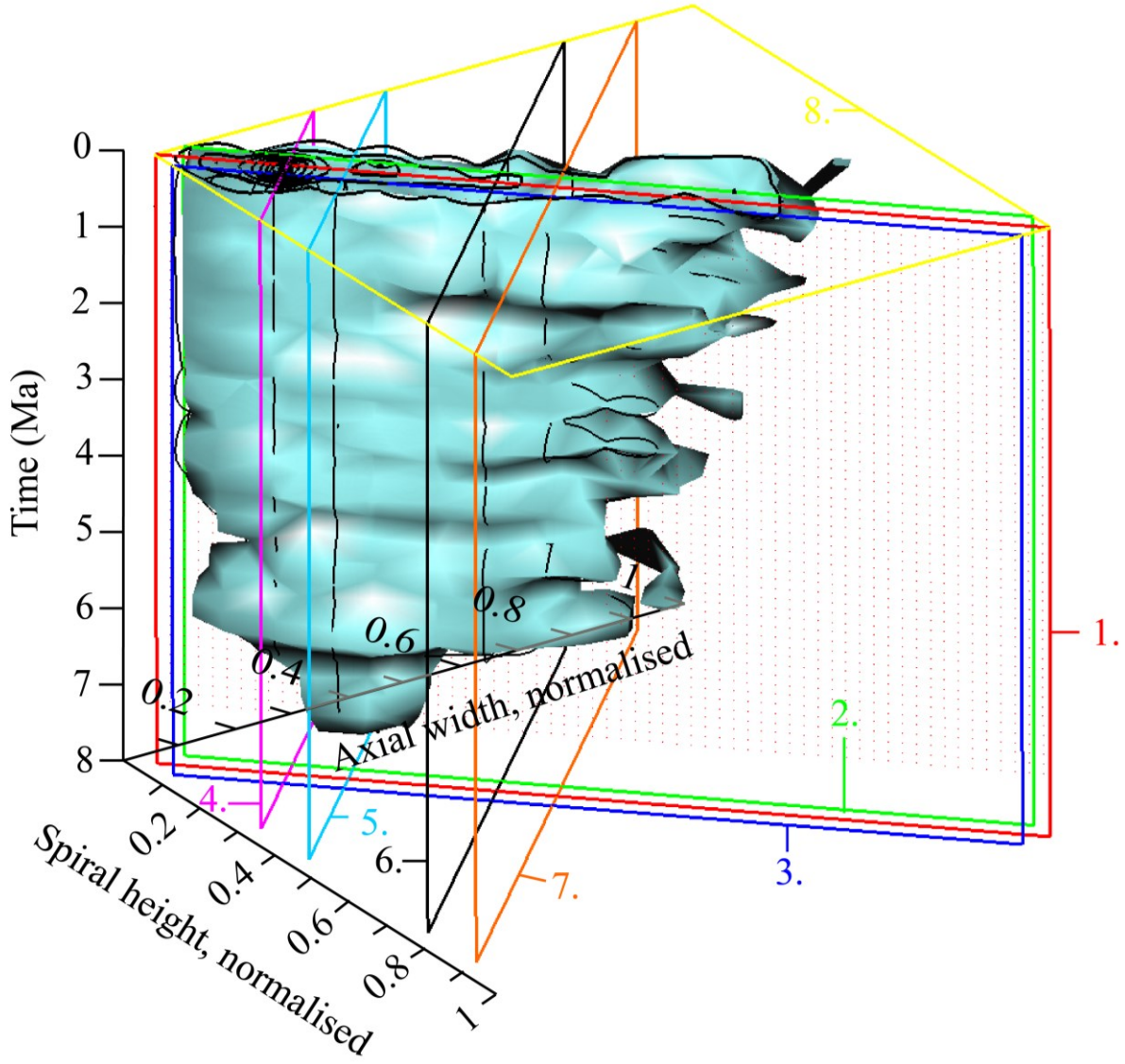

Figure A3.6: VDD of the normalized spiral height (δX), the normalized axial length (δY) and the age (Ma) for *G. menardii* for Hole U1476A. It shows the position of frontal and sagittal sections presented in Fig. 3.11 and A3.7-A12 as colored planes. Figure 3.11 is represented by the red frontal section 1. Frontal section 2 (green) has an offset of -0.05 (away from the reader, Fig. A3.4), while frontal section 3 (blue) has an offset of +0.05 (towards the reader, Fig. A3.7). Sagittal section 4 (violet, offset value = -0.68, Fig. A3.8), sagittal section 5 (light blue, offset = -0.55, Fig. A3.9), sagittal section 6 (black, offset = -0.23, Fig. A3.10) and sagittal section 7 (orange, offset = -0.1, Fig. 3.11) are orthogonal to frontal sections. Transversal plane 8 (yellow, offset = 0.4995, 0.004 Ma in Fig. 3.12) shows the contoured frequency with black lines representing intervals of 5. See also the file "U1476_3D_PDF.pdf" in the supplementary material.

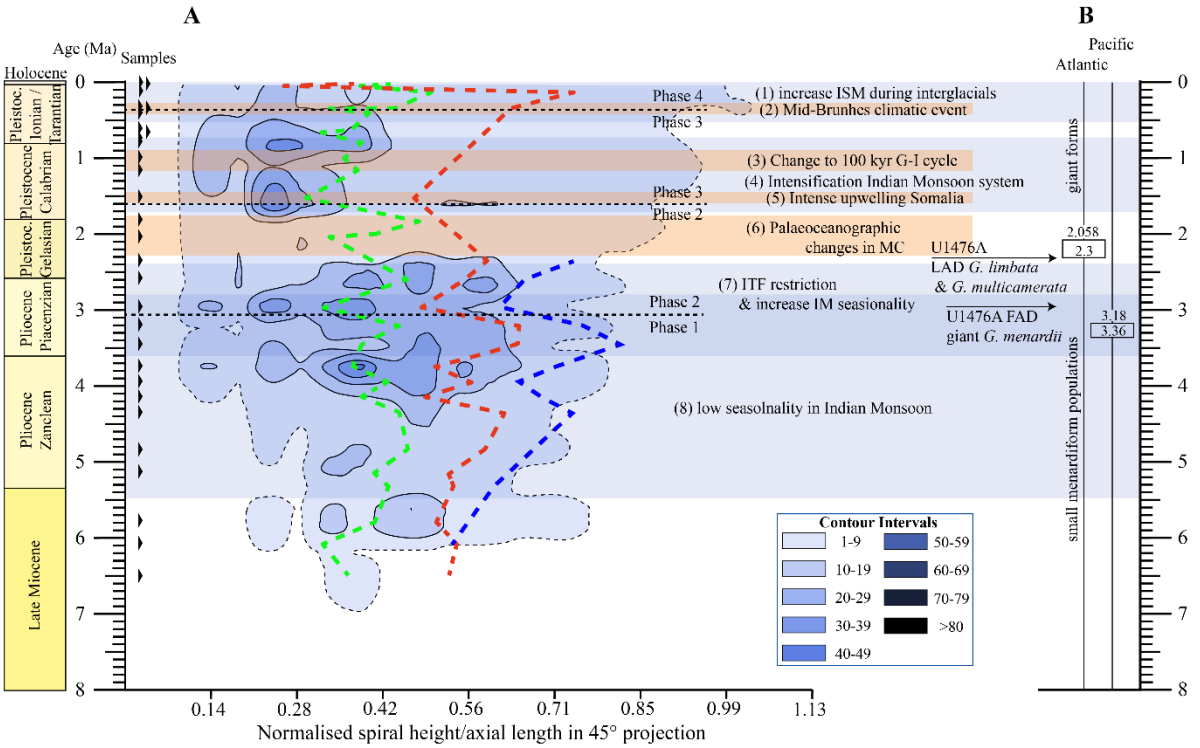

Figure A3.7: Frontal section with an offset value of -0.05 (away from the reader, no. 2 in Fig. A3.3) though the VDD of Hole U1476A in a palaeoceanographic context. The solid lines represent the contours with an interval of 10, the dashed line the interval line 1. See figure 3.11 for further explanation.

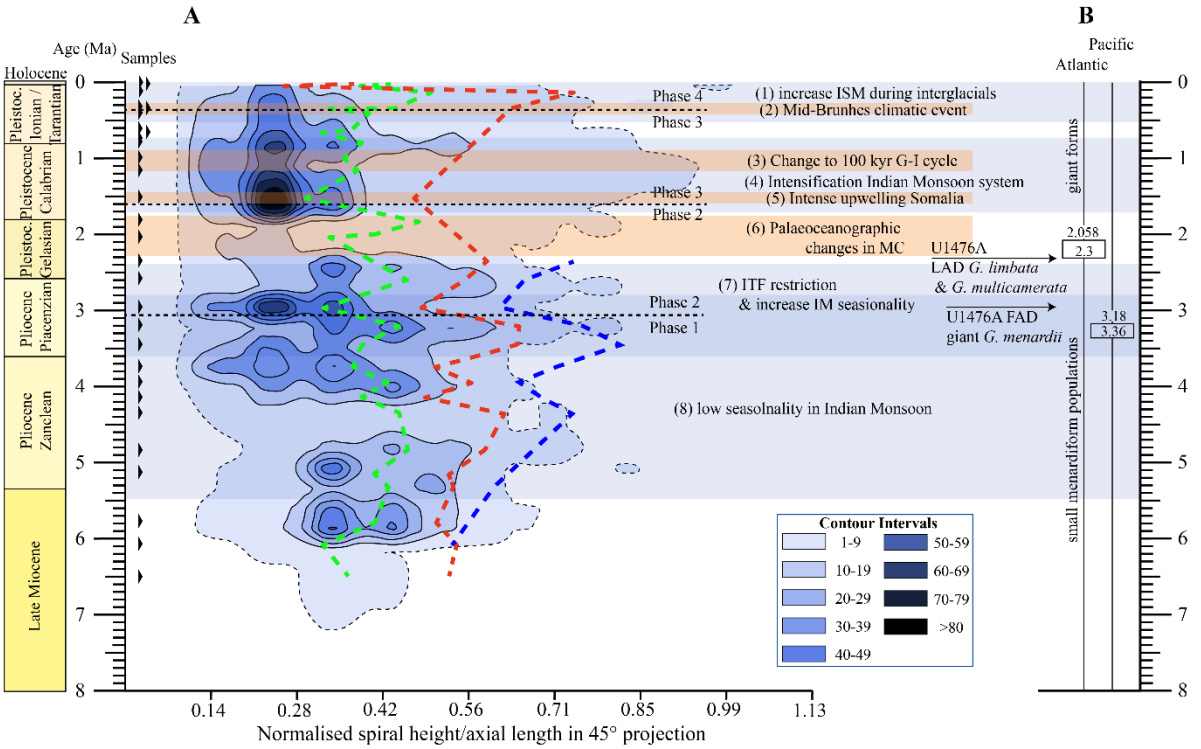

Figure A3.8: Frontal section with an offset value of +0.05 (towards the reader, no. 3 in Fig. A3.3) though the VDD of Hole U1476A in a palaeoceanographic context. The solid lines represent the contours with an interval of 10, the dashed line the interval line 1. See figure 3.11 for further explanation.

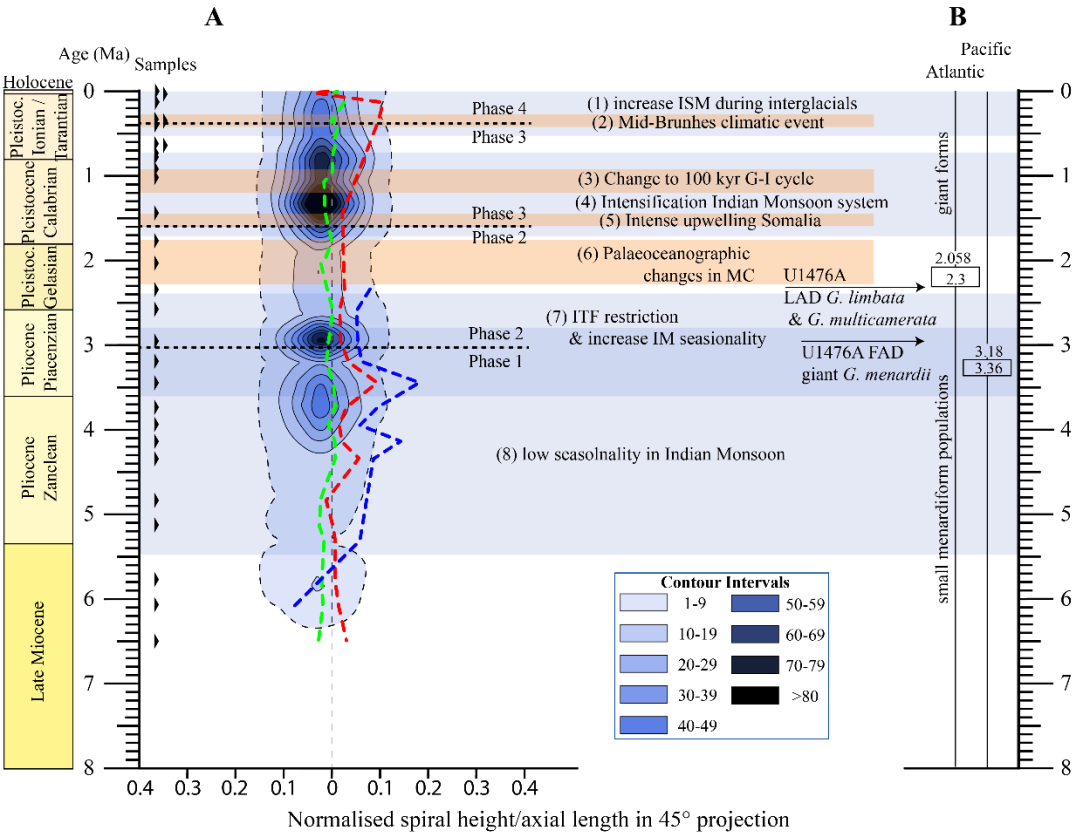

Figure A3.9: Sagittal section with an offset value of -0.68 (no. 4 in Fig. A3.3) though the VDD of Hole U1476A in a palaeoceanographic context. The solid lines represent the contours with an interval of 10, the dashed line the interval line 1. See figure 3.11 for further explanation.

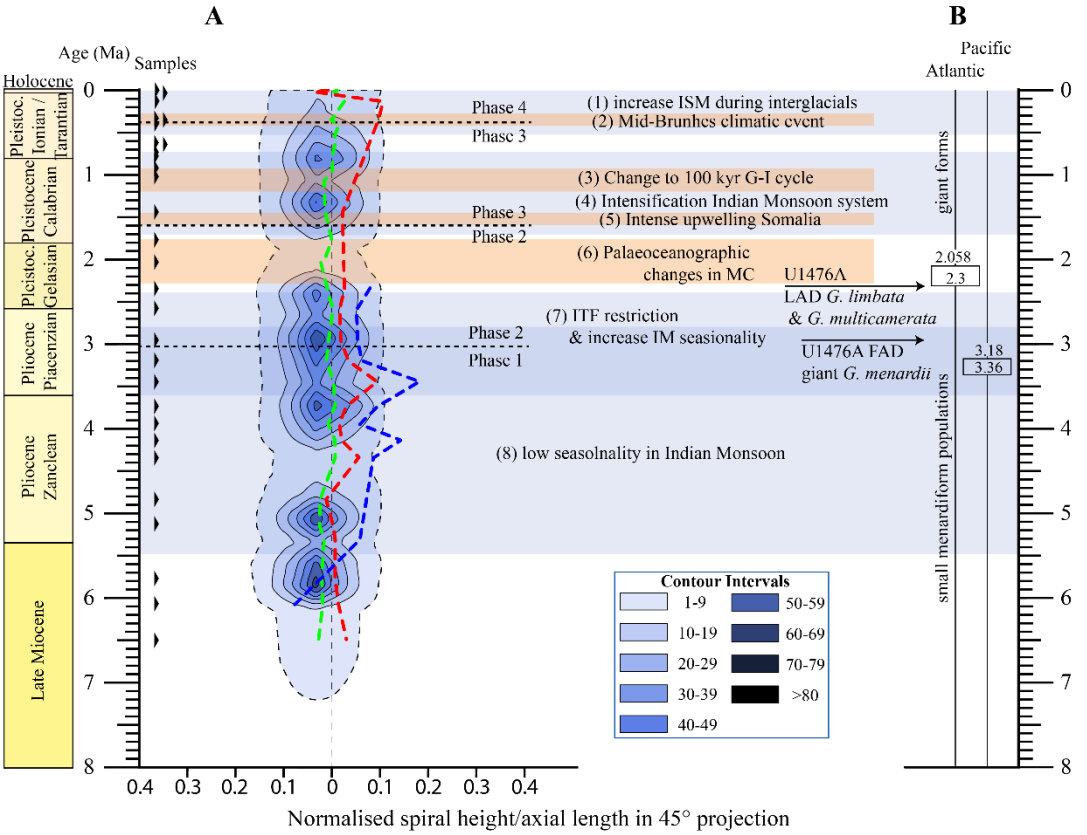

Figure A3.10: Sagittal section with an offset value of -0.55 (no. 5 in Fig. A3.3) though the VDD of Hole U1476A in a palaeoceanographic context. The solid lines represent the contours with an interval of 10, the dashed line the interval line 1. See figure 3.11 for further explanation.

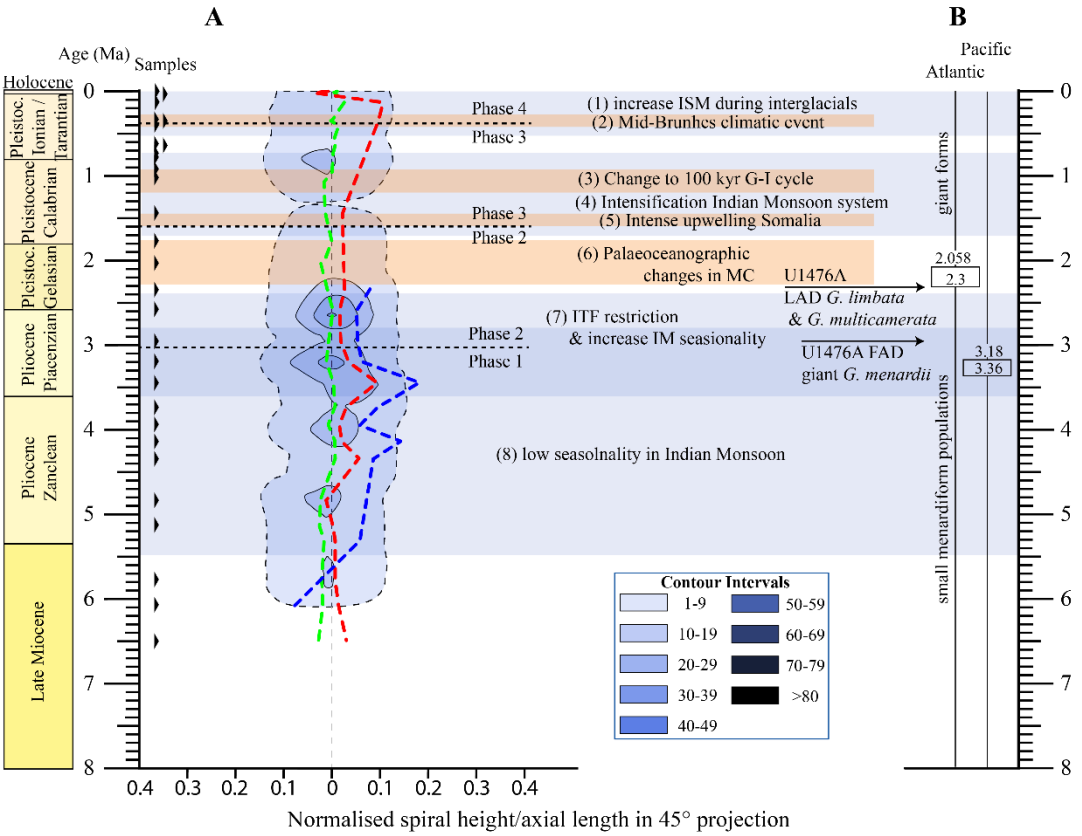

Figure A3.11: Sagittal section with an offset value of -0.23 (no. 6 in Fig. A3.3) though the VDD of Hole U1476A in a palaeoceanographic context. The solid lines represent the contours with an interval of 10, the dashed line the interval line 1. See figure 3.11 for further explanation.

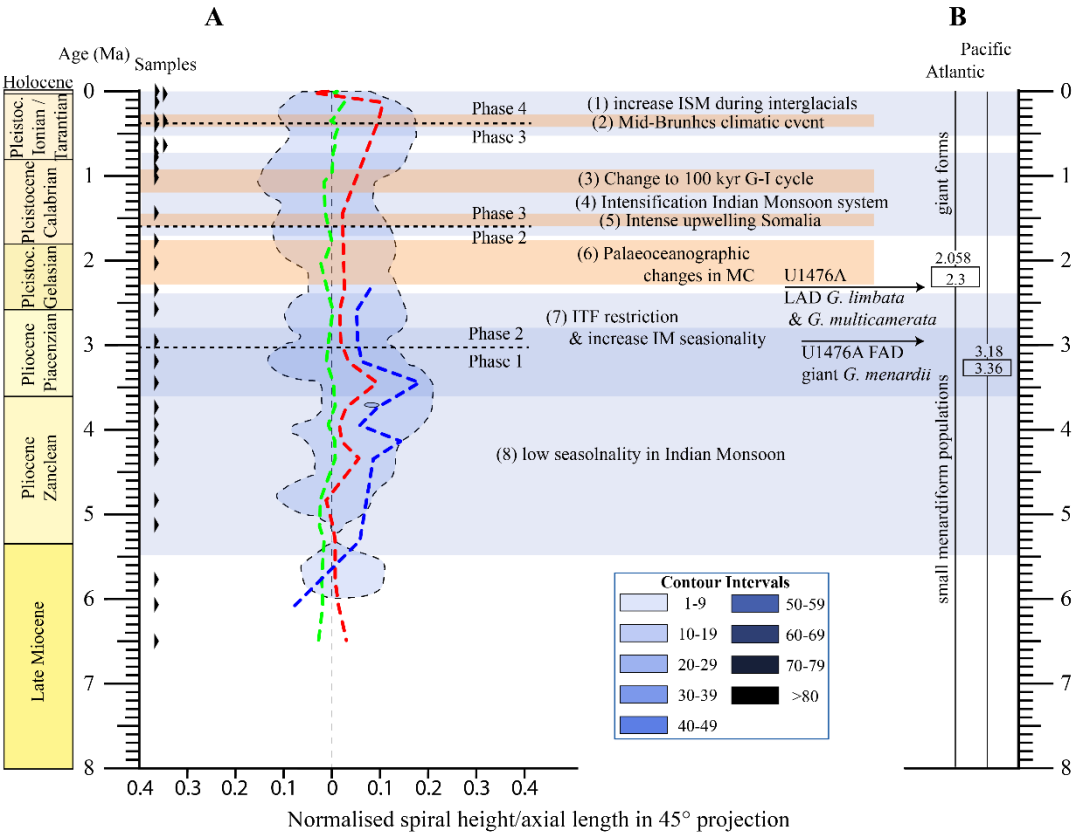

Figure A3.12: Sagittal section with an offset value of -0.1 (no. 7 in Fig. A3.3) though the VDD of Hole U1476A in a palaeoceanographic context. The solid lines represent the contours with an interval of 10, the dashed line the interval line 1. See figure 3.11 for further explanation.

Sample	Depth, CSF-A (m)	expected Age (Ma)	expected MIS Event	Depth, CCSF-A (m)	Age (Ma) van der Lubbe et al. (2021)	Comments	Difference "expected Age" - "Age (Ma) van der Lubbe et al. (2021)"	Sampled MIS event (van der Lubbe et al., 2021)
U1476A-1H-1, 7-8cm	0.075	0.004*	1^{R}	0.075	0.004^{+}		0.000	1
U1476A-1H-1, 72-73cm	0.725	0.018*	2^{R}	0.725	0.035^{+}	supposed glacial	0.017	2
U1476A-1H-2, 111-112cm	2.618	0.123*	$5e^{R}$	2.618	0.122^{+}		-0.001	5
U1476A-2H-1, 99-100cm	6.700	0.329*	$9e^{R}$	6.979	0.324^{+}		-0.005	9
U1476A-2H-1, 134-135cm	7.050	0.343*	$10a^{R}$	7.329	0.339^{+}	supposed glacial	-0.004	10
U1476A-2H-2, 113-114cm	8.341	0.403*	$11c^{R}$	8.620	0.394^{+}		-0.009	11
U1476A-2H-5, 98-99cm	12.693	0.61*	$15e^{R}$	13.331	0.615^{+}		0.005	15
U1476A-2H-6, 13-14cm	13.346	0.63*	$16a^{R}$	14.047	0.647^{+}	supposed glacial	0.017	16
U1476A-3H-1, 4-5cm	15.250	0.732*	$18b^{R}$	16.136	0.736^{+}		0.004	18
U1476A-3H-1, 119-120cm	16.400	0.78*	$19c^{R}$	17.077	0.778^{+}		-0.002	19
U1476A-3H-4,123-124cm	20.937	0.952**	$25e^{R}$	21.372	0.984^{++}		0.032	27
U1476A-3H-6,114-115cm	23.845	1.072**	31^{LR04}	24.249	1.148^{++}		0.076	35
U1476A-4H-6, 46-47cm	32.665	1.436**	47^{LR04}	32.974	1.514^{++}		0.078	51
U1476A-5H-5, 62-63cm	40.819	1.772**	63^{LR04}	41.040	1.818^{++}		0.046	67
U1476A-6H-2, 64-65cm	45.848	1.98**	75^{LR04}	46.014	1.982^{++}		0.002	75
U1476A-6H-3, 64-65cm	47.067	2.025**	77^{LR04}	47.276	2.027^{++}		0.002	77
U1476A-7H-3, 32-33cm	56.532	2.34**	91^{LR04}	57.437	-		-	-
U1476A-8H-1, 118-119cm	63.893	2.585**	103^{LR04}	65.339	-		-	-
U1476A-9H-2, 115-116cm	74.860	2.95**	$G17^{LR04}$	77.112	-		-	-
U1476A-10H-1, 98-99cm	82.685	3.19**	$KM5^{LR04}$	85.666	-		-	-
U1476A-11H-1, 65-66cm	91.861	3.44**	$MG5^{LR04}$	95.933	-		-	-
U1476A-12H-2, 11-12cm	102.322	3.725**	$Gi7^{LR04}$	107.638	-		-	-
U1476A-12H-7, 33-34cm	110.030	3.935**	$Gi17^{LR04}$	116.263	-		-	-
U1476A-13H-5, 98-99cm	117.187	4.13**	$Gi25^{LR04}$	124.271	-		-	-
U1476A-14H-4, 95-96cm	125.166	4.34**	$CN3^{LR04}$	132.615	-		-	-
U1476A-16H-4, 72-73cm	143.933	4.825**	$Si3^{LR04}$	151.765	-		-	-
U1476A-17H-6, 22-23cm	155.929	5.135**	$T7^{LR04}$	164.006	-		-	-
U1476A-18H-4, 49-50cm	162.701	5.31**	$TG5^{LR04}$	170.916	-		-	-
U1476A-19H-6, 101-102cm	175.721	5.78***	-	183.733	-		-	-
U1476A-20H-7, 21-22cm	185.917	6.07***	-	193.509	-		-	-

Sample	Depth, CSF-A (m)	expected Age (Ma)	expected MIS Event	Depth, CCSF-A (m)	Age (Ma) van der Lubbe et al. (2021)	Comments	Difference "expected Age" - "Age (Ma) van der Lubbe et al. (2021)"	Sampled MIS event (van der Lubbe et al., 2021)
U1476A-22H-4, 47-48cm	200.684	6.49***	-	209.395	-		-	-

Table A3.1: List of used samples from IODP LEG 361 Hole U1476A. The used age model is "Neptune model U1476A_loc95", which is deposited in the supplementary materials and in table 3.3. *: samples selected on the basis of magnetic susceptibility. **: samples selected by LR05 stack. ***: samples selected in stratigraphic vicinity to Knappertsbusch (2007, 2016) and Friesenhagen (2022). ^{R}: MIS-event nomenclature after Railsback et al. (2015). ^{LR04}: MIS-event nomenclature after Lisiecke & Raymo (2005).

Group	Event Name	Plotcode	Event-No. in Fig. 3.1	Top Depth CFS-A (m)	Bottom Depth CFS-A (m)	Gradstein et al. (2012), Age (Ma)	Berggren et al. (1995), Age (Ma)
F/184	T *Globigerinoidses ruber* pink	TGrp	1	2.22	3.7	0.12	0.12
F/184	B *Globigerinoidses ruber* pink	BGrp	3	7.92		0.4	0.4
F	TOP *Globorotalia tosaensis*	Ttos	5	15.44	15.9	0.61	0.65
F	TOP *Globigerinoides fistulosus*	Tfst	13	36.42	37.9	1.88	1.6
F	TOP *Globigerinoides obliquus extremus*	Tobe	15	39.42	40.9	1.98	1.7
F	BT *Globorotalia truncatulinoides*	Btrc	17	45.92	47.4	1.93	2
F	TOP *Globoquadrina altispira*	Talp	21	78.92	80.4	3.47	3.09
F	BT *Globigerinoides fistulosus*	Bfst	22	80.42	82.22	3.33	3.33
F	BT *Globorotalia tosaensis*	Btos	23	80.42	82.22	3.35	3.35
F	TOP *Sphaeroidinellopsis seminulina*	Tsem	24	94.92	96.4	3.59	3.12
F/184	T *Sphaeroidinellopsis kochi*	TSk	31	104.42	105.9	4.53	4.53
F	TOP *Globorotalia margaritae*	Tmgt	25	105.92	107.4	3.85	3.58
F	TOP *Globigerina nepentes*	Tnep	29	123.42	124.9	4.37	4.2
F	TOP *Globorotalia cibaoensis*	Tcbn	30	153.32	154.8	4.6	4.4
F	BT *Globorotalia tumida*	Btum	38	177.32	178.8	5.57	5.6
F	TOP *Globoquadrina dehiscens*	TGqd	39	177.32	177.8	5.92	5.8
F	BT *Globigerinoides conglobatus*	Bcgb	40	186.4	186.8	6.2	5.8
F	BT *Globorotalia margaritae*	Bmgt	42	197.82	199.3	6.08	6
F	BT *Pulleniatina primalis*	BPpr	43	203.92	205.41	6.6	6.4
N	B *E. huxleyi*	B Ehu	2	5.72	9.45	0.29	0.26
N	T *P. lacunosa*	T Pla	4	5.72	9.45	0.44	0.46
N	T *Reticulofonestra asanoi*	T Ras	6	17.45	18.95	0.91	0.897
N/184	T small *Gephyrocapsa acme*		7	21.95	23.45	1.02	1.01
N/184	B medium *Gephyrocapsa* spp.		8	23.45	24.76	1.04	1.69

Group	Event Name	Plotcode	Event-No. in Fig. 3.1	Top Depth CFS-A (m)	Bottom Depth CFS-A (m)	Gradstein et al. (2012), Age (Ma)	Berggren et al. (1995), Age (Ma)
N/184	B *Reticulofenestra asanoi*		9	25.45	26.95	1.14	1.16
N/184	B small *Gephyrocapsa acme*		10	26.95	28.45	1.24	1.22
N	T *H. sellii*	T Hse	11	28.45	29.95	1.34	1.47
N	T *C. macintyrei*	T Cma	12	32.8	34.19	1.6	1.59
N	T *D. brouweri*	T Dbr	14	43.85	45.95	1.93	1.95
N	T *D. triradiatus*	T Dtr	16	43.85	45.95	1.95	1.95
N	T *D. pentaradiatus*	T Dpe	18	58.45	61.45	2.39	2.5
N	T *D. surculus*	T Dsu	19	62.9	63.45	2.49	2.55
N	T *D. tamalis*	T Dta	20	69.45	70.95	2.8	2.78
N	T *Sphenolithus* spp.	T Sna	26	97.95	99.45	3.54	3.6
N	T *R. pseudoumbilicus*	T Rps	27	102.95	104.45	3.7	3.75
N	B *D. asymmetricus*	B Das	28	118.45	119.85	4.13	4.2
N	T *A. primus*	T Apr	33	129.39	129.95	4.5	4.8
N	T *C. acutus*	T Cac	32	148.43	150.45	5.04	4.57
N	B *C. rugosus*	B Cru	34	158.45	159.95	5.12	5
N	T *T. rugosus*	T Tru	35	161.45	162.95	5.28	5.34
N	B *C. acutus*	B Cac	36	164.45	165.95	5.35	5.34
N	T *D. quinqueramus*	T Dqu	37	169.45	172.45	5.59	5.6
N	T *A. amplificus*	T Aam	41	186.95	188.45	5.94	5.9
N	B *A. amplificus*	B Aam	44	215.45	216.95	6.91	6.6

Table A3.2: Biostratigraphic events of Site U1476 used for the applied Age-Depth model (see Fig. 3.2). The datums were translated from Gradstein et al. (2012) into Berggren et al. (1995) timescale. Reference: Biostratigraphic planktonic foraminifer datums (http://dx.doi.org/10.14379/iodp.proc.361.105.2017), Biostratigraphic calcareous nannofossil datums (http://dx.doi.org/10.14379/iodp.proc.361.105.2017).

Age (Ma)	Depth (CSF-A, m)	Depth (CCSF-A, m)
0	0	0
0.12	2.96	2.96
0.818	17.7	18.17
2.003	46.4	46.56
3.098	79.3	81.88
4.204	119.9	127.31
5.344	164	172.24
6.6	216.2	226.5

Table A3.3: Neptune model U1476A_loc95. Control points of the age-depth plot are given in CSF-A (m) depth. For calculation of the CCSF-A (m) depth, tables 10 and 11 in Hall et al. (217b) were used.

Chapter 4: Geometric morphometrics does not indicate speciation in the planktonic foraminifer *Globorotalia menardii* since the late Miocene

Thore Friesenhagen [1,2]
Bastien Mennecart [1]
Laura Dziomber [3]
Michael Knappertsbusch [1]

[1] Natural History Museum Basel, Augustinergasse 2, 4001 Basel, Switzerland
[2] University of Basel Department Umweltwissenschaften, Bernoullistrasse 32, CH-4056 Basel
[3] University of Bern, Institute of Plant Sciences, Paleoecology, Altenbergrain 21, 3013 Bern, Switzerland

Abstract

In the previous chapters of this dissertation, the occurrence of a new morphotype of the planktonic foraminifer *Globorotalia menardii* in the Atlantic Ocean was hypothesised for the early Pleistocene. This new morphotype shows an increase in test size as well as a permanent change in the predominant coiling direction, which abruptly occur between 2.5 Ma and 2 Ma.

In this chapter, a (semi-) landmark-based approach of the test outline in keel view is employed to track form (containing allometric signal) and shape (corrected for the allometric signal) evolution of *G. menardii* for the last 8 Myr at three tropical locations in the Atlantic, Pacific and Indian oceans. Principal Component Analyses were applied to recognise form changes in the morphospace through time to find evidence for differences in pre-Pliocene and Pliocene-Quaternary morphotypes.

The overall form and shape evolution in the Atlantic, Pacific, and Indian oceans show a high degree of overlap in the morphospace through time. This result suggests the existence of one single morphotype of *G. menardii* at the investigated sites since the late Miocene.

Consistent with the literature, the data show a covariation of test form and size. As form is thought to influence the sinking-velocity of the organism, the fluctuation in maximum and median form may be an adaption to variations in the environmental conditions.

The median shape evolution in the Atlantic and Indian Ocean reveals possible anagenetic tendencies in two time intervals. Between 4 Ma and 2.3 Ma in the Atlantic Ocean and from ca. 1.7 Ma until the present in the Indian Ocean, *G. menardii* evolved towards exhibiting a more pronounced apex and more concave development of the wall of the last chambers in comparison to populations within the other investigated sites, respectively. These intervals coincide with changes in the environmental conditions induced by major hydrographic and oceanographic changes due to the closure of the Central American Seaway in the Atlantic Ocean and by a strengthening of the Indian monsoon system in the Indian Ocean.

4.1 Introduction

The climatic conditions on earth changed during the last 8 Myr from a warm, relatively stable state into a world influenced by glacial cycles from 2.5 Ma onward (Zachos, 2003; Lisiecki and Raymo, 2005). Along with the climate, regional environmental conditions changed, which in turn affected onshore and offshore biotic communities all over the world (e.g. Leckie, 1989; Chaisson, 2003; von der Heydt and Dijkstra, 2005; Trauth et al., 2007; Jackson and O'Dea, 2013; O'Dea et al., 2016). Planktonic foraminifera (PF) are an interesting group of organisms to investigate the impact of long-term climate changes on communities and populations. These unicellular organisms are distributed in the worlds' oceans in huge numbers and built up a calcitic shells (test), which are used to investigate evolution (e.g. Pfuhl and Shackleton, 2004; Knappertsbusch, 2007a, 2016; Pearson and Coxall, 2014; Friesenhagen, 2022a; Chapter 3) and environmental (e.g. Nuber, 2020) changes through time. Many studies show an overall test-size increase of PF through time, which coincides with long-term changes in the climate (e.g. Huber, 2000; Schmidt et al., 2004; Schmidt et al., 2006; Knappertsbusch, 2007a, 2016, 2022; Schmidt et al., 2016; Brombacher et al., 2017a; Friesenahgen, 2022a; Chapter 3).

During the last 15 years, a number of studies have concentrated on test-size evolution of the PF *Globorotalia menardii* (Knappertsbusch, 2007a, 2016; Mary and Knappertsbusch, 2013; Mary and Knappertsbusch, 2015; Friesenhagen, 2022a; Chapter 3). During the Gelasian, this species exhibits a doubling of its size in the Atlantic Ocean between 2.5 Ma and 2 Ma (Knappertsbusch, 2007a, 2016; Friesenhagen, 2022a). The size increase is accompanied by a reversal in the predominant coiling direction of populations from dextral between 4 and 2 Ma to sinistral from 2 Ma until the present. This pattern was interpreted as being evidence for the occurrence of a new morphotype in the Atlantic, probably dispersed by the Agulhas Leakage from the Indian Ocean (Fig. 4.1; Knappertsbusch, 2016; Friesenhagen, 2022a; Chapter 3).

To further investigate the possibility of a pan-oceanic dispersal and transportation of morphotypes, the current study explores the evolution of the test form and shape of *G. menardii*. Using geometric morphometrics, changes in the test outline in keel view through time may provide new insight into the mode and tempo of *G. menardii*'s evolution and about the appearance of a new morphotype.

Geometric morphometrics is a statistical tool which allows the study of different aspects of the test form (which is a combination of shape and size and thus includes the allometric signal; Klingenberg, 2016) and shape (form corrected for size). It is widely used in different contexts of natural science (e.g. Thompson, 1917; Malmgren et al., 1983; Klingenberg & McIntyre, 1998; Mennecart et al., 2020). The approach of a landmark-based analysis of the test outline in

keel view has already been used to investigate the nature and mode of morphological evolution in PF. In the *Globorotalia tumida* lineage (Malmgren et al., 1983; Hull & Norris, 2009), a gradual transformation in shape was observed from the ancestorial *G. plesiotumida* into the extant *G. tumida* within 600 Kyr or even 44 Kyr at the Miocene-Pliocene boundary in the Indian and Pacific Ocean, respectively. The studies interpreted this observation as a case of punctuated gradualism.

Bicknell et al. (2018) recorded a rapid evolutionary transition between *Truncorotalia juanai* and *Truncorotalia* crassaformis between 5.1 Ma and 5.2 Ma. The changes in test shape were not gradual and intermediate types were missing. This event was suggested to represent a case of punctuated equilibrium, caused by a rapid regional evolution.

Analogous to these studies, the current study attempts to disentangle the tempo and mode of evolution in *G. menardii* by applying a semi-landmark based approach on the test outline of 15,368 *G. menardii* specimens. The extensive dataset, comprising data from the Ocean Drilling Program (ODP) Hole 667A in the Atlantic Ocean, the ODP Hole 806C in the Pacific Ocean and International Ocean Discovery Program (IODP) Hole U1476A in the Indian Ocean, is used to test the possibility of the Agulhas leakage hypothesis (Knappertsbusch, 2016). The investigation of tropical populations from the mentioned sites through time allows a pan-oceanic comparison, following Knappertsbusch's (2011) concept of "evolutionary prospection".

Similar to shifts in shape of the *G. plesiotumida-G. tumida* and *T.juanai-T. crassaformis* lineage, the observation of an abrupt shift in shape of *G. menardii* would indicate the appearance of a new morphotype in the Atlantic. If this new type or a similar shift in shape were observed earlier in the Indian Ocean, it would support the possibility of the Agulhas leakage hypothesis.

The Agulhas leakage is known to disperse Indian Ocean biota from the tropics throughout the transitional zone (Schiebel and Hemleben, 2017a) along the south-western coast of Africa into the South Atlantic (Norris, 1999; Caley et al., 2012; Villar et al., 2015).

The Agulhas leakage is known to disperse the tropical dwelling (Caley et al., 2012; Schiebel and Hemleben, 2017b, and references therein) *G. menardii* from the tropical Indian Ocean into the tropical realm of the Atlantic Ocean at least since 1.3 Ma (Caley et al., 2012). It may have introduced the new, giant5 morphotype to the tropical Atlantic in the early Pleistocene after the last direct connection to a tropical ocean, the Central American Seaway, was closed (Bartoli et al., 2005; Jackson and O`Dea, 2013; O'Dea et al., 2016).

4.2 Material and Methods

4.2.1 Material

4.2.1.1 Data

Data from the ODP Hole 667A (tropical East Atlantic, 4°34.15' N, 21°54.68' W; Fig. 4.1), IODP Hole U1476A (southwest Indian Ocean, 15°49.25′S, 41°46.12′E) and ODP Hole 806C (western tropical Pacific, 0°19.11'N, 159°21.70'E) were used in this study (Fig. 4.1). These sites are within suspected dispersal pathway of *G. menardii*. The eastern tropical Pacific Ocean is the first place in which the giant type was observed, while the eastern tropical Atlantic Ocean might be the end point of dispersal (Friesenhagen, 2022a; Chapter 3). Morphometric measurements and ages of samples from Hole 806C were taken from Knappertsbusch (2021). A list of samples used in this study is given in the Appendix (table 1-3). Information about sample ages and sample preparation for Holes 667A and U1476A are given in (Friesenhagen, 2022a, b) and Chapter 3.

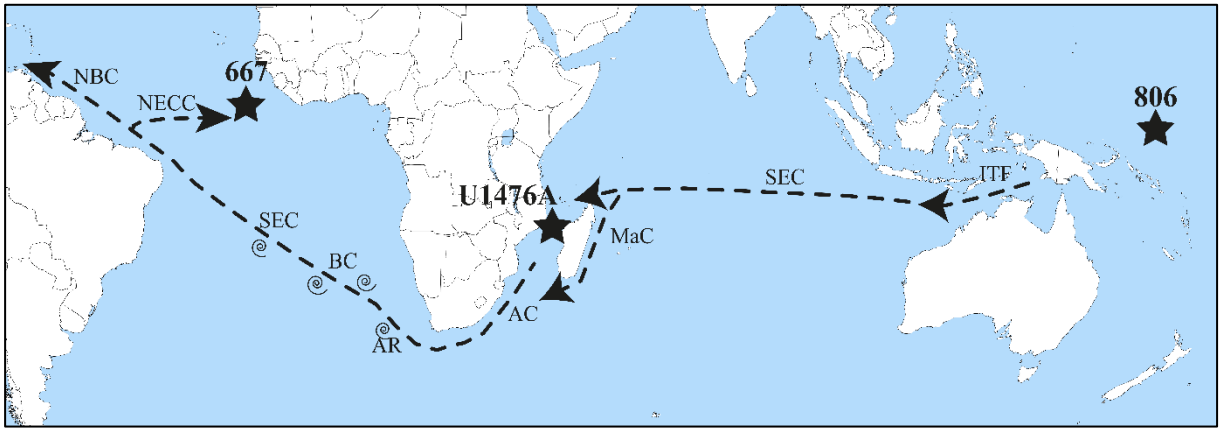

Figure 4.1: Locations of the investigated sites. Hole 667A is located in the eastern tropical Atlantic Ocean, Hole U1476A in the Mozambique Channel and Hole 806C in the western tropical Pacific Ocean. Currents, which may be important for the dispersal of *G. menardii*, are symbolised by arrows, following Shipboard Scientific Party (1998) and Tangunan et al. (2018). AC = Agulhas Current; AR = Agulhas Rings; BC = Benguela Current; ITF = Indonesian Throughflow; NBC = North Brazil Current; NECC = North Equatorial Counter Current; SEC = South Equatorial Current; SEMC = Southeast Madagascar Current

The age models for the holes, from which the data derive apply the Berggren et al. (1995) time scale to allow direct temporal comparison. For Hole 667A, foraminiferal and nannoplankton occurrence data as well magnetostratigraphic events were used to define the model (Friesenhagen, 2022a). Sample ages of Hole 806C were determined with isotopic data (Knappertsbusch, 2022), while for Hole U1476A planktonic foraminiferal and nannoplanktonic occurrence data were used to construct the age model (Chapter 3).

The recently published isotopic record for Site U1476 (van der Lubbe et al., 2021) reveals a discrepancy between the constructed age model and the dating by the isotopic record in the time

interval from 1 Ma to 2 Ma. This error involves a correction of the dating by up to 0.078 Ma (Chapter 3). However, as in this study the evolution is investigated for a time period of 8 Myr, this error does not impact the results and interpretation of this study.

4.2.1.2 Sample Preparation

Sample preparation for all three sites followed a similar protocol: for the present study, only specimens of the species *G. menardii menardii* were included (which will be referred to as *G. menardii* from now on). Identification of *G. menardii* is based on Kennett and Srinivasan (1983) and Bolli (1985). The reference collection "49 Cenozoic planktonic foraminiferal zones and subzones prepared by Bolli in 1985 – 1987" was consulted for comparison. Whenever possible, 200 menardiform specimens were picked from the >63µm fraction. The total number of *G. menardii* specimens used in this study is 15,368, including 4487 specimens from Hole 667A (Friesenhagen, 2022a), 5904 from Hole 806C (Knappertsbusch, 2022) and 4977 from Site U1476 (Chapter 3).

Morphological analysis of specimens is based on profiles in keel view. The keel position was shown to present the largest morphological variation to detect evolutionary changes (Malmgren et al., 1983) and already used in several morphological and shape studies (e.g. Lohman & Malmgren, 1983; Tabanick & Bookstein, 1990; Malmgren et al., 1983; Kucera & Malmgren, 1995; Spencer-Cervato & Thierstein, 1996; Scott et al., 2006; Knappertsbusch, 2007a; Hull & Norris, 2009; Pearson & Ezard, 2014; Knappertsbusch, 2016; Brombacher, Wilson & Ezard, 2017; Si & Berggren, 2017; Bicknell et al., 2018; Knappertsbusch, 2022; Friesenhagen, 2022a; Chapter 3). For this reason, specimens were glued in keel position on slides.

The sampled material is stored in the Natural History Museum Basel as reference collections to Friesenhagen (2022a), Knappertsbusch (2022) and Friesenhagen (in prep. a).

4.2.1.3. Imaging

Specimens from Hole 667A and 806C were orientated and imaged with system AMOR 1, using software version AMOR 3.28 (Knappertsbusch, 2009). Using the AMOR systems for the orientation and imaging of the specimens ensures that each specimen was objectively treated the same way. It reduces the bias of outline coordinates, that otherwise incur deviation due to by-hand orientation of the authors. Specimens from Hole U1476A were imaged using the newer twin system AMOR 2 (software version AMOR 4.2; Knappertsbusch and Eisenecker, 2022). A comparison of measurements taken on both devices confirm good coincidence with an average

error of outline coordinates of ±2.44 µm (0.69% of the mean radius) for the same specimen (Knappertsbusch and Eisenecker, 2022).

4.2.1.4 Image Treatment

Images obtained with system AMOR 1 and AMOR 2 are 640*480 pixel, 8-bit grey scale *Tiff* files (Fig. 4.2A). After conversion to black-white *Tiff* images, they were further processed with ImageJ, a freeware from the National Institute of Health (Rasband, 1997-2018). Processing steps comprise the removal of adhering particles, smoothing of the outline, enhancement of the contrast, the closing of single pixel embayments and the binarization of the image (.raw-files). From these RAW-files, cartesian outline coordinates (traced _T files, Fig. 4.2B) were extracted for each specimen, using the programme "*Trace_AMOR2_batch.exe*" from Knappertsbusch (2022). Different software versions of the trace-batch programme have been used due to technical differences between AMOR system 1 and 2 (Knappertsbusch and Eisenecker, 2022). Details about the programme versions applied for the different sites can be found in the corresponding studies (Hole 667A: Friesenhagen, 2022a; Hole 806C: Knappertsbusch, 2022; Hole U1476A: Chapter 3). All images, intermediate black&white files, RAW files, and the traced files are permanently stored on the internal media server of the Natural History Museum Basel and will be made available on the PANGAEA data repository website for Hole 806C (Knappertsbusch, 2021) and Hole 667A (Friesenhagen, 2022b). Data for Hole U1476A will be made available on PANGAEA (Friesenhagen, in prep. b).

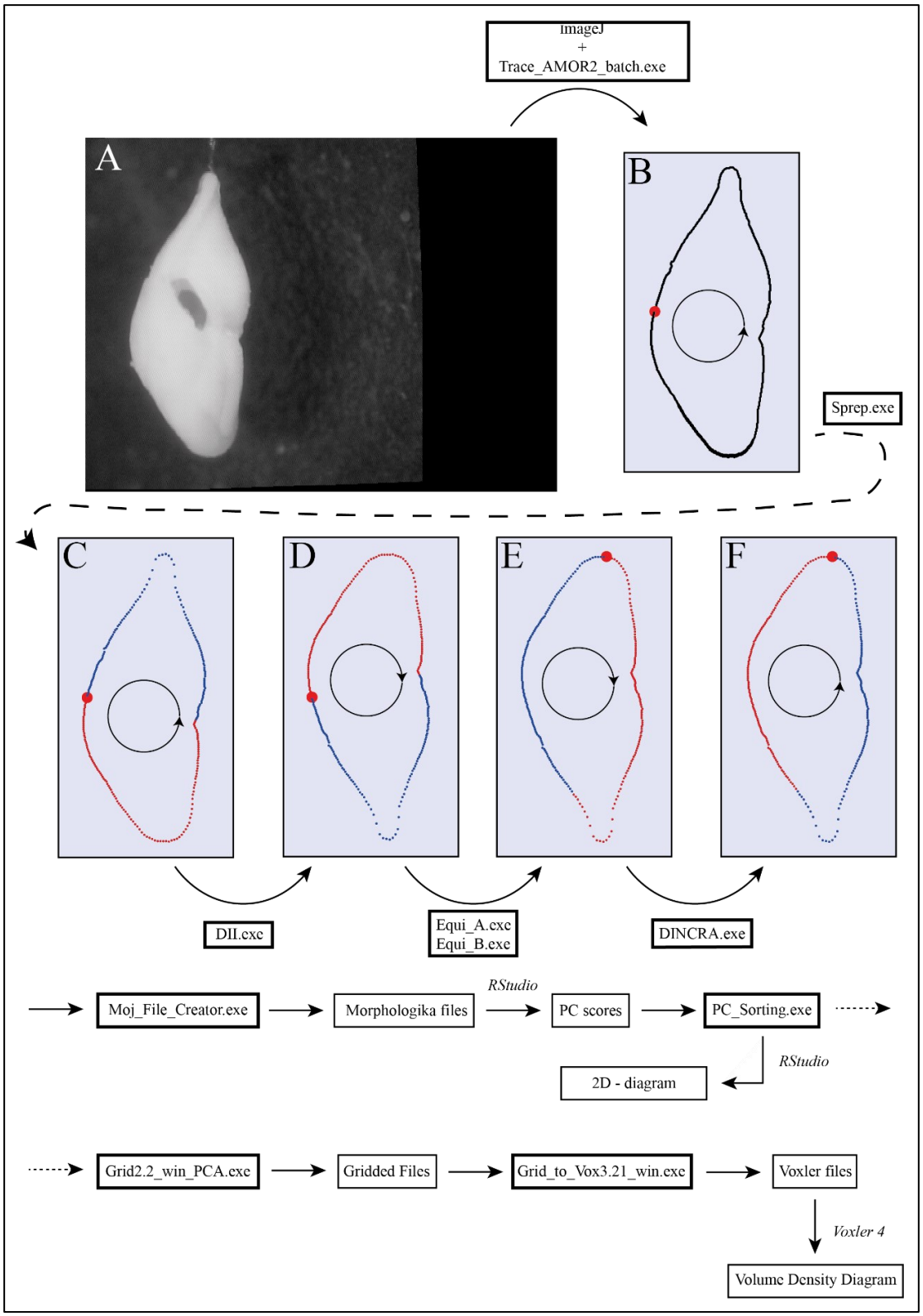

Figure 4.2: Steps from the initial image to outline coordinates. **A**: Image of a *G. menardii* specimen taken by AMOR. **B**: After binarization of the original image with ImageJ, the outline coordinates are determined with the programme "*Trace_AMOR2_batch.exe*". The bigger singular red dot symbolizes the first coordinate from where outline extraction started. The circle within the outline gives the direction the coordinates were read. **C**: Programme "*Sprep.exe*" was used to reduce outline coordinates to 250 equiangular interpolated coordinates. The small red dots represent the first 125 coordinates, blue are coordinates 126 to 250. **D**: Dextrally coiling specimens are vertically mirrored with the programme "*DII.exe*". **E**: The sequence of coordinates is resorted with the programmes "*Equi_A.exe*" and "*Equi_B.exe*". **F**: The two subsets from *Equi_A.exe* and *Equi_B.exe* were vertically flipped if specimens were dextral coiling.

From the traced files containing the cartesian outline coordinates, 250 interpolated equiangular outline coordinates for every specimen were taken with the programme "*Sprep*" ("_INT" files; Fig. 4.2C), which uses the centre of gravity as the point of origin for taking the coordinates. The first interpolated coordinate is set left from the centre of gravity at the same x-coordinate and then continuous in anticlockwise direction. The number of 250 coordinates had been chosen to ensure the preservation of details in form and shape, e.g. the convexity of the chamber wall of the last chamber(s) (Fig. 4.3). Programme "*Sprep*" is part of a suite of programmes developed by Knappertsbusch (2015) for outline analysis in menardiform globorotallids.

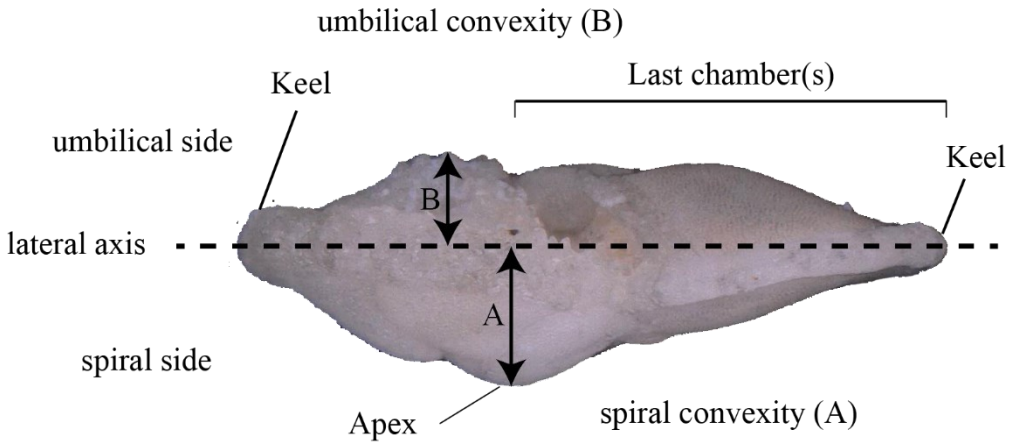

Figure 4.3: Morphometric parameters used to describe shape and form variation in keel view. In comparison to Fig. 2, the test was rotated anticlockwise by 90° to show the same orientation to warpgrid specimens in Fig. 4.4, 4.5, 4.6, 4.9, 4.10, and 4.11.

4.2.2 Treatment of outline coordinates

4.2.2.1 Treatment of interpolated outlines from sinistral and dextral forms

The treatment of interpolated outlines requires new software, which were programmed for Fortran 95 by Thore Friesenhagen and will be introduced in the following:

In order to enable a direct comparison of sinistral and dextral specimens, the y-value of the outline coordinates of dextrally coiling specimens was multiplied by "-1", using the programme "*DII.exe*" (Fig. 4.2D; code in supplement). However, the virtual inversion of dextrally coiling specimens with "*DII.exe*" also invert the listing of the coordinates from anticlockwise to clockwise. This is corrected in the third step (see further below).

In the second step, the coordinates were reorganised in such a way that the sequence of points of each specimen starts with the point having the highest y-value coordinate (= landmark no. 1, Fig. 4.4.2E), so that this first coordinate is topologically homologous throughout the datasets. This re-sorting of points was done with the programme "*Equi_A.exe*" (code in supplement). In

case that one file showed several coordinates with the same maximum y-value, the one in the centre was used ("*Equi_B.exe*", code in supplementary) (Fig. 4.2E). The neighbouring coordinate to the right was set as landmark no. 2. The remaining 248 coordinates were treated as semilandmarks (e.g. Si and Berggren, 2017; Shi, 2021). Semilandmarks are a series of landmark coordinates used to represent the form of homologous curves. Thus, semilandmarks across the sample display geometric homology (Gunz and Mitteriecker, 2013).

In the third step, coordinates of dextrally coiling specimens were re-sorted, so that coordinates are arranged in the same anticlockwise order as that of sinistrally coiling specimens ("*DINCRA.exe*", code in supplementary; Fig. 4.2F). The re-arrangement is necessary to standardise the direction of coordinates listing, as the admixture of clockwise and anticlockwise listing files would cause a miscalculation of mean and median form in the following Principal component analysis.

In the last step, input files for RStudio (see next section) were generated with the programme "*Moj_File_Creater.exe*" (Fig.4. 2; code in supplementary).

4.2.2.2 Analysis of variation in form and size: separation of shape from size and allometric effects

Allometry is the covariation in morphometric variables, i.e. the shape in the current study, with variation in size (Klingenberg, 1996). For *G. menardii*, allometric effects throughout ontogeny cause changes in the form (Brown, 2007; Mary, 2013; Schmidt et al., 2013; Caromel et al., 2016; Knappertsbusch et al., 2016). In keel view, small specimens exhibit a bulkier form with a relatively low spiral convexity (A; Fig. 4.3) and a relatively high umbilical convexity (B; Fig. 4.3) compared to large specimens. The latter show a relatively flattened, elongated test with relatively low umbilical and high spiral convexity.

4.2.2.2.1. Investigation of form

Form comprises information about shape and size of the studied objects (Klingenberg, 2016), which includes the allometric signal of *G. menardii*.

Variation in test form (dataset 1) is investigated by using the principal component analysis (PCA). The PCA "is a mathematical algorithm that reduces the dimensionality of the data while retaining most of the variation in the data set. It accomplishes this reduction by identifying directions, called principal components, along which the variation in the data is maximal" (Ringnér, 2008).

For the computation of the PCA, in a first step, a Procrustes fit was executed, using the function '*gpagen*' from the 'geomorph' package (Adams et al., 2021; V. 4.0.0). The Procrustes fit allows the analysis of the distribution of a set of forms and comprises three steps (Klingenberg & McIntyre, 1998; Klingenberg, 2016):

(1) the scaling of outlines and the determination of the centroid size, which is "the square root of the sum of squared distances of all the landmarks of an object from their centroid" (Klingenberg, 2016), (2) the superimposition of the centroid or centres of gravity and (3) the rotation to an optimal fit of the outlines by minimising the sum of squared distances between corresponding (semi-) landmarks.

In the next step, semilandmarks underwent sliding along the outline to minimize the bending energy. Bending energy is a measurement for the amount of non-uniform shape difference. Using a metaphor, it is the amount of energy which is required to bend a thin steel plate by a given amplitude between two points (Zelditch et al., 2004). The advantage of minimizing the bending energy is the reduction of the chance to generate artifacts, which might be induced by the artificial process of setting semilandmarks (Gunz and Mitteroecker, 2013; Bardua et al., 2019).

The PCA for the form was then performed with the function '*gm.prcomp*' (package 'geomorph' V. 4.0.0; Adams et al., 2021).

Warp grids (Gunz, Mitteroecker & Bookstein, 2005) were plotted for the minimum and maximum scores of the Principal Component (PC) axis with the function '*plotReftoTarget*' ('geomorph' package, V. 4.0.0; Adams et al., 2021). Based on the mean shape, warp grids visualise changes in shape along the corresponding axis.

4.2.2.2.2 Investigation of shape (allometry corrected)

Shape is defined as form which is corrected for size (Klingenberg, 2016). The correction includes the elimination of the allometric signal from the dataset.

In order to test the influence of size on the test form, i.e. the allometry, a regression of the centroid size and the regression score was computed, using 10,000 randomized permutation tests, with the function '*procD.lm*' ('geomorph' package V. 4.0.0; Adams et al., 2021). It was plotted with the function '*plot allometry*' ('geomorph' package V. 4.0.0; Adams et al., 2021).

The regression score is the projection of "data points in [Kendall's] shape space onto an axis in the direction of the regression vector". It represents the shape variable which has the maximal covariation with centroid size and is therefore the best option to summarise the relation between shape and size. The regression score combines the component of shape variation which is

predicted by the model and a residual part of variation which cannot be explained by allometry (Supplementary Fig. A4.1). Thus, "residuals" allow the investigation of that part of shape variation which is exclusively related to evolution and/or the morphological response to environmental changes. (Klingenberg, 2016)

Kendall's shape space represents "all possible shapes with a given number of landmarks and a given dimensionality" (Klingenberg, 2016; see also supplementary Fig. A4.2).

For the calculation of the residuals, the '*procD.lm*' function of the 'geomorph' package (V. 4.0.0; Adams et al., 2021) was used.

A PCA was carried out on the residuals to investigate the changes in shape caused by evolution and/or morphological adaptation to a changing environment.

The first two axes, which explain most of the morphological variance, were used for interpretation. Principal Component (PC) scores of those two axes were extracted and sorted for samples with the program "PC_sorting.exe" (Fig. 4.2; code in supplementary).

4.2.3 Graphical presentation

4.2.3.1 Univariate Plots

Univariate plots and statistics of Principal components, measures for allometry and centroid sizes were prepared with the freeware programme RStudio (V. 3.5.3; RStudio Team, 2020), using the packages psych (V 2.1.9; Revelle, 2018), ggplot2 (V 3.3.5; Wickham, 2016), pacman (V 0.5.1; Rinker & Kurkiewicz, 2018) and rio (V 0.5.27; Chan et al., 2018).

4.2.3.2 Volume-Density-Diagrams

Volume density Diagrams (VDDs) are very useful for visualizing and illustrating evolutionary tendencies in bivariate datasets through time (Knappertsbusch and Mary, 2012; Knappertsbusch, 2016, 2022.; Friesenhagen, 2022a & Chapter 3). In the present study, VDDs were constructed from principal component scores of axes 1 and 2 and plotted against time in order to quantify evolution of test form and shape in the investigated sites. Changes in the modal frequency within the morphospace through time and space are a useful tool to detect changes in the (form and shape) evolution of a population and can provide important signals of anagenetic evolution or cladogenetic splitting (Knappertsbusch, 2007a; 2016).

For this, the bivariate values of PC1 and PC2 were gridded and local frequencies F of binned values of PC1 and PC2 scores were determined. Binning was determined by the square root method following Scott and David (1979):

$$H = \max(x) / \sqrt{N}$$

where *H* is the bin width, *max(x)* the highest value in all used samples and *N* the maximum number of data points in the dataset comprising all samples of the three sites. The calculated bin width for the dataset 1 is 0.026689703, which was rounded to 0.025. The axes were subdivided into 20 bins, ranging from PC score -0.25 to 0.25. For the allometric-free dataset 2, a bin width of 0.10094 was calculated and rounded to 0.1. Again, the axes were scaled to 20 bins from -1 to +1.

The gridded files were generated using the program "*Grid2.2_win_PCA.exe*" (Fig. 4.2; code in supplement), which is a modified version of the programme "*Grid2.2_win.exe*" derived from Knappertsbusch (2015). In order to remove negative signs, the constant "0.25" was added to dataset 1 and the constant "1" was added to the dataset 2.

Binned values of PC1 and PC2, age, and the local frequency F, defined a four-dimensional cell called "voxel". Using the commercial software "Voxler 4", F can be illustrated by isosurfaces. The isosurfaces were calibrated following the procedure in Knappertsbusch (2022) to represent the frequency of one, corresponding to the extreme shapes. For dataset 1, values were calibrated to 0.8 for Hole 667A, to 0.84615 for Hole 806C and 0.68182 for Hole U1476A. For dataset 2, the value is 0.75 for Hole 667A, 0.83333 for Hole 806C and 1 for Hole U1476A.

For the generation of the input files, the programme "*Grid_to_Vox_PCA.exe*" (Fig. 4.2; code in supplement) was used, which is a modified version of programme "*Grid_to_Vox3.21_win.exe*" (Friesenhagen, 2022a, b; see also Knappertsbusch and Mery, 2012; Knappertsbusch, 2016, 2022).

4.3. Results

4.3.1 PCA of the original Dataset (1)

PC1 explains 49.59% of the total morphological variation (Fig. 4.4). For the most negative score of PC1, the form exhibits a relatively high spiral convexity (A, see Fig. 4.3), a low umbilical convexity (B, see Fig. 4.3) and flattened, elongated last chambers. The apex is readily identifiable due to the high A. For the most positive scores, the form changes to a relatively low A, high B and a smaller, shorten last chambers, while the apex is not as pronounced as it is at the most negative score.

The PC2 axis represents 20.98% of the total morphological variation. Along the PC2 axis, the form changes from a pronounced apex, a relatively high A and low B value and short, last chambers at the most negative score to a form with a relatively low A, high B value and prolonged, flattened last chambers at the most positive score.

Neither the main dataset nor a separation into site location, coiling, or age reveal any trends in morphospace evolution (Supplementary Fig. A4.3-5). However, the centroid size shows a trend. Bulkier specimens, which plot along the positive part of the PC1 axis, exhibit a small centroid size, while more elongated specimens tend to be located in the negative area of the PC1 axis with a large centroid size (Fig. 4.4). No trend is observed in the PC2 axis.

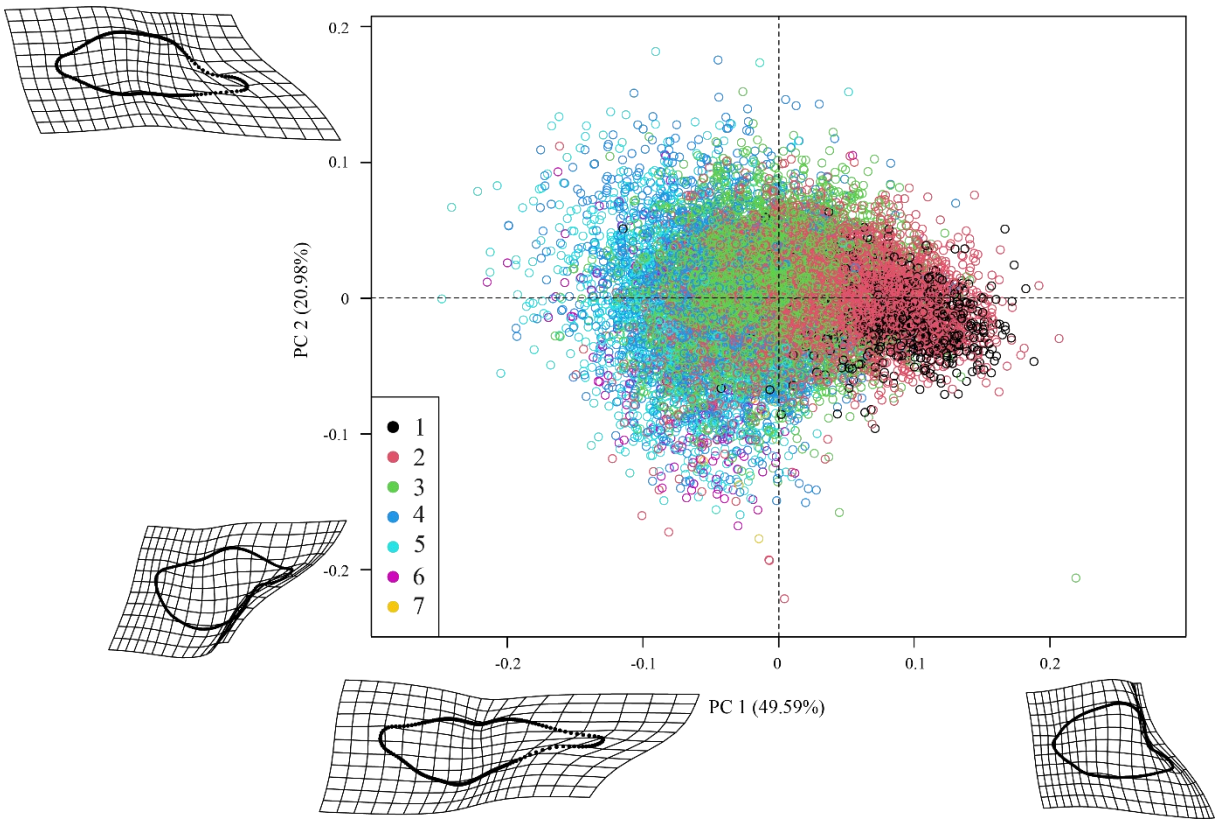

Figure 4.4: Plot of the PC1 axis versus the PC2 axis. The warpgrids show the extreme forms along the corresponding axis. The colours indicate classes of centroid size: black cycles (group 1) correspond to individuals with a centroid size between 0 and 999, red cycles (group 2) to 1000-1999, green (group 3) to 2000-2999, blue (group 4) to 3000-3999, turquois (group 3) to 4000-4999, purple (group 6) to 5000-5999 and yellow (group 7) to 6000-6999.

4.3.1.1. Evolution of PC1 and PC2 through time at Hole 667A (Atlantic Ocean)

At Hole 667A, the maximum scores of the PC1 axis are relatively stable throughout the entire investigated time interval (Fig. 4.5A, 4.6A). This means that the shape of the smallest specimens remains the same. They range from 0.1 (7.6 Ma) to 0.2 (3.69 Ma), which is characterised by a low A, high B value and relatively short last chambers. From 2 Ma to the present, the maximum scores exhibit a decreasing trend, so that spiral (A) and convexities (B) convexities become more similar, and the last chambers elongate and flatten.

Considering the minimum scores of the PC1 axis, the values are close to 0 at 7.96 Ma and 7.6 Ma, meaning that A and B are almost equal. They also indicate that the last chambers have an intermediate elongation and inflation in comparison to the extreme forms. From 7.11 Ma and

3.204 Ma, minimum values range between -0.05 and -0.15, so that A increases, B decreases and the last chambers become more elongated and flattened in comparison to 7.96 Ma and 7.6 Ma. At 2.88 Ma and 2.58 Ma, minimum scores approach again 0.

A strong, negative shift is observed between 2.58 Ma and 2.058 Ma from 0 to -0.15 along the PC1 axis. From 2 Ma to the present, the scores fluctuate between -0.1 and -0.22. Within this interval, these individuals exhibit the most flattened and elongated last chambers as well as the highest A and lowest B values in comparison to all specimens from Hole 667A.

In the mean and median scores, two phases can be recognised: in the first, from 7.98 Ma to 2.58 Ma, the scores are positive and range from ca. 0 to 0.1, so that specimens exhibit relatively short and inflated last chambers and larger B than A values. From 2.057 Ma to 0.003 Ma, a shift of mean and median scores towards 0 is observed for the second interval. In comparison to the first interval, specimens overall show more elongated and flattened last chambers and almost equal A and B values.

Along the PC2 axis (Fig. 4.5B, 4.7B), two major phases can be recognized. In the first phase, maxima are around 0 (7.98 Ma and 7.6 Ma) to 0.1 (7.11 Ma to 2.58 Ma). A gradual decrease is observed from 0.14 at 4.14 Ma to 0.05 at 2.58 Ma. Relative to the mean form, last chambers are elongated and flattened, while A decreases and B increases. In the second phase, the score increases to 0.14 at 2.06 Ma and fluctuates afterwards around 0.1 until 0.11 Ma and 0.003 Ma, where the score increases to 0.18. With this, A decreases and B increases.

Means and medians of PC2 remain stable (around 0), so that A and B are relatively equal.

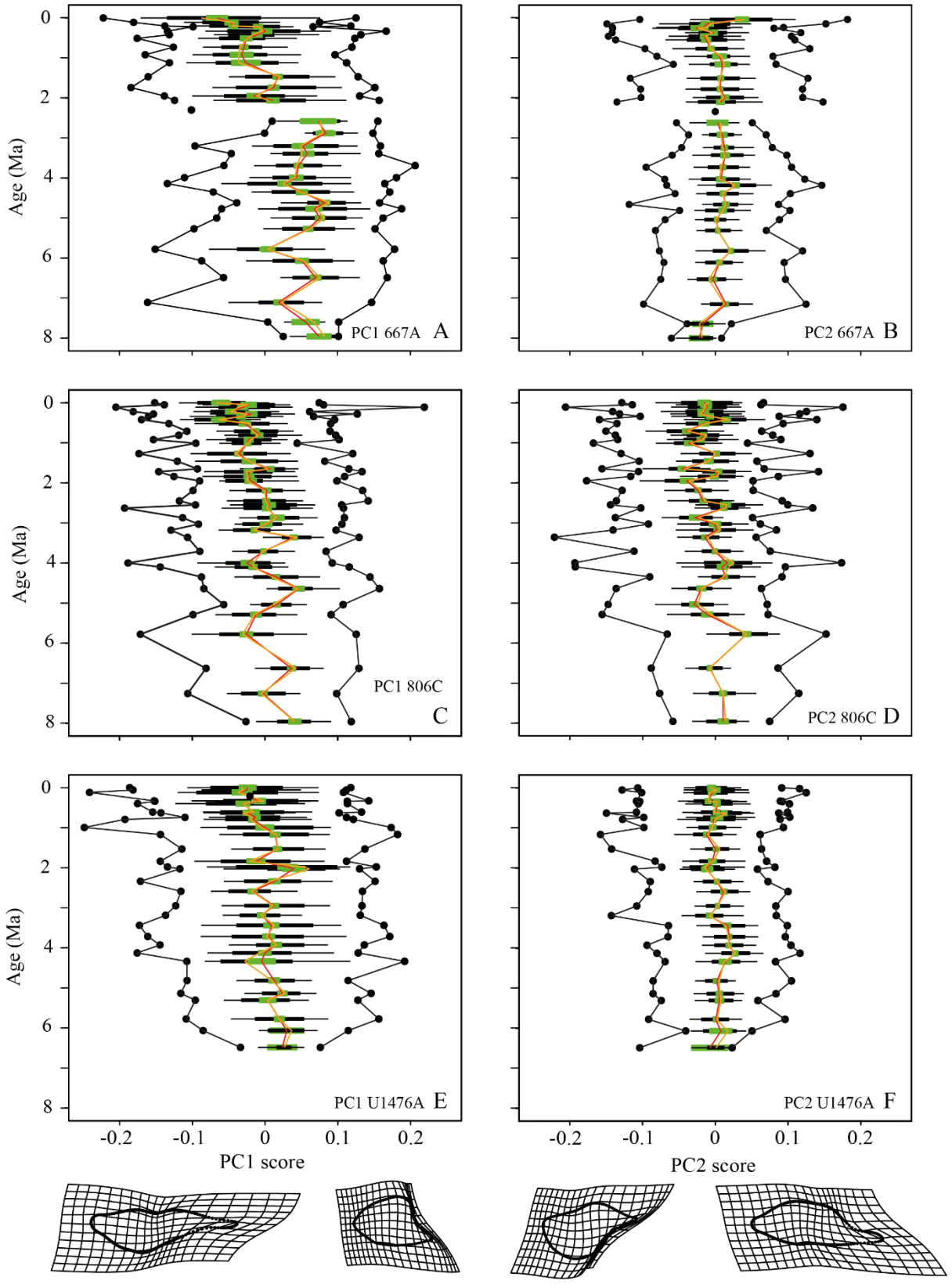

Figure 4.5: Plot of PC axes versus age. **A**: PC1 scores of Hole 667A. **B**: PC2 scores of Hole 667A. **C**: PC1 scores of Hole 806C. **D**: PC2 scores of Hole 806C. **E**: PC1 scores of Hole U1476A. **F**: PC2 scores of Hole U1476A. The black dots and lines represent maxima and minima of the PC scores. The horizontal, thin black bars represent 10 and 90 % sample percentiles, the thick black bars upper and lower quartiles, green bars show the confidence intervals about the mean. Means are connected by red line, medians by blue line. The warpgrids show the maximum form variation along the corresponding axis.

4.3.1.2 Evolution of PC1 and PC2 through time at Hole 806C (Pacific Ocean)

At Hole 806C, PC1 scores for populations are more stable in comparison to Hole 667A (Fig. 4.5C). Maxima fluctuate around 0.1 throughout the investigated time interval. One outlier is observed at 0.1 Ma (0.219), which is the most positive value for the entire dataset 1. It is a specimen with the smallest spiral, the largest umbilical convexities and the shortest last chamber.

Minima scores of PC1 suggest two intervals: from 7.96 Ma to 1.94 Ma, minima fluctuate around -0.1. Specimens have a greater spiral (A) than umbilical (B) convexity and relatively flattened, elongated last chambers. After 1.94 Ma until the present, there is a slight shift towards more negative scores from -0.1 to ~-0.15. Mean and median values exhibit an overall negative trend and decrease from ca 0.04 at 7.96 Ma to -0.06 at 0.004 Ma.

Along the PC2 axis, most maxima fluctuate around 0.1, although several peaks towards larger values can be observed (Fig. 4.5D). In general, A is relatively shortened in comparison to B. Overall, minimum scores decrease gradually from -0.05 (7.96 Ma) to -0.1 (0.004 Ma). The data show that changes in form throughout the investigated time interval are minor, although A slightly increases with time in comparison to B. Medians and means stay stable around 0.

4.3.1.3 Evolution of PC1 and PC2 through time at Hole U1476A (Indian Ocean)

Maxima of PC1 and PC2 scores are relatively constant and fluctuate between 0.1 and 0.2, representing forms with a relatively small A and high B value and small but inflated last chambers (Fig. 4.5E).

The minimum values of PC1 and PC2 scores change gradually from ca. -0.03 at 6.49 Ma to ca. -0.24 at 0.12 Ma and 0.985 Ma. This means that form changes from individuals with almost equal A and B to individuals with a high A and low B with elongated and flattened last chambers.

The mean and median PC1 and PC2 scores fluctuate from -0.03 to 0.06 between 6.49 Ma and 1 Ma, and almost gradually decreases to -0.03 until 0.004 Ma. Between 1 Ma to recent, A becomes larger, and the last chambers becomes increasingly flattened.

In case of PC2, little change is observed in means, medians and extreme values during the past 6.49 Ma (Fig. 4.5F).

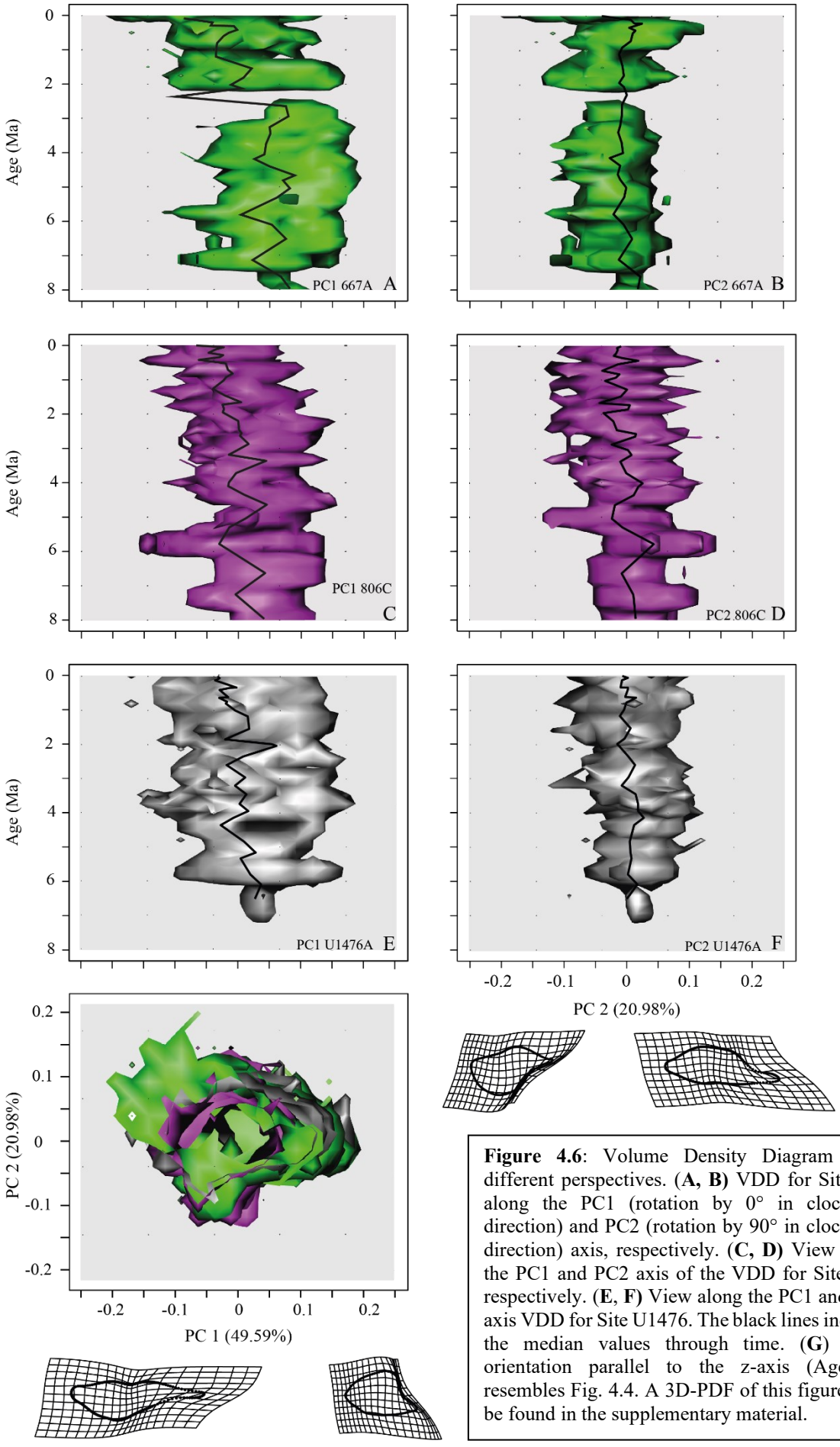

Figure 4.6: Volume Density Diagram from different perspectives. (**A, B)** VDD for Site 667 along the PC1 (rotation by 0° in clockwise direction) and PC2 (rotation by 90° in clockwise direction) axis, respectively. (**C, D)** View along the PC1 and PC2 axis of the VDD for Site 806, respectively. (**E, F)** View along the PC1 and PC2 axis VDD for Site U1476. The black lines indicate the median values through time. (**G**) VDD orientation parallel to the z-axis (Age). It resembles Fig. 4.4. A 3D-PDF of this figures can be found in the supplementary material.

4.3.1.4 Median Comparison of Dataset 1

PC1 median values of the investigated sites show an overall decrease through time (Fig. 4.5A, C, E; 6A, C, E; 7A). Interestingly, medians of PC1 from Hole 667A and 806C show an almost exact same pattern in the evolution from 8 Ma to ca. 4 Ma.

Overall, Hole 667A exhibits the more positive values of PC1 (pointing to shortened last chambers and a higher B value) in comparison to Hole 806C. From 4 Ma to 2.3 Ma, Hole 806C and U1476A show very similar values in PC1. Values evolve different for all sites between 2 Ma and 1 Ma, but values equal each other after 1 Ma.

In contrast to medians of PC1, those of PC2 remain fairly constant throughout the investigated time interval. Hole 667A and U1476A are similar through time and plot around 0 (Fig. 4.5B, D, F; 6B, D, F; 7B), while values of Site 806 show a slightly fluctuating pattern.

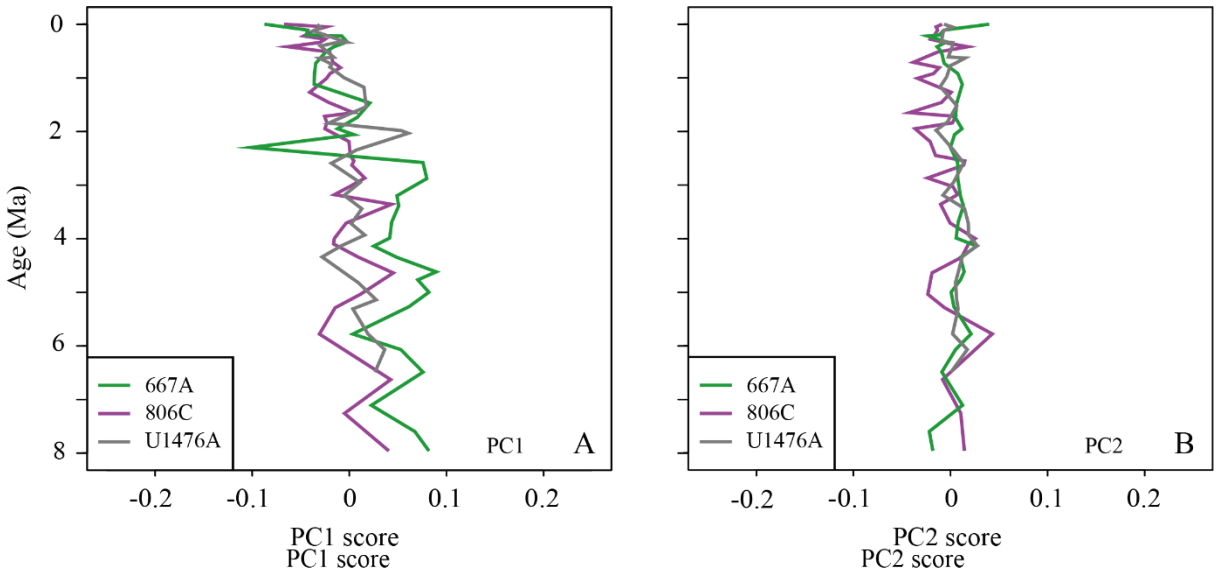

Figure 4.7: Median values for holes 667A (green line), 806C (purple) and U1476A (grey) through time. Medians of PC1 are shown in **A** and medians of PC2 in **B.**

4.3.2 Allometric signal

A regression between centroid size and regression score confirms a statistically significant covariation between form and centroid size (Fig. 4.8; *p*-value < 0.0001). Specimens with a larger centroid size tend to develop a more elongated and flattened form in comparison to specimens with a relatively low centroid size (Fig. 4.8). Allometry explains 22.7 % of the observed variance ($R^2 = 0.22717$) for the dataset consisting of the three cores.

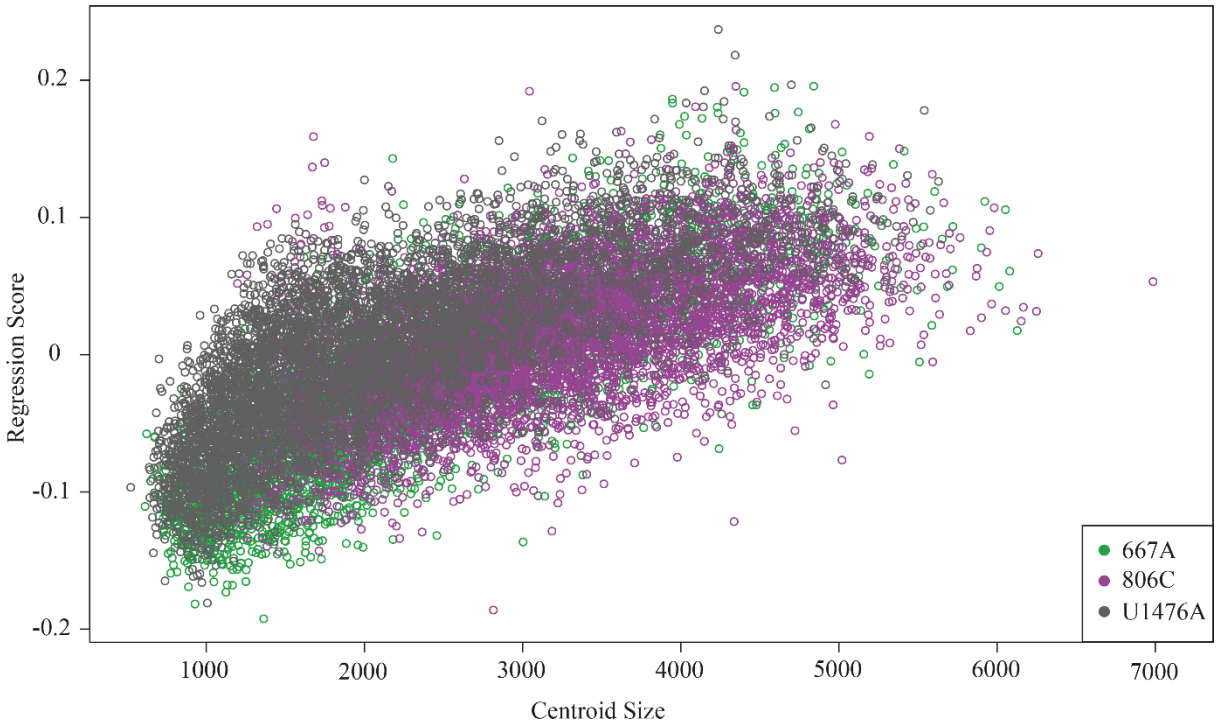

Figure 4.8: Plot of the centroid size versus the regression score. Green cycles symbolise specimens from Hole 667A, purple from Hole 806C and grey from Hole U1476A.

4.3.2.1 PCA of the allometry-free shape (Dataset 2)

As the current study seeks to investigate the shape variation which is not linked to size (allometry) but to evolution, a PCA on the residuals, representing the allometry-free shape, is performed.

None of the studied parameters (Site locality, age and coiling direction) show any trends (Fig. A4.6-8). Along the PC1 axis, the shape of the maximum score is defined by a high A and low B value, the apex is tapered, and the last chambers do not define the maximum B value (Fig. 4.9). The chamber walls of the last chambers are slight curved concavely.

On the contrary, the minimum shape is characterised by a more rounded apex, the maximum B value is defined by the final chambers and the walls of the last chambers are curved in a convex way. The first axis explains 12.21% of the total shape variation (Fig. 4.9).

The shape along the PC2 axis (11.13% of the total shape variation) varies from a relatively rounded apex, convex-shaped walls of the last chambers and a maximum B value, which is developed at the final chambers for the maximum score towards a tapered apex, a gradual to slightly concave shape of the last chambers wall and a less accentuated B at the last chambers for the most negative score.

The average shape (PC1 = 0, PC2 = 0) has straight walls in the last chambers, while the last chambers still define the highest B value.

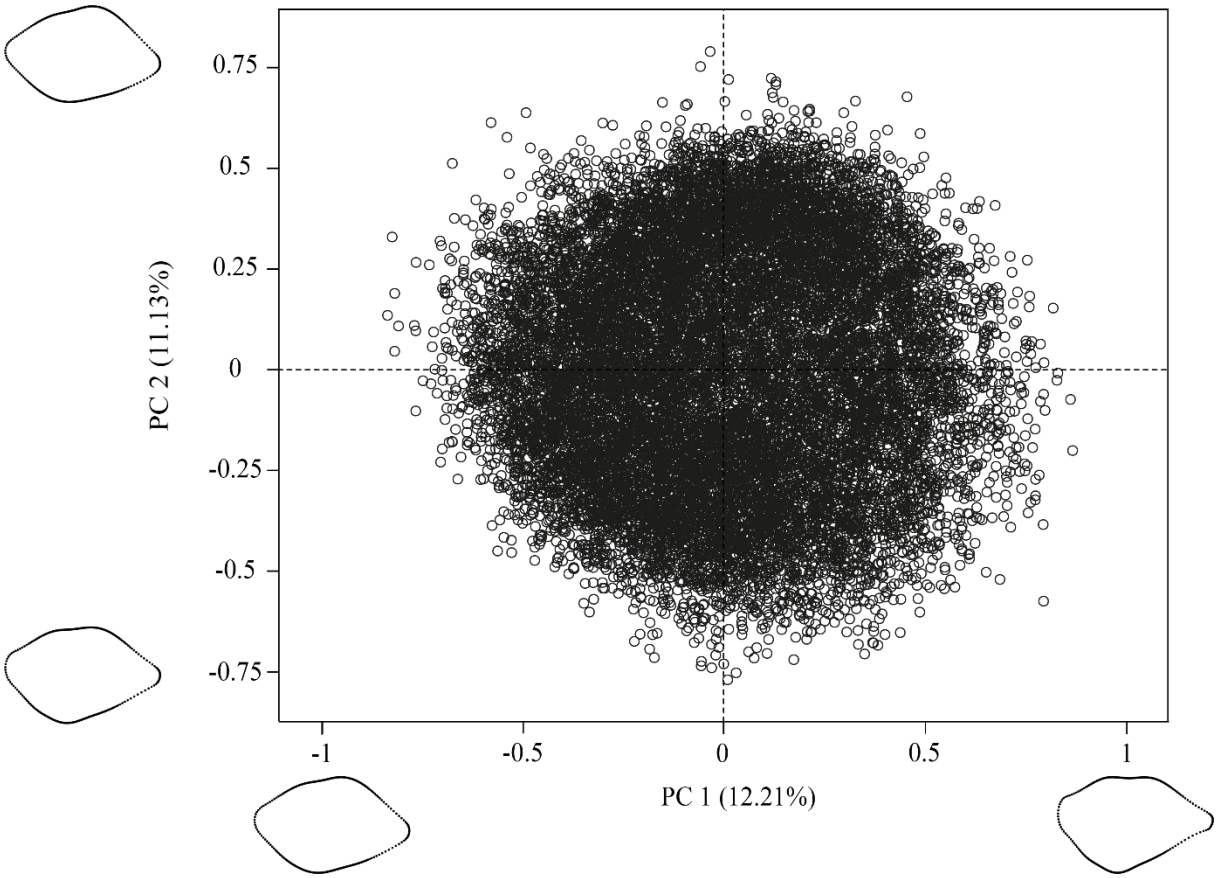

Figure 4.9: Plot of the shape (without allometric effects). PC1 versus PC2 for Holes 667A, 806C and U1476A. The outlines represent the extreme shape along the corresponding axis.

4.3.2.2 Hole 667A

Overall, PC1 values of the residuals show little change through time (Fig. 4.10A, 4.11A). Maxima fluctuate around 0.7, while minima show low variation as well (-0.7 - -0.5). A reduced variance is observed at 7.6 Ma. From 2.88 Ma to 2.34 Ma, a gradual increase in the minima is observed, causing a reduction in the variance. During this time interval, the shape changes towards a more rounded apex and straightening of the shape of the last chambers.

Means and medians exhibit negative peaks at 7.11 Ma, 5.78 Ma and 4.11 Ma (Fig. 4.10A, 4.12A). In the time interval from 4.11 Ma until 2.3 Ma, values gradually increase, tapering the apex and inducing the evolution towards an overall more concave wall shape of the last chambers. During the last 2 Myr, the values have a low variation, varying around -0.05.

Along the PC2 axis, minima and maxima change little through time (Fig. 4.10B, 4.11B). Maxima (minima) increase (decrease) from 7.96 Ma to 6.49 Ma, causing an increase in variance (Fig. 4.10A). Increase in maxima affect the shape to evolve towards a more rounded apex and a more convex shape of the last chambers, while towards more negative PC scores the apex becomes more tapered and the shape of the last chambers becomes more concave.

Values are relatively stable until 3.24 Ma, after which the variance decreases due to decreasing (increasing) maxima (minima). At 2.057 Ma, the lowest minimum (0.74) values correspond to a drastically increased maximum value of 0.645, resulting in a high variance, which stays stable until 0.003 Ma.

Means and medians exhibit a shift from ca. -0.3 to 0 between 7.96 Ma and 7.11 Ma, causing a slightly less tapered apex and a more distinct maximal B defined by a more straightened shape of the walls of the last chambers (10B, 12B). For the last 7 Myr, variation in values is low and varying around 0, only showing distinct negative peaks at 2.3 Ma (only one specimen) and at 0.003 Ma.

4.3.2.3 Hole 806C

Maxima (0.7), minima (~0.6), means and medians (~0) for PC1 stay relatively stable throughout the investigated time interval, so that there is low change in the variance (Fig. 4.10C, 4.11C). Fluctuations in the values are only observed for means and medians between 7.96 Ma and 5.29 Ma. Similar to the PC1 axis, fluctuation in the minima (~-0.6) and maxima (~0.5) along the PC2 axis is relatively low, so that the overall variance is stable through time (Fig. 4.10D, 4.11D).

High fluctuation is observed in the means and median of PC 1 and PC 2 throughout the last 8 Myr, which do not seem to follow any pattern (Fig. 4.10C, D; 4.12A, B).

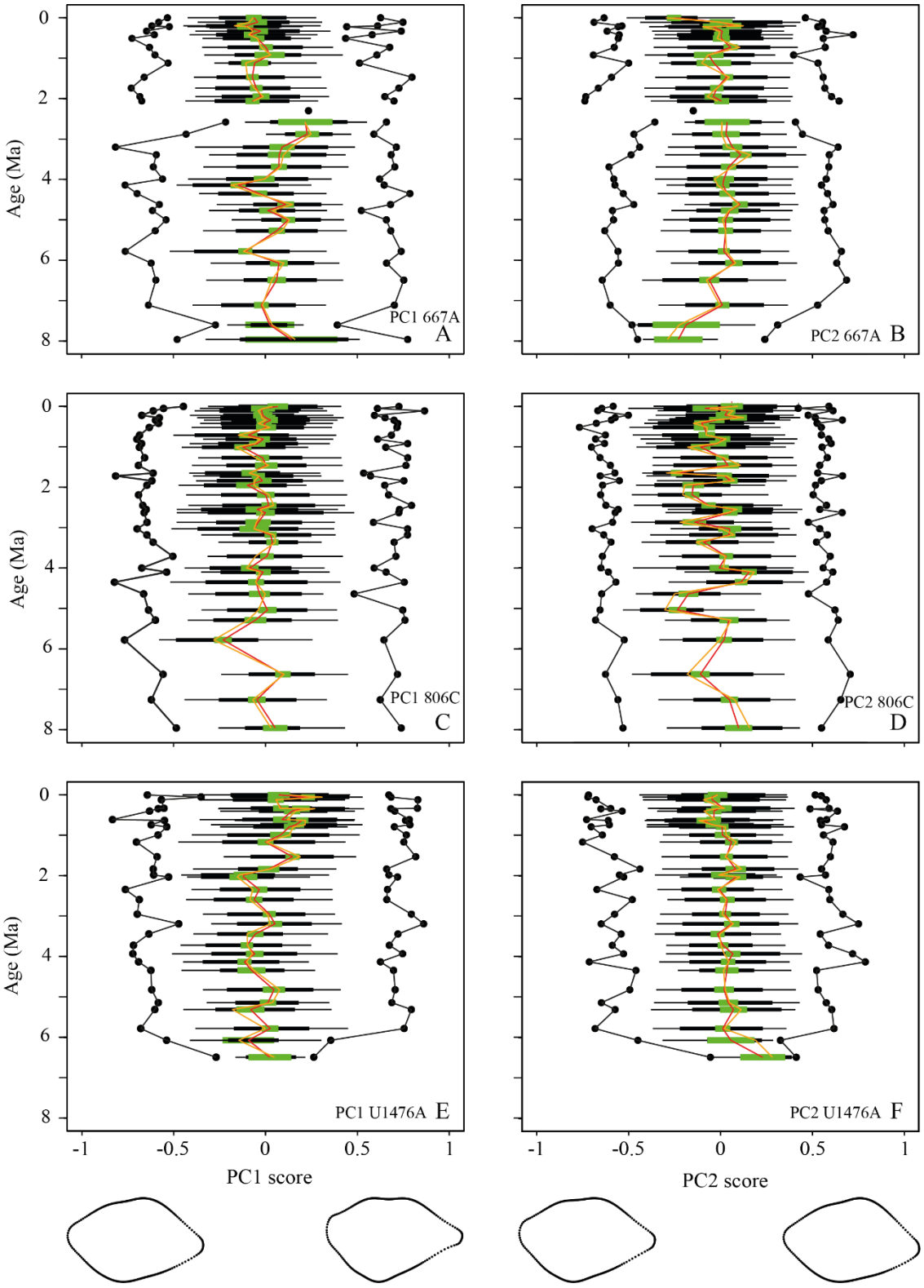

Figure 4.10: Plot of the residuals' PC1 scores for Hole 667A (**A**), Hole 806C (**C**) and Size U1476A (**E**) versus the age. Residuals' PC2 scores versus the age are given for Hole 667A in **B**, for Hole 806C in **D** and for Hole U1476A in **F**. For explanation of the symbols, see Fig. 5.

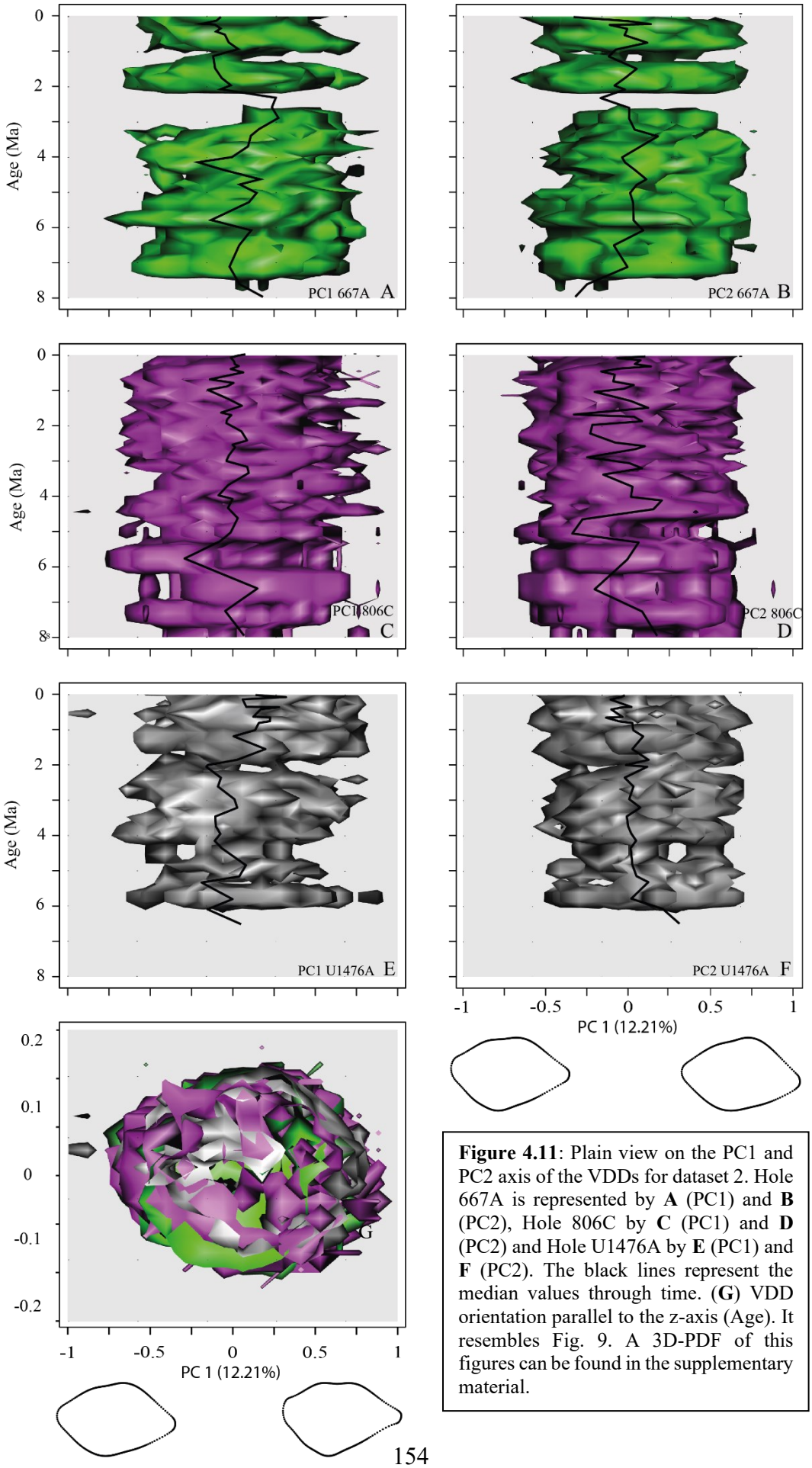

Figure 4.11: Plain view on the PC1 and PC2 axis of the VDDs for dataset 2. Hole 667A is represented by **A** (PC1) and **B** (PC2), Hole 806C by **C** (PC1) and **D** (PC2) and Hole U1476A by **E** (PC1) and **F** (PC2). The black lines represent the median values through time. (**G**) VDD orientation parallel to the z-axis (Age). It resembles Fig. 9. A 3D-PDF of this figures can be found in the supplementary material.

4.3.2.4 Hole U1476A

Variance in the PC 1 axis increases from 6.49 Ma until 5.78 Ma, because minima gradually decrease (-0.25 to -0.7) and maxima gradually increase (Fig. 4.10E, 4.11E). Thereafter, variance is stable due to low variation of minima and maxima though time.

Mean and median scores are relatively stable around 0 from 6.49 Ma until 1.98 Ma (Fig. 4.10E, 4.12A). Thereafter, a shift towards more positive values is observed, changing the shape towards an overall more concave wall shape of the last chamber and a more tapered apex.

Like PC1, an increase in the variance is observed from 6.49 Ma until 5.78 Ma in the PC2 axis (Fig. 4.10F, 4.11F). This coincides with a gradual decrease in the means and medians (Fig. 4.10F, 4.12B). Overall, variance does not change until 1.82 Ma, but two peaks are observed at 4.13 Ma and 3.19 Ma. Relative stability is also shown by means and medians from 5.78 Ma to 0.78 Ma and exhibit a shift to permanent negative values after 0.78 Ma.

4.3.2.5 Comparisons of medians of Dataset 2

Comparing the evolution of the PC1 medians through time, sites plot relatively close around value 0 (Fig. 4.12A). Hole 667A evolves differently compared to the other sites towards more positive values from 4.14 Ma until 2.3 Ma, while Hole U1476A shows more positive values from 1.77 Ma to the present in comparison to Hole 667A and 806C. In these phases, the shape of the wall of the last chamber becomes more concave, while the apex is more tapered.

PC2 medians are similar for the last 5.78 Myr for the investigated sites, varying around the value 0 (Fig. 4.12B). Before 5.78 Ma, medians exhibit site-specific patterns: Hole 667A evolves gradually from -0.288 towards positive values, expressed by a slightly more gradual wall shape

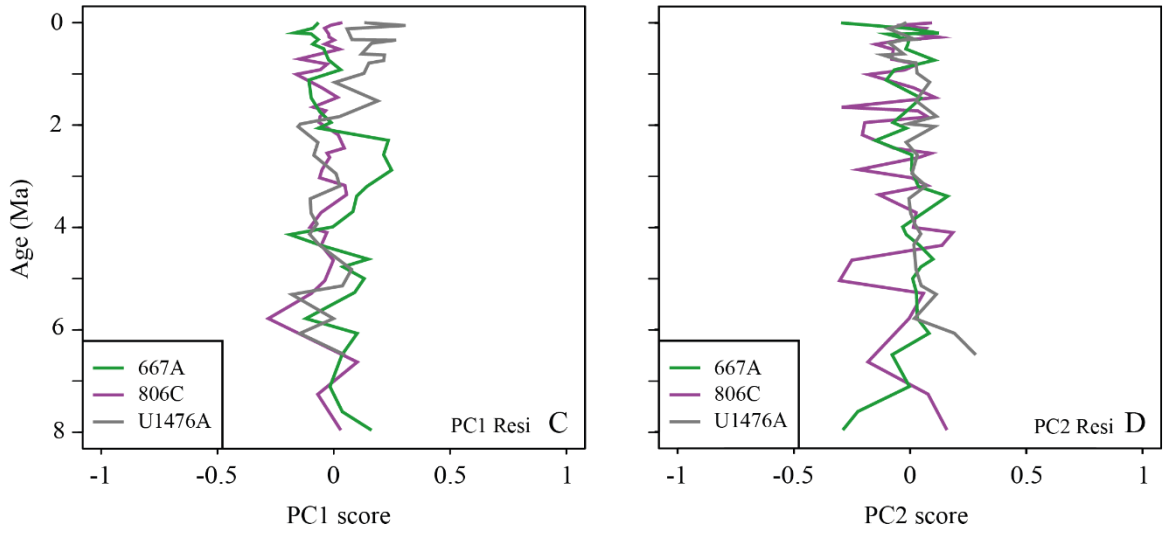

Figure 4.12: Median values of the residuals (shape) for Sites 667 (black line), 806 (red) and U1476 (blue) through time. Medians for PC1 are given in **C** and medians for PC2 in **D.**

of the last chamber and more tapered apex. Hole 806C and Hole U1476A evolve from positive (convex wall shape of the last chamber, more rounded apex) to ca. 0 at 6.625 Ma and 5.78 Ma (almost gradual wall shape of the last chamber), respectively.

4.4 Discussion

4.4.1 Allometry – How ontogeny and climate may have influenced the form evolution

4.4.1.1 Form changes throughout ontogeny and possible environmental influences

Form changes along the PC 1 axis of dataset 1 tend to coincide with changes in the centroid and thus test size of *G. menardii* (Fig. 4.4, 4.8). The change from an inflated form of juvenile towards a flattened, elongated form in adult *G. menardii* has already been observed in several studies (Brown, 2007; Knappertsbusch, 2007a, 2016; Mary, 2013; Caromel et al., 2016; Friesenhagen, 2022a; Chapter 3). The allometric pattern is perhaps a reaction of the organism to its changing habitat within the water column throughout ontogeny (Brown, 2007; Schiebel and Hemleben, 2017c), but detailed causal relationships are not secured until now. The trend towards a relative flattening of the test in keel view were discussed in context of a hydrodynamic adaption to maintain buoyancy (Scott, 1973) or to control settling velocity during growth (Caromel et al., 2014).

Following this argumentation, the trend towards more negative values of PC1 during at least the last 2 Myrs (Fig. 4.5A, 4.6A) suggests either a reaction to an increase in body size sensu Cope's Rule (e.g. Stanley, 1973) or hydrographic change of the habitat of *G. menardii*. For the PF *Globorotalia truncatulinoides*, Lohmann & Malmgren (1983) suggested oceanographic and hydrographic changing aspects in the South Atlantic and southern Indian Ocean to explain gradual change in its the test form for the last 0.7 Myr.

4.4.1.2 Form changes at locations through time

Dataset 1 reveals that the evolution of the form in keel-view differs among the oceans: in the Atlantic Ocean (Site 667A), minima of PC1 show several negative peaks, while minima of PC1 scores in the Pacific (Site 806C) and Indian Ocean (Site U1476A) decrease more gradually. This difference might be constituted in the different palaeoceanography of those oceans, which cause different environmental niches for *G. menardii* to thrive and possibly affecting its morphological development (Friesenhagen, 2022a).

In the Atlantic Ocean, the dominating oceanographic feature is the Atlantic Meridional Overturning Circulation (AMOC). It drives the global ocean conveyor belt and causes transport of warm and salty surface water from the South Atlantic Ocean into the North off Greenland and the Weddell Sea and returns as bottom water into the South Atlantic at depth as the North Atlantic Deep Water (McCarthy et al., 2017). Long-term changes in the dynamics of the AMOC are thought to impact test size (Friesenhagen, 2022a) because of its effect on surface water structure and thus influence the form evolution of *G. menardii* (Fig. 4.13).

Since the early Pleistocene, El Niño – Southern Oscillation (ENSO) drives the equatorial hydrography and oceanography of the Pacific Ocean (Wara et al., 2005; Chiang, 2009). In the normal, present state, there is a sea-surface temperature gradient between the eastern and the western tropical Pacific of ca. 4°C, establishing a deeper thermocline in the warmer western

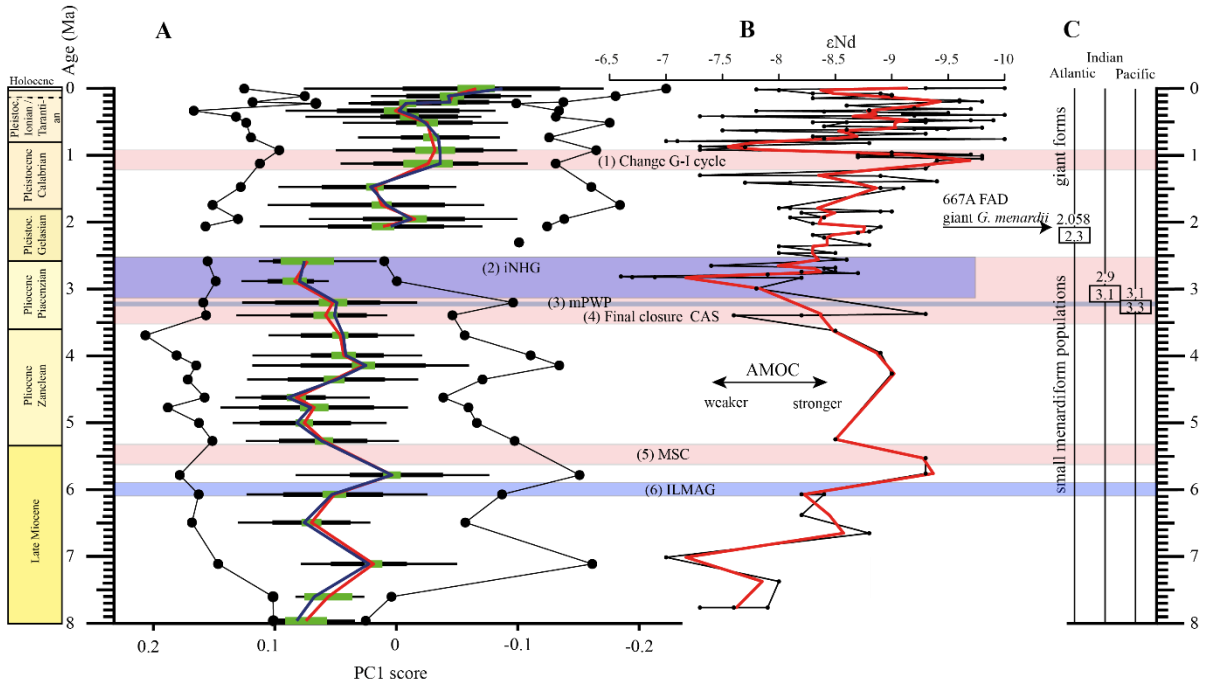

Figure 4.13: (**A**) PC1 axis for the eastern tropical Atlantic Ocean Hole 667A in a palaeoceanographic context. Please note that the PC1 axis is mirrored to facilitate an easier comparison in peaks of the εNd isotopic curve. Maxima and minima of PC1 are represented by black dots. Horizontal thin bars represent the 10 % to 90 % sample percentiles, thick black bars the upper and the lower quartiles about the median, and the green bars the confidence interval about the mean. The vertical red line illustrates means, the blue line the median. Coloured boxes: (1) Time interval in which a shift towards increased amplitude of glacial–interglacial cycles and a corresponding 100 Ka fluctuation in ice sheets is observed (Clemens et al., 1996; Ivanova, 2009). (2) Cooling trend leading to the NHG (Chapman, 2000). (3) Mid Pliocene warm period (mPWP; Haywood et al., 2016). (4) Time interval in which the final closure of the Central American Seaway (CAS) is supposed by Bartoli et al. (2005), Jackson and O`Dea (2013) and O'Dea et al. (2016). (5) Time interval of the Mediterranean Salinity Crisis (Krijgsman et al., 1999). (6) Intensification of the Late Miocene Antarctic Glaciation (ILMAG) (Chaisson and Ravelo, 1997). (**B**) The εNd isotopic curve at Site 1088 in the South Atlantic is taken from Dausmann et al. (2017), which is a proxy for the AMOC strength. The black line with circles represents the original data from Dausmann et al. (2017), the red line a smoothed version, produced with the RStudios' command 'smooth.spline' at the value of 0.35. (**C**) The boxes show the time intervals in which the giant *G. menardii* specimens occurred in the Atlantic, the Indian and the Pacific oceans, and in which the size increase is presumed to have taken place (Friesenhagen, 2022; Knappertsbusch, 2022; Chapter 3). The arrow shows the first appearance datum (FAD) of giant *G. menardii* at Hole 667A.

side and a shallower thermocline in the cooler eastern side (Wara et al., 2005). During El Niño events, sea-surface temperature and thermocline gradients decrease between the eastern and western tropical Pacific (Chiang, 2009). Reconstructions of the thermocline depth indicate that this system was established between 2.5 Ma and 1.7 Ma (Wara et al., 2005; van der Lubbe et al., 2021; Fig. 4.14). Palaeoceanography in the Indian Ocean is impacted by changes in the evolution of the Indian monsoon system (e.g. Gupta and Thomas, 2003; Ivanova, 2009; Chang et al., 2010; Zhisheng et al. 2011). It is very plausible that the long-term development of the Indian monsoon system had an impact on the evolution of tests of *G. menardii* (Fig. 4.15). As can be derived from figures 4.5 and 4.7, the pattern of evolution of form differs between the oceans from 2.5 Ma to 2 Ma: while there is a pronounced shift in minima of PC1 from -0.01 to -0.124 in the eastern tropical Atlantic (Fig 4.5A, 4.6A), a gradual shift is observed for populations from the western tropical Pacific and the Mozambique Channel (Fig. 4.5C, E; 4.6C, E; 3D-PDF in Supplementary material). The pattern of an abrupt shift observed in the Atlantic Ocean for *G. menardii* is similar to the shifts in form noticed for the transitions within the *G. plesiotumida-tumida* lineage at the Miocene-Pliocene boundary in the Indian Ocean

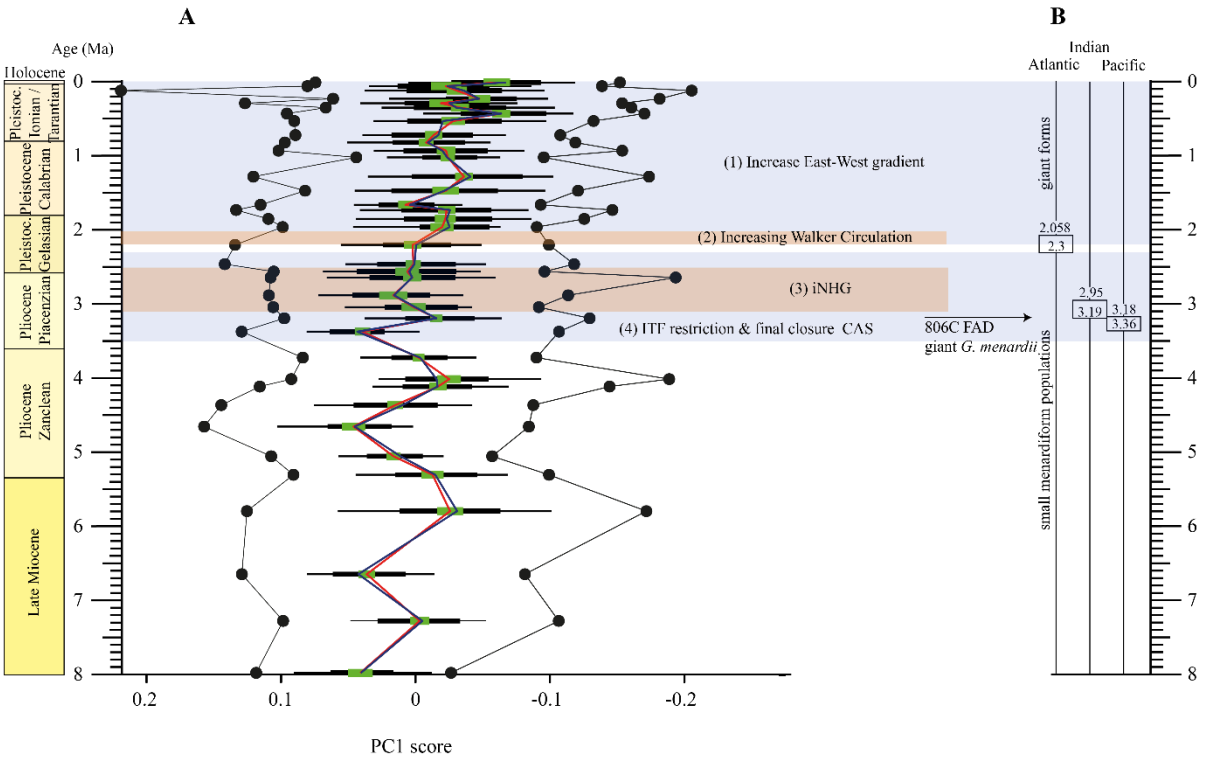

Figure 4.14: **(A)** PC1 axis for Hole 806C (western tropical Pacific Ocean) for *G. menardii* in a palaeoceanographical context. Please note that the PC1 axis is mirrored. See Fig. 4.13 for explanation of the symbols. (1) Increase in the East-West sea-surface temperature and thermocline gradient within the Pacfic Ocean (Wara et al., 2005; van der Lubbe et al., 2021). (2) Increase in the Walker Circulation (Etourneau et al., 2010). (3) Cooling trend leading to the NHG (Chapman, 2000). (4) Tectonic restriction of the Indonesian Throughflow (De Vleeschouver et al., 2019; Auer et al., 2019) and time interval of the final closure of the Central American Seaway. **(B)** First appearance date of the giant *G. menardii* type in the Atlantic, Indian and Pacific oceans. Furthermore, it marks the time intervals in which the giant type first occurred in the Atlantic Ocean (Friesenhagen, 2022) and in the Pacific Ocean (Knappertsbusch, 2022).

(Malmgren et al., 1983; Hull & Norris, 2009) and the *T. juanai-crassaformis* lineage in the early Pliocene in the west of New Zealand (Bicknell et al., 2018). In those studies, the rapid form change is interpreted as an interpunctured, evolutionary event within an otherwise gradual pattern (Malmgren et al., 1983) and quantum evolution (Simpson, 1953), respectively.

Thus, the (not so) rapid pattern at Hole 667A might be interpreted as a punctuated, evolutionary phase. In this case, an isolated *G. menardii* population in the Atlantic Ocean is proposed, which evolved differently between 4 Ma to 2.5 Ma, but abruptly developed similar test forms as populations in the Indian and Pacific oceans around 2 Myr. However, the accelerated form change can equally well be explained by large scale dispersal of specimens from the Indian Ocean. While the variation in PC1 in the Pacific and Indian Ocean stays relatively unchanged during 2.5 Ma and 2 Ma (5C, E; 6C, E), it strongly decreases in the Atlantic Ocean (5A, 6A). This decrease follows the closure of the Central American Seaway

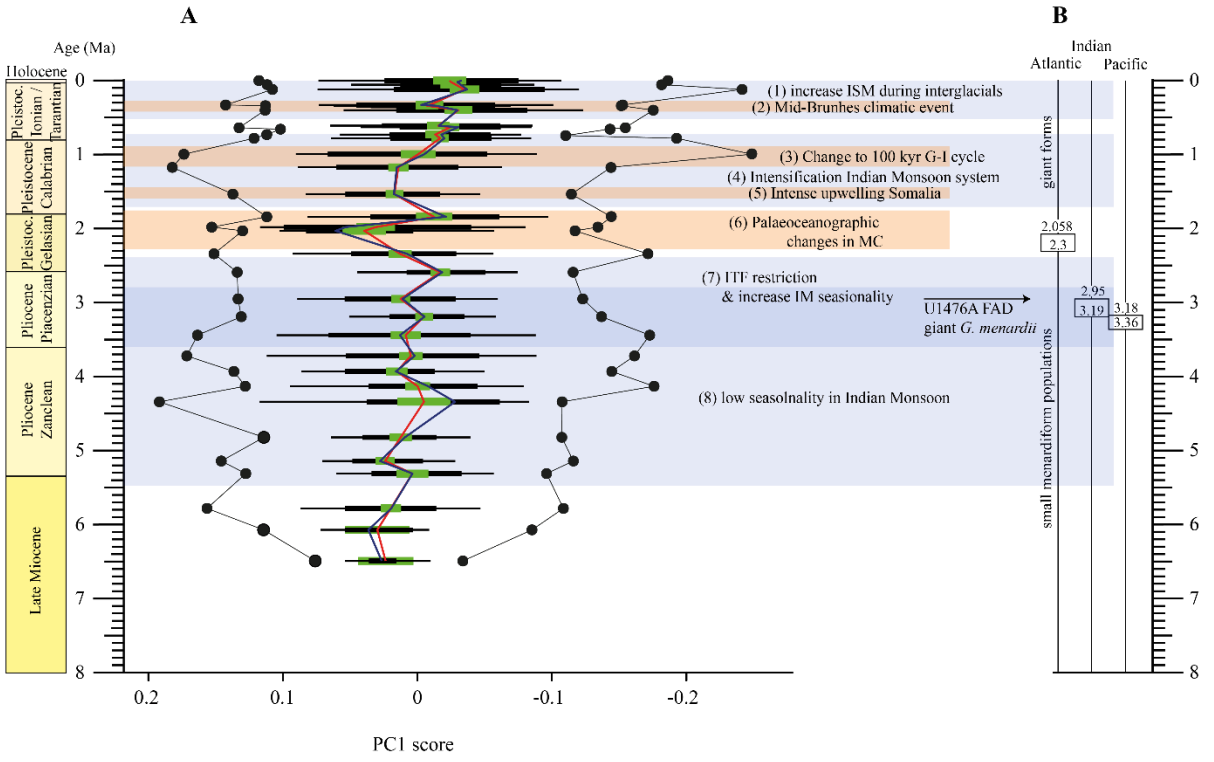

Figure 4.15: (**A)** PC1 axis for Hole U1476A for *G. menardii* in a palaeoceanographical context. Please note that the PC1 axis is mirrored. See Fig. 12 for explanation of the symbols. (1) Increase in the Indian Summer Monsoon (ISM) (Petrick et al., 2019). (2) Mid-Brunhes climatic event (Jansen et al., 1986). (3) Shift towards an increased amplitude of glacial-interglacial cycles and a corresponding 100 ka fluctuation in global ice sheets (Clemens et al., 1996; Ivanova, 2009). (4) Intensification of the Indian Monsoon system (Gupta, 1999). (5) Intense upwelling in the Somalia Basin (Gupta, 1999). (6) Palaeoceanographic changes in the Mozambique Channel (Tangunan et al., 2018). (7) Tectonic restriction of the Indonesian Throughflow (De Vleeschouver et al., 2019; Auer et al., 2019) and increase in the Indian Monsoon seasonality (Gupta & Thomas, 2003; Ivanova, 2009; Chang et al., 2010). (8) Low seasonality of the Indian Monsoon, strong Indian summer monsoon, weaker Indian winter monsoon (Gupta & Thomas, 2003). (**B)** First appearance date of the giant *G. menardii* type in the Atlantic, Indian and Pacific Ocean. Furthermore, it marks the time intervals in which the giant type first occurred in the Atlantic Ocean (Friesenhagen, 2022) and in the Pacific Ocean (Knappertsbusch, 2022). See Fig. 13 for further explanation.

(CAS; O'Dea et al. 2016), which is thought to have intensified the Northern Hemisphere Glaciation (Haug and Tiedemann, 1998; Bartoli et al., 2005; O'Dea et al., 2016) and having affected hydrography of the Atlantic Ocean (Haug and Tiedemann, 1998; Haug et al., 2001; Bartoli et al., 2005).

These environmental changes may have triggered a decrease in the form variation and probably led finally to the replacement of an Atlantic incumbent *G. menardii* type by Indian or Pacific newcomers via Agulhas faunal leakage. These newcomers had a high degree of morphological overlap in the Atlantic Ocean during the last 2 Ma.

The abrupt shift of the PC1 score in the Atlantic Ocean (2.3 Ma - 2.058 Ma) and the start of the gradual shift in the Indian and Pacific Ocean around 2 Ma in the minima and medians (Fig. 4.5A, C, E; 4.6A, C, E; 3D-PDF in Supplementary material) coincide with the dominance of the proposed new giant type in *G. menardii* (Friesenhagen, 2022a; Knappertsbusch, 2022; Chapter 3). This observation supports the dispersal hypothesis.

In contrast to PC1, form changes along the PC 2 axis (20.98 % of the total variation) do not trend along with any investigated morphometrical character or is defined by location.

4.4.2. The Shape Evolution of *G. menardii*

Maxima and minima values of dataset 2, the allometry-free shape, resemble each other for all investigated sites throughout the investigated time interval (Fig. 4.9; 4.10C, D; 4.11; 3D-PDF in supplementary material). The rather stable maxima and minima indicate no shape evolution in the extreme morphotypes, suggesting the existence of one single morphotype at the studied sites throughout the last 8 Myr. The results resemble that of Stewart (2003; see his Fig. 5.10A), who also observed a high degree of superposition in morphospace of *G. menardii* through time and could not distinguish different *G. menardii* subspecies in an eigenshape morphometric analysis of outlines in keel view.

However, the evolution of the median PC1 scores through time (Fig. 4.12C) suggests three intervals in the population's shape evolution, which coincide with major palaeogeographic and palaeoceanographic events.

In phase 1 between ca. 8 Ma and 4 Ma (Fig. 4.16, 4.17), median scores of the different sites exhibit similar pattern in their evolution. During this time, an exchange of tropical surface-water and *G. menardii* population between the oceans was possible (1) between the Atlantic and Pacific Ocean via the CAS and (2) between the Indian and Pacific Ocean via the Indonesian Throughflow (ITF). A direct exchange between the Indian and Atlantic Ocean was probably taking place via a "palaeo-Agulhas" leakage, although there are no hints for the existence during

the Pliocene (Petrick, 2014; Petrick et al., 2015), while the Agulhas Current was already established (Wright and Thunell, 1988; Petrick, 2014; Petrick et al., 2015).

In 5the second phase (ca. 4 Ma to 2 Ma), the restriction of the ITF (De Vleeschouver et al., 2019, Auer et al., 2019) and the final closure of the CAS (Chaisson, 2003; O'Dea et al., 2016) reduced the exchange of tropical surface-water and *G. menardii* population exchange between the oceans. Reorganisation of ocean surface currents (Haug and Tiedemann, 1998; Haug et al., 2001; Bartoli et al., 2005) could have triggered the start of an allopatric speciation event. This also affected the strength of the Agulhas current and probably the Agulhas leakage (Petrick,

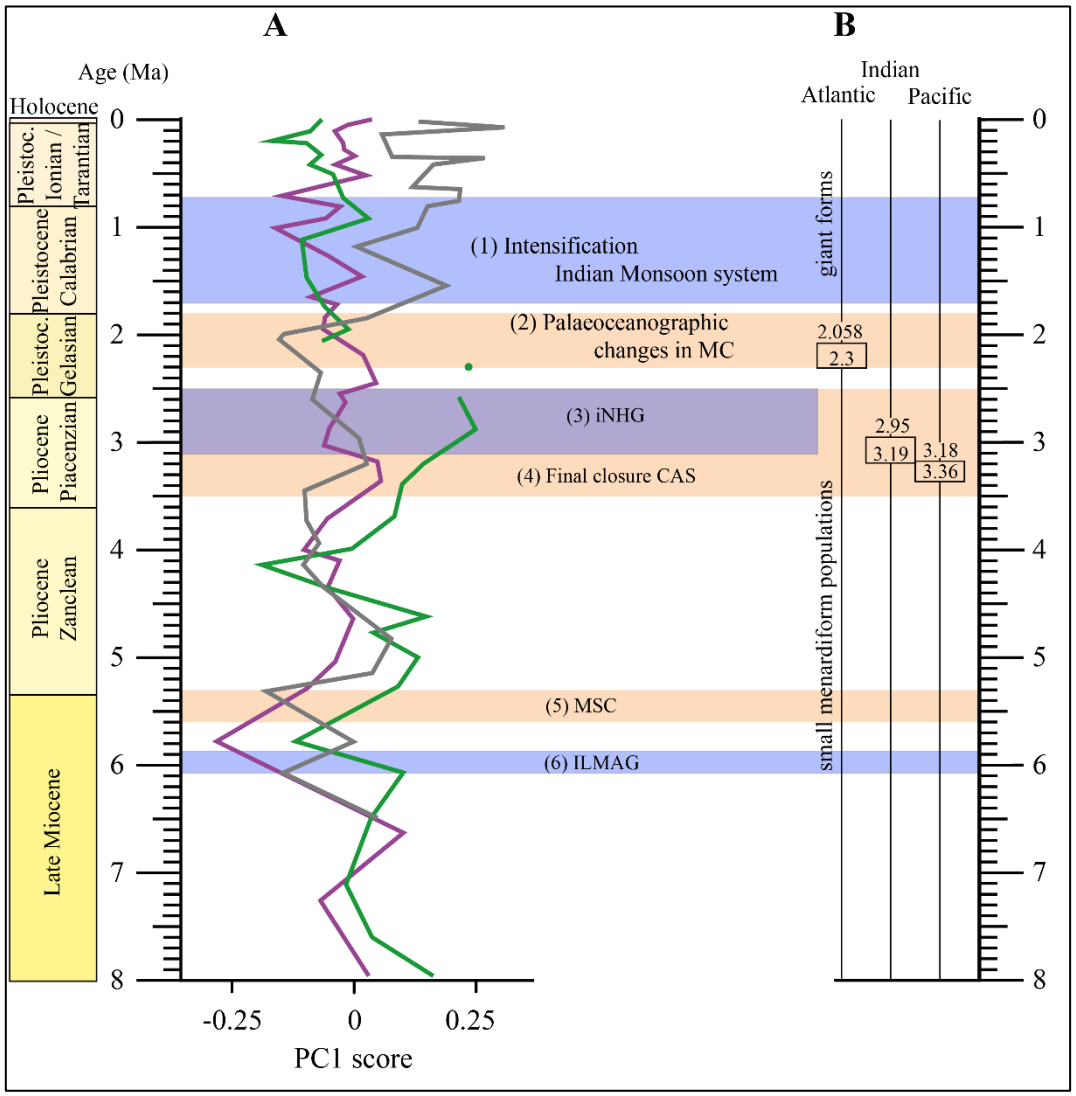

Figure 4.16: **(A)** Median values of the PC1 axis of dataset 2 in a palaeoceanographical context. The green line represents the medians for Hole 667A, the purple for Hole 806C and the grey for Hole U1476A. (1) Increase in the Indian Summer Monsoon (Petrick et al., 2019). (2) Palaeoceanographic changes in the Mozambique Channel (Tangunan et al., 2018). (3) Cooling trend leading to the NHG (Chapman, 2000). (4) Time interval in which the final closure of the CAS is supposed by Bartoli et al. (2005), Jackson and O`Dea (2013) and O'Dea et al. (2016). (5) Time interval of the Mediterranean Salinity Crisis (Krijgsman et al., 1999). (6) Intensification of the Late Miocene Antarctic Glaciation (ILMAG) (Chaisson and Ravelo, 1997). **(B)** First appearance date of the giant *G. menardii* type in the Atlantic, Indian and Pacific Ocean. Furthermore, it names the time intervals in which the giant type first occurred in the Atlantic Ocean (Friesenhagen, 2022), the Indian Ocean (Chapter 3) and in the Pacific Ocean (Knappertsbusch, 2022).

2014; Petrick et al., 2015). The mentioned palaeogeographic changes could have affected the environmental conditions in the Atlantic Ocean and impacted the habitat of *G. menardii*, initiating an anagenetic shift in the median shape of Atlantic populations. This anagenetic pattern is expressed by a shift towards more positive values at Hole 667A (Fig. 4.16, 4.17) and a decrease of the variance along the PC1 axis (Fig. 4.10A; 4.11A) in comparison to Hole 806C and U1476A. The latter two sites show a similar pattern throughout this time interval.

Between 2.5 Ma and 2 Ma, the median values of Hole 667A abruptly shifted back to values similar to that of Hole 806C and U1476A. This pattern probably denotes a drastic reduction or extinction of the incumbent Atlantic population and an isochronal dispersal of specimens from the Indian Ocean via a (re-)strengthening Agulhas Leakage (see also section 4.1; Knappertsbusch, 2016; Friesenhagen, 2022a; Chapter 3). It may also be explained by a drastic change in the thermocline habitat of *G. menardii*, triggered by initiation of the NHG due to the closure of the CAS and the possible reduction of the palaeo-Agulhas leakage.

In the third phase from ca. 2 Ma until the present, a pattern resembling anagenesis is observed in the Indian Ocean (Fig. 4.16, 4.17). A shift towards more positive values in the medians along the PC1 axis is exhibited in comparison to the similar and stable values of Hole 667A and 806C. This shift might be the consequence of permanent palaeoceanographic changes in the Mozambique Channel (Tangunan et al., 2018) after 2.2 Ma, an increased seasonality of the Indian monsoon (Ivanova, 2009; Chang et al., 2010) as well as changes in the intensity of the Indian Summer Monsoon (Zhisheng et al., 2011; Fig. 4.16).

The divergent form and shape evolution of *G. menardii* populations in the Atlantic Ocean between ca. 4 Ma and 2 Ma and the subsequent, rapid shift leading to superposition in morphospace during the last 2 Myr with the Indian and Pacific populations resembles the pattern observed in the test-size evolution and in the predominant-coiling-direction in the Atlantic and Indian ocean (Friesenhagen, 2022a, Chapter 3). The Agulhas leakage hypothesis was supposed to explain those observed pattern best. Therefore, it provides a plausible explanation for the shape and form evolution in the Atlantic Ocean.

However, the results do not exclude the possibility of a regional evolutionary event taking place in the Atlantic. For testing to which extent the (palae-) Agulhas faunal leakage influenced *G. menardii*'s evolution in the Atlantic Ocean, high-resolution size, form and shape studies for the investigated sites in the time interval from 2.5 Ma to 2 Ma are needed.

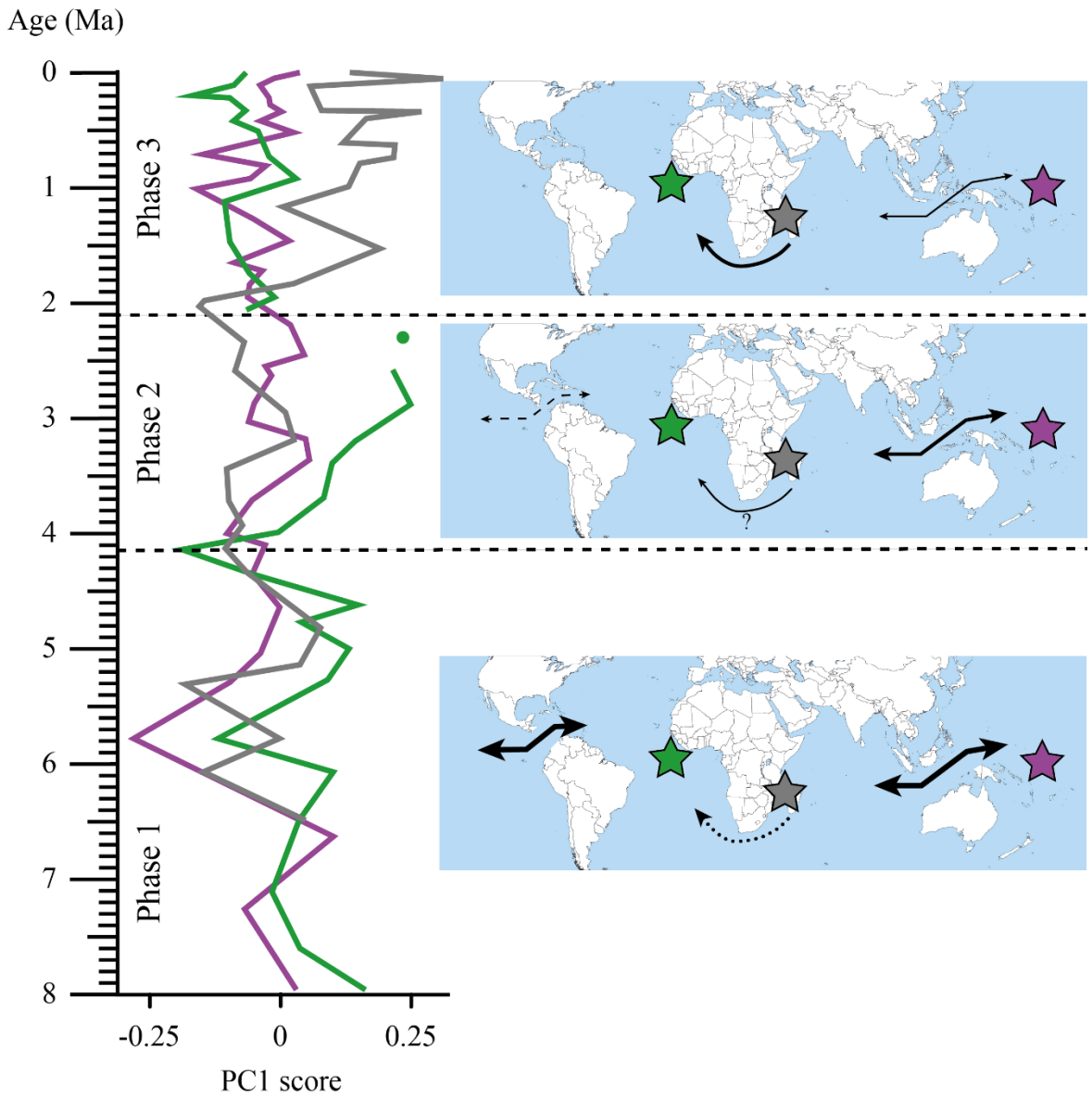

Figure 4.17: Median values of the PC1 axis of dataset 2 (allometry-free shape) of the three studied sites through time in comparison to schematic maps showing major palaeoceanographical and -geographical changes. The green line on the left represents the medians of Hole 667A, the purple one medians of Hole 806C and the grey one of Hole U1476A. **Phase 1 (> 4 Ma)**: Evolution of medians show the same pattern in the investigated holes, while the CAS and the ITF are open and a strong Agulhas Current was present (Wright and Thunell, 1988). This may include a palaeo-Agulhas Leakage (dotted arrow). This palaeoceanographic setting allowed an exchange of tropical surface waters and *G. menardii* populations between the oceans (bold arrows). **Phase 2 (ca. 2 Ma to 4 Ma)**: While medians of populations in Hole 806C and U1476A are similar, medians in Hole 667A evolve towards more positive values. The CAS became restricted and finally closed (dashed line; Chaisson, 2003; O'Dea et al., 2016), the ITF also became tectonically restricted (thinned arrow; De Vleeschouver et al., 2019; Auer et al., 2019), changing paths of major currents and probably weakened or ceased the Agulhas Current and the Agulhas leakage (arrow with '?'). This might have led to an isolation of Atlantic *G. menardii* populations and/or decreasing suitability of environmental conditions in the Atlantic for *G. menardii*. **Phase 3 (ca. 2 Ma until present)**: Hole 667A and 806C show similar values, while medians of Hole U1476A exhibit a permanent shift towards more positive values. This evolution coincides with a decreased tropical surface-water and *G. menardii* population exchange between the Indian and Pacific Ocean due to a further ITF restriction and a strong Agulhas Current as well as an established or restrengthened Agulhas Leakage. It indicates that either the Pacific morphotype (re-)entered the Atlantic or that the environmental conditions became suitable again for *G. menardii* to thrive in the Atlantic Ocean. The anagenetic pattern in the Indian Ocean may be explained by permanent changes in the oceanography of the Mozambique Channel after 2.2 Ma (Tangunan et al., 2018) and changes in the Indian monsoon system (Ivanova, 2009; Chang et al., 2010; Zhisheng et al., 2011).

4.5 Conclusions

1. The test-form (includes allometric effects) and -shape (allometry-free) analyses in the keel view of the planktonic foraminifer *G. menardii* for the last 8 Myr reveal a high degree of overlap in the morphospace of Atlantic, Pacific and Indian Ocean populations.
2. Lack of change in the extreme shapes indicate that there has been one single morphotype at the investigated sites throughout the late Miocene until the present. There is no evidence for the existence of different morphotypes in *G. menardii*.
3. Changes in the form evolution parallel changes in the test size throughout both ontogeny and time. Since the maximum test size was hypothesised to be influenced by changes in the environment induced by palaeoceanographic and palaeohydrographic alternations, the form may be indirectly affected by alterations in environmental conditions as well. This may explain the different pattern observed in the form evolution from 8 Ma to ca. 2 Ma between the Atlantic Ocean, exhibiting an interpunctuated pattern, and the Pacific and Indian Ocean, which show a gradual evolution.
4. Median-shape evolution indicate two phases, which show different values in comparison to the other investigated sites. They may be interpreted as the beginning of anagenetic evolution within the populations: From 4 Ma to ca. 2.3 Ma in the Atlantic Ocean and from ca. 1.7 Ma to the present in the Indian Ocean, *G. menardii* populations evolve towards more pronounced apex and convex walls of the last chamber at the corresponding site.
5. The Agulhas leakage hypothesis delivers a plausible explanation for the form and shape evolution of *G. menardii* in the Atlantic Ocean. However, the results of the current study do not provide unequivocal evidence for the Agulhas leakage hypothesis and cannot disprove the hypothesis of a punctuated evolutionary event taking place in the Atlantic Ocean.
6. For a final determination, detailed ontogenetic investigations and a conventional taxonomic classification of the proposed morphotypes, including differences in the wall structure, in the porosity and growth pattern, are needed.

Contribution of Contents

Friesenhagen designed the study, wrote new and adjusted existing programmes. He adjusted the R-script, processed the data, wrote the text and created the figures. Mennecart helped to design the study, critically reviewed the text and helped with the interpretation of the results. The initial R-script for the PCA was provided by Dziomber. Knappertsbusch provided the raw data from ODP Hole 806C and critically reviewed the text.

Code availability

The Fortran codes and programmes will be uploaded to the PANGAEA Data Repository and are stored at internal servers of the Natural History Museum Basel.

Data availability

Raw and intermediate and final data will be uploaded to the PANGAEA Data Repository and are stored at internal servers of the Natural History Museum Basel.

Sample availability

All sample material and residuals are stored in the collection of the Natural History Museum Basel as the reference collection to the dissertation of Friesenhagen.

Acknowledgements

Swiss National Science Foundation (SNSF; SNF-No.: 200021_169048/1 and 200021_169048/2) and Freiwillige Akademische Gesellschaft Basel (FAG) are highly acknowledged for funding and supporting this project.

We highly obligate the International Ocean Discovery Program (IODP) and its precursor organisation Ocean Drilling Program (ODP) for providing the investigated sample material.

We thank the Naturhistorisches Museum Basel for its support in any way.

Special thanks go to Alexandra Viertler, Mark Charran, Seraina Klopfstein and Tamara Spasojevic for their help with RStudio and the used code as well as discussions.

References

Adams, D., Collyer, M., Kaliontzopoulou, A., and Baken, E.: Geomorph: Software for geometric morphometric analyses. R package version 4.0., https://cran.r-project.org/-package=geomorph, version 4.0.1, 2021.

Auer, G., De Vleeschouwer, D., Smith, R. A., Bogus, K., Groeneveld, J., Grunert, P., Castañeda, I. S., Petrick, B., Christensen, B., Fulthorpe, C., Gallagher, S. J., and Henderiks, J.: Timing and Pacing of Indonesian Throughflow Restriction and Its Connection to Late Pliocene Climate Shifts, Paleoceanography and Paleoclimatology, 34, 635–657, https://doi.org/10.1029/2018pa003512, 2019.

Bardua, C., Felice, R. N., Watanabe, A., Fabre, A.-C., and Goswami, A.: A Practical Guide to Sliding and Surface Semilandmarks in Morphometric Analyses, Integrative Organismal Biology, 1, https://doi.org/10.1093/iob/obz016, 2019.

Bartoli, G., Sarnthein, M., Weinelt, M., Erlenkeuser, H., Garbe-Schönberg, D., and Lea, D. W.: Final closure of Panama and the onset of northern hemisphere glaciation, Earth and Planetary Science Letters, 237, 33–44, https://doi.org/10.1016/j.epsl.2005.06.020, 2005.

Berggren, W. A., Kent, D. V., Swisher, C. C., and Aubry, M.-P.: Geochronology, time scales and global stratigraphic correlation, vol. 54, chap. A Revised Cenozoic Geochronology and Chronostratigraphy, pp. 129–212, SEPM (Society for Sedimentary Geology), https://doi.org/10.2110/pec.95.04.0129, 1995.

Bicknell, R. D. C., Collins, K. S., Crundwell, M., Hannah, M., Crampton, J. S., and Campione, N. E.: Evolutionary Transition in the Late Neogene Planktonic Foraminiferal Genus Truncorotalia, iScience, https://doi.org/10.1016/j.isci.2018.09.013, 2018.

Bolli, H. M. and Saunders, J. B.: Plankton Stratigraphy, vol. 1, chap. 6. Oligocene to Holocene low latitude planktic foraminifera, pp. 155–262, Cambridge University Press, 1985.

Brombacher, A., Wilson, P. A., Bailey, I., and Ezard, T. H. G.: The Breakdown of Static and Evolutionary Allometries during Climatic Upheaval, The American Naturalist, 190, 350–362, https://doi.org/10.1086/692570, 2017.

Brombacher, A., Wilson, P. A., and Ezard, T. H. G.: Calibration of the repeatability of foraminiferal test size and shape measures with recommendations for future use, Marine Micropaleontology, 133, 21–27, https://doi.org/10.1016/j.marmicro.2017.05.003, 2017.

Brown, K. R.: Biogeographic and morphological variation in late Pleistocene to Holocene globorotalid foraminifera, PhD Thesis, University of Basel, https://edoc.unibas.ch/780/, 2007.

Caley, T., Jiraudeau, J., Malaizé, B., Rossignol, L., and Pierre, C.: Agulhas leakage as a key process in the modes of Quaternary climate changes, PNAS, 109, 6835–6839, https://doi.org/10.1073/pnas.1115545109, 2012.

Caromel, A. G. M., Schmidt, D. N., Phillips, J. C., and Rayfield, E. J.: Hydrodynamic constraints on the evolution and ecology of planktic foraminifera, Marine Micropaleontology, 106, 69–78, https://doi.org/10.1016/j.marmicro.2014.01.002, 2014.

Caromel, A. G. M., Schmidt, D. N., Fletcher, I., and Rayfield, E. J.: Morphological Change During The Ontogeny Of The Planktic Foraminifera, Journal of Micropalaeontology, 35, 2–19, https://doi.org/10.1144/jmpaleo2014-017, 2016.

Chaisson, W. P.: Vicarious living: Pliocene menardellids between an isthmus and an ice sheet, Geology, 31, 1085–1088, https://doi.org/10.1130/G19834.1, 2003.

Chaisson, W. P. and Ravelo, A. C.: Changes in upper water-column structure at Site 925, late Miocene-Pleistocene: planktonic foraminifer assemblage and isotopic evidence, in: Proceedings of the Ocean Drilling Program, edited by Shackleton, N. J., Curry, W. B., Richter, C., and Bralower, T. J., vol. 154, pp. 255–268, Ocean Drilling Program, https://doi.org/10.2973/odp.proc.sr.154.105.1997, 1997.

Chan, C.-H., Chan, G. C. H., Leeper, T. J., and Becker, J.: rio: A Swiss-army knife for data file I/O, https://cran.r-project.org/web/packages/rio/ https://github.com/leeper/rio, R package version 0.5.16, 2018.

Chang, Z., Xiao, J., Lü, L., and Yao, H.: Abrupt shifts in the Indian monsoon during the Pliocene marked by high-resolution terrestrial records from the Yuanmou Basin in southwest China, Journal of Asian Earth Sciences, 37, 166–175, https://doi.org/10.1016/j.jseaes.2009.08.005, 2010.

Chapman, M. R.: Biotic Response to Global Changes: The Last 145 Million Years, chap. The response of planktonic foraminifera to the Late Pliocene intensification of Northern Hemisphere glaciation, pp. 79–96, 115, Cambridge University Press, https://doi.org/10.1017/CBO9780511535505.007, 2000.

Chiang, J. C. H.: The Tropics in Paleoclimate, Annual Review of Earth and Planetary Sciences, 37, 263–297, https://doi.org/10.1146/annurev.earth.031208.100217, 2009.

Clemens, S. C., Murray, D. W., and Prell, W. L.: Nonstationary Phase of the Plio-Pleistocene Asian Monsoon, Science, 274, 943–948, https://doi.org/10.1126/science.274.5289.943, 1996.

Dausmann, V., Frank, M., Gutjahr, M., and Rickli, J.: Glacial reduction of AMOC strength and long–term transition in weathering inputs into the Southern Ocean since the mid–Miocene:

Evidence from radiogenic Nd and Hf isotopes, Paleoceanography, 32, 265–283, https://doi.org/10.1002/2016PA003056, 2017.

De Vleeschouwer, D., Auer, G., Smith, R., Bogus, K., Christensen, B., Groeneveld, J., Petrick, B., Henderiks, J., Castañeda, I. S., O'Brien, E., Ellinghausen, M., Gallagher, S. J., Fulthorpe, C. S., and Pälike, H.: The amplifying effect of Indonesian Throughflow heat transport on Late Pliocene Southern Hemisphere climate cooling, Earth and Planetary Science Letters, 500, 15–27, https://doi.org/10.1016/j.epsl.2018.07.035, 2018.

Etourneau, J., Schneider, R., Blanz, T., and Martinez, P.: Intensification of the Walker and Hadley atmospheric circulations during the PliocenePleistocene climate transition, Earth and Planetary Science Letters, 297, 103–110, https://doi.org/10.1016/j.epsl.2010.06.010, 2010.

Friesenhagen, T.: Test-size evolution of the planktonic foraminifer *Globorotalia menardii* in the eastern tropical Atlantic since the Late Miocene, Biogeosciences, 19, 777–805, https://doi.org/10.5194/bg-19-777-2022, 2022a.

Friesenhagen, T.: Archive to the evolutionary study about menardiform globorotallids (planktonic foraminifer) in the eastern tropical Atlantic Ocean ODP Hole 667A, PANGAEA Data Repository, doi: https://doi.org/10.1594/PANGAEA.940563, https://doi.pangaea.de/-10.1594/PANGAEA.940563, 2022b.

Friesenhagen, T.: Morphometric measurements of the planktonic foraminifer *Globorotalia menardii* from the Mozambique Channel provide new evidence for the Agulhas leakage hypothesis, in preparation a

Friesenhagen, T.: Archive to the evolutionary study about menardiform globorotaliids in the Indian Ocean IODP Hole U1476A, in preparation b

Gunz, P. and Mitteroecker, P.: SEMILANDMARKS: A METHOD FOR QUANTIFYING CURVES AND SURFACES, Hystrix, the Italian Journal of Mammalogy, 24, https://doi.org/10.4404/hystrix-24.1-6292, 2013.

Gunz, P., Mitteroecker, P., and Bookstein, F. L.: Semilandmarks in Three Dimensions, in: Developments in Primatology: Progress and Prospects, pp. 73–98, Kluwer Academic Publishers-Plenum Publishers, https://doi.org/10.1007/0-387-27614-9_3, , 2005.

Gupta, A. K.: Latest Pliocene through Holocene paleoceanography of the eastern Indian Ocean: benthic foraminiferal evidence, Marine Geology, 161, 63–73, https://doi.org/10.1016/S0025-3227(99)00056-0, 1999.

Gupta, A. K. and Thomas, E.: Initiation of Northern Hemisphere glaciation and strengthening of the northeast Indian monsoon: Ocean Drilling Program Site 758, eastern equatorial Indian

Ocean, Geology, 31, 47, https://doi.org/10.1130/0091-7613(2003)031<0047:ionhga>2.0.co;2, 2003.

Haug, G. H. and Tiedemann, R.: Effect of the formation of the Isthmus of Panama on Atlantic Ocean thermohaline circulation, Nature, 393, 673–676, https://doi.org/10.1038/31447, 1998.

Haug, G. H., Tiedemann, R., Zahn, R., and Ravelo, A. C.: Role of Panama uplift on oceanic freshwater balance, Geology, 29, 207–210, https://doi.org/10.1130/0091-7613(2001)029<0207:ROPUOO>2.0.CO;2, 2001.

Haywood, A. M., Dowsett, H. J., and Dolan, A. M.: Integrating geological archives and climate models for the mid-Pliocene warm period, Nature Communications, 7, https://doi.org/10.1038/ncomms10646, 2016.

Healy-Williams, N.: Morphological Changes in Living Foraminifera and the Thermal Structure of the Water Column, Western North Atlantic, PALAIOS, 4, 590, https://doi.org/10.2307/3514749, 1989.

Healy-Williams, N. and Williams, D. F.: Fourier analysis of test shape of planktonic foraminifera, Nature, 289, 485–487, https://doi.org/10.1038/289485a0, 1981.

Huber, R., Meggers, H., Baumann, K.-H., Raymo, M. E., and Henrich, R.: Shell size variation of the planktonic foraminifer Neogloboquadrina pachyderma sin. in the Norwegian'Greenland Sea during the last 1.3 Myrs: implications for paleoceanographic reconstructions, Palaeogeography, Palaeoclimatology, Palaeoecology, 160, 193–212, https://doi.org/10.1016/s0031-0182(00)00066-3, 2000.

Hull, P. M. and Norris, R. D.: Evidence for abrupt speciation in a classic case of gradual evolution, PNAS, 106, 21224–21229, https://doi.org/10.1073/pnas.0902887106, 2009.

Ivanova, E. V.: Paleoceanography of the Northern Indian Ocean: Linkages to Monsoon and Global Thermohaline Paleocirculation, in: The Global Thermohaline Paleocirculation, pp. 107–145, Springer Netherlands, https://doi.org/10.1007/978-90-481-2415-2_5, 2009.

Jackson, J. B. C. and O'Dea, A.: Timing of the oceanographic and biological isolation of the Caribbean Sea from the tropical eastern Pacific Ocean, Bulletin of Marine Science, 89, 779–800, http://dx.doi.org/10.5343/bms.2012.1096, 2013.

Jansen, J. H. F., Kuijpers, A., and Troelstra, S. R.: A Mid-Brunhes Climatic Event: Long-Term Changes in Global Atmosphere and Ocean Circulation, Science, 232, 619–622, https://doi.org/10.1126/science.232.4750.619, 1986.

Kennett, J. P. and Srinivasan, M. S.: Neogene planktonic foraminifera. A phylogenetic atlas, Hutchinson Ross Publishing Company, Stroudsburg, Pa. New York, NY, 1983.

Klingenberg, C. P.: Multivariate Allometry, in: Advances in Morphometrics, pp. 23–49, Springer US, https://doi.org/10.1007/978-1-4757-9083-2_3, 1996.

Klingenberg, C. P.: MorphoJ: an integrated software package for geometric morphometrics, Molecular Ecology Resources, 11, 353–357, https://doi.org/10.1111/j.1755-0998.2010.02924.x, 2011.

Klingenberg, C. P.: Size, shape, and form: concepts of allometry in geometric morphometrics, Development Genes and Evolution, 226, 113–137, https://doi.org/10.1007/s00427-016-0539-2, 2016.

Klingenberg, C. P. and McIntyre, G. S.: GEOMETRIC MORPHOMETRICS OF DEVELOPMENTAL INSTABILITY: ANALYZING PATTERNS OF FLUCTUATING ASYMMETRY WITH PROCRUSTES METHODS, Evolution, 52, 1363–1375, https://doi.org/10.1111/j.1558-5646.1998.tb02018.x, 1998.

Knappertsbusch, M. and Eisenecker, J.: Towards a Fleet of Robots for Orientation, Imaging, and Morphometric Analyses of Planktonic Foraminifera, Frontiers in Marine Science, 9, https://doi.org/10.3389/fmars.2022.798002, 2022.

Knappertsbusch, M. W.: Morphological variability of Globorotalia menardii (planktonic foraminifera) in two DSDP cores from the Caribbean Sea and the Eastern Equatorial Pacific, Carnets de Geologie, CG2007, 1–34, hal-00164930, 2007.

Knappertsbusch, M. W.: Evolution im marinen Plankton, Mitteilungen der Naturforschenden Gesellschaften beider Basel, pp. 3–14, https://doi.org/10.5169/seals-676589, 2011.

Knappertsbusch, M. W.: Morphometric data of menardiform globorotalids, https://doi.org/10.1594/PANGAEA.855898, 2015.

Knappertsbusch, M. W.: Evolutionary prospection in the Neogene planktic foraminifer Globorotalia menardii and related forms from ODP Hole 925B (Ceara Rise, western tropical Atlantic): evidence for gradual evolution superimposed by long distance dispersal?, Swiss Journal of Palaeontology, 135, 205–248, https://doi.org/10.1007/s13358-016-0113-6, 2016.

Knappertsbusch, M. W.: MorphCol 2004-2021. A collection of Fortran 77 programs for morphometry, https://micropal-basel.unibas.ch/Research/MORPHCOL/-SUPPL_27_Cal_AMOR2.pdf, 2019.

Knappertsbusch, M. W.: Commented archive to studies about the morphological evolution of menardiform globorotalids at Western Pacific Warm Pool ODP Hole 806C (Ontong-Java Plateau), https://doi.org/10.1594/PANGAEA.932504, 2021.

Knappertsbusch, M.: Morphological evolution of menardiform globorotalids at Western Pacific Warm Pool ODP Hole 806C (Ontong-Java Plateau) Evolution morphologique du groupe de

Globorotalia menardii au Site ODP 806C (Ontong-Java Plateau, Pacifique tropical occidental), Revue de Micropaléontologie, 74, 100608, https://doi.org/10.1016/j.revmic.2022.100608, 2022.

Knappertsbusch, M. W. and Mary, Y.: Mining morphological evolution in microfossils using volume density diagrams, Palaeontologica Electronica, 15, 1–29, https://doi.org/10.26879/278, 2012.

Knappertsbusch, M. W., Binggeli, D., Herzig, A., Schmutz, L., Stapfer, S., Schneider, C., Eisenecker, J., and Widmer, L.: AMOR – A NEW SYSTEM FOR AUTOMATED IMAGING OF MICROFOSSILS FOR MORPHOMETRIC ANALYSES, Palaeontologia Electronica, 12, http://palaeo-electronica.org/2009_2/165/index.html, 2009.

Krijgsman, W., Hilgen, F. J., Raffi, I., Sierro, F. J., and Wilson, D. S.: Chronology, causes and progression of the Messinian salinity crisis, Nature, 400, 652–655, https://doi.org/10.1038/23231, 1999.

Kucera, M. and Malmgren, B. A.: Latitudinal variation in the planktic foraminifer Contusotruncana contusa in the terminal Cretaceous ocean, Marine Micropaleontology, 28, 31–52, https://doi.org/10.1016/0377-8398(95)00078-x, 1996.

Leckie, R. M.: A palaeoceanographic model for the early evolutionary history of planktonic foraminifera, Palaeogeography, Palaeoclimatology, Palaeoecology, 73, 107–138, https://doi.org/10.1016/0031-0182(89)90048-5, 1989.

Lisiecki, L. E. and Raymo, M.: A Pliocene-Pleistocene stack of 57 globally distributed benthic d18O records, Paleoceanography, 20, https://doi.org/10.1029/2004PA001071, 2005.

Lohmann, G. P. and Malmgren, B. A.: Equatorward migration of Globorotalia truncatulinoides ecophenotypes through the Late Pleistocene: Gradual evolution or ocean change?, Paleobiology, 9, 414–421, https://doi.org/10.1017/s0094837300007879, 1983.

Malmgren, B. A., Berggren, W. A., and Lohmann, G. P.: Evidence for punctuated gradualism in the Late Neogene Globorotalia tumida lineage of planktonic foraminifera, Paleobiology, 9, 377–389, https://doi.org/10.1017/s0094837300007843, 1983.

Mary, Y.: Morphologic, biogeographic and ontogenetic investigation of Mid-Pliocene menardellids (planktonic foraminifera), PhD Thesis, University of Basel, https://doi.org/10.5451/unibas-006194467, 2013.

McCarthy, G., Smeed, D., Cunningham, S., and Roberts, C.: Atlantic Meridional Overturning Circulation, MCCIP Science Review 2017, pp. 15–21, https://doi.org/10.14465/2017.ARC10.002-ATL, 2017.

Mennecart, B., Guignard, C., Dziomber, L., Schulz, G., Müller, B., and Costeur, L.: Allometric and Phylogenetic Aspects of Stapes Morphology in Ruminantia (Mammalia, Artiodactyla), Frontiers in Earth Science, 8, https://doi.org/10.3389/feart.2020.00176, 2020.

Norris, R. D.: Reconstruction Ocean History, chap. Hydrographic and tectonic control of plankton distribution and evolution, pp. 173–193, Springer US, https://doi.org/10.1007/978-1-4615-4197-4, 1999.

Nuber, S.: Atmospheric CO2 across the Plio-Pleistocene, PhD Thesis, Cardiff University, http://orca.cf.ac.uk/134264/, 2020.

O'Dea, A., Lessios, H. A., Coates, A. G., Eytan, R. I., Restrepo-Moreno, S. A., Cione, A. L., Collins, L. S., de Queiroz, A., Farris, D. W., Norris, R. D., Stallard, R. F., Woodburne, M. O., Aguilera, O., Aubry, M.-P., Berggren, W. A., Budd, A. F., Cozzuol, M. A., Coppard, S. E., Duque-Caro, H., Finnegan, S., Gasparini, G. M., Grossman, E. L., Johnson, K. G., Keigwin, L. D., Knowlton, N., Leigh, E. G., Leonard-Pingel, J. S., Marko, P. B., Pyenson, N. D., Rachello-Dolmen, P. G., Soibelzon, E., Soibelzon, L., Todd, J. A., Vermeij, G. J., and Jackson, J. B. C.: Formation of the Isthmus of Panama, Science Advances, 2, https://doi.org/10.1126/sciadv.1600883, 2016.

Pearson, P. N. and Coxall, H. K.: Origin of the Eocene Planktonic Foraminifer Hantkenina by Gradual Evolution, Palaeontology, 57, 243–267, https://doi.org/10.1111/pala.12064, 2014.

Pearson, P. N. and Ezard, T. H. G.: Evolution and speciation in the Eocene planktonic foraminifer Turborotalia, Paleobiology, 40, 130–143, https://doi.org/10.1666/13004, 2014.

Petrick, B., McClymont, E. L., Felder, S., Rueda, G., Leng, M. J., and Rosell-Melé, A.: Late Pliocene upwelling in the Southern Benguela region, Palaeogeography, Palaeoclimatology, Palaeoecology, 429, 62–71, https://doi.org/10.1016/j.palaeo.2015.03.042, 2015.

Petrick, B., Martnez-Garcá, A., Auer, G., Reuning, L., Auderset, A., Deik, H., Takayanagi, H., De Vleeschouwer, D., Iryu, Y., and Haug, G. H.: Glacial Indonesian Throughflow weakening across the Mid-Pleistocene Climatic Transition, Scientific Reports, 9, https://doi.org/10.1038/s41598-019-53382-0, 2019.

Petrick, B. F.: Pliocene-Pleistocene evolution of Benguela upwelling and Agulhas Leakage in the SE Atlantic, PhD Thesis, Newcastle University, http://hdl.handle.net/10443/2728, 2014.

Pfuhl, H. A. and Shackleton, N. J.: Changes in coiling direction, habitat depth and abundance in two menardellid species, Marine Micropaleontology, 50, 3–20, https://doi.org/10.1016/s0377-8398(03)00063-x, 2004.

Rasband, W. S.: ImageJ, U.S. National Institute of Helath, https://imagej.nih.gov/ij/, https://-imagej.nih.gov/ij/, 1997–2018.

Revelle, W.: psych: Procedures for Psychological, Psychometric, and Personality Research, Northwestern University, Evanston, Illinois, https://CRAN.R-project.org/package=psych, R package version 1.8.12, 2018.

Ringnér, M.: What is principal component analysis?, Nature Biotechnology, 26, 303–304, https://doi.org/10.1038/nbt0308-303, 2008.

Rinker, T. W. and Kurkiewicz, D.: pacman: Package Management for R, Buffalo, New York, https://cran.r-project.org/web/packages/pacman/index.html, version 0.5.0, 2018.

RStudio Team: RStudio: Integrated Development Environment for R, RStudio, PBC., Boston, MA, http://www.rstudio.com/, 2020.

Schiebel, R. and Hemleben, C.: Ecology, in: Planktic Foraminifers in the Modern Ocean, chap. 7, pp. 209–230, Springer Berlin Heidelberg, https://doi.org/10.1007/978-3-662-50297-6_7, 2017a.

Schiebel, R. and Hemleben, C.: Classification and Taxonomy of Extant Planktic Foraminifers, in: Planktic Foraminifers in the Modern Ocean, e2019PA003738, chap. 2, pp. 11–110, Springer Berlin Heidelberg, https://doi.org/10.1007/978-3-662-50297-6_2, 2017b.

Schiebel, R. and Hemleben, C.: Introduction, in: Planktic Foraminifers in the Modern Ocean, chap. 1, pp. 1–9, Springer Berlin Heidelberg, https://doi.org/10.1007/978-3-662-50297-6_1, 2017c.

Schmidt, D. N., Thierstein, H. R., Bollmann, J., and Schiebel, R.: Abiotic Forcing of Plankton Evolution in the Cenozoic, Science, 303, 207–210, https://doi.org/10.1126/science.1090592, 2004.

Schmidt, D. N., Lazarus, D., Young, J. R., and Kucera, M.: Biogeography and evolution of body size in marine plankton, Earth-Science Reviews, 78, 239–266, https://doi.org/10.1016/j.earscirev.2006.05.004, 2006.

Schmidt, D. N., Rayfield, E. J., Cocking, A., and Marone, F.: Linking evolution and development: Synchrotron Radiation Xray tomographic microscopy of planktic foraminifers, Palaeontology, 56, 741–749, https://doi.org/10.1111/pala.12013, 2013.

Schmidt, D. N., Caromel, A. G. M., Seki, O., Rae, J. W. B., and Renaud, S.: Morphological response of planktic foraminifers to habitat modifications associated with the emergence of the Isthmus of Panama, Marine Micropaleontology, 128, 28–38, https://doi.org/10.1016/j.marmicro.2016.08.003, 2016.

Scott, D. W.: On optimal and data-based histograms, Biometrika, 66, 605–610, https://doi.org/10.1093/biomet/66.3.605, 1979.

Scott, G. H.: Ontogeny and shape in Globorotalia menardii, The Journal of Foraminiferal Research, 3, 142–146, https://doi.org/10.2113/gsjfr.3.3.142, 1973.

Shi, Y.: Heterochronic origin of spherical fusulinid foraminifera in the late Paleozoic, Paleobiology, 47, 115–133, https://doi.org/10.1017/pab.2020.53, 2020.

Shipboard Scientific Party: Site 667, in: Proc. ODP, Init. Repts. (Pt. B), 108, edited by Stewart, S. K. and Rose, W. D., 108, pp. 833–930, College Station, TX (Ocean Drilling Program), https://doi.org/10.2973/odp.proc.ir.108.112.1988, 1988.

Si, W. and Berggren, W. A.: Taxonomy, Stratigraphy and Phylogeny of the Middle Miocene Fohsella Lineage: Geometric Morphometric Evidence, Journal of Foraminiferal Research, 47, 310–324, https://doi.org/10.2113/gsjfr.47.4.310, 2017.

Simpson, G. G.: CHAPTER XII. Patterns or Modes of Evolution, in: The Major Features of Evolution, pp. 377–396, Columbia University Press, https://doi.org/10.7312/simp93764-015, 1953.

Spencer-Cervato, C. and Thierstein, H. R.: First appearance of Globorotalia truncatulinoides: cladogenesis and immigration, Marine Micropaleontology, 30, 267–291, https://doi.org/10.1016/s0377-8398(97)00004-2, 1997.

Stanley, S. M.: An explanation for Cope's Rule, Evolution, 27, 1–26, https://doi.org/10.1111/j.1558-5646.1973.tb05912.x, 1973.

Stewart, D. R. M.: Evolution of Neogene globorotaliid foraminifera and Miocene climate change, Doctoral dissertation, University of Bristol, 2003.

Tabachnick, R. E. and Bookstein, F. L.: The structure of individual variation in Miocene Globorotalia, Evolution, 44, 416–434, https://doi.org/10.1111/j.1558-5646.1990.tb05209.x, 1990.

Tangunan, D. N., Baumann, K.-H., Just, J., LeVay, L. J., Barker, S., Brentegani, L., De Vleeschouwer, D., Hall, I. R., Hemming, S., and Norris, R.: The last 1 million years of the extinct genus Discoaster: Plio-Pleistocene environment and productivity at Site U1476 (Mozambique Cannel), Palaeogeography, Palaeoclimatology, Palaeoecology, 505, 187–197, https://doi.org/10.1016/j.palaeo.2018.05.043, 2018.

Thompson, D. W.: On Growth and Form., University press, https://doi.org/10.5962/bhl.title.11332, 1917.

Trauth, M. H., Maslin, M. A., Deino, A. L., Strecker, M. R., Bergner, A. G. N., and Dühnforth, M.: High- and low-latitude forcing of Plio-Pleistocene East African climate and human evolution, Journal of Human Evolution, 53, 475–486, https://doi.org/10.1016/j.jhevol.2006.12.009, 2007.

van der Geer, A. A. E., Claessens, L. P. A. M., Rijsdijk, K. F., and Lyras, G. A.: The changing face of the dodo (Aves: Columbidae:Raphus cucullatus): iconography of the Walghvogel of Mauritius, Historical Biology, pp. 1–10, https://doi.org/10.1080/08912963.2021.1940996, 2021.

van der Lubbe, H. J. L., Hall, I. R., Barker, S., Hemming, S. R., Baars, T. F., Starr, A., Just, J., Backeberg, B. C., and Joordens, J. C. A.: Indo-Pacific Walker circulation drove Pleistocene African aridification, 598, 618–623, https://doi.org/10.1038/s41586-021-03896-3, 2021.

Villar, E., Farrant, G. K., Follows, M., Garczarek, L., Speich, S., Audic, S., Bittner, L., Blanke, B., Brum, J. R., Brunet, C., Casotti, R., Chase, A., Dolan, J. R., d'Ortenzio, F., Gattuso, J.-P., Grima, N., Guidi, L., Hill, C. N., Jahn, O., Jamet, J.-L., Le Goff, H., Lepoivre, C., Malviya, S., Pelletier, E., Romagnan, J.-B., Roux, S., Santini, S., Scalco, E., Schwenck, S. M., Tanaka, A., Testor, P., Vannier, T., Vincent, F., Zingone, A., Dimier, C., Picheral, M., Searson, S., Kandels-Lewis, S., Oceanscoordinators, T., Acinas, S. G., Bork, P., Boss, E., de Vargas, C., Gorsky, G., Ogata, H., Pesant, S., Sullivan, M. B., Sunagawa, S., Wincker, P., Karsenti, E., Bowler, C., Not, F., Hingamp, P., and Iudicone, D.: Environmental characteristics of Agulhas rings affect interocean plankton transport, Science, 348, 1261447, https://doi.org/10.1126/science.1261447, 2015.

von der Heydt, A. and Dijkstra, H. A.: Flow reorganizations in the Panama Seaway: A cause for the demise of Miocene corals?, Geohysical Research Letters, 32, https://doi.org/10.1029/2004GL020990, 2005.

Wara, M. W., Ravelo, A. C., and Delaney, M. L.: Permanent El Niño - Like Conditions During the Pliocene Warm Period, Science, 309, 758–761, https://doi.org/10.1126/science.1112596, 2005.

Wickham, H.: ggplot2: Elegant Graphics for Data Analysis, Springer-Verlag New York, https://doi.org/10.1007/978-3-319-24277-4, 2016.

Wright, J. D. and Thunell, R. C.: Neogene Planktonic Foraminiferal Biogeography and Paleoceanography of the Indian Ocean, Micropaleontology, 34, 193, https://doi.org/10.2307/1485752, 1988.

Zachos, J., Pagani, M., Sloan, L., Thomas, E., and Billups, K.: Trends, Rhythms, and Aberrations in Global Climate 65 Ma to Present, Science, 292, 686–693, https://doi.org/10.1126/science.1059412, 2001.

Zelditch, M. L., Swiderski, D. L., Sheets, H. D., and Fink, W. L.: Glossary, in: Geometric Morphometrics for Biologists, edited by Zelditch, M. L., Swiderski, D. L., Sheets, H. D., and

Fink, W. L., chap. Glossary, pp. 409–428, Elsevier, https://doi.org/10.1016/b978-012778460-1/50018-1, 2004.

Zhisheng, A., Clemens, S. C., Shen, J., Qiang, X., Jin, Z., Sun, Y., Prell, W. L., Luo, J., Wang, S., Xu, H., Cai, Y., Zhou, W., Liu, X., Liu, W., Shi, Z., Yan, L., Xiao, X., Chang, H., Wu, F., Ai, L., and Lu, F.: Glacial-Interglacial Indian Summer Monsoon Dynamics, Science, 333, 719–723, https://doi.org/10.1126/science.1203752, 2011.

Appendix

Sample	DEPTH, m.b.s.f. (m)	Age (Ma)
667A-1H-1, 4.4 cm	0.044	0.003
667A-2H-1, 31 cm	1.61	0.110
667A-2H-2, 16 cm	2.96	0.202
667A-2H-2, 50 cm	3.30	0.225
667A-2H-3, 60 cm	4.90	0.334
667A-2H-4, 33 cm	6.13	0.418
667A-2H-5, 15 cm	7.45	0.510
667A-2H-CC, 2 cm	10.51	0.730
667A-3H-2, 85 cm	13.15	0.920
667H-3H-4, 64 cm	15.94	1.120
667A-4H-1, 51 cm	20.81	1.470
667A-4H-3, 120 cm	24.50	1.735
667A-4H-5, 119 cm	27.49	1.950
667A-4H-6, 118 cm	28.98	2.057
667A-5H-2, 106 cm	32.36	2.300
667A-5H-5, 46 cm	36.26	2.580
667A-6H-1, 113 cm	40.43	2.880
667A-6H-4, 115 cm	44.95	3.204
667A-6H-6, 73 cm	47.53	3.390
667A-7H-3, 13 cm	51.93	3.690
667A-7H-6, 40 cm	56.94	3.990
667A-8H-1, 114 cm	59.44	4.140
667A-8H-4, 15 cm	62.95	4.350
667A-8H-CC, 16 cm	67.46	4.620
667A-9H-2, 66 cm	69.96	4.770
667A-9H-5, 1 cm	73.81	5.000
667A-10H-1, 98 cm	78.28	5.268
667A-10H-CC, 16 cm	86.46	5.780
667A-11H-2, 142 cm	89.72	6.070
667A-11H-6, 15 cm	94.45	6.490
667A-12H-4, 63 cm	101.43	7.110
667A-13H-1, 114 cm	106.94	7.600
667A-13H-4, 69 cm	110.99	7.960

Table 4.1: Samples investigated at ODP Hole 667A (Friesenhagen, 2022). It shows the sample depth in metre below seafloor (m.b.s.f) and the sample age in million years (Ma).

Sample	DEPTH, m.b.s.f. (m)	Age (Ma)
806C-1H-1,13-15cm	0.14	0.004
806C-1H-2,15-17cm	1.66	0.052
806C-1H-2,81-83cm	2.32	0.106
806C-1H-3,88-90cm	3.89	0.216
806C-1H-4,42-44cm	4.93	0.280
806C-2H-1,30-32cm	5.91	0.341
806C-2H-2,98-100cm	8.09	0.422
806C-2H-3,130-132cm	9.91	0.518
806C-2H-7,7-9cm	14.68	0.713
806C-3H-2,84-86cm	17.45	0.813
806C-3H-4,84-86cm	20.45	0.917
806C-3H-6,23-25cm	22.84	1.008
806C-4H-1,117-119cm	25.78	1.267
806C-4H-4,7-9cm	29.18	1.463
806C-4H-7,15-17cm	33.76	1.653
806C-5H-2,65-67cm	36.26	1.719
806C-5H-4,26-28cm	38.87	1.843
806C-5H-5,139-141cm	41.50	1.948
806C-6H-3,83-85cm	47.44	2.192
806C-6H-6,90-92cm	52.01	2.448
806C-7H-2,58-60cm	55.19	2.552
806C-7H-3,127-129cm	57.38	2.634
806C-8H-1,108-110cm	63.69	2.868
806C-8H-6,6-8cm	70.17	3.029
806C-9H-3,15-17cm	75.26	3.182
806C-10H-1,98-100cm	82.59	3.363
806C-11H-1,78-79cm	91.89	3.706
806C-12H-4,10-12cm	105.21	4.000
806C-12H-6,110-112cm	109.21	4.095
806C-14H-1,21-23cm	119.82	4.349
806C-15H-2,126-128cm	131.87	4.636
806C-17H-1,67-69cm	148.78	5.040
806C-18H-2,28-30cm	159.39	5.293
806C-20H-2,67-69cm	178.78	5.780
806C-23H-5,28-30cm	211.39	6.625
806C-26H-5,27-29cm	239.88	7.258
806C-29H-7,30-32cm	271.41	7.959

Table 4.2: Samples investigated at ODP Hole 806C (Knappertsbusch, 2022). It shows the sample depth in metre below seafloor (m.b.s.f) and the sample age in million years (Ma).

Sample	DEPTH, CSF-A (m)	Age (Ma)
U1476A-1H-1, 7-8cm	0.075	0.004^{+}
U1476A-1H-1, 72-73cm	0.725	0.035^{+}
U1476A-1H-2, 111-113cm	2.618	0.122^{+}
U1476A-2H-1, 99-101cm	6.700	0.324^{+}
U1476A-2H-1, 134-136cm	7.050	0.339^{+}
U1476A-2H-2, 113-115cm	8.341	0.394^{+}
U1476A-2H-5, 98-100cm	12.693	0.615^{+}
U1476A-2H-6, 13-15cm	13.346	0.647^{+}
U1476A-3H-1, 4-6cm	15.250	0.736^{+}
U1476A-3H-1, 119-121cm	16.400	0.778^{+}
U1476A-3H-4,123-125cm	20.937	0.985^{+}
U1476A-3H-6,114-115cm	23.845	1.158^{+}
U1476A-4H-6, 46-47cm	32.665	1.533^{+}
U1476A-5H-5, 61-63cm	40.819	1.829^{+}
U1476A-6H-2, 64-66cm	45.848	1.980^{+}
U1476A-6H-3, 64-66cm	47.067	2.027^{+}
U1476A-7H-3, 32-34cm	56.532	2.340
U1476A-8H-1, 118-120cm	63.893	2.585
U1476A-9H-2, 115-117cm	74.860	2.950
U1476A-10H-1, 98-99cm	82.685	3.190
U1476A-11H-1, 65-67cm	91.861	3.440
U1476A-12H-2, 11-13cm	102.322	3.725
U1476A-12H-7, 32-34cm	110.030	3.935
U1476A-13H-5, 98-100cm	117.187	4.130
U1476A-14H-4, 95-97cm	125.166	4.340
U1476A-16H-4, 72-74cm	143.933	4.825
U1476A-17H-6, 22-24cm	155.929	5.135
U1476A-18H-4, 49-51cm	162.701	5.310
U1476A-19H-6, 101-103cm	175.721	5.780
U1476A-20H-7, 21-23cm	185.917	6.070
U1476A-22H-4, 47-49cm	200.684	6.490

Table 4.3: Samples investigated at IODP Hole U1476A (Chapter 3). It shows the sample depth in metre below seafloor (m.b.s.f) and the sample age in million years (Ma). $^{+}$: Sample age defined by stable isotope data by van der Lubbe (2021).

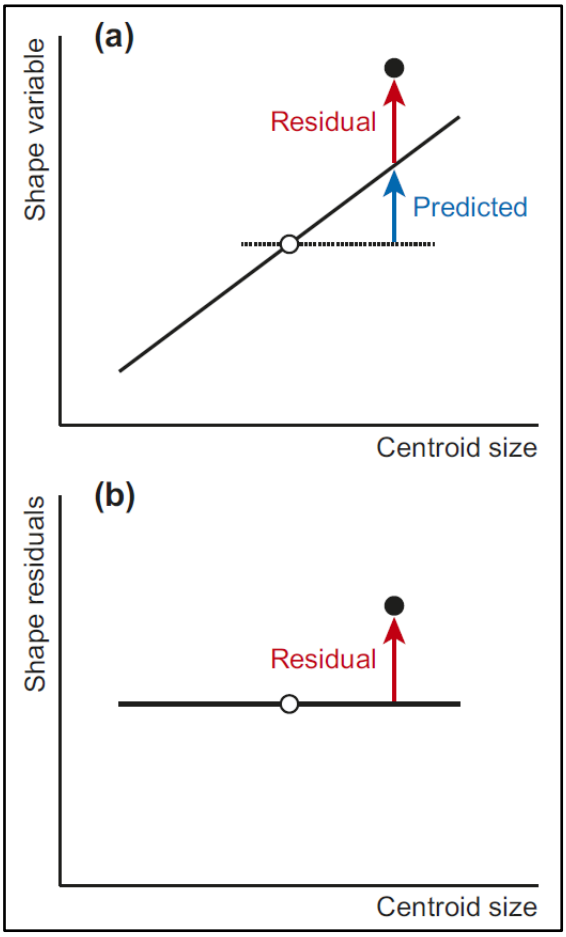

Figure A4.1: Size correction of the allometric regression via residuals. "(**a**) The decomposition of the shape deviations of each data point (black dot) from the sample average (hollow dot) into predicted and residual components. For each shape variable, the predicted component can be computed from the deviation in size of the specimen of interest from the average size in the sample and the slope of the regression line (solid line). (**b**) Size correction by using residuals from the regression. For the residual component of variation, there is the same expected value for shape regardless of the size of a specimen (horizontal line)" (Klingenberg, 2016). Figure 4.6 in Klingenberg (2016).

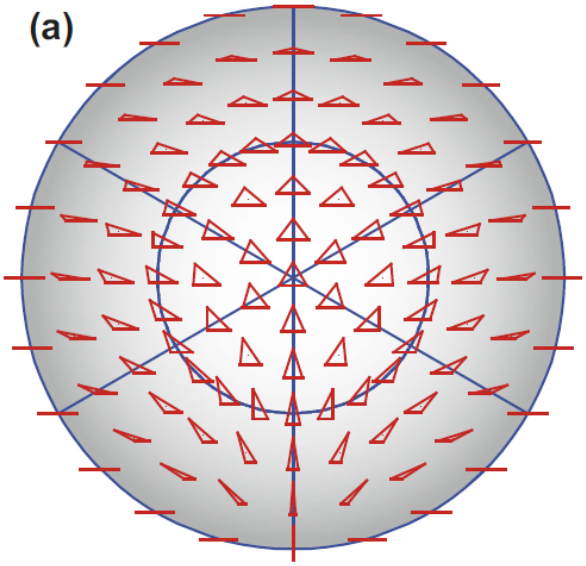

Figure A4.2: "Kendall's shape space for triangles. (**a**) A view of one half of the shape space for triangles with some examples shown in the respective locations. The "pole" corresponds to an equilateral triangle. The equator contains the flat triangles where all three vertices are on a straight line. The six "meridians" correspond to isosceles triangles. The hidden hemisphere of the shape space contains mirror images of the triangles visible in this diagram" (Klingenberg, 2016). Figure 5a in Klingenberg (2016).

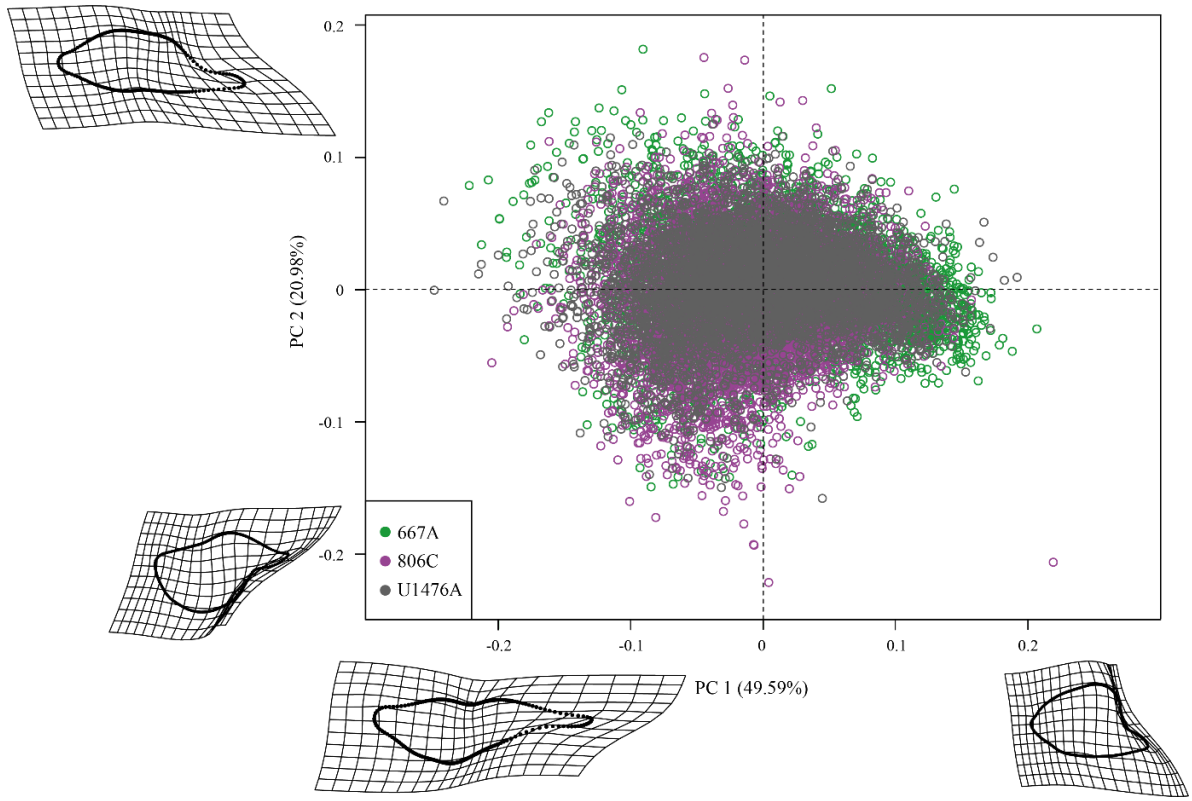

Figure A4.3: Plot of the PC1 axis versus the PC2 axis of all specimens for dataset 1, green dots representing specimens from Hole 667A, purple from Hole 806C and grey from Hole U1476A. The warpgrids show the extreme shape along the axes.

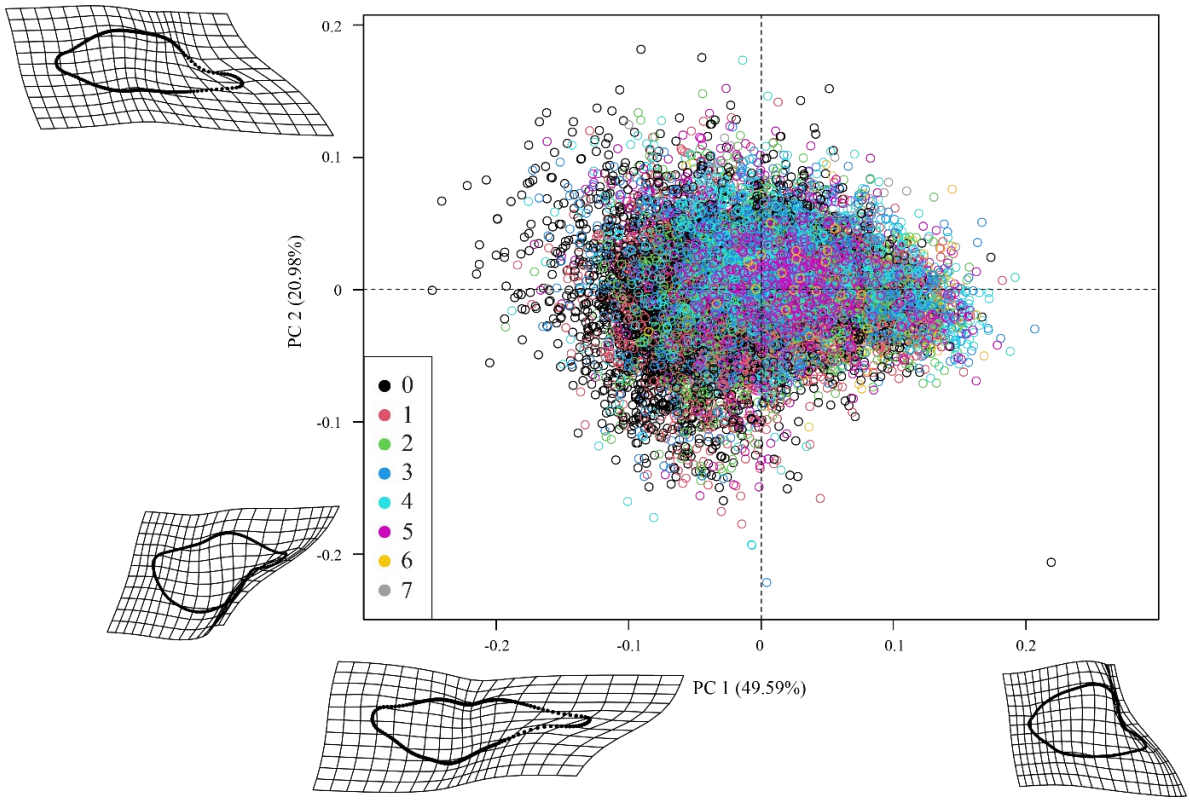

Figure A4.4: Plot of the PC1 axis versus the PC2 axis of all specimens for dataset 1. The colours indicate age classes: black cycles (0) correspond to individuals with an age between 0 Ma and 1 Ma, red cycles (1) between 1 Ma – 2 Ma, green (2) between 2 Ma – 3 Ma, blue (3) between 3 Ma – 4 Ma, turquois (4) between 4 Ma – 5 Ma, purple (5) between 5 Ma – 6 Ma, yellow (6) between 6 Ma – 2 Ma and grey (7) between 7 Ma – 8 Ma . The warpgrids show the extreme shape along the axes.

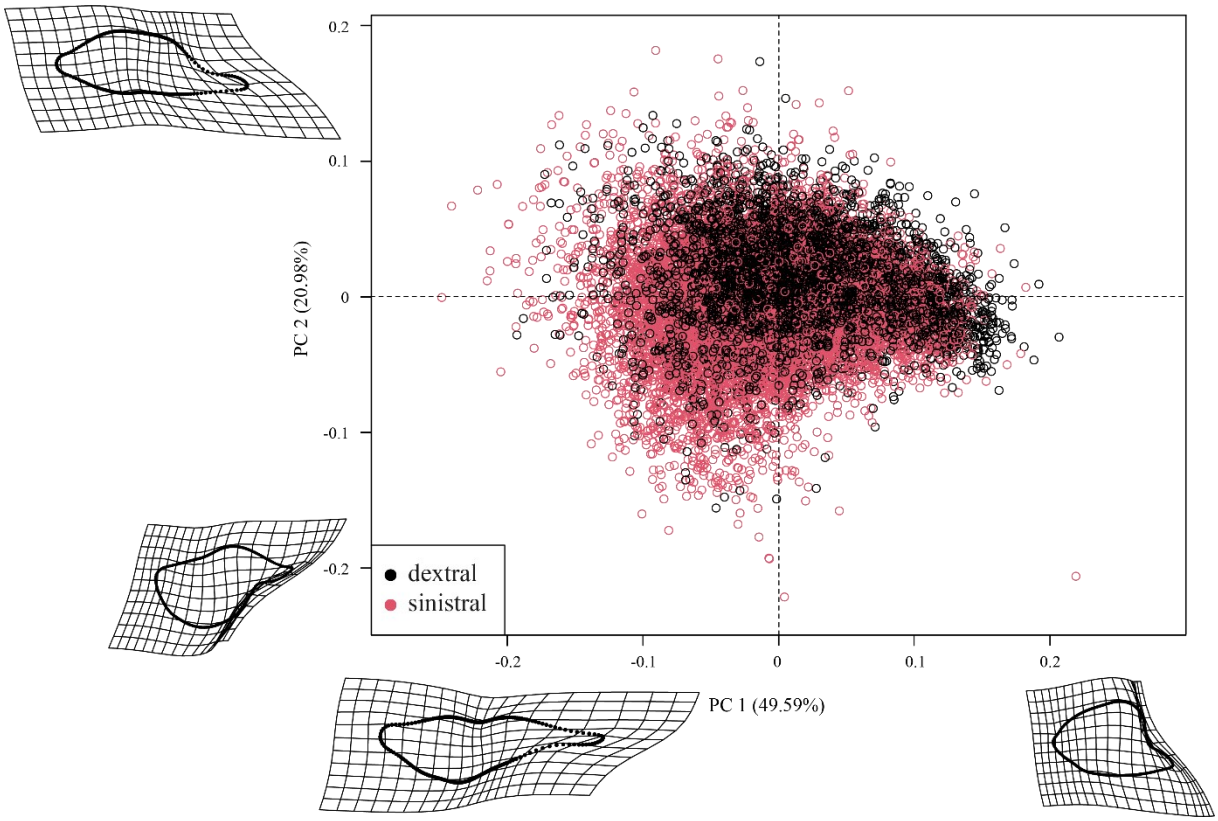

Figure A4.5: Plot of the PC1 axis versus the PC2 axis of all specimens for dataset 1. Black circles represent specimens with a dextral coiling direction, red specimens with a sinistral coiling direction. The warpgrids show the extreme shape along the axes.

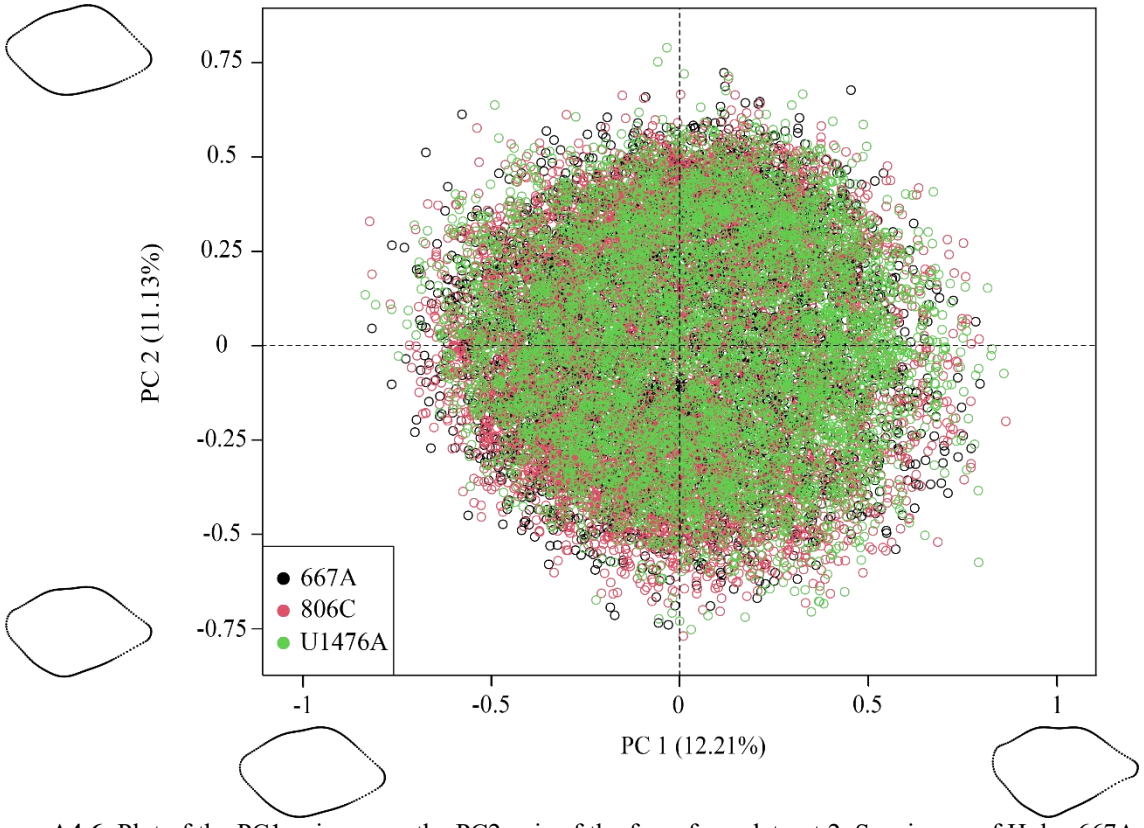

Figure A4.6: Plot of the PC1 axis versus the PC2 axis of the form from dataset 2. Specimens of Holes 667A are represented by black, specimens of Hole 806C by red and specimens of Hole U1476A by green cycle. The outlines represent the extreme shape along the corresponding axis.

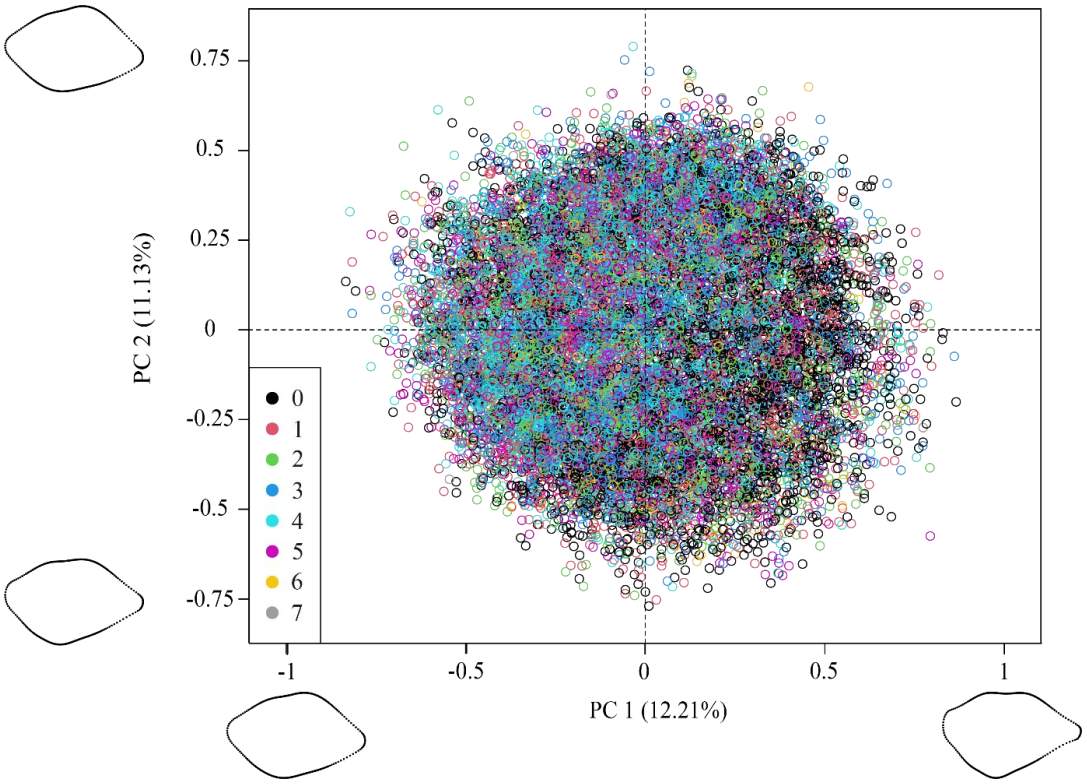

Figure A4.7: Plot of the PC1 axis versus the PC2 axis of all specimens for dataset 2. The colours indicate age classes: black cycles (0) correspond to individuals with an age between 0 Ma and 1 Ma, red cycles (1) between 1 Ma – 2 Ma, green (2) between 2 Ma – 3 Ma, blue (3) between 3 Ma – 4 Ma, turquois (4) between 4 Ma – 5 Ma, purple (5) between 5 Ma – 6 Ma, yellow (6) between 6 Ma – 2 Ma and grey (7) between 7 Ma – 8 Ma . The warpgrids show the extreme shape along the axes.

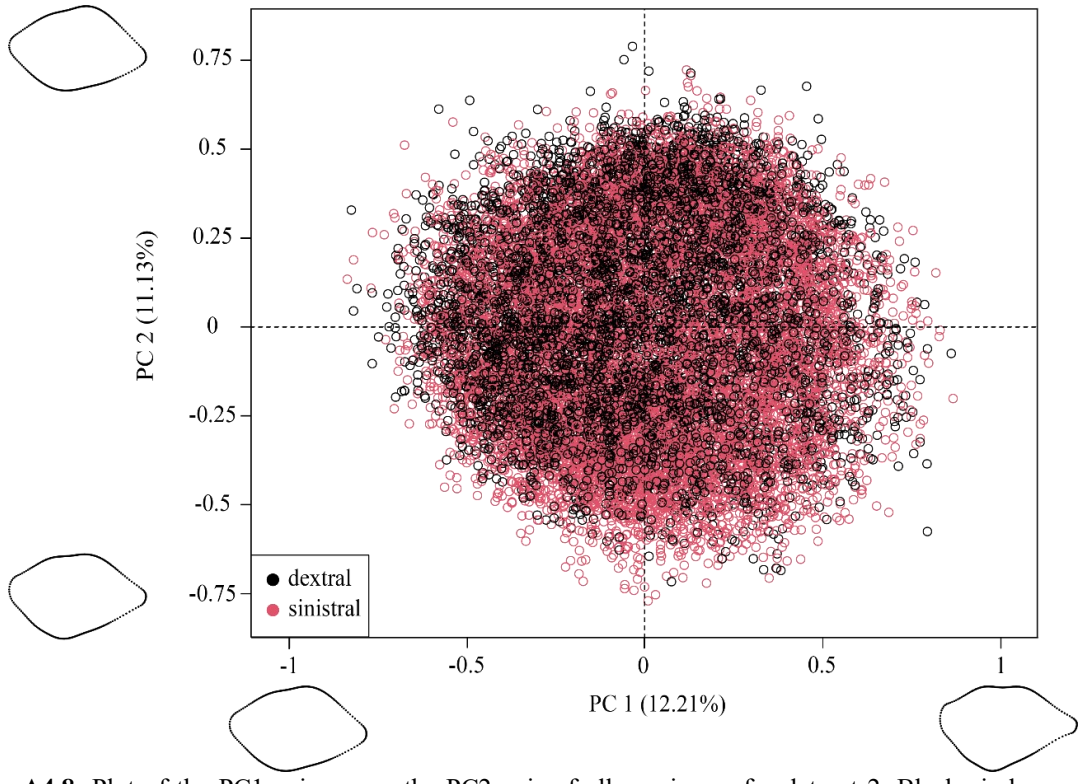

Figure A4.8: Plot of the PC1 axis versus the PC2 axis of all specimens for dataset 2. Black circles represent specimens with a dextral coiling direction, red specimens with a sinistral coiling direction. The warpgrids show the extreme shape along the axes.

Chapter 5: Synopsis, Conclusion, and Outlook

5.1 Synopsis

5.1.1 Results and implications for the Agulhas leakage hypothesis

The Agulhas leakage hypothesis is a plausible model to explain the observations from measurements of morphometric parameters and geometric morphometrics of the planktonic foraminifer *Globorotalia menardii* in the early Pleistocene.

The investigation of the evolution of the spiral height (δX) and axial length (δY) of 14,542 menardiform globorotaliid specimens for the eastern tropical Atlantic Ocean ODP Hole 667A and the tropical Indian Ocean IODP Hole U1476A in the Mozambique Channel shows an overall increase in the maximum test-size since the late Miocene.

At Hole 667A, test-size evolution exhibits several peaks between 8 Ma and 2.5 Ma. Between 2.58 Ma and 2.057 Ma, the maximum test size more than doubles and shows no major changes until the present. This predates the first occurrence of the giant type in the Atlantic Ocean by at least ca. 0.1 Myr. The observed pattern at Hole 667A resembles that of previous works in the Atlantic Ocean (Knappertsbusch, 2007, 2016). It indicates that the test-size evolution follows the same pattern within the Atlantic Ocean and is not restricted to regional areas.

At Hole U1476A in the Mozambique Channel, the maximum test-size evolution shows an overall gradual increase throughout the last 6.5 Myr. This pattern was also observed in the eastern and western Pacific Ocean (Knappertsbusch, 2007, 2022). The axial length (δY) exceeded that of the Atlantic Ocean between 3 Ma and 2 Ma and indicates that a giant type was dispersed from the Indian Ocean via the Agulhas leakage into the Atlantic Ocean between 2.58 Ma and 2.057 Ma.

Additional support for the Agulhas leakage hypothesis derives from the change in the predominant coiling direction of populations of *G. menardii*. From ca. 5 Ma until 2.58 Ma, dextrally coiling specimens dominated the populations in the Atlantic Ocean. Between 2.58 Ma and 2.057 Ma, the predominant coiling direction changes to almost exclusively sinistral. This moment coincides with the size increase to more than 1000 µm in δY. If the giant morphotype is characterised by a maximum δY of >1000 µm and a predominant sinistral coiling direction, this type already occurred at 2.95 Ma at Hole U1476A. This date predates their first appearance in the Atlantic Ocean by 0.9 Myr. Data from Knappertsbusch (2022) suggest that the giant morphotype already occurred at 3.19 Ma in the western Pacific Ocean and indicates that the giant morphotype originated in the Pacific Ocean.

The investigation of form and shape evolution of the tests of *G. menardii* by using geometric morphometrics of outline coordinates are consistent with the Agulhas leakage hypothesis as well. The evolution of the form, which includes the allometric signal, exhibits a similar pattern to the size evolution in the investigated sites, as form covariates with size during ontogeny. A decrease in the variation of form is observed for Atlantic Ocean populations in the interval between 4 Ma and 2.58 Ma, which coincides with major palaeoceanographic reconfigurations due to the closure of the Panamanian Isthmus (O'Dea et al., 2016). It is followed by an increase in variation until 2.057 Ma, and the morphospace of Atlantic Ocean populations superimposes that of Indian and Pacific Ocean populations. Form in the Indian and western Pacific oceans developed gradually through time, which may display anagenesis, and does not indicate the occurrence or evolution of a new morphotype. The superposition in morphospace after 2.057 Ma suggests the pan-oceanic presence of a single morphotype.

Extreme shapes do not change through time for the investigated sites. It suggests the existence of one morphotype for the last 8 Ma. The median shape exhibits two time intervals of divergent trends which may reflect anagenetic patterns: from ca. 4 Ma until 2.58 Ma in the Atlantic Ocean and from ca. 2 Ma until the present in the Indian Ocean. Those time intervals coincide with major palaeoceanographic changes and may indicate anagenetic speciation events.

Test-form and -shape evolution are consistent with the Agulhas leakage hypothesis, but cannot prove it. This is due to the fact that, in contrast to test size, the proposed new, giant morphotype in the Atlantic Ocean cannot be distinguished from the potential precursor by shape and form in keel view.

Size, form and shape variation decreases from 2.88 Ma until 2.3 Ma in the Atlantic Ocean, and drastically increases between 2.3 Ma and 2.057 Ma. This trend indicates a decrease in suitability of the Atlantic Ocean environment for the incumbent morphotype. The drastic increase in variance can be explained by the dispersal of the new, giant morphotype from the Indian Ocean via the Agulhas leakage.

5.1.2 Evolution of the *G. menardii-G. limbata-G. multicamerata* lineage

The investigation of the test-size evolution of the *G. menardii-G. limbata-G. multicamerata* lineage in the Atlantic and Indian oceans shows that, on average, *G. multicamerata* develops the largest test size and *G. menardii* the smallest, while *Globorotalia limbata* ranks in between. This is in accordance with previous studies (Knappertsbusch, 2007, 2016; Mary, 2013; Mary and Knappertsbusch, 2013, 2015).

In the Atlantic Ocean, the test-size evolution of *G. multicamerata* and *G. limbata* diverges from that of *G. menardii* in the time interval from ca. 5.5 Ma to 4 Ma, which was also observed in the western tropical Atlantic Ocean (Knappertsbusch, 2016). After 4 Ma, this trend reverses. The convergent trend ends with the extinction of *G. limbata* and *G. multicamerata*. Assuming that maximum size develops during optimal environmental conditions, (Hecht, 1976; Schmidt et al., 2006), the diverging trend could point to environmental conditions, which were more suitable for *G. limbata* and *G. multicamerata* than for *G. menardii*. This might be an indication for different ecologies of the three species.

In the Indian Ocean, the last appearance of *G. multicamerata* was observed at 2.34 Ma, which is in agreement with previous studies in the Indian Ocean (Hall et al., 2017). This last appearance date differs from that given in Berggren et al. (1995) (3.09 Ma) and Wade et al. (2011) (2.99 Ma). Specimens with seven chambers in the final whorl, identified as *G. limbata* following the pragmatic approach of classifying species by the number of the chambers in the final whorl, were sporadically found during the last 2 Myr and may point to a pseudoextinction of this morphospecies as was proposed by Knappersbusch (2016).

The relative abundance of *G. multicamerata* and *G. limbata* is lower in the Indian Ocean in comparison to the Atlantic Ocean, which may be caused by the different palaeoceanographic settings of Atlantic and the Indian oceans.

The data could not reveal any quantitative morphometric characteristics or parameter in keel view, which allows a unequivocal discrimination of *G. menardii*, *G. limbata*, and *G. multicamerata*.

5.1.3 Possible influences on test size (evolution) of menardiform globorotaliids

The overall increase in the maximum test-size in the Atlantic Ocean and the largely gradual increase in the Indian Ocean might reflect Cope's rule, which proposes an evolutionary increase in body size through time.

The evolution of mean, median and maximum test-size evolution in the Atlantic Ocean shows a similar trend to the evolution of the strength of the Atlantic Meridional Overturing Circulation (AMOC), especially in the time interval between 8 Ma and ca. 2.5 Ma. Changes in the pattern of means and medians in the Indian Ocean coincide with long-term changes in the Indian monsoon.

These observations suggest that major changes in the (palae-)oceanographic drivers have had an influence on the size evolution of menardiform globorotaliids probably by affecting the

regional hydrographic structure of the water column and thus the thermocline habitat of menardiform globorotaliids.

However, these coinciding trends are currently only observational. The causal relationship between changes in the oceanographic features and the test size of menardiform globorotaliids, the thermocline hypothesis, remain hypothetical and has to be tested in future studies.

5.2 Conclusions

The results show that evolutionary prospection is a promising strategy and methodology to study and disentangle the tempo and mode of evolution in marine microfossils.

Morphometric measurements from the Atlantic and the Indian Ocean throughout the last 8 Ma and 6.5 Ma, respectively, of a total of 14,542 menardiform globorotaliids is in accordance with the hypothesis of the dispersal of a new, giant *G. menardii* morphotype from the Indian Ocean into the Atlantic Ocean via the Agulhas leakage between 2.3 Ma and 2.057 Ma in the early Pleistocene. If the giant morphotype is defined to have a maximum axial length of >1000 µm and a predominant sinistral coiling direction, data from the literature (Knappertsbusch, 2022) suggest the first occurrence of the giant type in the Pacific Ocean. From there, it was transported into the Indian Ocean via surface currents throughout the Indonesian throughflow and subsequently into the Atlantic Ocean by the Agulhas leakage.

The pattern in test-size evolution in the Atlantic Ocean and the Indian Ocean exhibit similar trends to the reconstructed strength of the AMOC and the changes in the Indian monsoon system through time, respectively. It indicates an influence of major palaeoceanographic drivers onto the test-size evolution of *G. menardii*, probably due to their influence on the regional hydrography and thus the thermocline habitat of *G. menardii*.

Shape and form evolution of *G. menardii* do not suggest the evolution of a new morphotype since the late Miocene. While form seem to be driven by major (palae-)oceanographic drivers, as it covaries with size, those drivers seem to have a reduced influence on shape evolution through time.

Interspecific variation in the test size shows an overall diverging trend in the size evolution of *G. menardii*, *G. limbata* and *Globorotalia multicamerata* in the early to mid-Pliocene. As this trend reverses in the late Pliocene, this pattern should be considered as being driven by environmental influences rather than permanent genetic evolution. The measurements did not allow to define a characteristic, which enables an unequivocal distinction of those species.

This underlines the importance of extensive studies of morphometric measurements in PF. They do not only allow to track evolution through time, but the strategy of evolutionary prospection increases the knowledge of temporal and spatial evolution and distribution pattern.

5.3 Outlook for future research

The presented results of the morphometric measurements and geometric morphometrics (test-size, -shape and -form evolution) are consistent with the Agulhas leakage hypothesis, but do not provide unequivocal evidence for this or the alternative hypothesis of a punctuated evolutionary event in the Atlantic Ocean.

(1) In a first step, classical, detailed morphological descriptions, including the investigation of differences in the microstructure of the test, i.e. the wall structure and porosity, as well as growth curves of the proposed new, giant morphotype and its ancestor type will clarify if they are distinct.

(2) An expansion of the dataset by the measurement of geochemical and stable isotopes chamber-by-chamber, for example by laser ablation techniques or secondary ion mass spectrometry (SIMS), in the investigated populations through time and space will give evidence for changes in the habitat and ontogeny of *G. menardii*, which may be indicative for different species and the hypothesis of an incumbency replacement within the Atlantic Ocean. Such an isotopic record will also provide information about ecological preferences and the change of those through time, e.g. changes in the depth habitat within the watercolumn or the ability to be capable of bearing symbionts. The chamber-by-chamber isotopic record will also help to test interspecific ecological differences between *G. menardii*, *G. limbata* and *G. multicamerata* during ontogeny.

(3) As the results suggest the first occurrence of the giant type in the Pacific Ocean, the investigation of additional sites through time in the eastern and central Indian Ocean, e.g. the Bay of Bengal or along the Ninetyeast Ridge and in the western and eastern tropical Pacific Ocean, would help to locate the area of the first occurrence of the new type. Sampling along the Brazilian coast in the Southern Atlantic Ocean will provide information about the evolution of menardiform globorotaliids in the southern hemisphere and if the evolution differs due to alternation of the (palae-)oceanographic and hydrography.

(4) High-resolution biostratigraphic studies for the time interval from ca. 2.6 Ma to 2 Ma at all investigated sites and additional localities will allow to determine the location and exact timing of the first occurrence of the giant type in the Atlantic Ocean. This provides insight into the geographical distribution pattern and gives evidence for potential influences of environmental

conditions on distribution. It could reveal, if the new, giant morphotype and the precursor type showed a temporal and spatial overlap in their occurrence.

(5) The investigation of the ecology of extant *G. menardii* will allow to interpret the fossil record of this species in a palaeoecological and palaeoenvironmental context. Information about test size, geochemical and stable isotope measurements, occurrence data, population size and which ontogenetic stages are present in which quantity, taken from sediment traps compared to the contemporaneous observed environmental conditions, e.g. by CTD data, could help greatly in palaeoenvironmental reconstructions based on the fossil record of *G. menardii*. Insight into the relationship between test morphology and environmental conditions can be used to test the thermocline hypothesis.

(6) This thesis demonstrates the high potential of evolutionary prospection to describe evolutionary processes in the evolution of menardiform globorotaliids. The use of this strategy in other microfossil groups seems very promising, as it would allow to receive a broader view on evolutionary processes and if those mechanisms work the same.

References

Berggren, W. A., Kent, D. V., Swisher, C. C., and Aubry, M.-P.: Geochronology, time scales and global stratigraphic correlation, vol. 54, chap. A Revised Cenozoic Geochronology and Chronostratigraphy, pp. 129–212, SEPM (Society for Sedimentary Geology), https://doi.org/10.2110/pec.95.04.0129, 1995.

Hall, I. R., Hemming, S. R., LeVay, L. J., Barker, S., Berke, M. A., Brentegani, L., Caley, T., Cartagena-Sierra, A., Charles, C. D., Coenen, J. J., Crespin, J. G., Franzese, A. M., Gruetzner, J., Han, X., Hines, S. K. V., Jimenez Espejo, F. J., Just, J., Koutsodendris, A., Kubota, K., Lathika, N., Norris, D. R., Periera dos Santos, T., Robinson, R., Rolinson, J. M., Simon, M. H., Tangunan, D., van der Lubbe, J. J. L., Yamane, M., and Zhang, H.: Site U1476, in: Proceedings of the International Ocean Discovery Program, International Ocean Discovery Program, http://dx.doi.org/10.14379/iodp.proc.361.105.2017, 2017.

Hecht, A. D.: An ecologic model for test size variation in Recent planktonic foraminifera; applications to the fossil record, The Journal of Foraminiferal Research, 6, 295–311, https://doi.org/10.2113/gsjfr.6.4.295, 1976.

Knappertsbusch, M.: Morphological evolution of menardiform globorotalids at Western Pacific Warm Pool ODP Hole 806C (Ontong-Java Plateau) Evolution morphologique du groupe de Globorotalia menardii au Site ODP 806C (Ontong-Java Plateau, Pacifique tropical occidental), Revue de Micropaléontologie, 74, 100608, https://doi.org/10.1016/j.revmic.2022.100608, 2022.

Knappertsbusch, M. W.: Morphological variability of Globorotalia menardii (planktonic foraminifera) in two DSDP cores from the Caribbean Sea and the Eastern Equatorial Pacific, Carnets de Geologie, CG2007, 1–34, hal-00164930, 2007.

Knappertsbusch, M. W.: Evolutionary prospection in the Neogene planktic foraminifer Globorotalia menardii and related forms from ODP Hole 925B (Ceara Rise, western tropical Atlantic): evidence for gradual evolution superimposed by long distance dispersal?, Swiss Journal of Palaeontology, 135, 205–248, https://doi.org/10.1007/s13358-016-0113-6, 2016.

Mary, Y.: Morphologic, biogeographic and ontogenetic investigation of Mid-Pliocene menardellids (planktonic foraminifera), PhD Thesis, University of Basel, https://doi.org/10.5451/unibas-006194467, 2013.

Mary, Y. and Knappertsbusch, M. W.: Worldwide morphological variability in Mid-Pliocene menardellid globorotalids, Marine Micropaleontology, 121, 1–15, https://doi.org/10.1016/j.marmicro.2015.09.001, 2015.

O'Dea, A., Lessios, H. A., Coates, A. G., Eytan, R. I., Restrepo-Moreno, S. A., Cione, A. L., Collins, L. S., de Queiroz, A., Farris, D. W., Norris, R. D., Stallard, R. F., Woodburne, M. O., Aguilera, O., Aubry, M.-P., Berggren, W. A., Budd, A. F., Cozzuol, M. A., Coppard, S. E., Duque-Caro, H., Finnegan, S., Gasparini, G. M., Grossman, E. L., Johnson, K. G., Keigwin, L. D., Knowlton, N., Leigh, E. G., Leonard-Pingel, J. S., Marko, P. B., Pyenson, N. D., Rachello-Dolmen, P. G., Soibelzon, E., Soibelzon, L., Todd, J. A., Vermeij, G. J., and Jackson, J. B. C.: Formation of the Isthmus of Panama, Science Advances, 2, https://doi.org/10.1126/sciadv.1600883, 2016.

Schmidt, D. N., Lazarus, D., Young, J. R., and Kucera, M.: Biogeography and evolution of body size in marine plankton, Earth-Science Reviews, 78, 239–266, https://doi.org/10.1016/j.earscirev.2006.05.004, 2006.

Wade, B. S., Pearson, P. N., Berggren, W. A., and Pälike, H.: Review and revision of Cenozoic tropical planktonic foraminiferal biostratigraphy and calibration to the geomagnetic polarity and astronomical time scale, Earth-Science Reviews, 104, 111–142, https://doi.org/10.1016/j.earscirev.2010.09.003, 2011.